


5-2015

# MULTILEVEL DEREGULATION OF SURVIVAL MECHANISMS IN NPM-ALK+ T-CELL LYMPHOMA

Deeksha Vishwamitra

Follow this and additional works at: [http://digitalcommons.library.tmc.edu/utgsbs\\_dissertations](http://digitalcommons.library.tmc.edu/utgsbs_dissertations)

 Part of the [Hematology Commons](#), [Laboratory and Basic Science Research Commons](#), [Medical Cell Biology Commons](#), and the [Medical Molecular Biology Commons](#)

---

## Recommended Citation

Vishwamitra, Deeksha, "MULTILEVEL DEREGULATION OF SURVIVAL MECHANISMS IN NPM-ALK+ T-CELL LYMPHOMA" (2015). *UT GSBS Dissertations and Theses (Open Access)*. Paper 554.

This Dissertation (PhD) is brought to you for free and open access by the Graduate School of Biomedical Sciences at DigitalCommons@The Texas Medical Center. It has been accepted for inclusion in UT GSBS Dissertations and Theses (Open Access) by an authorized administrator of DigitalCommons@The Texas Medical Center. For more information, please contact [laurel.sanders@library.tmc.edu](mailto:laurel.sanders@library.tmc.edu).

**MULTILEVEL DEREGULATION OF SURVIVAL  
MECHANISMS IN NPM-ALK<sup>+</sup> T-CELL LYMPHOMA**

A

DISSERTATION

Presented to the Faculty of  
The University of Texas  
Health Science Center at Houston  
and  
The University of Texas  
MD Anderson Cancer Center  
Graduate School of Biomedical Sciences  
in Partial Fulfillment

of the Requirements

for the Degree of

DOCTOR OF PHILOSOPHY

by

Deeksha Vishwamitra, M.S.  
Houston, Texas

May 2015

**Dedication**

*To my dearest parents,*

*Thank you for your unconditional love, pride, teachings, and giving me the wings to soar,*

*I love you forever and always*

## **Acknowledgements**

Firstly, I would like to thank my supervisor Dr. Hesham M. Amin for being an incredible mentor to me over the years. I am truly grateful for his constant belief in me, even at times when I had doubts, as well as for his praise. He has exemplified qualities that will help me grow as a scientist and has equipped me with all the skills needed to endure the scientific world. I learned so much through him as well as working in his lab, and have achieved greater things than I ever thought imaginable because of him.

Secondly, I would like to thank the members of my Supervisor Committee: Dr. Russell Broaddus, Dr. Jeffrey Frost, Dr. Gary E. Gallick, and Dr. Joseph A. Ludwig. I sincerely thank each of these members for their support and encouragement over the years. They provided positive feedback and recognized the extent of this thesis work from the beginning. They also exemplify qualities which I hope to encompass throughout my scientific journey.

Thirdly, I would like to thank the members of the Amin lab, both past and present: Ping Shi, Suraj Konnath George, Wenyu Shi, Ghazaleh Eskandari, Desiree Wilson, and Roxsan Manshouri. They have assisted me in several research experiments and I am grateful for their help.

Finally, I would like to thank my family and friends for their continuous encouragement through this journey. The road seemed so much shorter, easier, and better because of it.

# MULTILEVEL Deregulation of Survival Mechanisms in NPM-ALK<sup>+</sup> T-Cell Lymphoma

Deeksha Vishwamitra, M.S.

Advisory Professor: Hesham M. Amin, M.D.

The anaplastic lymphoma kinase (ALK) is a single chain transmembrane receptor tyrosine kinase that belongs to the insulin receptor superfamily. Other members of this superfamily include the insulin receptor (IR), type I insulin-like growth factor receptor (IGF-IR), and the leukocyte tyrosine kinase. The common structural finding among these tyrosine kinases is the YXXYY motif present within their respective tyrosine kinase domains. Binding of its ligands causes ALK receptor homodimerization and protein kinase activation. ALK has been previously shown to play a significant role during early developmental stages. In human embryos, the expression of ALK is mainly seen in the nervous system but it decreases at birth. A variety of structural rearrangements have been identified in the *ALK* gene, such as mutations, overexpression, and translocations, often leading to the production of oncogenic proteins found in several different types of human cancers, such as nucleophosmin-anaplastic lymphoma kinase-expressing anaplastic large-cell lymphoma (NPM-ALK<sup>+</sup> ALCL). The oncogenic potential of NPM-ALK has been demonstrated by several studies using *in vitro* assays as well as transgenic mouse models.

NPM-ALK<sup>+</sup> ALCL is an aggressive subset of T-cell lymphoma that predominantly occurs in children and young adults. It comprises approximately 85% of ALK<sup>+</sup> ALCL cases and is characterized by the translocation t(2;5)(p23;q35) that leads to the fusion between the *NPM* gene on chromosome 5q35 and the *ALK* gene on chromosome 2p23 generating the *NPM-ALK* oncogene, which encodes the expression of NPM-ALK chimeric tyrosine kinase. NPM-

ALK induces lymphomagenic effects through the formation of the constitutively activated NPM-ALK/NPM-ALK homodimers, which phosphorylate/activate downstream survival-promoting proteins including JAK/STAT, PI3K/AKT, and MAP kinase. NPM-ALK resides in the cytoplasm; nonetheless, it is also capable of forming the wild type NPM/NPM-ALK heterodimers that translocate to the nucleus through the nuclear localization signal site present in wild type NPM.

IGF-IR is a homodimeric protein that is composed of two extracellular  $\alpha$  and two transmembranous  $\beta$  subunits connected by disulfide bonds. Similar to ALK, its expression plays an important role during early developmental stages. Mouse models have confirmed the importance of IGF-IR in prenatal and postnatal growth through its interactions with the growth hormone. The result of activation of IGF-IR during these stages is survival and proliferation of cells resulting in developmental growth of tissues such as skeletal and cardiac muscles. It also plays a critical role during growth of the mammary gland during pregnancy and lactation. It has been previously shown that *Igf1r* null mice develop generalized organ hypoplasia, such as developmental delays in bone ossification, abnormalities in the central nervous system, and they prematurely die because of underdevelopment of their lungs that leads to respiratory failure. Recently, it has been shown that IGF-IR overexpression significantly contributes to the establishment and progression of different types of cancer and to the emergence of therapeutic resistance. These effects have been extensively investigated in solid tumors including breast, prostate, lung, ovary, skin, and soft tissue cancers.

We have recently demonstrated that, compared with normal human T lymphocytes and reactive lymphoid tissues, the expression and activation of IGF-IR are remarkably upregulated in NPM-ALK<sup>+</sup> ALCL. We also demonstrated that IGF-IR physically associates and directly interacts with NPM-ALK. Nonetheless, the exact mechanisms for the up-

regulation of IGF-IR and NPM-ALK in this lymphoma are not fully characterized. *We hypothesized that multilevel deregulation of survival mechanisms contributes to aberrant NPM-ALK and IGF-IR expression, which supports the survival and progression of NPM-ALK<sup>+</sup> ALCL.*

**Table of Contents**

APPROVAL SHEET .....	i
TITLE PAGE .....	ii
DEDICATIONS .....	iii
ACKNOWLEDGMENTS.....	iv
ABSTRACT .....	v
TABLE OF CONTENTS .....	viii
LIST OF ILLUSTRATIONS .....	x
LIST OF TABLES .....	xii
LIST OF ABBREVIATIONS .....	xiii
INTRODUCTION.....	1
1.1 NPM-ALK <sup>+</sup> anaplastic large cell lymphoma .....	2
1.2 NPM.....	3
1.2.1 Roles of NPM.....	3
1.2.2 Structure of NPM .....	4
1.3 ALK.....	7
1.3.1 Role of ALK.....	7
1.3.2 Structure of ALK.....	7
1.3.3 ALK and disease.....	11
1.4 NPM-ALK.....	11
1.4.1 NPM-ALK structure and function.....	11
1.4.2 NPM-ALK signaling .....	16
1.5 Overview of the insulin-like growth factor system.....	20
1.6 IGF-I.....	21
1.7 IGF-IR .....	25
1.7.1 IGF-IR structure and signaling.....	25
1.7.2 Physiological and pathological roles of IGF-IR.....	30
RATIONALE, HYPOTHESIS, AND SPECIFIC AIMS.....	33
RESULTS .....	43
3.1 Transcriptional regulation of IGF-IR .....	44
3.1.1 Introduction .....	45
3.1.2 Transcriptional regulation of IGF-IR: Transcription Factors .....	46



3.1.2.1 Materials and Methods .....	47
3.1.2.2 Results .....	58
3.1.3 Transcriptional regulation of IGF-IR: Gene Amplification .....	75
3.1.3.1 Materials and Methods .....	76
3.1.3.2 Results .....	78
3.2 Discussion for Aim 1 .....	82
3.3 Post-transcriptional regulation of IGF-IR .....	87
3.3.1 Introduction .....	88
3.3.2 Post-transcriptional regulation of IGF-IR: miRNAs .....	89
3.3.2.1 Materials and Methods .....	90
3.3.2.2 Results .....	101
3.3.3 Post-transcriptional regulation of IGF-IR: mRNA stability .....	124
3.4.3.1 Materials and Methods .....	125
3.4.3.2 Results .....	127
3.4 Discussion for Aim 2 .....	130
3.4.1 Supplemental .....	136
3.5 Post-translational regulation of IGF-IR .....	149
3.5.1 Introduction .....	150
3.5.2 Post-translational regulation of IGF-IR: SUMOylation .....	151
3.5.2.1 Materials and Methods .....	152
3.5.2.2 Results .....	159
3.5.3 Post-translational regulation of IGF-IR: IGF-I .....	184
3.5.3.1 Materials and Methods .....	185
3.5.3.2 Results .....	187
3.6 Discussion for Aim 3 .....	192
3.6.1 Supplemental .....	198
CONCLUSIONS.....	204
FUTURE DIRECTIONS .....	213
BIBLIOGRAPHY .....	214
VITAE.....	230

## List of Illustrations

### INTRODUCTION

<b>Figure 1.</b> Structure of NPM.....	5
<b>Figure 2.</b> Structure of human ALK .....	9
<b>Figure 3.</b> The t(2;5)(p23;q35) translocation resulting in NPM-ALK fusion protein .....	14
<b>Figure 4.</b> NPM-ALK and its downstream signaling pathways .....	18
<b>Figure 5.</b> Overview of the IGF system.....	21
<b>Figure 6.</b> Structure of IGF-IR .....	26
<b>Figure 7.</b> IGF-IR signaling.....	28

### RATIONALE, HYPOTHESIS, AND SPECIFIC AIMS

<b>Figure 8.</b> Expression of IGF-IR in NPM-ALK <sup>+</sup> ALCL cell lines .....	37
<b>Figure 9.</b> Association and functional interactions between NPM-ALK and IGF-IR .....	38
<b>Figure 10.</b> NPM-ALK does not regulate IGF-IR expression.....	41

### TRANSCRIPTIONAL REGULATION OF IGF-IR: TRANSCRIPTION FACTORS

<b>Figure 11.</b> The expression of Ik-1 and MZF1 is decreased in NPM-ALK <sup>+</sup> ALCL cell lines and human primary tumors .....	62
<b>Figure 12.</b> Ik-1 and MZF1 interact with and bind to the <i>IGF-IR</i> gene promoter .....	66
<b>Figure 13.</b> Ik-1 and MZF1 decrease IGF-IR mRNA and protein expression and the phosphorylation of downstream targets .....	70
<b>Figure 14.</b> Transfection of Ik-1 and MZF1 decreases the viability, proliferation, migration, and anchorage-independent colony formation of NPM-ALK <sup>+</sup> ALCL cells.....	73

### TRANSCRIPTIONAL REGULATION OF IGF-IR: GENE AMPLIFICATION

<b>Figure 15.</b> FISH analysis of IGF-IR gene (red signal) and chromosome enumeration 15 (green signal; CEP15), which detects centromere 15, copy numbers in normal T lymphocytes and NPM-ALK <sup>+</sup> ALCL cell lines .....	79
---	----

### POSTTRANSCRIPTIONAL REGULATION OF IGF-IR: MIRNA

<b>Figure 16.</b> Array analysis of differential expression of miR in NPM-ALK <sup>+</sup> ALCL cell lines vs. normal T lymphocytes.....	102
<b>Figure 17.</b> miR-30a and miR-30d decrease <i>IGF-IR</i> -3'-UTR activity.....	106
<b>Figure 18.</b> miR-30a and miR-30d decrease IGF-IR protein expression, but not <i>IGF-IR</i> mRNA expression in NPM-ALK <sup>+</sup> ALCL cells.....	108
<b>Figure 19.</b> miR-30a and miR-30d decrease cell proliferation, migration, and colony forming potential in NPM-ALK <sup>+</sup> ALCL cell lines. ....	111
<b>Figure 20.</b> 5'aza increases miR-30a and miR-30d expression in NPM-ALK <sup>+</sup> ALCL cells..	114
<b>Figure 21.</b> Inducible miR-30a and miR-30d mouse model.....	119
<b>Figure 22.</b> miR-30a and miR-30d suppress NPM-ALK <sup>+</sup> ALCL tumor growth <i>in vivo</i> . ....	120

<b>Figure 23.</b> Adequate induction of miR-30a and miR-30d expression by administration of 4-OHT in mice.....	122
--	-----

## POSTTRANSCRIPTIONAL REGULATION OF IGF-IR: MRNA STABILITY

<b>Figure 24.</b> IGF-IR mRNA expressed in NPM-ALK <sup>+</sup> ALCL cells exhibits prolonged decay time compared with <i>IGF-IR</i> mRNA from normal human T lymphocytes.....	128
--	-----

## SUPPLEMENTAL

<b>Figure S1.</b> miR-30a and miR-30d are downregulated in MCF-7 and SW-480 cells.....	137
<b>Figure S2.</b> miR-30a and miR-30d decrease IGF-IR protein expression, but not <i>IGF-IR</i> mRNA expression in MCF-7 and SW-480 cells.....	139
<b>Figure S3.</b> miR-30a and miR-30d decrease cell proliferation, migration, and colony forming potential in MCF-7 and SW-480 cells.....	141
<b>Figure S4.</b> Breast mouse model with inducible expression of miR-30a or miR-30d.....	143
<b>Figure S5.</b> miR-30a and miR-30d suppress breast tumor growth <i>in vivo</i> .....	145
<b>Figure S6.</b> Doxycyclin increased efficiently the levels of miR-30a and miR-30d <i>in vivo</i> ....	147

## POSTTRANSLATIONAL REGULATION OF IGF-IR: SUMOYLATION

<b>Figure 25.</b> SUMO binding motifs within NPM-ALK amino acid sequence.....	160
<b>Figure 26.</b> SUMO is upregulated in NPM-ALK <sup>+</sup> ALCL cells.....	162
<b>Figure 27.</b> NPM-ALK is SUMOylated.....	167
<b>Figure 28.</b> NPM-ALK is SUMOylated at Lys <sup>24</sup> and Lys <sup>32</sup> .....	169
<b>Figure 29.</b> SUMOylation promotes the stability of NPM-ALK protein.....	171
<b>Figure 30.</b> NPM-ALK is predominantly expressed in the nucleus.....	174
<b>Figure 31.</b> SENP1 decreases NPM-ALK nuclear expression.....	176
<b>Figure 32.</b> SENP1 decreases cell viability, proliferation, and colony formation potential in NPM-ALK <sup>+</sup> ALCL cells.....	179
<b>Figure 33.</b> Schematic model illustrating the SUMOylation of NPM-ALK.....	182

## POSTTRANSLATIONAL REGULATION OF IGF-IR: IGF-I

<b>Figure 34.</b> Expression of IGF-I in NPM-ALK <sup>+</sup> ALCL cell lines.....	188
<b>Figure 35.</b> NPM-ALK does not affect the levels of expression of IGF-IR and IGF-I.....	190

## SUPPLEMENTAL

<b>Figure S7.</b> IGF-IR is SUMOylated.....	197
<b>Figure S8.</b> IGF-IR and pIGF-IR are expressed in the cytoplasm, whereas pIGF-IR is also expressed in the nucleus after IGF-I stimulation.....	199
<b>Figure S9.</b> SENP1 decreases IGF-IR nuclear and cytoplasmic expression.....	201

## CONCLUSIONS.....

<b>Figure 36.</b> Mechanisms contributing to deregulated survival mechanisms in NPM-ALK <sup>+</sup> ALCL.....	208
--	-----

## List of Tables

### TRANSCRIPTIONAL REGULATION OF IGF-IR: TRANSCRIPTION FACTORS

<b>Table 1.</b> Sequence of primers used to construct the 3 fragments (F1, F2, and F3) of the human <i>IGF-IR</i> gene promoter.....	50
<b>Table 2.</b> The amplification conditions used in Touchdown PCR for the construction of 3 fragments of the human <i>IGF-IR</i> gene promoter.....	51
<b>Table 3.</b> PCR conditions used for DNA ligation for the construction of the human <i>IGF-IR</i> gene promoter .....	52
<b>Table 4.</b> Sequences of the primers used to construct the 3 mutated fragments of human IGF-IR luciferase reporter (F1, F2, and F3). .....	53
<b>Table 5.</b> Sequences of the primers flanking potential binding sites (BS) of Ik-1 and MZF1 within the human IGF-IR promoter used in the RT-PCR reactions following the ChIP assay. ....	55
<b>Table 6.</b> Ik-1 and MZF1 can potentially bind with <i>IGF-IR</i> gene promoter.....	59

### POSTTRANSCRIPTIONAL REGULATION OF IGF-IR: MIRNA

<b>Table 7.</b> PCR conditions for miRNA reverse transcription.....	93
<b>Table 8.</b> PCR conditions for WT IGF-IR 3'UTR construction.....	94
<b>Table 9.</b> PCR conditions Quick Ligation .....	95
<b>Table 10.</b> PCR conditions for mutated IGF-IR 3'UTR construction. ....	96

### POSTTRANSLATIONAL REGULATION OF IGF-IR: SUMOYLATION

<b>Table 11.</b> Primers used to create NPM-ALK <sup>K24R</sup> and NPM-ALK <sup>K32R</sup> constructs by site-directed mutagenesis.....	154
--	-----

**List of Abbreviations**

ALCL: anaplastic large cell lymphoma

ALK: anaplastic lymphoma kinase

AR: androgen receptor

BAD: Bcl-2-associated death promoter

Bcl-2: B-cell lymphoma 2

Bcl-XL: B-cell lymphoma extra large

CHOP: cyclophosphamide, doxorubicin, vincristine, and prednisone

CNS: central nervous system

EGR1: early growth response protein 1

ER: endoplasmic reticulum

ERK: extracellular signal regulated kinase

FRS2: fibroblast growth factor receptor substrate 2

GH: growth hormone

GIST: gastrointestinal stromal tumor

Grb2: growth factor receptor bound protein

HR: hybrid receptor

ICD: intracellular domain

IGF: insulin like growth factor

IGF-IR: type I insulin-like growth factor receptor

IR: insulin receptor

IRS: insulin receptor substrate

JAK: Janus kinase

JNK: c-Jun N terminal kinase

LDL<sub>A</sub>: low-density lipoprotein class A

Lys: lysine

MAM: memprin, A5 protein and receptor tyrosine phosphatase mu

Mcl-1: myeloid leukemia cell differentiation protein

miR: microRNA

mTOR: mammalian target of rapamycin

NES: nuclear export signal

NLS: nuclear localization signal

NPM: nucleophosmin

PI3K: phosphoinositol 3-kinase

PLC- $\gamma$ : phospholipase C-gamma

PTCH: Patched protein

SENP: sentrin specific protease

Shc: src homology and collagen protein

SHH: sonic hedgehog

SHP1: Src homology region 2 domain-containing phosphatase-1

SMO: Smoothed protein

SP1: specificity protein 1

STAT: signal transducer and activator of transcription

SUMO: small ubiquitin like modifier

TIMP1: tissue inhibitor of metalloproteinase

TM-spanning: transmembrane spanning

Tyr: tyrosine

WT1: Wilm's tumor suppressor

YXXYY motif: tyrosine residue, followed by 3 amino acids, followed by 2 tyrosine residues

## **Introduction**

### 1.1. NPM-ALK<sup>+</sup> T-cell anaplastic large cell lymphoma

Anaplastic large cell lymphoma (ALCL) is a high-grade non-Hodgkin's T-cell lymphoma that was originally described as universally expressing the tumor necrosis factor receptor CD30/Ki-1 [1, 2]. Morphological features typically include large anaplastic cells with abundant cytoplasm and distinct, often "horse-shoe" shaped, nuclei [3]. However, it is agreed now that ALCL is a misnomer as it is not unusual for this lymphoma to represent in the form of small lymphoma cells without notable anaplastic features. ALCL constitutes 3 to 5% of adult malignant lymphomas and comprises 10 to 30% of malignant lymphomas in children and young adults [3, 4]. The lymphoma is slightly more predominant in males. ALCL usually presents as a widespread stage III/IV neoplasm, with a rapidly progressive course. It is considered an aggressive type of lymphoma because patients typically present with B symptoms (fever, weight loss, and night sweats), generalized lymphadenopathy, and frequent extranodal involvement [1].

Approximately 60-80% of ALCL cases harbor an aberration involving the anaplastic lymphoma kinase (*ALK*) gene that encodes the expression of the ALK protein (ALK<sup>+</sup> ALCL). The expression of ALK holds prognostic significance as ALK<sup>-</sup> ALCL patients show a much reduced 5-year survival rate compared to ALK<sup>+</sup> ALCL patients [5, 6]. Although several chromosomal translocations involving *ALK* have been identified in ALK<sup>+</sup> ALCL, approximately 85% of these lymphomas are characterized by the translocation t(2;5)(p23;q35) that generates the fusion between the *NPM* gene on chromosome 5q35 to the *ALK* gene on 2p23 that forms the oncogenic fusion protein NPM-ALK, which is the defining feature of NPM-ALK<sup>+</sup> ALCL [1, 5-8]. Because NPM-ALK expression is the most common and because cell lines have been developed only from the NPM-ALK<sup>+</sup> variant, in this work we will refer to this lymphoma as NPM-ALK<sup>+</sup> ALCL.



First-line treatment using doxorubicin-based polychemotherapy is encouraging in some cases, in which 60-80% of NPM-ALK<sup>+</sup> ALCL patients initially respond favorably, with a 5-year relapse-free survival of 60%, and a 5-year overall survival of 70% [9, 10]. Anthracycline-based chemotherapy regimens, including CHOP (cyclophosphamide, doxorubicin, vincristine, and prednisone), have also provided favorable results. Radiation or stem cell transplantation in combination with CHOP is oftentimes utilized in more advanced cases, in which large localized masses are found [9, 10]. However, as many as 40% of these patients relapse, develop resistance, and eventually die, suggesting the need for specific and more effective therapeutics. Recently, selective ALK inhibitors have been developed; nonetheless, most of these inhibitors have been tested in solid tumors, with the majority being in lung cancer patients [11-14]. Notably, mutations of ALK have quickly developed in some of the NPM-ALK<sup>+</sup> ALCL patients that were treated with such inhibitors, indicating that the battle against this aggressive lymphoma is far from over [15, 16].

## **1.2. NPM**

**1.2.1. Roles of NPM:** NPM is a ubiquitously expressed RNA-binding nucleolar phosphoprotein that is encoded by chromosome 5q35. It is believed to be involved in regulating numerous processes that leads to maintaining cellular homeostasis. For instance, it is involved in the transport of pre-ribosomal particles during ribosome biogenesis, response to stress stimuli such as UV irradiation and hypoxia, the maintenance of genomic stability through the control of chromosome segregation, and DNA-repair processes. Furthermore, it is highly involved in gene transcription where it regulates chromatin condensation and decondensation events [17].

**1.2.2. Structure of *NPM*:** NPM protein has a molecular weight of approximately 38 kDa. The numerous functions of NPM are largely attributed to the diversity of its structural characteristics (**Figure 1**). The N-terminus contains a hydrophobic segment that is essential for oligomerization and chaperone activity. Immediately following this segment are two acidic stretches that are important for binding histones during DNA transcription processes [17-19]. The ribonuclease activity stems from the middle portion of NPM, the region between the two acidic domains. Finally, the C-terminal domain contains segments comprising basic amino acids that are important for nucleic-acid binding. These basic regions are followed by aromatic stretches, which house two tryptophan residues (288 and 290) located within the nuclear-localization signal (NLS) that are required for nuclear localization of the protein [17, 20]. In addition, NPM includes a nuclear-export signal (NES) that mediates NPM's ability to shuttle from the nucleus [21].

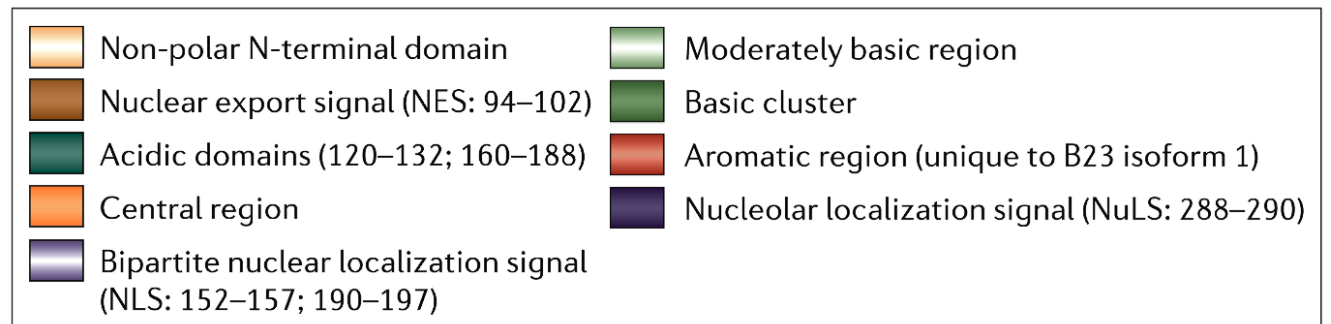
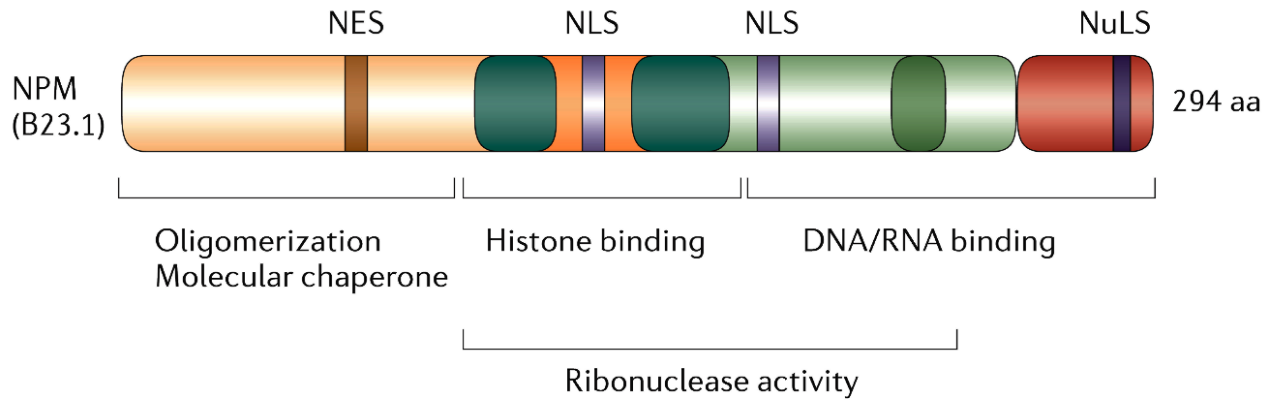


**FIGURE 1. Structure of NPM.** Starting from the N-terminus, the protein contains one hydrophobic segment that is involved in oligomerization as well as chaperone activity, followed by two acidic stretches that are important for binding to histones. The central portion between the two acidic domains is required for ribonuclease activity, together with the C-terminus domain, which contains basic regions involved in nucleic-acid binding. The basic clusters are followed by an aromatic stretch, which contains two tryptophan residues (288 and 290) that are required for nucleolar localization of the protein. In addition, NPM includes a nuclear-localization signal (NLS) and a nuclear-export signal (NES). **Adapted with permission from Macmillan Publishers Ltd on behalf of Cancer Research UK: [Nature Reviews Cancer] (Grisendi S, Mecucci C, Falini B, Pandolfi PP. Nucleophosmin and cancer. Nat Rev Cancer. 2006 Jul;6(7):493-505.), copyright 2006.**

### 1.3. ALK

**1.3.1. Role of ALK:** Physiologically, the expression of ALK is largely restricted to neuronal tissues at early developmental stages, as indicated by the high expression of *ALK* mRNA in the central nervous system (CNS) during mouse embryogenesis [22-24]. ALK expression diminishes after birth, reaching minimal levels at 3 weeks of age, and subsequently maintained at low levels during adult stages [22]. Based on these observations, it is believed that ALK is a critical regulator of neuronal development and function of the CNS. For example, it has been demonstrated that the ALK-IgG Fc hybrid protein, in which the extracellular region of ALK is substituted with the mouse IgG Fc domain, induces neurite differentiation and outgrowth of PC12 cells, mediated through the MAPK pathway [25]. In addition, it has also been demonstrated that specific antibody-mediated inhibition of ALK leads to prevention of the binding of the Src homology and collagen domain protein (Shc) to ALK, which causes subsequent MAPK inactivation and decreased neuronal differentiation. Similarly, inhibition of the ALK-activated MAPK pathway decreases neurite outgrowth, further strengthening the idea that neuronal differentiation induced by ALK is mediated via the MAPK pathway [26, 27]. In addition to Shc, the fibroblast growth factor receptor substrate 2 (FRS2) has also been reported to be recruited to a novel non-consensus phosphotyrosine site within ALK and contributes to ALK-induced neuronal differentiation [27].

**1.3.2. Structure of ALK:** ALK is a receptor tyrosine kinase whose structure is highly conserved within species, as well as within members of the insulin receptor superfamily, especially in regards to their kinase domains. The common structural finding among these tyrosine kinases is the YXXXYY (indicating a tyrosine (Y), followed by 3 non-tyrosine amino acid residues, and then 2 additional tyrosine residues) motif present within their

respective tyrosine kinase domains. It has been reported that the first tyrosine residue (Tyr<sup>1278</sup>) within the YXXYY motif is the principal site to become phosphorylated during the autoactivation process of ALK [28, 29].

The *ALK* gene is located on chromosome 2p23 that encodes for a single chain transmembrane receptor tyrosine kinase of 180 kDa (**Figure 2**). The extracellular portion of ALK contains an N-terminal signal peptide followed by two MAM domains (meprin, A5 protein and receptor tyrosine phosphatase mu) that flank one LDLa domain (low-density lipoprotein class A), followed by a glycine rich (G-rich) region. The N-terminus region is capable of undergoing N-linked glycosylation, which increases the molecular weight of ALK by 20kDa. Although the precise function of the LDLa domain is unknown, it has been proposed as the ligand binding domain. Similarly, the function of the MAM domains remains to be identified, however, they are thought to be involved in cell-to-cell interactions [30]. In addition, the G-rich domains are believed to be required for ALK function, as point mutations within this region render loss of ALK function [31]. The intracellular domain (ICD) consists of a transmembrane (TM)-spanning segment that essentially connects the extracellular region to the PTK domain; the ICD also contains ATP binding sites and putative binding sites for various interacting proteins including insulin receptor substrate 1 (IRS-1), Shc, phosphoinositide 3-kinase (PI3K) and phosphoinositide phospholipase C-gamma (PLC- $\gamma$ ) distributed throughout [22, 23, 32].

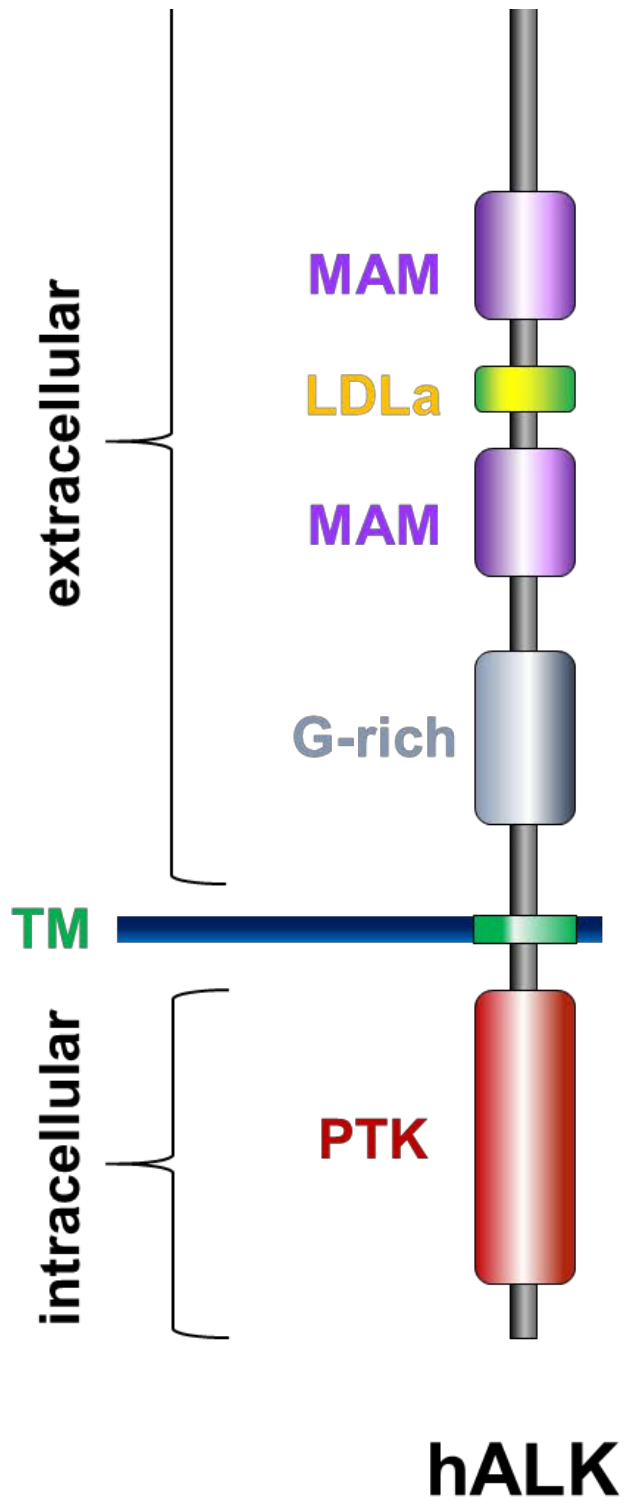


**FIGURE 2. Structure of human ALK.** The N-terminal region of ALK comprises two MAM domains (amino acids 264–427 and 480–626), one LDLa domain (amino acids 453–471), and a glycine rich (G-rich) region (amino acids 816–940). A transmembrane (TM)-spanning segment connects the extracellular region with the protein tyrosine kinase domain - containing intracellular region (amino acids 1116–1383). **Adapted with permission from PMC [Biochemical Journal] (Palmer RH, Vernersson E, Grabbe C, Hallberg B. Anaplastic lymphoma kinase: signalling in development and disease. Biochem J. 2009 May 27;420(3):345-61.), copyright 2009.**



**1.3.3. *ALK and disease:*** Alterations involving *ALK* have been implicated in various diseases, with the initial discovery of the NPM-*ALK* fusion protein in NPM-*ALK*<sup>+</sup> ALCL in 1994 [33, 34]. In addition to NPM-*ALK*, other *ALK* fusion proteins have been identified in ALCL, inflammatory myofibroblastic tumors, non-small cell lung cancer, diffuse large B-cell lymphoma, and squamous cell carcinoma [35-38]. Recently, overexpression of *ALK* has been reported to play a role in malignant transformation of cell lines and tumors, as well as activating point mutations in *ALK*, as in the case of neuroblastoma [39-49].

## **1.4. NPM-*ALK***

**1.4.1. *NPM-ALK structure and function:*** The most distinguishable feature in NPM-*ALK*<sup>+</sup> ALCL is the presence of the translocation t(2;5)(p23;q35) that generates the fusion between the *NPM* gene on chromosome 5q35 to the *ALK* gene on 2p23 to form the chimeric oncogene *NPM-ALK*, that encodes for NPM-*ALK* fusion protein [7] (**Figure 3; upper panel**). The t(2;5)(p23;q35) translocation juxtaposes the N-terminal domain of the *NPM* gene (amino acids 1-117) to the C-terminal domain of the *ALK* gene that codes for the entire cytoplasmic region of the *ALK* protein. As a consequence, the *ALK* gene is under the control of the highly active *NPM* promoter, which induces continual transcription of *NPM-ALK* gene and results in the silencing of the *ALK* regulatory and promoter regions that normally suppress *ALK* expression in normal lymphocytes. This leads to the constitutive activation of the NPM-*ALK* protein because the oligomerization domain of NPM and activation of the kinase catalytic domain of *ALK* are preserved.

Because the truncation of NPM during the translocation does not conserve its C-terminal domain, the nuclear localization signals are absent in the chimeric protein. Similarly, the extracellular and transmembrane regions of *ALK* are also not present, thereby rendering

ALK entirely cytoplasmic. The NPM-ALK protein is able to form homodimers with other NPM-ALK moieties or heterodimers by cross-linking with wild-type NPM. The formation of homodimers results in the constitutive activation of the ALK tyrosine kinase domain contained in the NPM-ALK fusion protein and the induction of downstream signaling via the JAK/STAT3, MEK/ERK1/2, or the PI3K/AKT pathways (detailed in section 1.4.2). The NPM/NPM-ALK heterodimers, on the other hand, translocate to the nucleus, primarily from the ability of wild type NPM to translocate to the nucleus (**Figure 3; lower panel**). There is considerable evidence suggesting that the nuclear localization of NPM-ALK is not required for the development of lymphoma, and therefore, the biological consequences of nuclear localization of NPM-ALK are not known [50, 51]. However, the importance of NPM in the transforming abilities of NPM-ALK has been demonstrated through experiments in which deletion of the NPM portion of the fusion protein abolishes transformation events; the process of dimerization through NPM oligomerization domain essentially mimics ligand binding and therefore, gives NPM-ALK its transforming abilities [52].

The oncogenic properties of NPM-ALK have been demonstrated *in vitro* in a variety of cell types, such as mouse NIH-3T3 and Fr3T3, as well as Rat-1 cells, and several hematopoietic cell lines such as the myeloid line 32Dcl3 and the lymphocytic cell line Ba/F3 [50-54]. Transformation occurs in primary mouse bone marrow cells retrovirally transduced with NPM-ALK, which was reversed upon treatment with PI3K inhibitors [54]. In addition, cells transfected with NPM-ALK are able to grow colonies in soft-agar, providing further support for the transforming abilities of NPM-ALK. These properties have also been demonstrated *in vivo*. For example, bone marrow expressing human NPM-ALK is able to induce lymphoid malignancies in lethally irradiated mice [53, 55]. Furthermore, transgenic mice expressing NPM-ALK under the control of the CD4 promoter develop CD30<sup>+</sup> NPM-

ALK<sup>+</sup> T-cell lymphoma [56]. Of important note is that in all NPM-ALK transgenic mouse models, significant numbers of tumors were plasma cell or B-cell neoplasms, strongly suggesting that NPM-ALK is not the only factor contributing to the immunophenotypic, pathophysiological, and clinical features as known in humans.

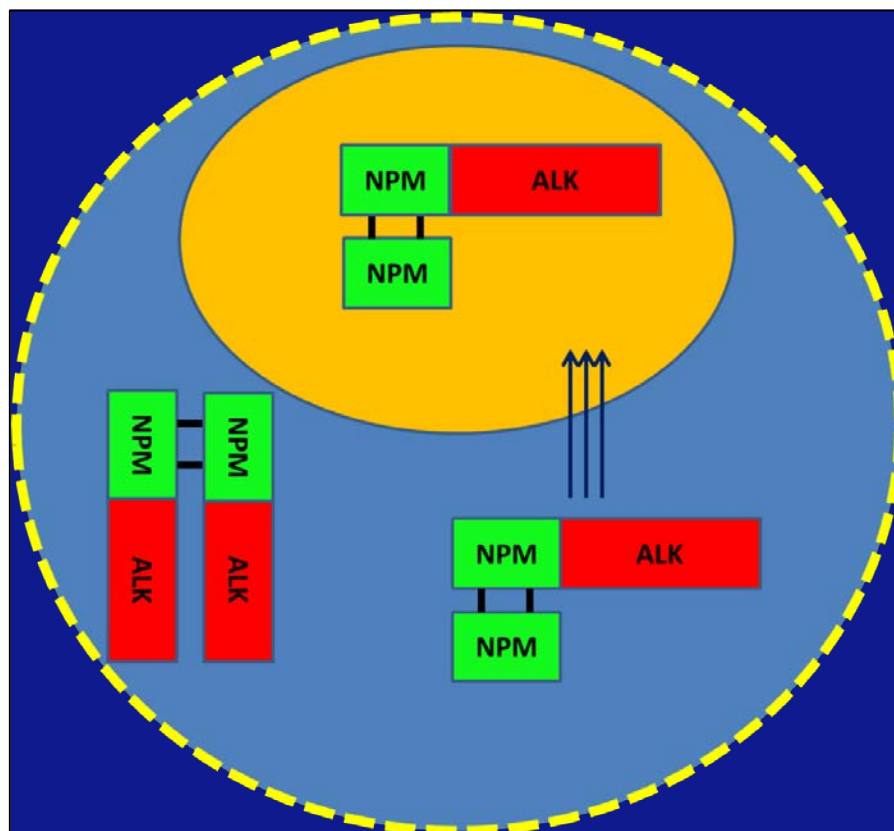
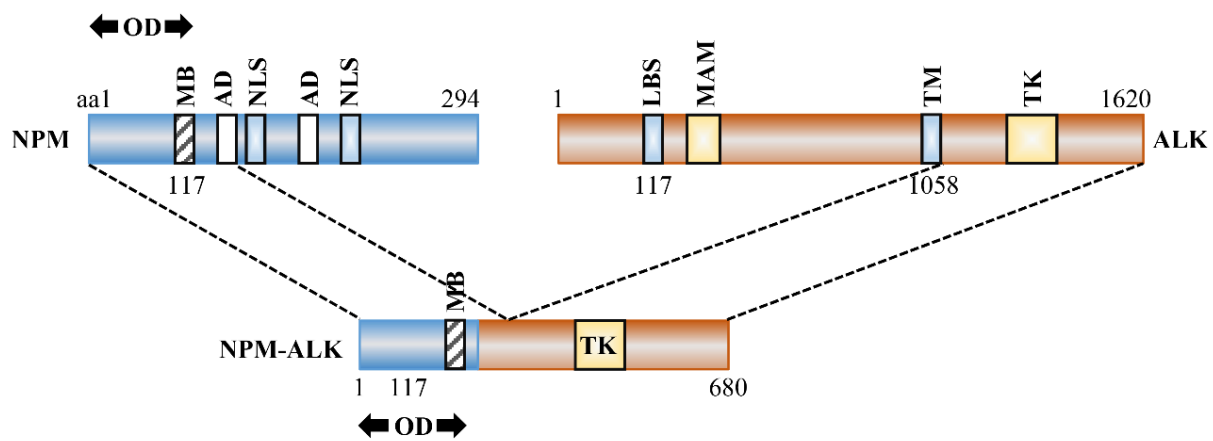


**FIGURE 3. The t(2;5)(p23;q35) translocation resulting in NPM-ALK fusion protein.** *Upper panel*, the t(2;5)(p23;q35) translocation juxtaposes the N-terminal domain of the *NPM* gene (amino acids 1-117) to the C-terminal domain of the *ALK* gene that encodes the entire cytoplasmic region of the *ALK* protein. The NPM-ALK fusion protein retains the oligomerization domain with the metal binding region of NPM and the tyrosine kinase domain and the cytoplasmic tail of *ALK*. **Reprinted from Anaplastic Lymphoma Kinase: Role in specific tumours, and development of small molecule inhibitors for cancer therapy: Ardini E, Magnaghi P, Orsini P, Galvani A, Menichincheri M. Anaplastic Lymphoma Kinase: role in specific tumours, and development of small molecule inhibitors for cancer therapy. Cancer Lett. 2010 Dec 28;299(2):81-94., with permission from Elsevier.** *Lower panel*, NPM-ALK is able to form homodimers with other NPM-ALK moieties in the cytoplasm as well as heterodimers with wild type NPM that allow *ALK* to translocate to the nucleus.

**1.4.2. NPM-ALK signaling:** The predominant signaling system in the cell survival mechanisms maintained by NPM-ALK is the signal transducer and activator of transcription 3 (STAT3) pathway either through Janus kinase-3 (JAK3)-dependent or independent mechanisms [57-59]. NPM-ALK can directly phosphorylate STAT3 [60, 61] and/or activate JAK3, which subsequently activates STAT3 [62] (**Figure 4**). Under normal circumstances, the SH2-containing ubiquitously expressed tyrosine-specific protein phosphatase-1 (SHP1) functions to inhibit ALK-mediated signaling by dephosphorylating ALK or its interacting proteins, namely Src and JAK. In NPM-ALK<sup>+</sup> ALCL, SHP1 is methylated, and therefore loses its expression, resulting in the enhancement of STAT3 signaling. Phosphorylated STAT3, in turn, translocates to the nucleus and up-regulates the expression of molecules involved in anti-apoptotic mechanisms such as B cell leukemia/lymphoma 2 (Bcl-2), Bcl-xL, and myeloid cell leukemia sequence 1 (Mcl-1), or key cell cycle regulators such as survivin, cyclin D3, and C/EBP $\beta$  [58, 63, 64]. We have also demonstrated previously that STAT3 plays a direct role in upregulating the tissue inhibitor of metalloproteinase-1 (TIMP1) in ALK<sup>+</sup> ALCL, and that expression of TIMP1 is associated with high level of STAT3 activation in this disease [65]. Also, there has been evidence that STAT5, particularly STAT5b, may act promote survival in NPM-ALK<sup>+</sup> ALCL through the activation of JAK2 [66, 67]. *In vitro* and *in vivo* studies using anti-STAT5b inhibitors resulted in impairment of NPM-ALK-induced cell transformation by inducing apoptosis. In contrast, it has also been shown that STAT5a is epigenetically silenced in this lymphoma [68]. In this regard, STAT5a acts as a tumor suppressor by reciprocally inhibiting NPM-ALK expression.

NPM-ALK also exerts proliferation signals through the activation of Ras, Raf-1, MEK1/2, and ERK1/2 by the direct binding of IRS-1, Src, and Shc to the autophosphorylated tyrosine residues located in the substrate-binding domain of ALK [7, 52] (**Figure 4**). This

induces the interaction between the SHP2-Grb2 (growth factor receptor-bound protein 2) and the ALK/Shc complex, which in turn enhances the phosphorylation of ERK1 and ERK2 through Src. Phosphorylation of ERK1 and ERK2 leads to the phosphorylation of the mammalian target of rapamycin (mTOR), which stimulates protein translation, ribosome biogenesis, and cap-dependent translation of mRNA [69]. In addition, NPM-ALK phosphorylates JUN N-terminal kinase (JNK) that up-regulates the activity of certain oncogenic transcription factors, such as AP1, which leads to uncontrolled proliferation due to repression of p21 and subsequent upregulation of cyclins [70]. Lastly, PLC- $\gamma$  directly binds to ALK, catalyzes the conversion of diacylglycerol and inositol triphosphate, triggering the release of  $\text{Ca}^{2+}$  from the endoplasmic reticulum (ER) to activate protein kinase C, leading to cell cycle progression [54].

Survival signaling can also occur through the PI3K/AKT pathway primarily by eliciting anti-apoptotic signals by NPM-ALK (**Figure 4**). NPM-ALK activates PI3K, which in turn activates the serine/threonine kinase, AKT, and results in the enhancement of survival signals by phosphorylating the cyclin-dependent kinase inhibitor p27 and increasing its proteosomal degradation [71]. Activation of AKT also results in inhibition of the function of pro-apoptotic proteins such as Bcl-2 antagonist of cell death (BAD) [72]. Concurrently, activated AKT phosphorylates and deactivates the FOXO3a transcription factor, which sustains FOXO3a in the cytoplasm, preventing its translocation to the nucleus and subsequent transcription of pro-apoptotic and cell cycle inhibitory genes [73]. This also leads to upregulation of cyclin D2, which is involved in G1-S cell cycle progression. Furthermore, mTOR is also activated by PI3K/AKT signaling through the induction of sonic hedgehog (SHH) expression. Binding of SHH to its receptor, Patched (PTCH), activates Smoothed (SMO) co-receptor by Patched, which results in activation of the GLI1 transcription factor and subsequently cyclin D2 [74].

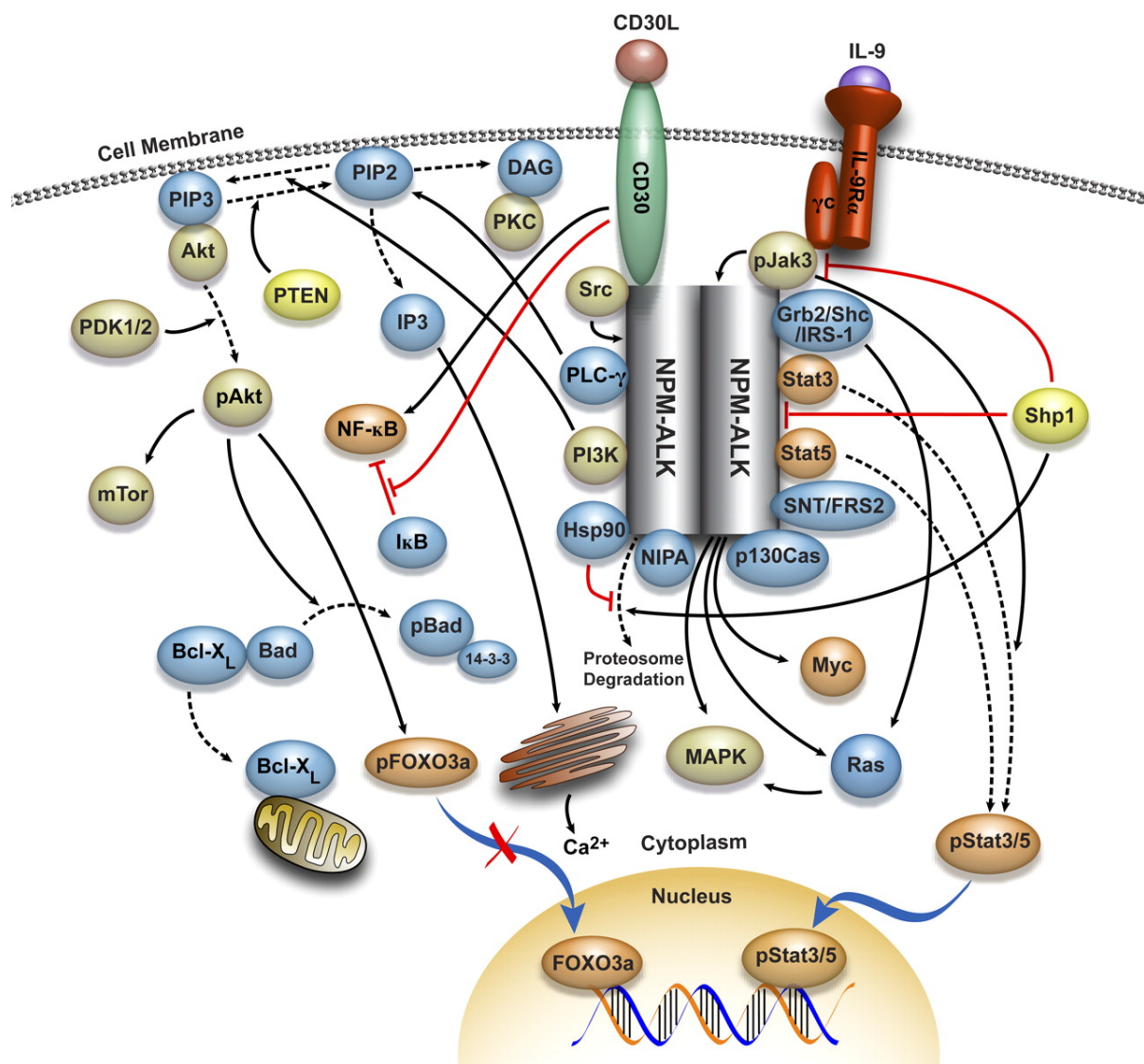




**FIGURE 4. NPM-ALK and its downstream signaling pathways.** The NPM-ALK fusion protein is aberrantly expressed and activates canonical signaling pathways, including Ras/Mek/Erk and PI3K/Akt cascades. The STAT3 signaling pathway has a central role in NPM-ALK-mediated transformation. **Adapted from Pathobiology of ALK<sup>+</sup> anaplastic large-cell lymphoma: Amin HM, Lai R. Pathobiology of ALK<sup>+</sup> anaplastic large-cell lymphoma. Blood.2007 Oct 1;110(7):2259-67., Copyright 2007, with direct permission from BLOOD.**

### 1.5. Overview of the insulin-like growth factor system

The insulin-like growth factor (IGF) system plays significant roles in both embryonic and postnatal development as well as important functions in normal adult physiology. The IGF system includes 4 receptors: insulin receptor (IR), type I insulin-like growth factor receptor (IGF-IR), IGF-IIR, and the hybrid receptors (HR) consisting of one-half IR and one-half IGF-IR. These receptors interact with at least three ligands: insulin, IGF-I, and IGF-II (**Figure 5**). The IR, IGF-IR, and IGF-IIR have strongest binding affinity for their respective ligand, whereas binding of insulin to IGF-IR and IGF-I to IR are approximately 100-fold less. IGF-I and IGF-II signaling is mediated through IGF-IR; however, IGF-I has a 4-5-fold higher binding affinity. The IGF system also includes 6 regulatory proteins known as IGF binding proteins that regulate IGF signaling [75].

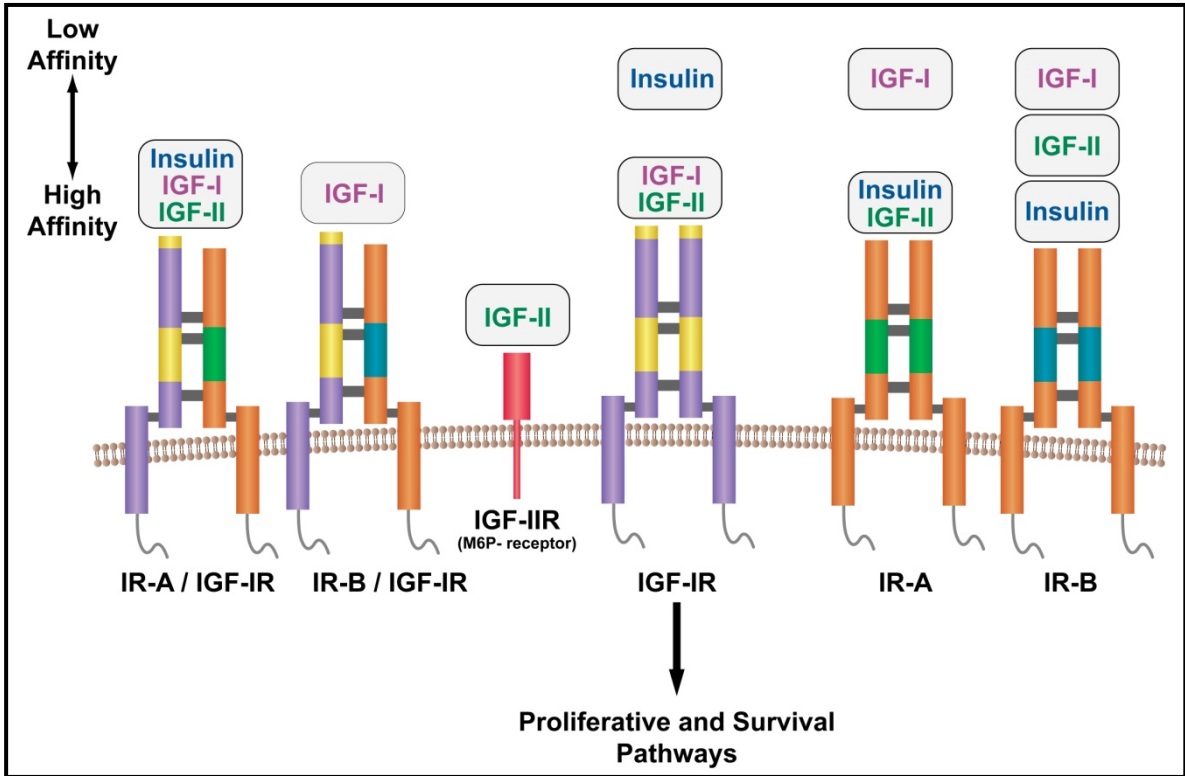


**FIGURE 5. Overview of IGF system.** The IGF system consists of 4 receptors: IR, IGF-IR, IGF-IIR, and HR. These receptors interact with at least three ligands: insulin, IGF-1, and IGF-II. In addition, the IGF system also includes 6 regulatory proteins called IGF binding proteins that regulate IGF signaling.

## 1.6. IGF-I

IGF-I is a single chain peptide that shares 62% homology with IGF-II and 40% homology with proinsulin [75]. Evidence shows that IGF-I is synthesized in a variety of tissues and cultured cell types, suggesting that the protein may have autocrine and paracrine effector functions, unlike insulin, which is stored within cells of a particular tissue (pancreas) and has mainly autocrine effects [76-80]. Liver secretion of IGF-I is regulated by the growth hormone (GH), which signals peripheral tissues to grow, whereas insulin is tightly regulated by glucose uptake [79, 81, 82]. Therefore, insulin is primarily associated with inducing metabolic effects, whereas IGF-I is essentially a growth factor and an anabolic agent.

IGF-I is the primary ligand for IGF-IR. There is increasing evidence that IGF-I might provide a major link between IGF-IR and the development of cancers through its regulatory effects on normal cell proliferation, differentiation, and apoptosis. Although most cancers do not secrete IGF-I, high concentrations of circulating IGF-I in serum appear to contribute to the growth, maintenance, and progression of cancers of the breast, lung, and colon [83-87]. For example, previous studies have demonstrated that colonic epithelium in acromegalic patients is characterized by increased proliferation that is proportional to serum IGF-I levels [88]. Also, *in vitro* and *in vivo* experiments showed that prostate cancer is mitogenically responsive to IGF-I [84]. Several mouse models have shown reduced proliferation of androgen-dependent prostate cancer cells in IGF-I deficient hosts relative to control hosts, testifying to the strong mitogenic properties of IGF-I [89].

IGF-I appears to tightly control both positive and negative regulators of the cell cycle primarily through the interaction with IGF-IR. It has been previously documented that IGF-I increases cell proliferation by amplifying DNA synthesis and upregulating *cyclin D1* mRNA

expression, which allows entry into the S phase of the cell cycle. Using skeletal myoblasts, it was demonstrated that the early effects of IGF-I during cell cycle progression are associated with the stabilization of Rb1 phosphorylation, which is typical of proliferating cells. Subsequently, upregulation of *CDK4* and *cyclin D1* gene expression further maintains Rb1 phosphorylation [83]. In another study using neocortical neural progenitor cells, *in vitro* addition of IGF-I induced rapid increase in cyclin D1 and cyclin D3. This led to a further increase in cyclin E, which also assists in the G1/S phase transition. Simultaneously, observed decrease in CDK inhibitors p27 and p57 suggested that downregulation of negative regulators of cell cycle also contributes to the mitogenesis induced by IGF-I. These effects were further demonstrated *in vivo*, where injection of IGF-I led to increased DNA synthesis and number of S phase cells, with simultaneous increase in phosphorylated/activated AKT, cyclin D1, and cyclin E [90]. Endogenous blockade of IGF-I with an anti-IGF-I antibody led to decreased DNA synthesis, upregulation of p27 and p57, as well as prevention of cyclin E mRNA expression. Interestingly, it has been demonstrated that the effects exerted by IGF-I are primarily induced through the PI3K/Akt pathway. Blocking this pathway, but not the MAPK/Erk pathway, inhibited the mitogenic potential of IGF-I [90]. These data suggest that the strong mitogenic potential of IGF-I is essentially mediated through IGF-IR.

## 1.7. IGF-IR

**1.7.1. IGF-IR structure and signaling:** IGF-IR is a receptor tyrosine kinase consisting of two identical  $\alpha$  subunits and two identical  $\beta$  subunits that are connected by disulfide bonds to form the functional homodimeric receptor complex. The  $\alpha$  subunit is entirely extracellular and contains a cysteine rich domain that forms the primary binding site for its ligands IGF-I and, to a lesser affinity, IGF-II and insulin. The  $\beta$  subunit includes an extracellular domain, a 24-residue hydrophobic transmembrane domain, and a larger cytoplasmic region that shares 84% homology with the IR [91, 92]. Tyrosine 950 is the binding site for its substrates, IRS-1 and Shc, among others. The intracellular region of the  $\beta$  subunit contains an ATP binding site at lysine 1003. It also contains a kinase domain encompassing the activation loop made up of three critical tyrosine residues at positions 1131, 1135, and 1136 (form part of the YXXYY moiety), which become phosphorylated upon ligand binding. Residue 1136 is particularly important in that it maintains the conformational stability of the  $\beta$  subunit. The C-terminus domain contains several tyrosine and serine residues that are phosphorylated to probably induce mitogenic effects, but how they actually contribute to normal and malignant IGF-IR signaling is still not fully understood [92] (**Figure 6**).

Binding of IGF-IR to its ligands causes the phosphorylation of tyrosine residues located in the intracellular portion of its  $\beta$  subunit. Once phosphorylated, tyrosine 950 provides a docking site for its substrates IRS-1-4 and Shc proteins. Upon substrate binding, downstream signaling is activated through PI3K/AKT, MAPK or STAT pathways and may stimulate cancer cell growth in an autocrine/paracrine manner [93-95] (**Figure 7**).

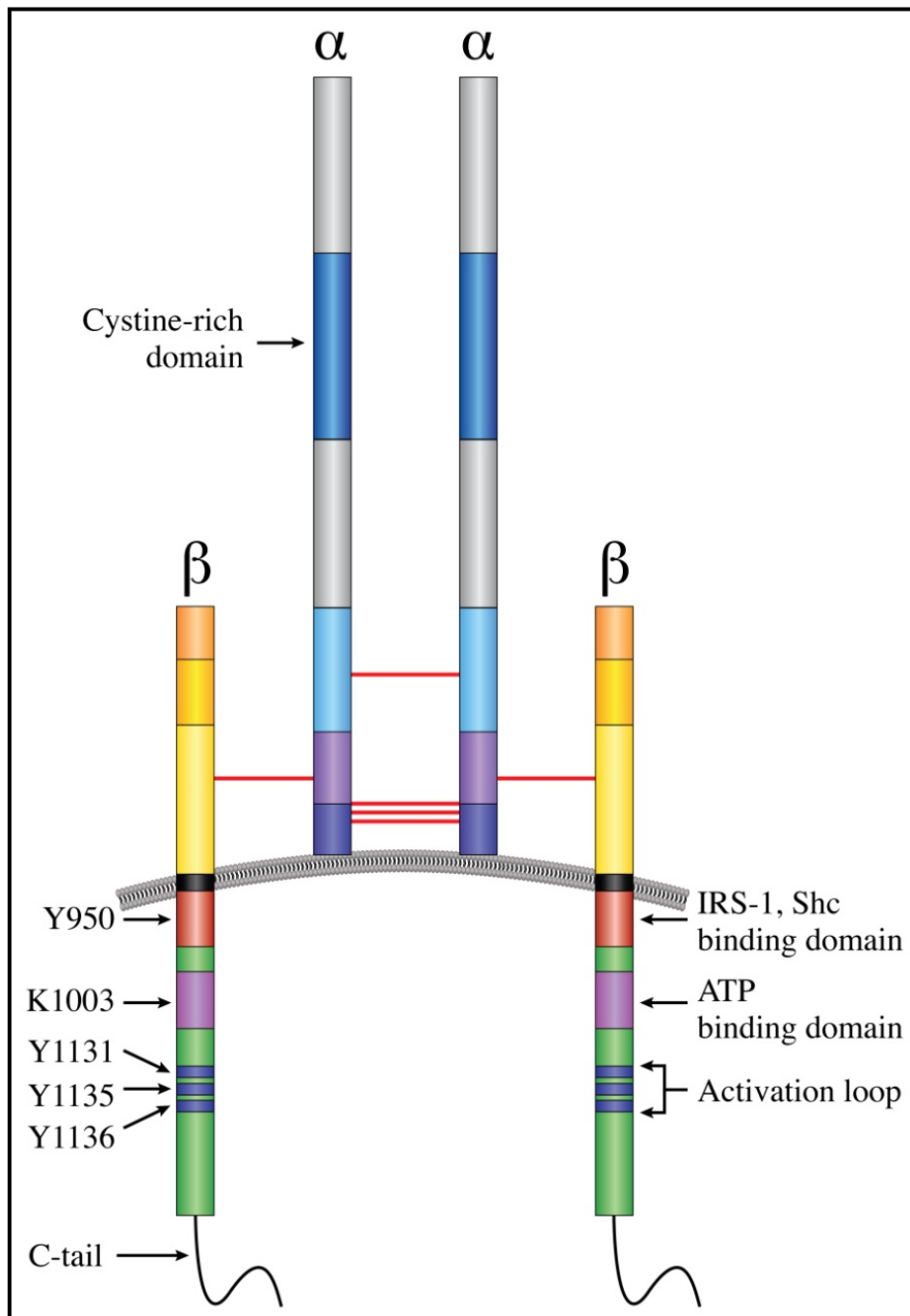




**FIGURE 6. Structure of IGF-IR.** IGF-IR is a transmembrane homodimeric receptor tyrosine kinase that is composed of two identical extracellular  $\alpha$  subunits and two identical transmembranous  $\beta$  subunits connected by disulfide bridges. The  $\alpha$  subunit contains a cysteine rich domain where the ligand binds. The cytoplasmic regions of the  $\beta$  subunits contain residues involved in the activation of IGF-IR. Y950 is the binding site for its primary substrates IRS-1 and Shc; K1003 is the ATP binding domain; and Y1131, Y1135, and Y1136 make up the activation loop of the kinase domain, which is followed by the C-terminus.

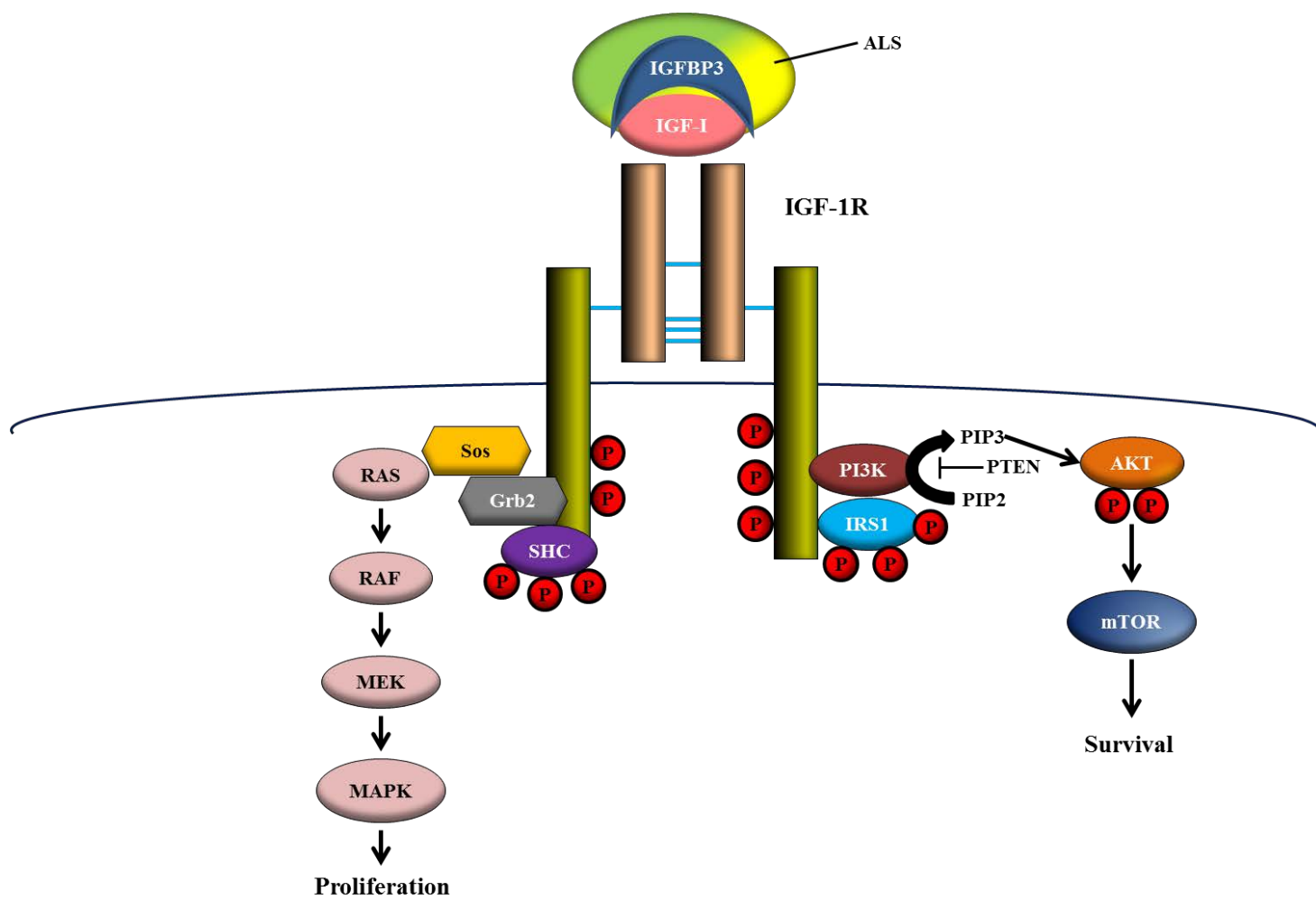


**FIGURE 7. IGF-IR signaling.** Binding of IGF-IR to its ligands causes the phosphorylation of tyrosine residues present in the intracellular portion of its  $\beta$  subunit. Once phosphorylated, Y950 provides a docking site for its substrates IRS-1-4 and Shc domain protein. Upon substrate binding, downstream signaling is activated through PI3K/AKT, MAPK, or JAK/STAT pathways. Adapted from **Kojima S, Inahara M, Suzuki H, Ichikawa T, Furuya Y. Implications of insulin-like growth factor-I for prostate cancer therapies. Int J Urol. 2009 Feb;16(2):161-7. Copyright 2008 by JOHN WILEY AND SONS. Reproduced with permission of JOHN WILEY AND SONS in the format Dissertation via Copyright Clearance Center.**

**1.7.2. Physiological and pathological roles of IGF-IR:** Mouse models have signified the importance of IGF-IR in prenatal and postnatal growth, especially in regards to genetic imprinting. The outcome of activation of IGF-IR during these stages is survival and proliferation of mitosis-competent cells resulting in growth of tissues such as skeletal and cardiac muscles [76, 80, 96-99]. IGF-IR also plays roles related to the growth of mammary gland during pregnancy and lactation. It has been previously shown that *Igf1r* null mice develop generalized organ hypoplasia, including developmental delays in bone ossification and abnormalities in the central nervous system [76, 80, 100-103]. During embryonic development, the IGF-IR pathway is also involved in the development of limb buds. Mice lacking the entire *Igf1r* gene typically exhibit dramatic reduction in body mass, testifying to the strong growth-promoting effect of this receptor, and they die at birth due to severe respiratory failure [100]. Mice carrying only one functional copy of *Igf1r* are normal, but demonstrate ~45% decrease in their body mass [100].

Aberrant activation of the IGF-IR pathway is also strongly associated with initiating cancer growth [86, 93, 96, 104-115]. Evidence in the last 20 years has emerged to support that IGF-IR overexpression plays a significant role in the development and progression of tumors, metastatic potential, and resistance to therapies. Studies have shown that IGF-IR induces its oncogenic effects through the inhibition of apoptosis and induction of transformation, metastasis, and angiogenesis. Moreso, it has been documented that IGF-IR can induce ligand-independent tumor cell progression, a process that is highly reliant on the level of expression of IGF-IR that deems it as constitutively active. In other words, exceeding a certain threshold for IGF-IR expression results in the lack of need for exogenous ligand stimulation. For example, treatment of RM11A cells (a murine breast cancer cell line with *high levels* of IGF-IR) with exogenous IGF-I, IGF-II or serum did not enhance the

proliferative/survival advantage [116]. On the other hand, the ability of RM11A cells expressing *low levels* of IGF-IR to respond to IGF stimulation was found to be robust, most likely to be due to the activation of the endogenous murine IGF-IR. Therefore, it was proposed that high expression of IGF-IR results in constitutive activation of the IGF-IR independent of the presence of ligands [116]. In addition, autoactivation of IGF-IR, when expressed at sufficient levels, has previously been shown in cells lacking IGF-IR that have been transfected with different levels of IGF-IR [117]. Furthermore, IGF-IR regulates properties that cause the malignant cells to overcome anchorage-independent growth, allowing them to acquire characteristics directly relevant to enduring detachment and migration that are essential attributes for metastasis [118].

It has been shown that the number of IGF-IR molecules present in cells plays a key role in its transforming properties [117, 119]. In fibroblasts, IGF-IR number needs to be greater than 20,000 receptors per cell to enable mitogenesis after stimulation with IGF-I. Similarly, in a pancreatic cell line, the observed increase in receptor number from 40,000 to 100,000 receptors/cell is in the range required to enable IGF-I-stimulated growth and therefore may be of central importance for pancreatic tumor growth. Based on these findings, it is concluded that only a small increment in the number of receptors per cell can induce the transforming properties of IGF-IR in different types of tumors [117, 119].

In solid tumors, some studies for the role of the IGF system have been performed using breast cancer cell lines, and found that one of the mechanisms that IGF-IR was activated both *in vitro* and *in vivo* was through IGF-I: 1) serum IGF-I may act as a stimulatory molecule to induce the proliferation of breast cancer cells in an endocrine manner and/or 2) stromal cells that surround the tumorigenic cells serve as a paracrine stimulator of the mitogenic signal [110, 120-123]. It has been demonstrated that there is hindrance of cell proliferation by

cancer cells when IGF-IR activation is inhibited. One possible mechanism is the lack of interaction of IGF-I with IGF-IR, which results in interrupting the signaling pathway. In prostate cancer, IGF-I is believed to directly stimulate the androgen receptor (AR) via crosstalk with IGF-IR on prostatic epithelial cells to induce its pathogenesis, progression, and metastasis [124]. Similarly, the oncogenic effects of IGF-IR are documented in colon cancer. IGF-IR is overexpressed in colon cancer, compared to normal colonic mucosa and IGFs in colonic malignant mucosa are shown to exert their effects via the IGF-IR only [88, 114].

In contrast to the widely studied solid tumors, not many studies have been performed to examine the role of IGF-IR in hematological neoplasms, and most of the studies have focused on plasma cell myeloma [125, 126]. In addition, our lab has demonstrated the contributions of IGF-IR signaling to the pathogenesis of other hematological neoplasms including mantle cell lymphoma and chronic myeloid leukemia [127-130].

### **Rationale, Hypothesis, and Specific Aims**

The scope of this project is to further current understanding of the pathobiology of NPM-ALK<sup>+</sup> ALCL. Our findings may provide a framework that could be useful to tailor novel selective and specific therapeutic strategies for NPM-ALK<sup>+</sup> ALCL.

There has been substantial evidence supporting the importance of NPM-ALK in the pathogenesis of NPM-ALK<sup>+</sup> ALCL, highlighted in section 1.4.1. Oncogenic effects are induced by NPM-ALK interaction with several proteins that regulate cell survival and growth [131]. Notably, the mechanisms leading to NPM-ALK overexpression and activation in this neoplasm are still unclear. In this regard, we have recently shown that NPM-ALK is post-transcriptionally regulated by microRNA-96 [132].

Previous experiments performed in our lab demonstrated that IGF-IR is overexpressed in NPM-ALK<sup>+</sup> ALCL cell lines and primary tumors than normal human T lymphocytes and reactive lymphoid tissues, which provide preliminary findings for this project [128] (**Figure 8**). Moreover, we found that novel reciprocal functional interactions exist between IGF-IR and NPM-ALK. Our previous results suggest that the two kinases physically associate to maintain their tyrosine phosphorylation and kinase activation levels. We demonstrated that IGF-IR and NPM-ALK directly interact through a positive feedback loop that appears to exist between NPM-ALK and IGF-IR through specific tyrosine (Y) residues, Y644 or Y664, located within the C terminus of NPM-ALK that maintains NPM-ALK phosphorylation status. A single mutation within Y644 or Y664 that changes these residues to phenylalanine decreased substantially the association between IGF-IR and NPM-ALK and phosphorylation levels, although not entirely [128] (**Figure 9**). Generation of a double mutation, NPM-ALK<sup>Y644,664F</sup>, completely eliminated the association between IGF-IR and NPM-ALK, which provides strong evidence to support a direct role of IGF-IR in maintaining the phosphorylation status of NPM-ALK for the latter to subsequently activate/phosphorylate



downstream proteins [113]. In addition, we have shown that IGF-IR can also maintain NPM-ALK protein stability; because specific targeting of IGF-IR by siRNA significantly decreased NPM-ALK basal protein levels [127]. Based on its dual influence on NPM-ALK phosphorylation and stability, IGF-IR most likely represents an important survival entity in this lymphoma.

Reciprocally, NPM-ALK appears to play a crucial role in maintaining the phosphorylation of IGF-IR at Y1131, and thereby sustains its downstream signaling. In support of this idea, specific targeting of NPM-ALK by siRNA decreased IGF-IR phosphorylation significantly [128]. However, NPM-ALK does not appear to contribute to IGF-IR protein stability. Specific targeting of NPM-ALK by siRNA resulted in substantial decrease of NPM-ALK protein, but changes in IGF-IR mRNA or protein expressions were not observed, even over prolonged periods of time. These important observations suggest that NPM-ALK does not contribute to IGF-IR overexpression, but mainly to its phosphorylation and downstream signaling process [113] (**Figure 10**).

*Because the mechanisms underlying the survival of NPM-ALK<sup>+</sup> ALCL are not completely understood, we hypothesized that multilevel deregulated mechanisms contribute to aberrant expression of IGF-IR and NPM-ALK, which enhances the survival potential of this aggressive lymphoma.* To test this hypothesis, the following set of specific aims were performed:

**Specific Aim 1: Transcriptional regulation of IGF-IR.**

- a. Transcription factors: We identified novel transcription factors that regulate the expression of *IGF-IR* and test their biological significance in NPM-ALK<sup>+</sup> ALCL.
- b. Gene amplification: *IGF-IR* gene amplification has been observed in different types of cancers including malignant melanoma and breast and pancreatic

cancers. We examined whether *IGF-IR* gene amplification exists in NPM-ALK<sup>+</sup> ALCL.

**Specific Aim 2: Posttranscriptional regulation of IGF-IR.**

- a. MicroRNA: We identified potential deregulated microRNAs that contribute to IGF-IR upregulation and test their biological significance in NPM-ALK<sup>+</sup> ALCL.
- b. RNA stability: We tested whether *IGF-IR* mRNA decay rate contributes to up-regulation of IGF-IR expression in NPM-ALK<sup>+</sup> ALCL.

**Specific Aim 3: Posttranslational regulation of NPM-ALK and IGF-IR.**

- a. SUMOylation: We examined whether SUMOylation contributes to posttranslational stabilization of IGF-IR and NPM-ALK in NPM-ALK<sup>+</sup> ALCL.
- b. Deregulation of IGF-I: We examined whether NPM-ALK potentiates IGF-IR signaling via upregulation of IGF-I expression.

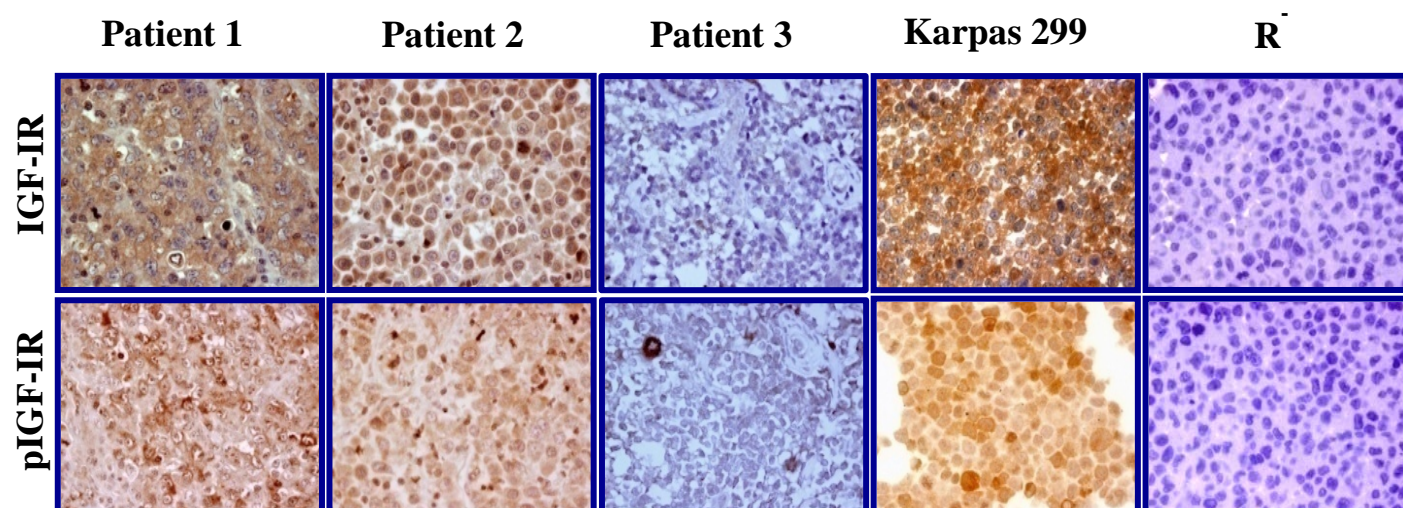
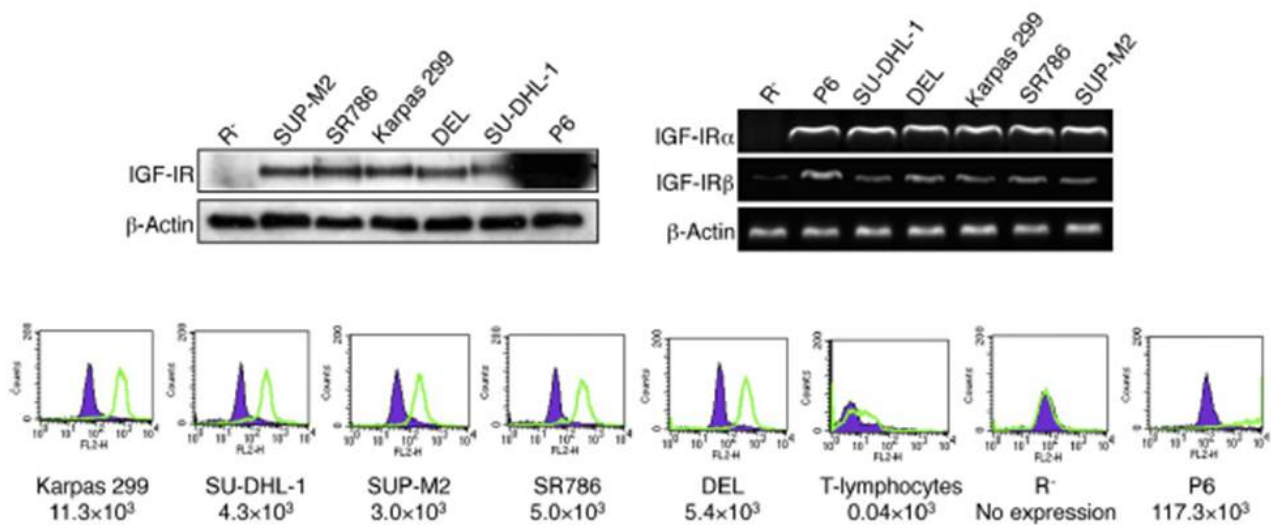


**FIGURE 8. Expression of IGF-IR in NPM-ALK<sup>+</sup> ALCL cell lines.** *Upper panel*, WB studies showed overexpression of IGF-IR protein in NPM-ALK<sup>+</sup> ALCL cell lines. R<sup>-</sup> and P6 cell lines were used as negative and positive controls for the expression of IGF-IR, respectively. It is important to note that the overexpression of IGF-IR in P6 cells has been artificially over-induced and does not represent a physiologic level. RT-PCR shows the presence of *IGF-IR* mRNA in the NPM-ALK<sup>+</sup> ALCL cell lines as well as in the P6 cell line. Although *IGF-IRα* mRNA is not detectable in R<sup>-</sup> cells, these cells appear to express very low levels of *IGF-IRβ* mRNA. Quantitative flow cytometric analysis shows that the NPM-ALK<sup>+</sup> ALCL cell lines express significantly higher levels of IGF-IR compared with normal human T lymphocytes. Using flow cytometry, the estimated numbers of IGF-IR molecules/cell are shown to be much more abundant in NPM-ALK<sup>+</sup> ALCL cell lines compared with normal human T-cells. *Lower panel*, immunohistochemical staining of ALK<sup>+</sup> ALCL patient specimens illustrates that 89% and 86% of patient samples were positive for IGF-IR and pIGF-IR expression, respectively. Patients 1 and 2 represent positive cases, and patient 3 represents a negative case. Karpas 299 and R<sup>-</sup> were used as positive and negative controls, respectively. **Adapted by direct permission from BLOOD (Shi P, Lai R, Lin Q, Iqbal AS, Young LC, Kwak LW, Ford RJ, Amin HM. IGF-IR tyrosine kinase interacts with NPM-ALK oncogene to induce survival of T-cell ALK<sup>+</sup> anaplastic large-cell lymphoma cells. Blood. 2009 Jul 9;114(2):360-70.), copyright 2009.**

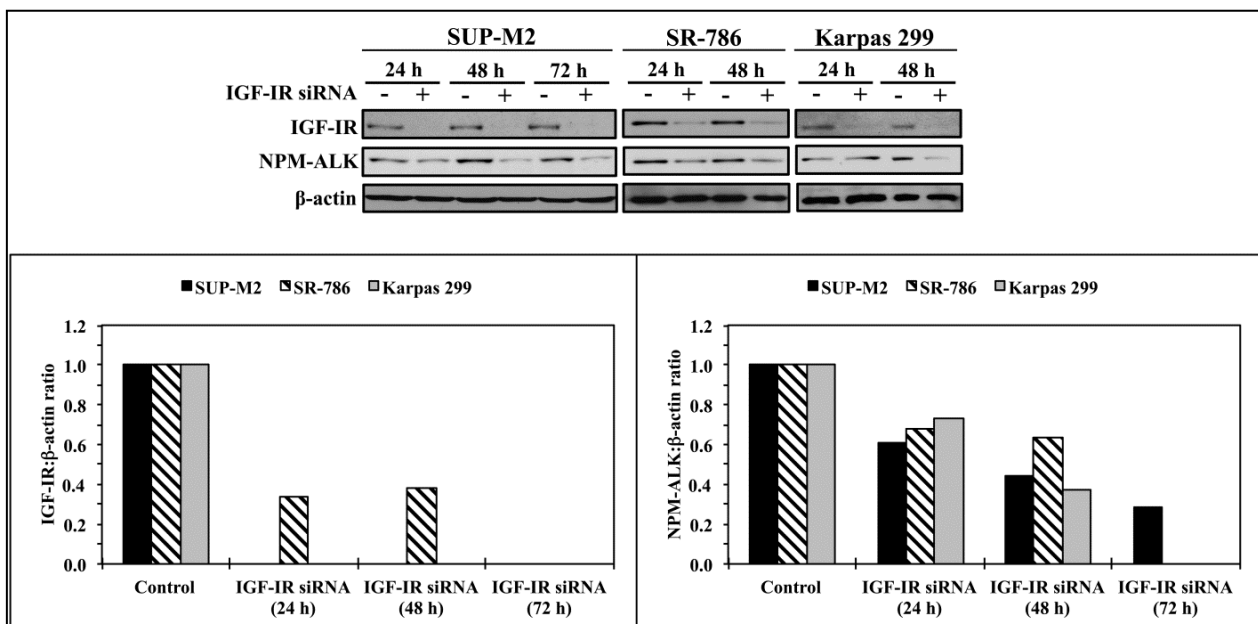
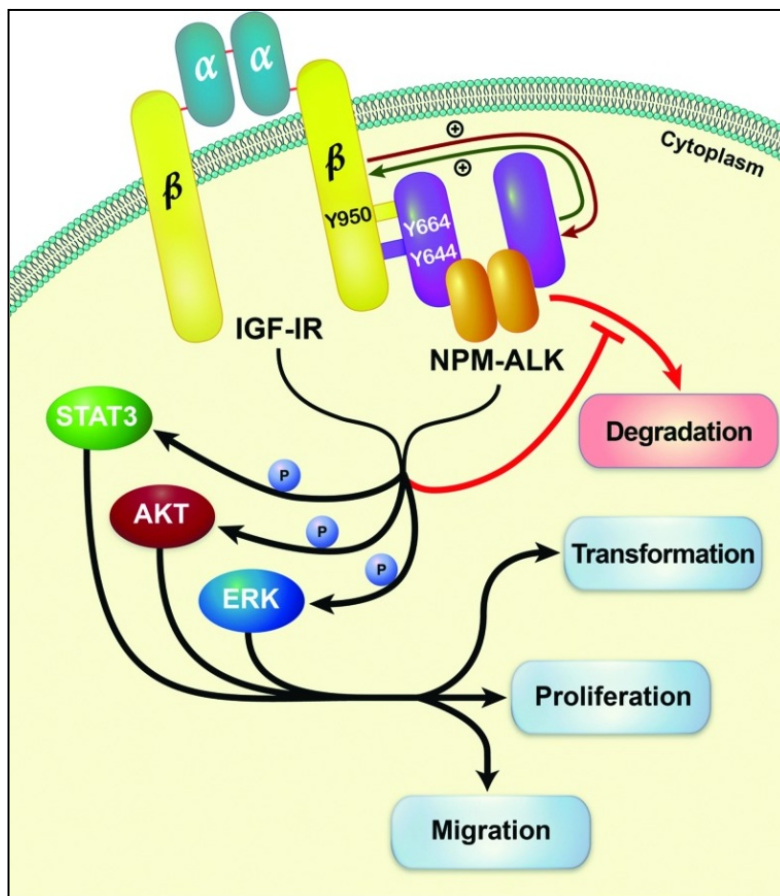


**FIGURE 9. Association and functional interactions between NPM-ALK and IGF-IR.** *Upper panel*, NPM-ALK and IGF-IR are physically associated through Y644 and Y664 of NPM-ALK and Y950 of IGF-IR. Through this association, the phosphorylation and tyrosine kinase activity of the two oncogenic proteins are maintained at high levels, and this leads to up-regulation of the phosphorylation of the common downstream targets including STAT3, AKT, and ERK. Such effects enhance the transformation, proliferation, and migration of NPM-ALK<sup>+</sup> T-cell lymphoma cells. In addition, the physical association between NPM-ALK and IGF-IR, in the presence of Hsp90 (not shown), appears to sustain the stability of NPM-ALK protein. *Lower panel*, specific targeting of IGF-IR by siRNA significantly decreased NPM-ALK protein expression levels over prolonged time; densitometric analysis of the IGF-IR:β-actin and NPM-ALK:β-actin ratios are shown below the WB. **Adapted with permission from PMC [Neoplasia] (Shi B, Vishwamitra D, Granda JG, Whitton T, Shi P, Amin HM. Molecular and functional characterizations of the association and interactions between nucleophosmin-anaplastic lymphoma kinase and type I insulin-like growth factor receptor. Neoplasia. 2013 Jun;15(6):669-83.), copyright 2013.**

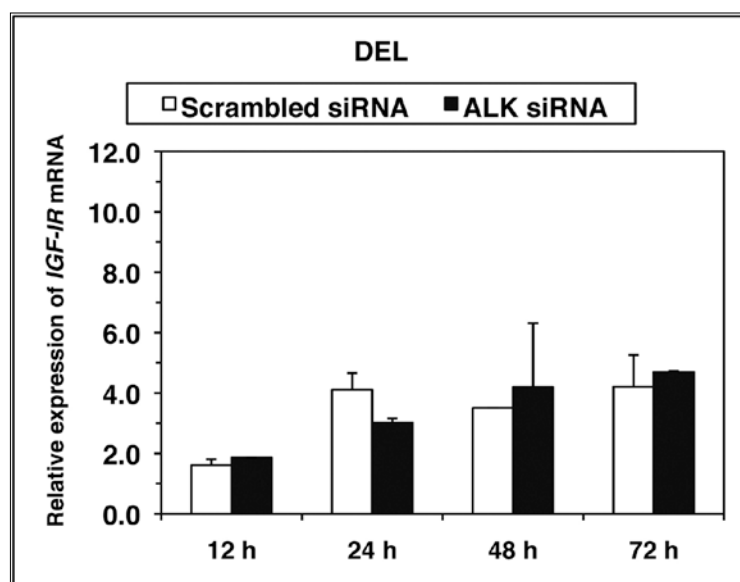
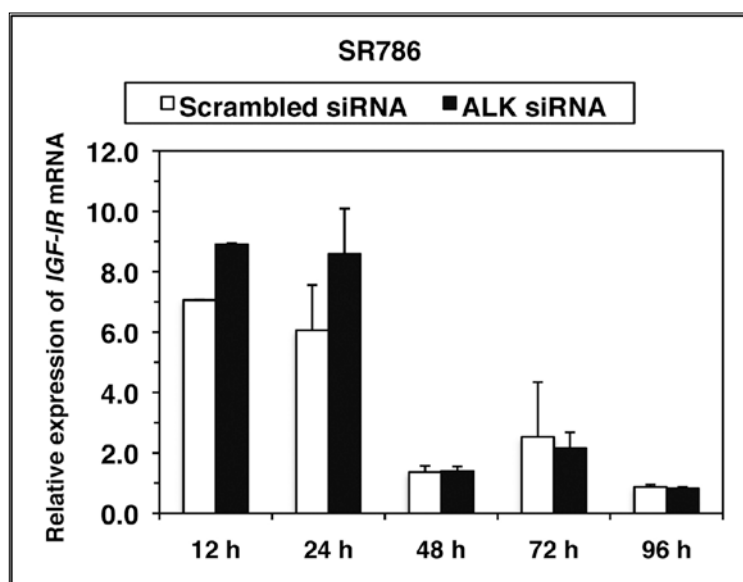
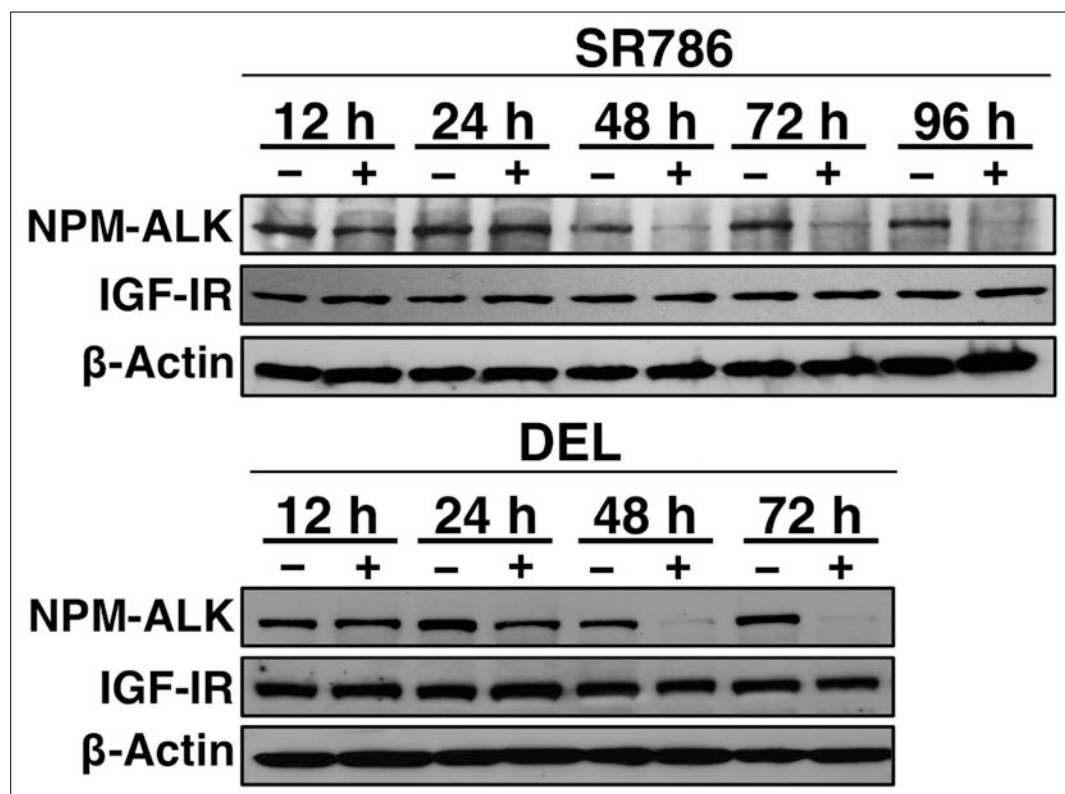


**FIGURE 10. NPM-ALK does not regulate IGF-IR expression.** *Upper panel*, specific targeting of NPM-ALK by siRNA significantly decreased NPM-ALK protein expression, but changes in IGF-IR protein expression were not observed even after 96 h. *Lower panel*, no change in *IGF-IR* mRNA expression was observed after sufficient knockdown of NPM-ALK by siRNA.



## **Results**

### **3.1. Transcriptional Regulation of *IGF-IR***

### 3.1.1. Introduction

Deregulated expression, activation or inactivation of transcription factors plays critical roles in tumorigenesis. Additionally, signaling via major oncogenic pathways is tightly controlled through transcription factors that have the ability to regulate the expression of target genes that are directly relevant to the corresponding oncogenic pathways, resulting in either induction or inhibition of tumor formation and progression. Under physiological conditions, genes are regulated by specific upstream transcriptional regulators, whereas in cancer cells, aberrant activation or inactivation of these transcription factors leads to deregulated expression of oncogenes or tumor suppressor genes that affect tumor development and progression. Only a few transcription factors have been shown to bind the *IGF-IR* gene promoter (15q26.3) and modulate its activity through stimulation or inhibition. These transcription factors include Sp1, WT1, E2F1, STAT1, and EGR-1 [26-34].

Gene amplification is indicative of a copy number increase of a particular segment on a chromosome. It is prevalent in some tumors and is associated with overexpression of the amplified genes. The presence of *IGF-IR* gene amplification and its clinical relevance has been investigated in a limited number of solid cancers including breast, lung, and gastrointestinal stromal tumors (GISTs) [133-139]. Of these cancers, gene amplification was detected only in small subgroups of patients with non-small cell lung cancer and GISTs [134]. *IGF-IR* amplification correlated positively with high IGF-IR protein expression and lymph node metastasis.

In this aim, we examined whether increased IGF-IR expression in NPM-ALK<sup>+</sup> ALCL may be explained by transcriptional aberrancies, such as deregulated transcription factors and/or *IGF-IR* gene amplification.

*The following section is published in Vishwamitra D, Curry CV, Alkan S, Song YH, Gallick GE, Kaseb AO, Shi P, Amin HM. The transcription factors Ik-1 and MZF1 downregulate IGF-IR expression in NPM-ALK(+) T-cell lymphoma. Mol Cancer. [accepted].*

### **3.1.2. Transcriptional Regulation of *IGF-IR*: Transcription Factors**

### 3.1.2.1. Materials and Methods

**Web-based transcription factor search algorithms** – To identify transcription factors that potentially bind the human *IGF-IR* gene promoter, 3 web-based transcription factor search algorithms were searched: Genomatix ([www.genomatix.de/](http://www.genomatix.de/)), and MATCH (<http://www.gene-regulation.com/pub/programs.html>), and TFSearch (we used this transcription factor search algorithm when we initiated the study, but we noticed that now it has been removed and the website is not available for online support. Importantly, the findings we obtained from TFSearch matched exactly the findings gathered from Genomatix and MATCH).

**Cell lines** – Five NPM-ALK<sup>+</sup> ALCL cell lines were used in this study: Karpas 299, SUP-M2, SR-786, DEL, and SU-DHL-1 (DSMZ, Braunschweig, Germany). The R<sup>-</sup> cell line (mouse 3T3-like fibroblasts with targeted ablation of *Igflr* gene; gift from Dr. Renato Baserga, Thomas Jefferson University, Philadelphia, PA) was used as the host cell line for luciferase assay studies (8). Normal human peripheral blood CD3<sup>+</sup> pan-T lymphocytes were used in some experiments (catalog number: PB009-1F; StemCell Technologies, Vancouver, BC, Canada). In addition, Jurkat cells (ATCC, Manassas, VA) were used as a positive control for the expression of Ik-1 and MZF1 [140, 141]. The T lymphocytes as well as the Jurkat and NPM-ALK<sup>+</sup> ALCL cell lines were maintained in Roswell Park Memorial Institute (RPMI) 1640 medium supplemented with 10% fetal bovine serum (FBS) (Sigma, St. Louis, MO), glutamine (2 mM), penicillin (100 U/mL), and streptomycin (100 µg/mL) at 37°C in humidified air with 5% CO<sub>2</sub>. Dulbecco's Modified Eagle's Medium (DMEM) supplemented with 10% FBS was used to culture the R<sup>-</sup> under the same conditions.

**Antibodies** – The following antibodies were used: pIGF-IR<sup>Y1131</sup> (3021), pALK<sup>Y1604</sup> (Y664 in NPM-ALK; 3341), pAKT<sup>S473</sup> (4051), and Ikaros (5443) (Cell Signaling Technology, Danvers, MA); IRS-1 (ab40777), AKT (ab8805), NPM (ab52644), and MZF1 (ab64866) (Abcam, Cambridge, MA); IGF-IR (396700; Life Technologies, Grand Island, NY); pIRS-1<sup>S639</sup> (sc-22300; Santa Cruz Biotechnology, Santa Cruz, CA); ALK (M719501-2; Dako, Carpinteria, CA); c-Myc (631206, Clontech Laboratories, Mountain View, CA); IGF-I (05-172; Millipore, Billerica, MA); and  $\beta$ -actin (A-5316; Sigma).

**Western blotting** – Cells were lysed using lysis buffer containing 25 mM HEPES (pH 7.7), 400 mM NaCl, 1.5 mM MgCl<sub>2</sub>, 2 mM EDTA, 0.5% Triton X-100, 0.1 mM PMSF, 2 mM DTT, and phosphatase and protease inhibitor cocktails (Thermo Scientific, Rockford, IL). Protein concentrations were measured using the Bio-Rad protein assay, and optical density values were obtained using an ELISA plate reader (Bio-Tek Instruments, Winooski, VT). Proteins (50  $\mu$ g) were resolved by electrophoresis on 8% SDS-PAGE and then transferred to PVDF membranes and probed with specific primary antibodies and then with appropriate horseradish peroxidase-conjugated secondary antibodies (GE Healthcare, Waukesha, WI). Proteins were detected using a chemiluminescence-based kit (Amersham Life Sciences, Arlington Heights, IL).

In addition, a commercially available kit (Qproteome Tissue Kit, Qiagen, Valencia, CA) was used to perform Western blot assay to measure Ik-1 and MZF1 protein levels in formalin-fixed and paraffin-embedded (FFPE) tissue sections from NPM-ALK<sup>+</sup> ALCL patients (approval of the Institutional Review Board was obtained prior to performing human tissue analysis). Briefly, tissue sections mounted on glass slides were examined and tumor areas were identified and marked. Next, sections were deparaffinized, and tumor areas were excised from the slides and transferred into 1.5-mL collection tubes.  $\beta$ -Mercaptoethanol (6

μL) was admixed with the provided Extraction Buffer EXB Plus (94 μL) and then added to the excised tissues. Tissue tubes were incubated on ice for 5 min and then the contents were mixed by vortexing and incubated on a heating block at 100°C for 20 min. Using an oven with rotators, samples were incubated at 80°C for 2 h with agitation at 750 rpm. After incubation, tubes were cooled at 4°C for 1 min. The samples were centrifuged for 15 min at 14,000 *g* at 4°C. The supernatant containing the extracted proteins was collected. For quantification of protein yield, the Bio-Rad assay was used as described above.

***RNA extraction, cDNA synthesis, and relative quantitative PCR (qPCR)*** – Total RNA was isolated and purified using the RNeasy Mini Kit (Qiagen). Briefly,  $1 \times 10^6$  cells were collected by centrifugation at 200 *g* for 5 min, washed twice in phosphate-buffered saline (PBS), and subjected to lysis and homogenization with Buffer RLT using QiaShredder spin columns (Qiagen). Homogenized cells were re-suspended in an equal volume of 70% ethanol and passed through the spin columns. Cells were then washed once using Buffer RW1 and twice using Buffer RPE (Qiagen). Total RNA was collected upon elution with RNase-free water. Optical density was detected using spectrophotometry (NanoDrop 2000, Thermo Fisher Scientific, Waltham, MA).

cDNA synthesis was performed using the Superscript III RT protocol (Invitrogen, Carlsbad, CA). Approximately 0.3 μg total RNA was used for reverse transcription. Briefly, total RNA, oligo deoxy-thymine (dT), and deoxytrinucleotide triphosphate (dNTP) were admixed, and the final volume was adjusted to 10 μL using RNase-free water. The RNA mixture and primer were denatured at 65°C for 5 min and then placed on ice. The master reaction mixture consisting of 10× cDNA synthesis buffer, 0.1 M DTT, RNaseOUT, SuperscriptIII RT, MgCl<sub>2</sub>, and RNase-free H<sub>2</sub>O was prepared on ice and vortexed gently.

Then, 10  $\mu$ L of the reaction mixture was pipetted into each reaction tube on ice. Samples were transferred to a thermal cycler preheated to the appropriate cDNA synthesis temperature and incubated at 50°C for 60 min and then at 85°C for 5 min. Finally, 1.0  $\mu$ L RNase H was added and the samples were incubated at 37°C for 20 min to remove template RNA.

Relative qPCR was used to measure the levels of *IGF-IR* mRNA in NPM-ALK<sup>+</sup> ALCL cell lines after transfection with Ik-1 or MZF1 expression vectors (Open Biosystems, Pittsburgh, PA) using reactions containing reverse-transcribed cDNA, *IGF-IR* primer/probe, and Taqman Mastermix (Applied Biosystems, Grand Island, NY). 18S ribosomal RNA was used as the endogenous control.

**Transfection** – Cells were transfected with Ik-1 or MZF1 expression plasmids using electroporation and the Amaxa 4D Nucleofector System (solution SF, program CA-150; Lonza, Walkersville, MD) and then incubated for 48 h. In some experiments, scrambled or ALK siRNA (Dharmacon, Pittsburgh, PA) was transfected into NPM-ALK<sup>+</sup> ALCL cell lines by using the same approach.

**Construction of the human IGF-IR gene promoter** – Three different fragments of the human *IGF-IR* gene promoter were amplified using genomic DNA (Promega, Madison, WI). Briefly, 500 ng of genomic DNA was added to HotStarTaq plus Q solution additive mixture (Qiagen) and subjected to Touchdown PCR. The PCR primers and amplification conditions are shown in Table 1 and Table 2, respectively.

**TABLE 1.** Sequence of the primers used to construct the 3 fragments (F1, F2, and F3) of the human *IGF-IR* gene promoter.

Primer Name	Sequence
F1 (Forward)	5'-CTC TCC TCG AGC CAC TCT GGG C-3'
F1 (Reverse)	5'-CAA GAC GTG CGG AGC GGA GC-3'
F2 (Forward)	5'-TCC GCA CGT CTT GGG GAA CC-3'



<b>F2</b> (Reverse)	5'-GCC CCG AAG TCC GGG TCA CA-3'
<b>F3</b> (Forward)	5'-GAC TCC GCG TTT CTG CCC CTC-3'
<b>F3</b> (Reverse)	5'-CTC CAC TCG TCG GCC AGA GC-3'

**TABLE 2.** The amplification conditions used in Touchdown PCR for the construction of 3 fragments of the human *IGF-IR* gene promoter ( $\infty$ : hold).

<b>Phase 1</b>	<b>Step</b>	<b>Temperature</b>	<b>Time</b>
1	Denature	95°C	15 min
2	Denature	95°C	30 sec
3	Anneal	70°C	45 sec
		-1.0°C*	
4	Elongate	72°C	1 min
Repeat steps 2-4 (15 times)			
<b>Phase 2</b>	<b>Step</b>	<b>Temperature</b>	<b>Time</b>
5	Denature	95°C	30 sec
6	Anneal	60°C	45 sec
7	Elongate	72°C	1 min
Repeat steps 5-7 (25 times)			
<b>Termination</b>	<b>Step</b>	<b>Temperature</b>	<b>Time</b>
8	Elongate	72°C	5 min
9	Halt reaction	4°C	15 min
10	Hold	4°C	$\infty$

\*Every time steps 2-4 were repeated, the annealing temperature was decreased by 1.0°C/cycle until the estimated melting temperature was reached.

PCR products were run on 1.5% agarose gel, excised, and purified using the Qiaquick Gel Extraction Kit (Qiagen). The PCR products were then subcloned at a 1:5 molar ratio into the pGEM vector using the TA cloning system (Promega). The ligated products were transformed using MaxEfficiency DH5 $\alpha$ -competent cells (Invitrogen) overnight at 37°C, and positive clones were selected and verified by PCR and direct DNA sequencing. Clones

containing the correct insert were amplified in ampicillin containing Luria-Bertani (LB) broth (Corning Costar, Corning, NY). Plasmids were isolated and purified using the Purelink Quick Plasmid Miniprep Kit (Invitrogen). To construct reporter plasmids containing the human *IGF-IR* gene promoter fragments, the pGEM plasmids and the PGL4.17 luciferase vector (Promega) were subjected to restriction enzyme digestion using ZraI/SpeI (Promega) and EcoICRI/NheI (New England Biolabs, Ipswich, MA). After digestion, DNA was ligated at room temperature using T4 DNA ligase (Promega) and the PCR conditions shown in Table 3.

**TABLE 3.** PCR conditions used for DNA ligation for the construction of the human *IGF-IR* gene promoter ( $\infty$ : hold).

<b>Temperature</b>	<b>Time</b>
22°C	30 min
20°C	30 min
18°C	30 min
16°C	30 min
14°C	30 min
12°C	30 min
10°C	30 min
8°C	30 min
6°C	30 min
4°C	30 min
4°C	$\infty$

Ligated products were confirmed by agarose gel electrophoresis and transformed using DH5 $\alpha$ -competent cells. Positive clones were selected, subjected to plasmid isolation and purification using the Miniprep Kit, and verified by PCR and direct DNA sequencing.

**Site-directed mutagenesis and luciferase assay** – Mutated human *IGF-IR* luciferase reporter constructs were generated using the QuickChange II XL Site Directed Mutagenesis Kit (Agilent Technologies, Santa Clara, CA) and a set of primers depicted in Table 4.

**TABLE 4.** Sequences of the primers used to construct the 3 mutated fragments of human *IGF-IR* luciferase reporter (F1, F2, and F3).

<b>Primer Name</b>	<b>Sequence</b>
<b>F1 (Forward)</b>	5'-CAA GAG CCC CAG CCG GGA GAA AGG GGA C-3'
<b>F1 (Reverse)</b>	5'-GTC CCC TTT CTC CCG GCT GGG GCT CTT G-3'
<b>F2 (Forward)</b>	5'-CAG AAA CGC GGA GCG CCG GCC ACC-3'
<b>F2 (Reverse)</b>	5'-GGT GGC CGG CGC TCC GCG TTT CTG-3'
<b>F3 (Forward)</b>	5'-GCC AGA GCG AGA GCG CCA AAT CCA GGA CAC-3'
<b>F3 (Reverse)</b>	5'-GTG TCC TGG ATT TGG CGC TCT CGC TCT GGC-3'

**Luciferase assay** – For luciferase assays, R<sup>-</sup> cells were transfected using Lipofectamine 2000 reagent. Briefly, 1 x 10<sup>6</sup> R<sup>-</sup> cells were seeded in 6-well plates. The following day, plasmids were incubated in 100 µL OptiMEM media for 5 min at room temperature. Simultaneously, 7 µL lipofectamine was incubated in a separate tube. Then, the contents of the plasmid tubes were added to the lipofectamine and incubated for 20 min at room temperature. Finally, the plasmid mixtures were added to the corresponding plate wells containing the R<sup>-</sup> cells.

Luciferase assay was performed with the Dual Glo Luciferase Kit (Promega) after co-transfecting the R<sup>-</sup> cells with the reporter plasmids containing the wild-type or mutated *IGF-IR* promoter fragments or *NPM* promoter (kind gift from Dr. Qishen Pang, Cincinnati Children's Hospital, Cincinnati, OH) along with Ik-1 or MZF1 expression plasmids using Lipofectamine 2000 (Invitrogen) for 48 h. Cells were trypsinized, washed twice with sterile PBS, and plated in a 96-well luminometer plate. An equal volume of Dual-Glo reagent was added and incubated for 10 min for cell lysis to occur. Firefly luminescence readings were

obtained using a plate reader (PolarStar Omega, BMGLabTech, Cary, NC). Finally, the Dual-Glo Stop & Glo reagent was added and incubated for 10 min. Renilla luminescence readings were obtained using the above methods.

***Chromatin immunoprecipitation (ChIP) assay*** – Because NPM-ALK<sup>+</sup> ALCL cells contain low levels of endogenous Ik-1 and MZF1, expression plasmids containing full-length Ik-1 or MZF1 were constructed by transferring the inserts into a c-Myc-tagged expression vector (pCMV-Myc-N; Clontech). Briefly, the original expression vectors containing Ik-1 or MZF1 as well as pCMV-Myc-N were subjected to digestion using the restriction enzymes NotI/SalI for Ik-1 or XhoI/ECORI for MZF1 (Promega). Digested products were verified by agarose gel electrophoresis and then excised and ligated using the HD InFusion system (Clontech). Ligated products were transformed using DH5 $\alpha$ -component cells, and positive clones were selected and verified by PCR.

ChIP assays were performed using the Pierce Agarose ChIP Kit (Thermo Scientific). Briefly, at 48 h post-transfection, cells were cross-linked using 1% formaldehyde, and cell pellets were lysed and re-suspended in a buffer containing 0.6  $\mu$ L Micrococcal Nuclease (ChIP grade) and subjected to sonication on ice (Output 6; six 15 sec pulses, followed by 45 sec rest periods; Sonic Dismembrator, model 100; Thermo Fisher Scientific). Five microliters of digested chromatin was separated for the 10% input. The remaining sonicated samples were immunoprecipitated overnight at 4°C on a rocking platform using the c-Myc-Tag antibody and the provided plugged spin columns. Following overnight incubation, ChIP-grade Protein A/G Plus agarose beads were incubated for 2 h with the lysate at 4°C on a rocking platform. The samples were then washed and reverse cross-linked at 65°C for 40 min. The immunoprecipitated samples and input were eluted in a buffer containing 5 M NaCl

and 20 mg/mL Proteinase K. Finally, chromatin DNA was recovered and purified using the DNA Clean-Up column and subjected to Touchdown PCR using HotStarTaq Master Mix and Q solution and a set of primers shown in Table 5. PCR products were run on 1.5% agarose gel.

**TABLE 5.** Sequences of the primers flanking potential binding sites (BS) of Ik-1 and MZF1 within the human *IGF-IR* promoter used in the RT-PCR reactions following the CHIP assay.

<b>Primer Name</b>	<b>Sequence</b>
<b>Ik-1 BS2</b> (Forward)	5'-CGG GGG CAT TGT TTT TGG AG-3'
<b>Ik-1 BS2</b> (Reverse)	5'-CGG GTT CCC CAA GAC GTG-3'
<b>Ik-1 BS3</b> (Forward)	5'-TCT TGT TTA CCA GC ATTA ACT CGC-3'
<b>Ik-1 BS3</b> (Reverse)	5'-CCT CTC TCG AGT TCG CCT G-3'
<b>Ik-1 BS4</b> (Forward)	5'-CGC CGC TTT GTG TGT GTC-3'
<b>Ik-1 BS4</b> (Reverse)	5'-GCC GCC TCC TCC CTC A-3'
<b>MZF1 BS2</b> (Forward)	5'-GCG GGG GCA TTG TTT TTG GA-3'
<b>MZF1 BS2</b> (Reverse)	5'-CCG GGT TCC CCA AGA CGT G-3'
<b>MZF1 BS3</b> (Forward)	5'-GCG CGT GTC TCT GTG TGC-3'
<b>MZF1 BS3</b> (Reverse)	5'-GCG AGT TAA TGC TGG TAA ACA A-3'
<b>MZF1 BS4</b> (Forward)	5'-GTG TGT GTC CTG GAT TTG GGA-3'
<b>MZF1 BS4</b> (Reverse)	5'-GCA GAA ACG CGG AGT CAA AAT-3'
<b>MZF1 BS5</b> (Forward)	5'-CGG CCC TTC GGA GTA TTG T-3'
<b>MZF1 BS5</b> (Reverse)	5'-CAA GTC TCA AAC TCA GTC TTC G-3'

**MTS assay** – Cell viability was evaluated using a CellTiter 96 AQueous One Solution Cell Proliferation 3-(4,5-dimethylthiazol-2-yl)-5-(3-carboxymethoxyphenyl)-2-(4-sulfophenyl)-2H-tetrazolium (MTS) assay kit (Promega). Cells were seeded in 96-well plates ( $1.0 \times 10^4$  cells/well) in 100  $\mu$ L RPMI supplemented with 10% FBS. Twenty microliters of MTS reagent were added, and the cells were incubated at 37°C in a humidified 5% CO<sub>2</sub> chamber for 4 h. Optical density measurements were obtained at 490 nm using an ELISA plate reader.

***BrdU assay*** – Cell proliferation was measured using a BrdU assay kit (ExAlpha Biologicals, Shirley, MD). Briefly,  $2.0 \times 10^5$  cells/mL were plated into a 96-well plate. BrdU (1:500 dilution) was added, and the plate was incubated for 24 h at 37°C. Cells were then fixed for 30 min at room temperature. After the cells were washed, anti-BrdU antibody was added for 1 h followed by peroxidase goat anti-mouse IgG conjugate (1:2000 dilution) for 30 min. Next, the 3,3',5,5'-tetramethylbenzidine peroxidase substrate was added, followed by incubation for 30 min at room temperature in the dark. The acid Stop Solution was then added and the plate was read at 450 nm using an ELISA plate reader.

***Cell migration assay*** – Cell migration was analyzed using 24-well Transwell plates with polycarbonate membranes (Corning Costar). Briefly, cells transfected with Ik-1 or MZF1 in serum-free culture medium were loaded into the upper compartment, and 500 ng/mL IGF-I (R&D Systems, Minneapolis, MN) in serum-free medium was loaded into the lower compartment. As controls, non-transfected cells in serum-free medium were loaded into the upper compartment with/without IGF-I added into the lower compartment. Plates were incubated for 4 h at 37°C, and cells migrating through the membrane into the lower chamber were counted using a particle counter and size analyzer (Beckman Coulter, Brea, CA).

***Anchorage-independent colony formation assay*** – Methylcellulose (Methocult H4230; StemCell Technologies) (3.0 mL) was added to 15-mL tubes. Empty vector- (EV-), Ik-1- or MZF1-transfected cells were added in a 1:10 (v/v) ratio to the methylcellulose tubes and mixed well by gentle inversion. One milliliter of the mix was divided into 24-well plates in triplicate. Plates were placed in a humidified incubator at 37°C in 5% CO<sub>2</sub> for 7 days. Then, *p*-iodonitrotetrazolium violet was added for 24 h for staining. Colonies were visualized using the AlphaImager system (Alpha Innotech Corporation, San Leandro, CA). In an additional

experiment, SUP-M2 cells were incubated for 21 days, and the results were similar to those of the shorter incubations.

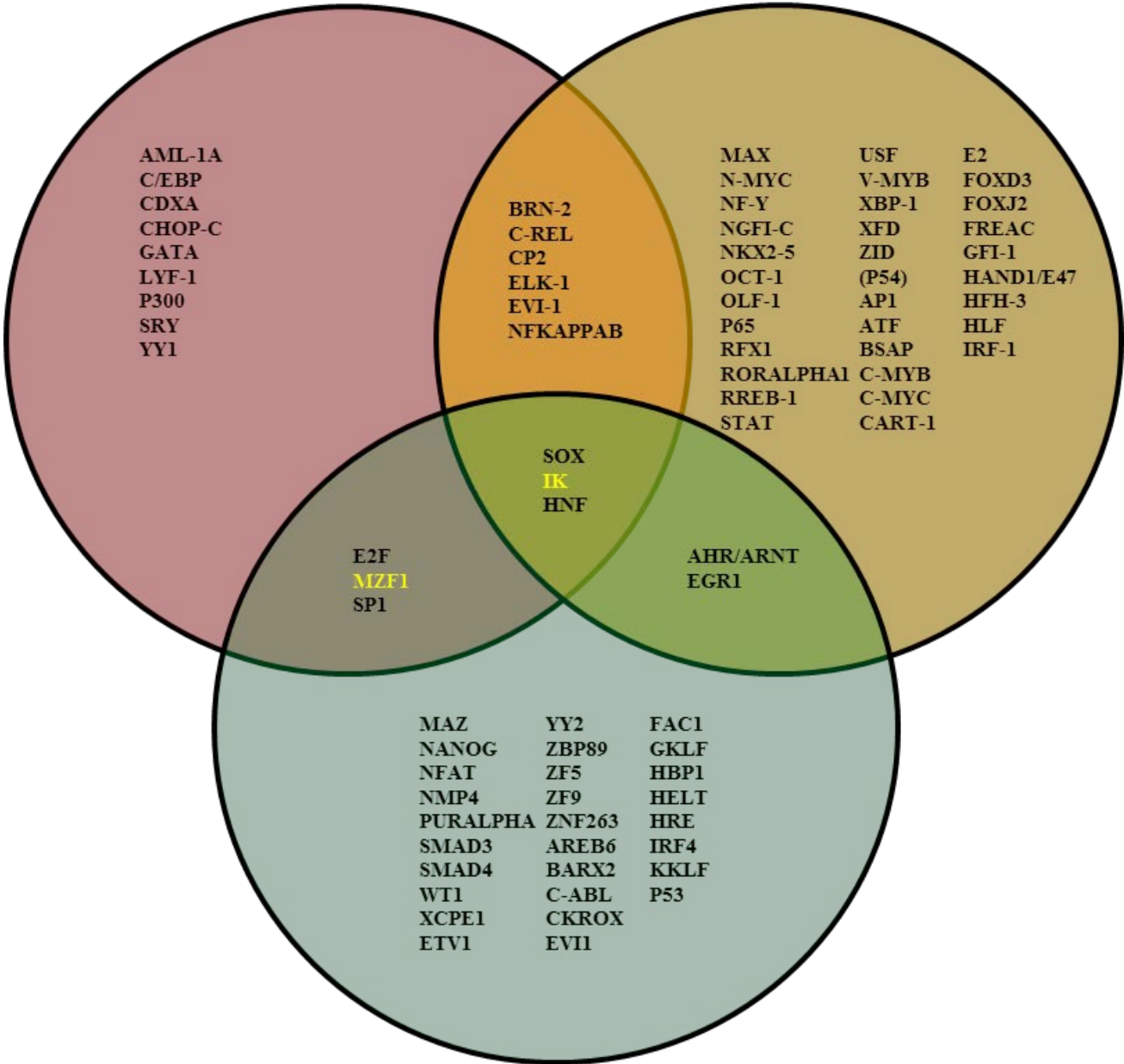
### 3.1.2.2. Results

*Identification of the transcription factors Ikaros isoform-1 (Ik-1) and myeloid zinc finger 1 (MZF1) as capable to potentially bind with the IGF-IR gene promoter:* The TFSearch, MATCH, and Genomatix transcription factor search algorithms identified multiple potential transcription factors. We elected to focus on Ik-1 and MZF1 because: their 1) matrix similarity thresholds to bind with the *IGF-IR* gene promoter are  $> 0.9$ , which has been predicted collectively by the 3 algorithms [the matrix similarity threshold represents the quality of the match between the transcription factor binding sequence and arbitrary parts of the promoter sequence, and is used to minimize false positive results] (**Table 6**); 2) contribution to the transcriptional regulation of *IGF-IR* expression has not been previously described; 3) role in the pathogenesis of NPM-ALK<sup>+</sup> T-cell lymphoma is not known; and 4) contribution to normal and abnormal hematopoiesis has been established by the transcription factors [141-145].



### TF Search®

### Match®

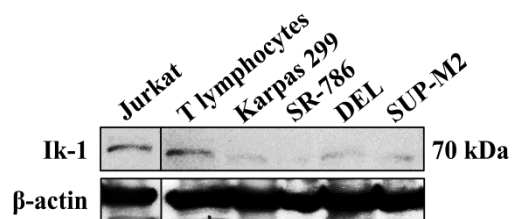


### Genomatix®

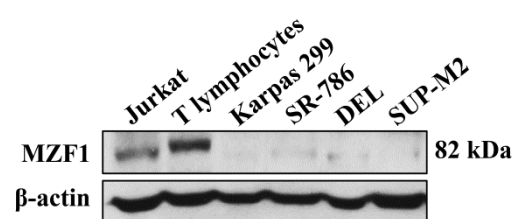
**TABLE 6. Ik-1 and MZF1 can potentially bind with *IGF-IR* gene promoter.** Three online-based software search algorithms (Genomatix, MATCH, and TESSearch) predicted several transcription factors that could potentially bind with *IGF-IR* gene promoter. Ik-1 and MZF1 were predicted by 3 and 2, respectively, of the 3 software algorithms, with the highest probability of  $> 0.09$ .

*Expressions of Ik-1 and MZF1 are significantly decreased in NPM-ALK<sup>+</sup> ALCL:* Western blotting was used to first analyze 4 NPM-ALK<sup>+</sup> ALCL cell lines (Karpas 299, SR-786, SUP-M2, and DEL) and normal human T lymphocytes for the expression of Ik-1 and MZF1. The expression levels of Ik-1 and MZF1 were significantly decreased in the 4 cell lines compared to the normal T lymphocytes (**Figure 11A and 11B**). Jurkat cells were used as positive controls for the expression of Ik-1 and MZF1. Densitometric analysis of the expression of Ik-1 and MZF1 relative to  $\beta$ -actin is shown (**Figure 11C**). In addition, examination of the expression levels of Ik-1 and MZF1 in protein lysates extracted from 15 FFPE patient tissues showed patterns of expression similar to cell lines. Ik-1 and MZF1 expressions were decreased in 87% and 100% of the patient's samples, respectively, compared to normal T lymphocytes (**Figure 11D**). Densitometric analysis of the expression of Ik-1 and MZF1 relative to  $\beta$ -actin is shown (**Figure 11E**).

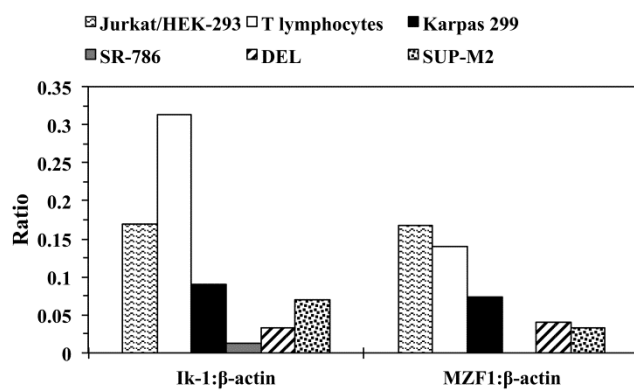
A



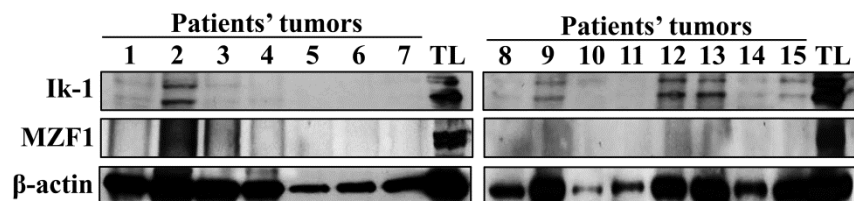
B



C



D



E

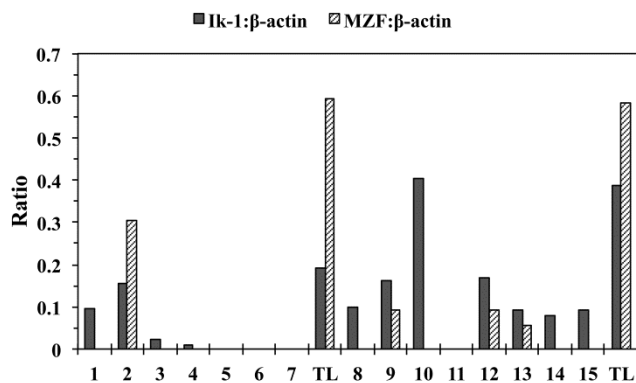


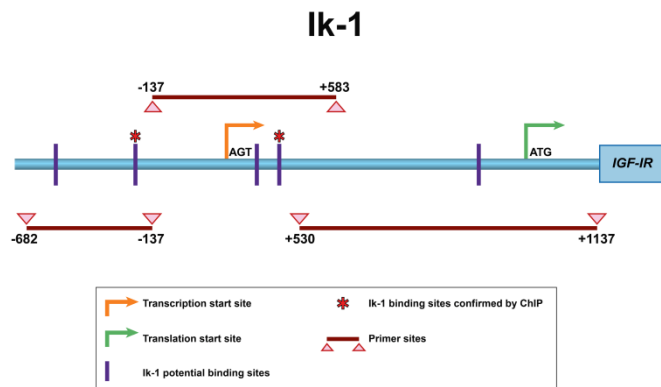
**FIGURE 11. The expression of Ik-1 and MZF1 is decreased in NPM-ALK<sup>+</sup> ALCL cell lines and human primary tumors.** (A) WB shows that Ik-1 levels were lower in 4 NPM-ALK<sup>+</sup> ALCL cell lines than in T lymphocytes. Jurkat cells were used as a positive control.  $\beta$ -actin represents the level of proteins loaded in each lane. (B) Similarly, MZF1 levels were lower in the lymphoma cell lines than in normal human T-cells. Jurkat cells served as a positive control.  $\beta$ -actin reflects the level of proteins loaded in each lane. (C) Densitometric analysis of the Ik-1/MZF1 Western blotting bands relative to the  $\beta$ -actin bands depicted in (A) and (B) further demonstrated that the expression of these two transcription factors is decreased in NPM-ALK<sup>+</sup> ALCL cell lines vs. T-cells and positive control cell lines. (D) Western blotting assay showing that the expression of Ik-1 and MZF1 were lower in ALK<sup>+</sup> ALCL specimens from patients than in T lymphocytes.  $\beta$ -actin reflects the level of total proteins loaded in each lane. Variability in  $\beta$ -actin levels is due to the poor quality of some of the FFPE tumor sections. (E) Densitometric studies analyzing the Ik-1/MZF1: $\beta$ -actin ratio of the Western blotting bands shown in (D).

***Ik-1 and MZF1 bind the IGF-IR promoter and regulate its activity:*** To elucidate whether Ik-1 and MZF1 can bind and regulate the *IGF-IR* gene promoter, a luciferase assay was performed using 3 different fragments of the human *IGF-IR* promoter construct (F1: -682/-137, F2: -137/+583, F3: +530/+1137; illustrated in **Figure 12A and 12B**) along with either EV, Ik-1 or MZF1 expression plasmids. In addition, a second luciferase assay was performed simultaneously using mutated versions of the promoter fragments that were sequentially deleted at the corresponding binding sites. Ik-1 and MZF1 significantly decreased the luciferase activity of the F1 and F2, but not the F3, regions of the human *IGF-IR* promoter (**Figure 12C**). In contrast, Ik-1 and MZF1 did not decrease the luciferase activity of the mutated forms of the *IGF-IR* promoter (**Figure 12C**). These results suggest that each of these transcription factors can interact with binding sites located within the F1 and F2 regions, but not the F3 region.

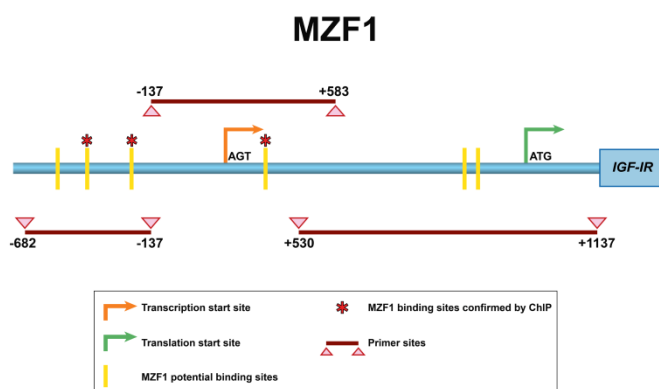
The 3 web-based transcription factor search algorithms also predicted 5 potential binding sites for Ik-1 and 6 potential binding sites for MZF1 within the *IGF-IR* promoter (**Figure 12A and 12B**). To determine which of these sites is responsible for Ik-1 or MZF1 interactions with the *IGF-IR* promoter, a ChIP assay was performed. Because there are low levels of endogenous Ik-1 and MZF1 in the cells, Karpas 299 and SR-786 cells were transfected with Myc-tagged Ik-1 or MZF1 (c-Myc-Ik-1 or c-Myc-MZF1) expression constructs or with empty vector (EV). Using a c-Myc antibody, the transcription factors were immunoprecipitated and the sonicated chromatin was used to perform an RT-PCR analysis using primers flanking the potential binding sites for Ik-1 and MZF1 within the human *IGF-IR* promoter. The ChIP assay identified 2 binding sites (BS2 and BS4) for Ik-1 and 3 binding sites for MZF1 (BS2, BS3, and BS4) (**Figure 12D, 12E**; the sites are depicted in **11A and 11B**). The RT-PCR (2 different sets of primers were tried) showed nonspecific binding in the

ChIP assay for Ik-1 BS1 and BS5, and for MZF1 BS1 and BS6 (data not shown). This nonspecific binding could possibly be due to the instability of the primers to bind to and amplify the extreme beginning and end of the *IGF-IR* gene promoter.

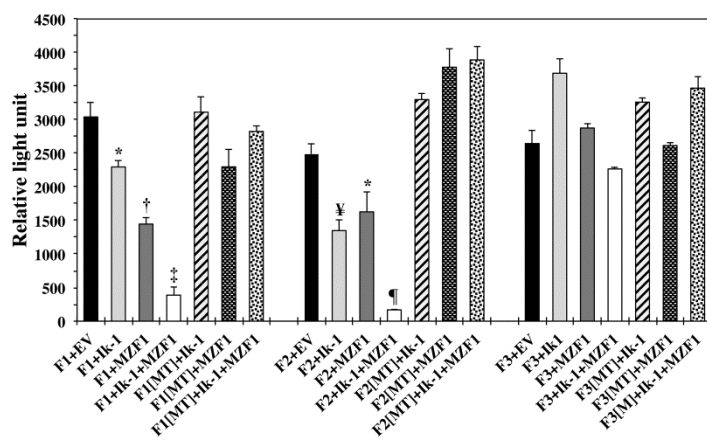
A



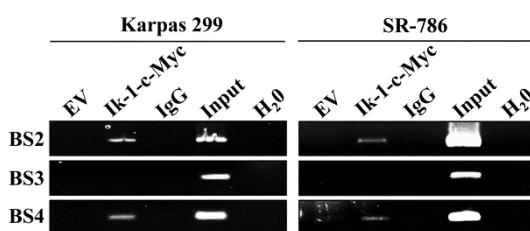
B



C



D



E

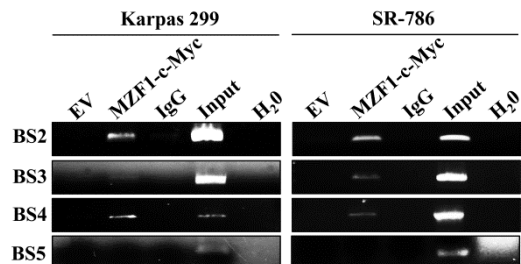




**FIGURE 12. Ik-1 and MZF1 interact with and bind to the *IGF-IR* gene promoter.** (A)

The general structure of the *IGF-IR* gene promoter, including the transcription and translation start sites is shown. The 3 PCR fragments used to perform the luciferase assay (F1: -682/-137, F2: -137/+583, F3: +530/+1137) as well as 5 sites that could potentially bind with Ik-1 are shown. \*: 2 sites that were shown to bind with Ik-1 by the ChIP assay. (B) The 3 PCR fragments used to perform the luciferase assay and 6 sites that could potentially bind with MZF1 are depicted. \*: 3 sites that were confirmed by the ChIP assay as binding sites for MZF1. (C) Luciferase assay performed in R<sup>-</sup> cells, which lack endogenous IGF-IR expression, demonstrates that transfection of Ik-1 or MZF1 induced a marked decrease in *IGF-IR* promoter activity at concomitantly transfected F1 and F2, but not at F3, of the *IGF-IR* gene promoter (\*:  $P < 0.05$ ; \*\*:  $P < 0.01$ ; \*\*\*:  $P < 0.001$  compared with EV). Importantly, Ik-1 and MZF1 failed to induce their effects when F1 and F2 were mutated (MT) at their potential binding sites. The results are shown as means  $\pm$  SE of 3 consistent experiments. (D) ChIP assay shows that Ik-1 binds with binding site 2 (BS2) and BS4 of the *IGF-IR* gene promoter. As shown, controls including EV, IgG, input, and H<sub>2</sub>O worked properly. The 2 binding sites are identified by an (\*) in (A). (E) ChIP assay confirms that MZF1 is capable of binding with the *IGF-IR* gene promoter at BS2, BS3, and BS4, which are marked by an (\*) in (B). Positive and negative controls worked properly.

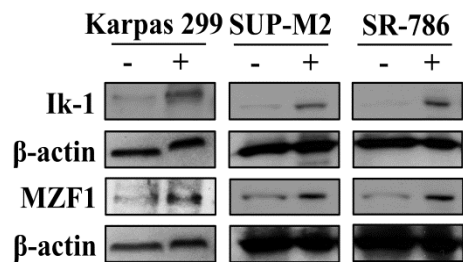
***Ik-1 and MZF1 decrease IGF-IR mRNA and protein levels in NPM-ALK<sup>+</sup> ALCL cells:***

Next, we sought to explore the effects of up-regulating the expression of Ik-1 and MZF1 in NPM-ALK<sup>+</sup> ALCL cells. Sufficient transfection of Karpas 299, SUP-M2, and SR-786 cells with Ik-1 or MZF1 expression plasmids resulted in a significant decrease in *IGF-IR* mRNA expression (**Figure 13A and 13B; Figure 13C and 13D**). In contrast, EV failed to elicit similar effects. These effects resulted in significant decrease in IGF-IR protein levels, and subsequently, its activated/phosphorylated form, pIGF-IR. Furthermore, Ik-1- and MZF1-induced downregulation of IGF-IR was followed by decreases in several downstream signaling proteins that are important for the IGF-IR signaling axis, such as pAKT<sup>Ser437</sup> and pIRS-1<sup>Ser639</sup> (**Figure 13E**). No significant changes were detected in total AKT levels, but unexpectedly Ik-1 and MZF1 decreased total IRS-1 levels. When the *IRS-1* gene promoter sequence was analyzed using the 3 web-based transcription factor search algorithms, we discovered that Ik-1 and MZF1 have the potential to bind to the *IRS-1* gene promoter, which may explain this unexpected finding.

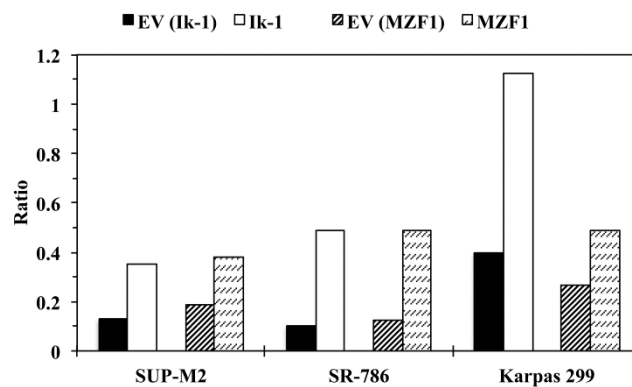
The ectopic expression of Ik-1 and MZF1 resulted in significant decrease in NPM-ALK and pNPM-ALK levels (**Figure 13E**). When we entered the NPM-ALK sequence into the three web-based algorithms, we found that neither of these transcription factors have potential binding sites within the *NPM* gene, which is where the promoter for *NPM-ALK* resides. In addition, WB analysis failed to demonstrate changes in wild type NPM protein after transfection of Ik-1 or MZF1, providing evidence that Ik-1 and MZF1 are not directly regulating NPM-ALK (**Figure 13E**). Moreover, the luciferase activity of the full length *NPM* promoter remained unchanged after transfection with Ik-1 or MZF1 (**Figure 13F**). These observations allude to the possibility that the decrease NPM-ALK protein levels is most

likely the result of decreases in IGF-IR, which is consistent with our previous results showing that IGF-IR sustains the stability of NPM-ALK protein.

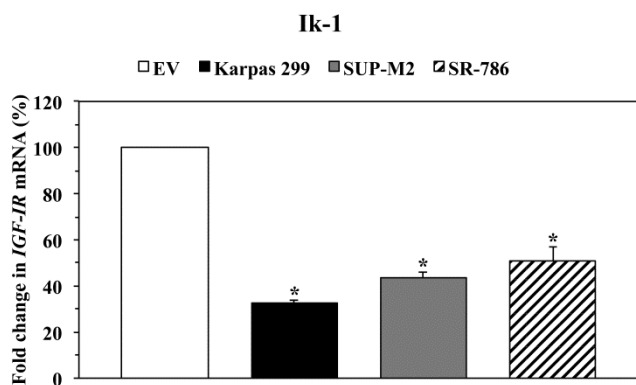
A



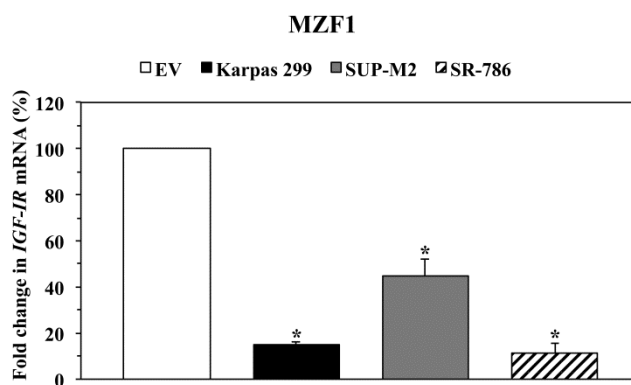
B



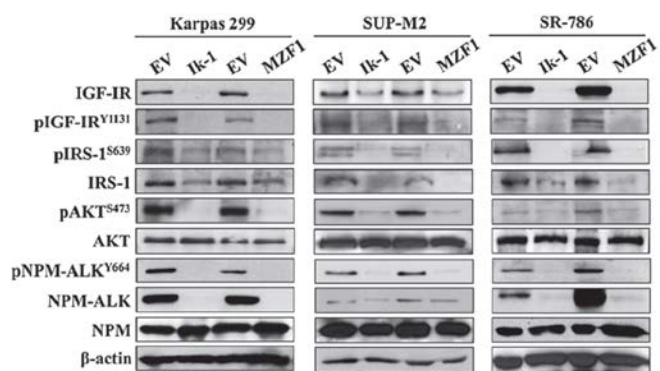
C



D



E



F

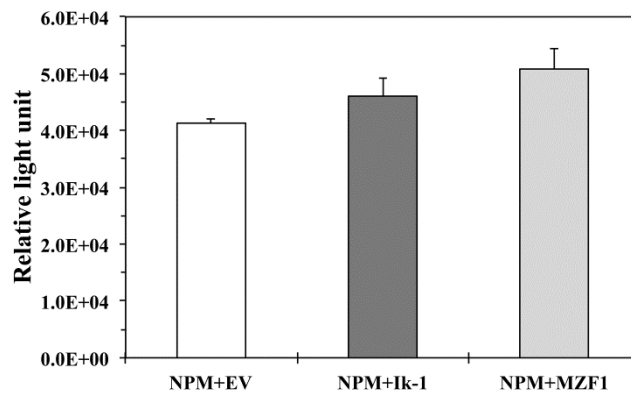


**FIGURE 13. Ik-1 and MZF1 decrease IGF-IR mRNA and protein expression and the phosphorylation of downstream targets.** (A) WB demonstrates increased expression levels of Ik-1 and MZF1 proteins at 48 h after transfection into 3 NPM-ALK<sup>+</sup> ALCL cell lines.  $\beta$ -actin shows equal protein loading. (B) Densitometric studies illustrate the ratio of the Ik-1 or MZF1 protein to  $\beta$ -actin. The ratios support increased expression of the corresponding transfection factor after transfection. (C) Transfection of Ik-1 remarkably decreased *IGF-IR* mRNA levels in Karpas 299, SUP-M2, and SR-786 cell lines (\*: < 0.0001 compared with EV). (D) Similarly, transfection of MZF1 induced a significant decrease in *IGF-IR* mRNA levels (\*: < 0.0001 compared with EV). The results depicted in (C) and (D) represent the means  $\pm$  SE of 3 experiments. (E) WB shows that transfection of Ik-1 and MZF1 into Karpas 299, SUP-M2, and SR-786 cell lines induced marked downregulation of IGF-IR protein, which was also associated with decreased pIGF-IR levels. Moreover, the decrease in IGF-IR/pIGF-IR expression levels was associated with decreased phosphorylation of important IGF-IR targets including IRS-1, AKT, and NPM-ALK. Whereas the basal levels of AKT remained unchanged, notable decrease in IRS-1 protein was observed. The 3 web-based transcription factor search algorithms showed that Ik-1 and MZF1 could potentially bind with the *IRS-1* gene promoter. In contrast, searching these algorithms did not support potential binding of Ik-1 or MZF1 and the *NPM* gene promoter, where the expression of NPM-ALK protein is regulated at the transcriptional level. (F) In line with lack of potential binding/interaction between Ik-1 or MZF1 and the *NPM* gene promoter, a luciferase assay performed in R<sup>-</sup> cells shows that transfection of Ik-1 and MZF1 does not decrease the *NPM* promoter activity. The results represent means  $\pm$  SE of 3 consistent experiments.

*Ik-1 and MZF1 decrease the viability, proliferation, migration, and anchorage-independent colony formation of NPM-ALK<sup>+</sup> ALCL cells:* A series of cellular assays were performed to test the biological impact of forced expression of Ik-1 and MZF1 in NPM-ALK<sup>+</sup> ALCL. Transfection of Karpas 299, SUP-M2, and SR7-86 with Ik-1 or MZF1, but not EV, decreased the cell viability of the NPM-ALK<sup>+</sup> ALCL cells (**Figure 14A and 14B**). In addition, cell proliferation was significantly reduced by the two transcription factors (**Figure 14C and 14D**). Furthermore, migration in response to IGF-I was significantly hindered in the three cell lines (**Figure 14E**). Finally, Ik-1 and MZF1 abrogated the potential of NPM-ALK<sup>+</sup> ALCL cells to form colonies in methylcellulose (**Figure 14F and 14G**).

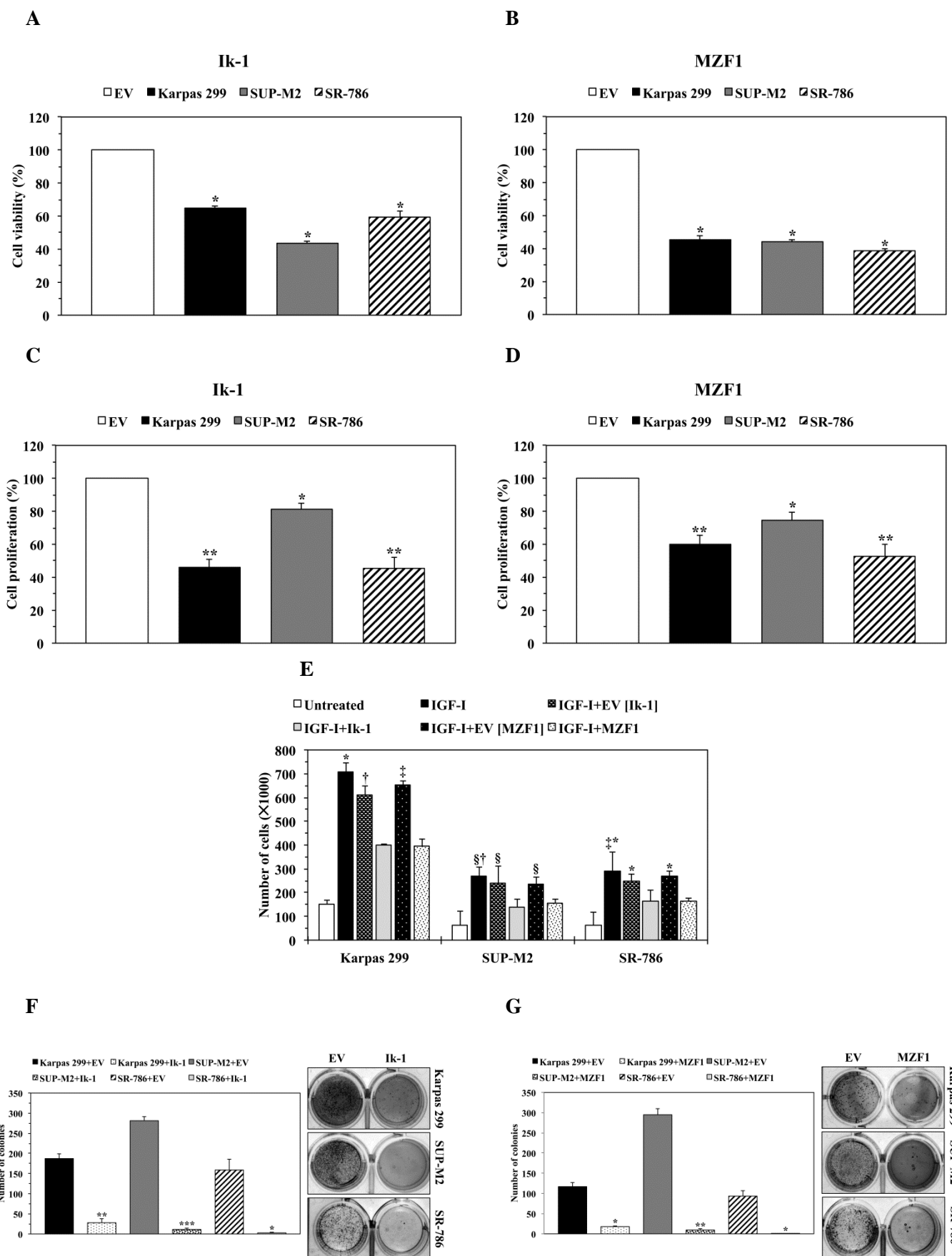


**FIGURE 14. Transfection of Ik-1 and MZF1 decreases the viability, proliferation, migration, and anchorage-independent colony formation of NPM-ALK<sup>+</sup> ALCL cells.** (A) Compared with EV, transfection of Ik-1 was associated with significant decreases in the viability of the NPM-ALK<sup>+</sup> ALCL cells Karpas 299, SUP-M2, and SR-786 at 48 h after transfection (\*:  $P < 0.0001$ ). (B) In a similar fashion, transfection of MZF1 into these cells induced marked decreases in their viability (\*:  $P < 0.0001$ ). (C) Ik-1 significantly decreases the proliferation of the NPM-ALK<sup>+</sup> ALCL cell lines (\*:  $P < 0.05$ ; \*\*:  $P < 0.01$ ). (D) In addition, transfection of MZF1 reduced the proliferation of these cells (\*:  $P < 0.05$ ; \*\*:  $P < 0.01$ ). (E) IGF-I stimulated the migration of Karpas 299, SUP-M2, and SR-786 cells. Whereas this effect was profoundly reduced when cells were treated with IGF-I and simultaneously transfected with Ik-1 or MZF1; transfection of EV failed to induce similar effects (for Karpas 299, \*:  $P < 0.0001$  in IGF-I vs. IGF-I+Ik-1 and IGF-I+MZF1, †:  $P < 0.01$  in IGF-I+EV [Ik-1] vs. IGF-I+Ik-1, ‡:  $P < 0.001$  in IGF-I+EV [MZF1] vs. IGF-I+MZF1; for SUP-M2, §:  $P < 0.05$  in IGF-I vs. IGF-I+Ik-1, IGF-I+EV [Ik-1] vs. IGF-I+Ik-1 and IGF-I+EV [MZF1] vs. IGF-I+MZF1, †:  $P < 0.01$  in IGF-I vs. IGF-I+MZF1; for SR-786, \*:  $P < 0.0001$  in IGF-I vs. IGF-I+MZF1, IGF-I+EV [Ik-1] vs. IGF-I+Ik-1, and IGF-I+EV [MZF1] vs. IGF-I+MZF1, ‡:  $P < 0.001$  in IGF-I vs. IGF-I+Ik-1). (F) Ik-1 abrogated anchorage-independent colony formation of Karpas 299, SUP-M2, and SR-786 cells at 7 days after transfection (\*:  $P < 0.05$ ; \*\*:  $P < 0.01$ ; \*\*\*:  $P < 0.001$  compared with EV). The numbers of the colonies are shown in the left panel, and representative examples from cells transfected with EV or Ik-1 are shown in the right panel. (G) Furthermore, MZF1 halted NPM-ALK<sup>+</sup> ALCL cells' anchorage-independent colony formation in methylcellulose at 7 days after transfection (\*:  $P < 0.05$ ; \*\*:  $P < 0.01$  compared with EV). The numbers of the colonies are shown in the left panel, and representative examples from cells transfected with EV or MZF1 are shown in the right panel. Results illustrated in Fig. 14 are means  $\pm$  SE of at least 3 consistent experiments.



### **3.1.3. Transcriptional Regulation of *IGF-IR*: Gene Amplification**

### 3.1.3.1. Materials and Methods

**Cell Lines** – Five characterized NPM-ALK<sup>+</sup> ALCL cell lines were used in this study including Karpas 299, DEL, SUP-M2, SR-786, and SU-DHL-1. Normal T lymphocytes were purchased from StemCell Technologies (Catalog # 70024, Vancouver, British Columbia). Lymphoma cell lines and T lymphocytes were maintained in RPMI 1640 medium (HyClone, South Logan, Utah) supplemented with 10% FBS, glutamine (2 mM), penicillin (100 U/ml), and streptomycin (100 µg/ml) at 37°C in a humidified 5% CO<sub>2</sub> in air chamber.

**Cytospins** – Cytospins were prepared from NPM-ALK<sup>+</sup> ALCL cell lines and normal T lymphocytes. Approximately 100,000 cells were suspended in RPMI medium and pipetted into cytospin chambers. Cells were suspended onto slides using the following conditions: 700 rpm, high acceleration, for 5 min. Once completed, the slides were allowed to dry and fixed immediately in ice cold 100% methanol (-20°C) for 5 min. Thereafter, slides were air dried and stored in -20°C until FISH was performed.

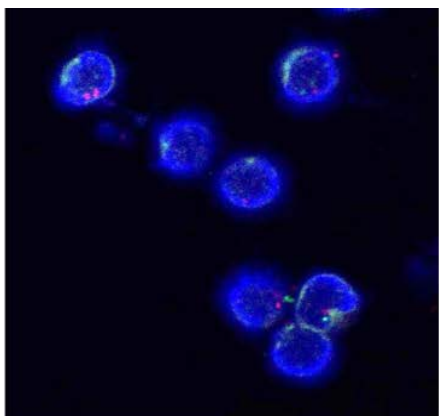
**Fluorescent in situ hybridization (FISH)** – Human T lymphocytes and NPM-ALK<sup>+</sup> T-cell lymphoma cells ( $1 \times 10^5$  cells) suspended in RPMI were pipetted into cytospin chambers. Cytospin slides were prepared (700 rpm at high 25 acceleration for 5 min). The cytospin slides were fixed in ice cold 100% methanol, and stored at -20°C until FISH was performed. We adopted a previously described approach to perform FISH assay and analysis [136]. The SureFish probes and kit from Agilent Technologies were used. Briefly, 1.0 µL of *IGF-IR* FISH probe (G100168R) and 1.0 µL of chromosome enumeration probe 15 (CEP15; G100543G), which identify centromere 15, were mixed gently in Agilent FISH hybridization buffer. Cytospin slides were prepared and placed in gradually increasing concentrations of ethanol (70%, 85%, and 100%), each for 1 min at room temperature. After allowing the

slides to dry, 5.0  $\mu$ L of probe/hybridization buffer mixture were added to the slides, and cover slips were applied. Hybridization was then accomplished by using the ThermoBrite system (Abbott Molecular, Abbott Park, IL). The slides were first incubated at 78°C for 5 min to denature the DNA, and then incubated at 37°C for 24 h. Thereafter, cover slips were removed and slides were placed and agitated in Wash buffer 1 (73°C) for 2 min. Subsequently, slides were transferred and agitated at room temperature for 2 min in Wash Buffer 2. The slides were air dried in the dark at room temperature, followed by pipetting DAPI (1.0  $\mu$ g/mL in PBS). DAPI was then removed, and slides were mounted with ProlongGold antifade media (P36934, Invitrogen, Grand Island, NY) and viewed using the FV1000 confocal microscope (Olympus America, Center Valley, PA).

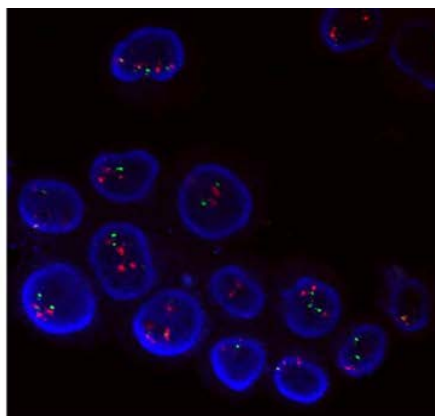
FISH scoring was performed in 55 nonoverlapping nuclei per slide. The means of the *IGF1R* gene and CEP15 copy numbers per cell, number of cells with two or fewer, three, and four or more copies of *IGF1R* and CEP15 signals, and *IGF1R*-to-CEP15 ratio were obtained.

### 3.1.3.2. Results

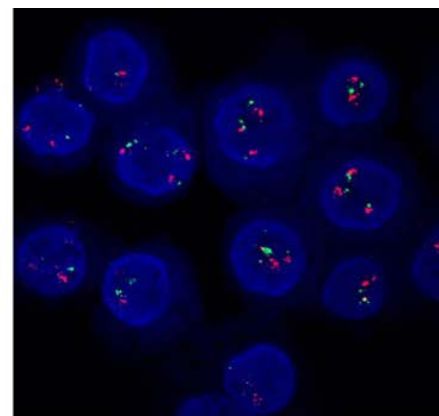
***IGF-IR is not amplified in NPM-ALK<sup>+</sup> ALCL cell lines:*** We analyzed *IGF-IR* gene probe signal (red) and the chromosome 15 pericentromeric (CEP) probe signal (green) in approximately 55 nonoverlapping nuclei in 5 NPM-ALK<sup>+</sup> ALCL cell lines (Karpas 299, SR-786, SUP-M2, SU-DHL-1, and DEL) and normal T lymphocytes prepared on cytopins by FISH (**Figure 15**). Also, we measured the additional parameters that are listed in **Figure 15**. While normal T lymphocytes *IGF-IR* copy number was approximately 2 copies/cell, the median *IGF-IR* gene copy number in the cell lines was 3 copies/cell. However, the median *CEP15* gene copy number in the cell lines analyzed by FISH was 2.5 copies/cell. Considering that the ratio between *IGF-IR* gene copy number-to-*CEP15* gene copy number is 1.1, we conclude that there is no apparent *IGF-IR* gene amplification in NPM-ALK<sup>+</sup> ALCL cells.



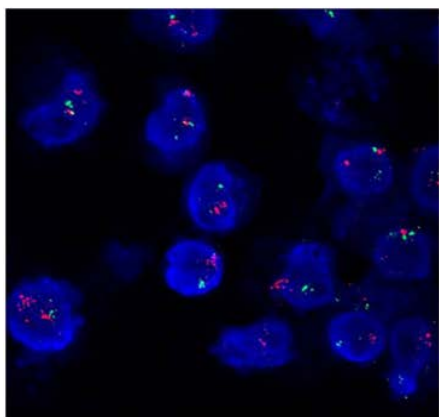
**T lymphocytes**



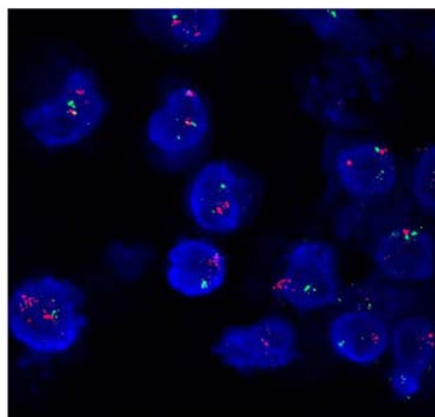
**Karpas 299**



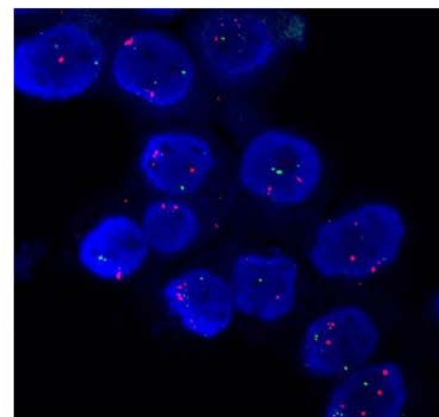
**SR-786**



**DEL**



**SUP-M2**



**SU-DHL-1**

**T lymphocytes**

Average # of IGFIR/cell	1.418181818
Average # of CEP15/cell	1.436363636
IGFIR: CEP15 Ratio	0.910714286
# of cells with 2 or fewer: CEP15	55
# of cells with 3: CEP15	0
# of cells with 4 or more: CEP15	0
# of cells with 2 or fewer: IGFIR	55
# of cells with 3: IGFIR	0
# of cells with 4 or more: IGFIR	0

**Karpas 299**

80

Average # of IGFIR/cell	3.018181818
Average # of CEP15/cell	2.563636364
IGFIR: CEP15 Ratio	1.177304965
# of cells with 2 or fewer: CEP15	35
# of cells with 3: CEP15	7
# of cells with 4 or more: CEP15	13
# of cells with 2 or fewer: IGFIR	19
# of cells with 3: IGFIR	21
# of cells with 4 or more: IGFIR	15

**SR786**

Average # of IGFIR/cell	4.181818182
Average # of CEP15/cell	3.890909091
IGFIR: CEP15 Ratio	1.074766355
# of cells with 2 or fewer: CEP15	16
# of cells with 3: CEP15	6
# of cells with 4 or more: CEP15	33
# of cells with 2 or fewer: IGFIR	13
# of cells with 3: IGFIR	8
# of cells with 4 or more: IGFIR	34

**DEL**

Average # of IGFIR/cell	4.436363636
Average # of CEP15/cell	4.436363636
IGFIR: CEP15 Ratio	1
# of cells with 2 or fewer: CEP15	5
# of cells with 3: CEP15	11
# of cells with 4 or more: CEP15	39
# of cells with 2 or fewer: IGFIR	4
# of cells with 3: IGFIR	10
# of cells with 4 or more: IGFIR	41

**SUPM2**

Average # of IGFIR/cell	2.545454545
Average # of CEP15/cell	1.945454545
IGFIR: CEP15 Ratio	1.308411215
# of cells with 2 or fewer: CEP15	46
# of cells with 3: CEP15	4
# of cells with 4 or more: CEP15	5
# of cells with 2 or fewer: IGFIR	31
# of cells with 3: IGFIR	12
# of cells with 4 or more: IGFIR	12

**SUDHL1**

Average # of IGFIR/cell	2.654545455
Average # of CEP15/cell	2.127272727
IGFIR: CEP15 Ratio	1.247863248
# of cells with 2 or fewer: CEP15	37
# of cells with 3: CEP15	12
# of cells with 4 or more: CEP15	6
# of cells with 2 or fewer: IGFIR	24
# of cells with 3: IGFIR	17
# of cells with 4 or more: IGFIR	14

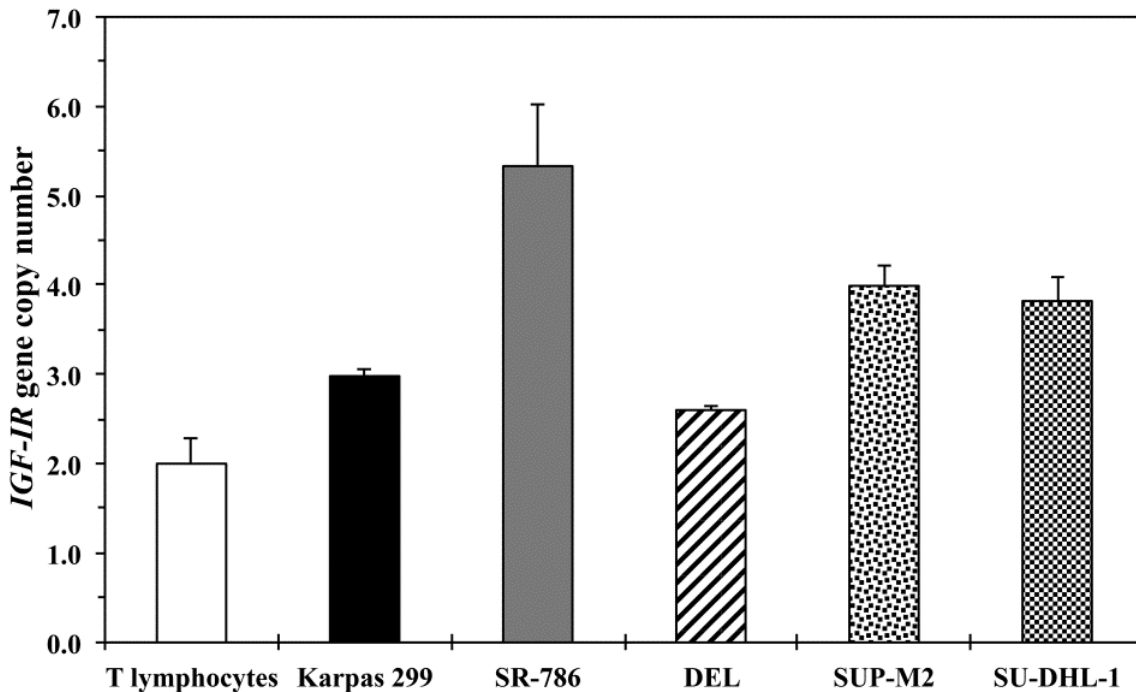


**FIGURE 15. FISH analysis of *IGF-IR* gene (red signal) and chromosome enumeration 15 (green signal; CEP15), which detects centromere 15, copy numbers in normal human T lymphocytes and NPM-ALK<sup>+</sup> ALCL cell lines.** FISH studies show no evidence to support amplification of *IGF-IR* gene in NPM-ALK<sup>+</sup> ALCL cells. As shown in the table, the *IGF-IR*-to-CEP15 ratio was consistently < 2.0 in the T lymphocytes as well as in the NPM-ALK<sup>+</sup> T-cell lymphoma cells.

### 3.2. Discussion for Aim 1

In this aim, we show that previously unidentified defects in transcriptional machinery contribute to the pathogenesis of NPM-ALK<sup>+</sup> ALCL. Firstly, we found that, compared with their expression in normal human T lymphocytes, the transcription factors Ik-1 and MZF1 are markedly decreased in NPM-ALK<sup>+</sup>ALCL cell lines and lymphoma tumors from patients. Substantial evidence is provided to support that Ik-1 and MZF1 possess the ability to bind specific sites residing within the IGF-IR gene promoter and inhibit its activity. In agreement with these observations, ectopic expression of Ik-1 and MZF1 in NPM-ALK<sup>+</sup> ALCL cells causes remarkable downregulation of the expression of IGF-IR mRNA and protein. Also, transfection of Ik-1 and MZF1 was associated with decreased cell viability, proliferation, migration, and anchorage independent colony formation of NPM-ALK<sup>+</sup> ALCL cells, asserting the tumor suppressing impact of Ik-1 and MZF1 in this lymphoma. Secondly, we failed to identify IGF-IR gene amplification in the lymphoma cells after measuring *IGF-IR* gene and *CEP15* pericentromeric gene copy numbers.

It has been previously shown that Ik-1 induces tumor-suppressing effects primarily in hematopoietic cellular elements [146-148]; nonetheless, the contribution of MZF1 to tumorigenesis is more diverse as it may induce oncogenic or tumor suppressor effects in hematopoietic and non-hematopoietic cells [149-154]. The *IGF-IR* gene promoter is tightly regulated during mammalian development, and during the embryonic and early postnatal stages it induces the transcription of high levels of *IGF-IR* mRNA, which decreases to much lower levels during growth [155]. The *IGF-IR* gene promoter is a TATA-less and CAAT-less promoter, and like other structurally similar promoters, the *IGF-IR* promoter is GC-rich [156-158]. The transcription of the *IGF-IR* gene is therefore initiated from an 11 basepair unique site contained within an “initiator” motif similar to the ones present in the terminal



deoxynucleotidyl transferase and adenovirus middle late gene promoters [157, 159, 160]. Although levels of expression of IGF-IR during physiological and pathological conditions can be rigorously determined at the transcriptional level [161], relatively few transcription factors have been shown to be capable of binding with and regulating the expression of the *IGF-IR* gene promoter. The multiple GC boxes present in this promoter form potential binding sites for members of the zinc-finger transcription factor family. In line with this possibility, earlier studies using rat *IGF-IR* gene promoter showed that Sp1, a zinc-finger transcription factor, binds with GC boxes located within the 5'-flanking region and one homopurine/homopyrimidine motif (CT element) in the 5'-untranslated region of *IGF-IR* gene promoter to enhance its activity [159, 162].

The *IGF-IR* gene promoter also includes cis-elements for members of the early growth response family of zinc-finger proteins including the WT1 Wilms tumor suppressor, which, in contrast with Sp1, downregulates the expression of *IGF-IR* [163, 164]. Indeed, increased expression of WT1 protein was associated with a reciprocal decrease in the expression of IGF-IR protein and receptor number in prostate cancer cells, and downregulation of WT1 increased IGF-IR expression in glioblastoma [165, 166]. Albeit less extensively studied, E2F1 and EGR-1 are also implicated in the positive regulation, and STAT1 in the negative regulation of *IGF-IR* gene expression [167-169]. In addition to the direct regulatory effects of Sp1 and WT1, several studies have elucidated indirect contributions of oncogenic and tumor suppressor proteins to the regulation of the *IGF-IR* gene expression through interactions with these two transcription factors. In breast cancer, BRCA1 appears to suppress the *IGF-IR* promoter activity, but there is no evidence to support BRCA1 binding and direct interactions with the *IGF-IR* promoter. Instead, BRCA1 most likely suppresses the activity of the *IGF-IR* promoter through the sequestration of Sp1 [170, 171].

Similarly, in breast cancer cells, the estrogen receptor enhances *IGF-IR* gene promoter activity via interactions with Sp1 and WT1 [172, 173]. Also, MCF7 breast cancer cells that express caveolin-1 demonstrate much higher levels of *IGF-IR* gene promoter activity, and the effects of caveolin-1 on the *IGF-IR* gene promoter were mediated through Sp1 [174]. Furthermore, the tumor suppressor transcription factor, Kruppel-like factor 6 (KLF6), activates *IGF-IR* gene transcription through synergy with Sp1 [175]. Moreover, it was found that wild-type p53 downregulates *IGF-IR* gene expression and mutated p53 enhances this expression [176-178]. The regulatory mechanisms conferred by p53 also do not involve specific binding with the *IGF-IR* gene promoter but seem to be mediated, at least partially, by protein-protein interactions between p53 and Sp1.

We have also previously demonstrated that NPM-ALK and IGF-IR are physically associated, and it appears that this physical association, through interactions with Hsp90, enhances the stability of NPM-ALK protein [127]. In the current study, the decrease in IGF-IR expression after Ik-1 and MZF1 transfection was also associated with pronounced decrease in NPM-ALK basal protein levels. Although these results agree with our previous observations, we sought to investigate whether Ik-1 or MZF1 is capable of regulating the expression of NPM-ALK directly at the transcriptional level. The web-based transcription factor search algorithms failed to predict potential binding sites between the *NPM* gene promoter, where the transcription of the *NPM-ALK* chimeric oncogene is driven [34], and either Ik-1 or MZF1. Furthermore, a luciferase assay using an *NPM* reporter construct showed that transfection of Ik-1 and MZF1 does not affect *NPM* promoter activity or protein levels. Therefore, our current results indicate that the decrease in NPM-ALK protein levels occurs secondarily to Ik-1- and MZF1-induced downregulation of IGF-IR protein expression.

The Ik-1 and MZF1 transcription factors play physiological roles in the development of normal hematopoiesis [142-145]. In the present work we describe for the first time in any type of cancer cell the negative regulation of *IGF-IR* gene expression by Ik-1 and MZF1 transcription factors. Ik-1 regulates transcription by binding to specific consensus binding sites (C/TGGGAA/T) within target promoters [179]. Similarly, MZF1's 13 zinc fingers are separated into 2 arms, and each arm has the ability to independently bind to specific binding sites within the promoters of target genes: the first domain of fingers 1-4 (ZN 1-4) binds to the sequence 5'-AGTGGGGA-3', and the second domain of fingers 5-13 (ZN 5-13) binds the core sequence 5'-CGGGnGAGGGGGAA-3' [144]. Similar to other transcription factors that bind with *IGF-IR* gene promoter, we found that Ik-1 and MZF1 possess the potential to bind with sequences located both upstream and downstream of the transcription start site within the 5'-flanking region as well as within the 5'-untranslated region. Specifically, potential binding sites for Ik-1 are located at nucleotides -504/-491, -138/-125, +77/+90, +427/+440, and +1011/+1024, and potential binding sites for MZF1 are located at nucleotides -504/-496, -299/-291, -138/-130, +501/+514, +919/+928, and +1011/+1019 (binding sites confirmed by ChIP are underlined). To our knowledge, these binding sites have not been previously described to bind with any of the transcription factors that are known to regulate *IGF-IR* gene. Among the previously described transcription factors, Sp1, E2F1, and EGR-1 showed a greater net change in promoter activity at binding sites located downstream of the transcription start site [162, 168, 169]. While this pattern was similar to Ik-1, MZF1 demonstrated a greater net change in *IGF-IR* promoter activity at binding sites located upstream of the transcription start site, which resembles the inhibitory effects induced by WT1 [163].

I $\kappa$ -1- and MZF1-induced downregulation of IGF-IR was associated with decreased levels of its activated/phosphorylated form, pIGF-IR. These effects induced downregulation of the phosphorylation levels of the molecular targets of IGF-IR including IRS-1, AKT, and NPMALK. Whereas basal levels of AKT remained unchanged, the basal levels of IRS-1 decreased after transfection of I $\kappa$ -1 and MZF1. To further analyze this unexpected finding, we searched the web-based transcription factor algorithms and found that the *IRS-1* gene promoter contains sites that could potentially function as targets for I $\kappa$ -1 and MZF1 transcriptional activity. It is important to mention that IRS-1 is also a downstream target of NPM-ALK phosphorylation activity [52]. Although further analysis is required to support this idea, we cannot completely rule out that I $\kappa$ -1 and MZF1 act as tumor suppressors in this lymphoma through targeting the expression of *IGF-IR* and *IRS-1*.

It is important, however, to emphasize that deregulated systems underlying the pathogenesis of NPM-ALK<sup>+</sup> ALCL are complex owing to the fact that they originate from more than one defective regulatory mechanism [131]. Although our results provide strong evidence that the aberrant decrease in the expression of I $\kappa$ -1 and MZF1 transcription factors contributes to upregulation of an important oncogenic protein, i.e., IGF-IR, we elected to investigate whether other transcriptional mechanisms exist to further enhance *IGF-IR* expression. Our experiments failed to support the presence of *IGF-IR* gene amplification, an aberrant transcriptional mechanism, in NPM-ALK<sup>+</sup> ALCL. IGF-IR gene amplification has been previously reported in small subgroups of patients with solid tumors such as lung cancer [136, 138]. To this end, our data suggest a model in which upregulation of *IGF-IR* in NPM-ALK<sup>+</sup> ALCL results from defects in transcriptional mechanisms, which reflects the complexity of survival signaling in this lymphoma.

### **3.3. Posttranscriptional Regulation of IGF-IR**

### 3.3.1. Introduction

Modifications of mRNA stability and/or translational efficiency through the posttranscriptional regulation of mRNAs are increasingly reported in cancer. MicroRNAs (miRs) constitute a family of 19- to 24- noncoding nucleotide RNAs that regulate gene expression posttranscriptionally through direct targeting of the 3'-UTR of the mRNA. There has been substantial evidence indicating that miRs are aberrantly expressed in many human cancers and may function as oncogenes or tumor suppressors; thus contributing significantly to cancer development and progression [180, 181]. Recently, there have been a few studies examining miRs that play a role in the pathogenesis of NPM-ALK<sup>+</sup> ALCL [182-185]. In our lab, we identified substantial decrease in basal expression levels of miR-96 and miR-26a in NPM-ALK<sup>+</sup> ALCL than normal human T lymphocytes [61, 132]. Importantly, we found that miR-96 induces negative regulatory effects on the expression of NPM-ALK protein, and miR-26a downregulates the expression of iNOS protein. However, the regulation of IGF-IR by miRs in NPM-ALK<sup>+</sup> ALCL has not been studied previously.

Another mechanism in which oncogenes, growth factors, cytokines, and cell-cycle regulatory genes are regulated posttranscriptionally is by controlling the rate of their mRNA turnover. In support of this view, mRNA turnover directly impacts signaling pathways that are often overactive in cancer, suggesting an important posttranscriptional component in regulating the expression of target mRNAs. In this aim, we hypothesized whether increased IGF-IR expression may be explained by posttranscriptional aberrancies, such as deregulated miRs and delayed mRNA turnover.

### **3.3.2. Posttranscriptional Regulation of IGF-IR: MicroRNA**

### 3.3.2.1. Materials and Methods

**Microarray analysis** – Total RNA isolation was performed using the Trizol reagent (Invitrogen, Grand Island, NY). RNA labeling and hybridization on miR array chips were performed as previously described [186]. Briefly, 5 µg of total RNA from each sample was biotin-labeled by reverse transcription using 5' biotin end-labeled random octomer oligo primer. Hybridization of biotin-labeled cDNA was carried out on a miR array chip (MD Anderson Cancer Center, Version 5.0), which contains 678 human miR genes in duplicate. Hybridization signals were detected by biotin binding of a streptavidin–Alexa647 conjugate by using an Axon GenePix 4000B scanner and the images were quantified by GenePix 6.0 software (Axon Instruments, Union City, CA).

**Web-based software** – In order to identify potential binding sites for miR-30a or miR-30d in the *IGF-IR*-3'-UTR, 3 web-based algorithms were used: MiRANDA (<http://www.microrna.org/microrna/home.do>), PicTar (<http://pictar.mdc-berlin.de>), and TargetScan (<http://www.targetscan.org>).

**Cell lines** – Five NPM-ALK<sup>+</sup> ALCL cell lines were used in this study including Karpas 299, DEL, SUP-M2, SR-786, and SU-DHL-1 (DSMZ, Germany). Normal T lymphocytes were purchased from StemCell Technologies (Catalog # 70024, Vancouver, British Columbia). The R<sup>-</sup> cells (mouse 3T3-like fibroblasts with targeted ablation of *Igf1r*) were a generous gift from Dr. R. Baserga (Thomas Jefferson University, Philadelphia, PA) and were used as the host cell line for luciferase assay studies [100]. The lymphoma cell lines and normal T lymphocytes were maintained in RPMI 1640 medium (HyClone, South Logan, Utah) supplemented with 10% FBS (Sigma, St. Louis, MO), glutamine (2 mM), penicillin (100 U/ml), and streptomycin (100 µg/ml) at 37°C in a humidified 5% CO<sub>2</sub> in air chamber.



Dulbecco's Modified Eagle Medium (DMEM), supplemented with 10% FBS was used to culture the R<sup>-</sup> cells under the same above conditions.

***MiR isolation from formalin-fixed and paraffin embedded (FFPE)*** – miRs were extracted from formalin-fixed, paraffin-embedded tissue sections prepared from tumor samples using the High Pure FFPE RNA Micro Kit (Roche Applied Science, Indianapolis, IN). First, FFPE tissue sections were marked for areas of interest and subjected to the following deparaffinization conditions: xylene (2 changes, 10 min each), 100% ethanol (2 changes, 10 min each), and deionized water (1 change, until ready for tissue excision). Tissue areas were excised using a blade and placed in microcentrifuge tubes. Tubes were spun to bring contents to the bottom of the tube. To each sample, 100  $\mu$ L Paraffin Tissue Lysis Buffer (provided in kit), 16  $\mu$ L 10% SDS, and 40  $\mu$ L Proteinase K working solution were added. Samples were vortexed and incubated in a 55°C water bath for 3 h. Next, 325  $\mu$ L binding buffer was added to each sample and transferred into the High Pure Filter tube attached to a 2mL collection tube (provided in kit). Tubes were centrifuged 30 sec at 10,000  $\times$  g. Following centrifugation, the flow through was discarded and samples were washed 2 times with 500  $\mu$ L Wash buffer working solution, then once again with 300  $\mu$ L Wash buffer working solution. Finally, the tubes were centrifuged at 13,000  $\times$  g for 1 min to dry the filter. The High Pure Tube was placed in a clean 1.5 mL microcentrifuge tube and solution containing miRs were eluted 2 times with 20  $\mu$ L nuclease-free water.

***RNA extraction, cDNA synthesis, and quantitative real time PCR (qPCR)*** – Total RNA was isolated and purified using RNeasy Mini Kit (Qiagen, Valencia, CA). Briefly,  $1-2 \times 10^6$  cells were collected by centrifugation at 200 $\times$  g for 5 min, washed twice in sterile PBS, and subjected to lysis and homogenization by RNA Lysis (RLT) buffer using QiaShredder spin columns. Homogenized cells were resuspended in an equal volume of 70% ethanol and

passed through provided spin columns. Two additional washing steps were performed with appropriate buffers: Buffer RW1 and Buffer RPE. Total RNA was collected upon elution with nuclease-free water. Optical density readings were read using DNA/Protein Analyzer (Beckman Coulter, Fullerton, CA)

cDNA synthesis for IGF-IR was performed through a two-step procedure using Superscript III RT protocol (Invitrogen, Carlsbad, CA). Approximately 0.3  $\mu\text{g}$  total RNA was used for reverse transcription. First, total RNA, oligo (dT), and dNTP mix were added to a mixture that was adjusted to a final volume of 10  $\mu\text{L}$  with nuclease-free water. This mixture was denatured by incubating at 65°C for 5 min and then placed on ice. Second, a master reaction mix consisting of 10 $\times$  cDNA synthesis buffer, 0.1 DTT, RNaseOUT, SuperscriptIII RT,  $\text{MgCl}_2$  and nuclease-free water was prepared on ice and vortexed gently. Approximately 10  $\mu\text{L}$  of master mix was pipetted into each sample tube on ice bringing the final volume to 20  $\mu\text{L}$ . The samples were then transferred to a thermal cycler preheated to the appropriate cDNA synthesis temperature and incubated for 60 min at 50°C, then terminated at 85°C for 5 min. 1  $\mu\text{L}$  of RNase H was added and samples were incubated at 37°C for 20 min to remove template RNA.

cDNA synthesis for miR-30a and miR-30d was performed using the TaqMan MicroRNA Reverse Transcription Kit (Applied Biosystems). Briefly, 100 mM dNTPs (with dTTP), MultiScribe™ Reverse Transcriptase (50 U/ $\mu\text{L}$ ), 10 $\times$  Reverse Transcription (RT) Buffer, RNase Inhibitor (20 U/ $\mu\text{L}$ ), and nuclease-free water was combined with total RNA in the ratio of 7  $\mu\text{L}$  RT master mix: 5  $\mu\text{L}$  total RNA (300 ng/reaction). Samples were mixed gently and centrifuged to bring the solution to the bottom of the tube. To each sample, 12  $\mu\text{L}$  of the master mix prepared above containing total RNA and 3  $\mu\text{L}$  of 5 $\times$  RT primer from each assay

set was added into the corresponding RT reaction tube for a final volume of 15  $\mu$ L/reaction. The samples were vortexed, centrifuged briefly, and transcribed using the following PCR conditions:

**Table 7.** PCR conditions for miRNA reverse transcription

Steps	Time	Temperature
Hold	30 min	16°C
Hold	30 min	42°C
Hold	5 min	85°C
Hold	$\infty$	4°C

qPCR was used to quantitate the levels of *IGF-IR* mRNA in NPM-ALK<sup>+</sup> ALCL cell lines after transfection with miR-30a and miR-30d using the reverse transcribed cDNA, *IGF-IR* gene expression assay primer/probe, and Taqman Mastermix (Applied Biosystems). The primer/probe sets used were obtained from Applied Biosystems (sequences not provided by the manufacturer). 18S ribosomal RNA was used as the endogenous control.

qPCR was used to examine the expression levels for miR-30a and miR-30d using the reverse transcribed cDNA, miR-30a, miR-30d or RNU48 gene expression assay primer/probe, and Taqman Mastermix (no AmpErase UNG) (Applied Biosystems). The primer/probe sets used were obtained from Applied Biosystems (sequences not provided). RNU48 was used as the endogenous control.

**Transfection** – Transfection of NPM-ALK, control mimic, miR-30a, miR-30d (Dharmacon) or with vectors used to create stable cell lines was performed by electroporation using Amaxa nucleofection system in 100  $\mu$ L cuvettes (Lonza; Solution V, Program A-023) and thereafter, cells were incubated for 48 h. For luciferase assays, R<sup>-</sup> cells were transfected using

Lipofectamine 2000 reagent. Briefly,  $1 \times 10^6$  R<sup>-</sup> cells were seeded in 6 well plates overnight. The following day, plasmids were incubated in 100  $\mu$ L Optimem media for 5 min at room temperature. Simultaneously, 7  $\mu$ L of Lipofectamine reagent was incubated in a separate tube. Thereafter, the tubes containing plasmids and the tubes containing Lipofectamine reagent were combined and incubated for a further 20 min at room temperature. Finally, the mixture was added to the corresponding well in the 6 well plates containing R<sup>-</sup> cells and incubated for 48 h.

***Cloning of IGF-IR 3'-UTR*** – IGF-IR 3'-UTR luciferase plasmid containing miR-30 binding site was constructed by the following approach: IGF-IR was amplified from genomic DNA (50 ng) using the HotStar Taq Mastermix, primers and PCR conditions listed in Table 2.

**Table 8.** PCR conditions for WT IGF-IR 3'-UTR construction

<u>Primer Name</u>	<u>Sequence</u>	
<b>WT IGF-IR 3'-UTR Forward</b>	5'-GTGTCCGCATCTTTCTGGTC-3'	
<b>WT IGF-IR 3'-UTR Reverse</b>	5'-GGATCACAAACACACATTTGC-3'	
<u>Step</u>	<u>Temperature</u>	<u>Time</u>
1. Initial activation step	95°C	15 min
2. 3-step cycling (35 cycles)		
Denaturation:	94°C	1 min
Annealing:	55°C	1 min
Extension:	72°C	1 min
3. Final extension:	10 min	72°C

The PCR products were run on 1.5% agarose gel, excised, and purified using the QIAquick gel extraction kit (Qiagen). Subsequently, DNA was ligated into pCR 2.1-TOPO vector using the TOPO TA cloning system (catalog # 451641; Invitrogen). Briefly, 4  $\mu$ L of

fresh PCR product, 1  $\mu$ L of Salt Solution, 1  $\mu$ L of pCR 2.1-TOPO vector, and 5  $\mu$ L of nuclease-free water were admixed and incubated for 5 min at room temperature. Thereafter, ligated products were immediately transformed using DH5 $\alpha$  competent cells and plated on ampicillin resistant agar plates coated with 40 mg/mL X-gal overnight at 37°C. White colonies were picked and amplified using ampicillin containing LB broth overnight at 37°C with shaking at 225 rpm and subjected to miniprep using QIAprep Miniprep kit (Qiagen). Plasmid sequence was confirmed using direct sequencing. In order to create the luciferase reporter plasmid containing the *IGF-IR* 3'-UTR, the pCR 2.1-TOPO-IGF-IR-3'-UTR plasmid and the pGL4.17 luciferase vector (Promega) were subjected to restriction enzyme digest using *Hind* III and *Eco* RV restriction enzymes (New England Biolabs, Ipswich, MA). Restriction enzyme digested products were run on a 1.5% agarose gel and purified using the QIAquick gel extraction kit. Resulting DNA was ligated using the Quick Ligation kit (Catalog # M2200S; New England Biolabs) and the following PCR conditions in Table 3:

**Table 9.** PCR conditions for Quick Ligation

<u>Temperature</u>	<u>Time</u>
22°C	30 min
20°C	30 min
18°C	30 min
16°C	30 min
14°C	30 min
12°C	30 min
10°C	30 min
8°C	30 min
6°C	30 min

4°C	30 min
4°C	∞

Ligated products were subjected to transformation as described above. The WT *IGF-IR* 3'-UTR luciferase vector was used as a template to create mutated (MUT) *IGF-IR* 3'-UTR luciferase constructs using the Quickchange II XL site-directed mutagenesis kit (Agilent Technologies), primers and PCR conditions listed in Table 4.

**Table 10.** PCR conditions for mutated *IGF-IR* 3'-UTR construction

**MUT *IGF-IR* 3'-UTR Forward**

5'-TAGTCAGTTGACGAAGATCTGGTCAAGAACTAATTAATGTTTCATT-3'

**MUT *IGF-IR* 3'-UTR Reverse**

5'-AATGAAACATTTAATTAGTTCCTTGACCAGATCTTCGTCAACTGACTA-3'

<u>Step</u>	<u>Temperature</u>	<u>Time</u>
1.	95°C	1 min
2.*	95°C	50 sec
	60°C	50 sec
	68°C	6 min
3.	68°C	7 min

\*Step 2 is repeated for a total of 18 cycles

MUT *IGF-IR* 3'-UTR luciferase plasmids were transformed, purified, and verified using the above procedures.

**Luciferase assay** – Luciferase assay was performed with the Dual Glo Luciferase kit (Promega) after cotransfecting R<sup>-</sup> cells with the reporter plasmids containing the wild type or mutated *IGF-IR* 3'-UTR constructs along with control mimic, miR-30a or miR-30d. Cells were washed with sterile PBS, scraped, and plated in a 96 well luminometer plate. Thereafter, the Dual-Glo Reagent (75 µL) was added and incubated for 10 min at room temperature for cell lysis to occur. Firefly luminescence readings were obtained using a

luminometer. Finally, the Dual-Glo Stop & Glo reagent was added in equal volume to original culture media volume and incubated for 10 min at room temperature. Renilla luminescence readings were obtained using the above methods.

**Western blotting** – Cells were collected and lysed using lysis buffer containing 25 mM HEPES (pH 7.7), 400 mM NaCl, 1.5 mM MgCl<sub>2</sub>, 2 mM EDTA, 0.5% Triton X-100, 0.1 mM PMSF, 2 mM DTT, phosphatase inhibitor, and protease inhibitor cocktails (Thermo Scientific). Protein concentrations were measured using Bio-Rad protein assay and OD values were obtained using an ELISA plate reader (Bio-Tek Instruments, Winooski, VT). Proteins (50 µg) were electrophoresed on 8% SDS-PAGE. The proteins were transferred to PVDF membranes and probed with specific primary antibodies and then with appropriate horseradish peroxidase-conjugated secondary antibodies (GE Healthcare, Cardiff, UK). Proteins were detected using chemiluminescence-based kit (Amersham Life Sciences, Arlington Heights, IL).

**Antibodies** – The following antibodies were used: pIGF-IR<sup>Y1131</sup> (3021), pALK<sup>Y1604</sup> (Y664 in NPM-ALK; 3341), pAKT<sup>S473</sup> (4051), integrin  $\alpha$ 5 (4705), and integrin  $\beta$ 1 (9699) (all from Cell Signaling Technology, Danvers, MA); IRS-1 (ab40777) and AKT (ab8805) (Abcam, Cambridge, MA); IGF-IR (396700, Life Technologies, Grand Island, NY); pIRS-1<sup>S639</sup> (sc-22300, Santa Cruz Biotechnology, Santa Cruz, CA); ALK (M719501-2, Dako, Carpinteria, CA); and  $\beta$ -actin (A-5316, Sigma).

**Colony formation assay** – Transfected cells were resuspended to eliminate clumping and then added in a 1:10 (v/v) ratio to 3 mL methylcellulose (MethoCult H4230 (NPM-ALK<sup>+</sup> ALCL cells) or MammoCult 04100 (for MCF-7); Stemcell Technologies) in 15 mL tubes. Tubes were tightly capped, and the mix was gently inverted several times. Then, 1.0 mL of the mix was divided into 24-well plates in triplicates. Plates were placed in a humidified

incubator at 37°C in 5% CO<sub>2</sub> for 7 days and then *p*-iodonitrotetrazolium violet was added for 24 h for staining. Colonies were visualized using AlphaImager system (Santa Clara, CA).

***Cell proliferation assay*** – Cell proliferation was measured using the 5-bromo-2'-deoxyuridine (BrdU) assay kit (ExAlpha, Shirley, MA). Briefly,  $2 \times 10^5$  cells/mL was plated into a 96-well plate. The BrdU label (1:500 dilution) was added, and the plate was incubated for 24 h at 37°C. Cells were fixed for 30 min at room temperature, incubated with anti-BrdU antibody for 1 h after washing, followed by peroxidase goat anti-mouse IgG conjugate (1:2000 dilution) for 30 min. Thereafter, the 3,3',5,5'-tetramethylbenzidine peroxidase substrate was added and incubated for 30 min at room temperature in the dark. Thereafter, the acid Stop Solution was used to stop the reaction and the plate was read at 450 nm using an ELISA plate reader.

***Cell migration assay*** – Cell migration was studied using 24-well transwell plates with polycarbonate membranes (Corning Costar, Tewksbury, MA). Briefly, treated NPM-ALK<sup>+</sup> ALCL cells were serum-starved for 24 hours, then loaded in serum-free RPMI 1640 medium onto the upper compartment. Simultaneously, 500 ng/mL insulin-like growth factor I (IGF-I) (R&D Systems, Minneapolis, MN) was loaded in serum free culture medium onto the lower compartment. For control cells, untransfected cells were incubated with or without IGF-I in the lower compartment. Plates were incubated for 4 h at 37°C, and cells migrating through the membrane into the lower chamber were counted using a particle counter and size analyzer (Coulter).

***5'-aza-cytidine treatment*** –  $1 \times 10^6$  NPM-ALK<sup>+</sup> ALCL cells were plated in 24 well plates. 5 μM 5'-aza-cytidine (Catalog # A2385; Sigma Aldrich) was added to the wells and the plate



was incubated for 5 h. Thereafter, cells were collected by centrifugation (200× *g* for 5 min), washed once with PBS, and subjected to RNA extraction.

**Stable cell lines** – To generate Karpas 299 tamoxifen-inducible stable cells, vectors containing miR-30a (pEGFP/RFP-miR-30a) or miR-30d (pEGFP/RFP-miR-30d) were used (catalog # v-0923, CelluTron, Baltimore, MD). The vector expressing Cre recombinase (pCreER-IRES-Puro) was also used (catalog # v-0924, CelluTron). Karpas 299 cells were transfected with empty vector or miR-30a or miR-30d expression vectors by electroporation (as described above). Forty-eight hours post transfection, 2.5 µg/mL blasticidin was added to culture media and the cells were incubated for 2 weeks. Thereafter, sorting by flow cytometry was performed to isolate the GFP<sup>+</sup> cells, which indicate that the miR vector of interest is present. Furthermore, sorted cells were collected and expanded to become the subsequent “host cell line.” The “host cell lines” were then transfected with the second vector expressing Cre recombinase by electroporation. After 48 h, 0.1 µg/mL puromycin was added for 1 week. Subsequently, stable cells expressing either empty vector or miR along with the Cre recombinase vector were expanded and maintained in media containing 1.5 µg/mL blasticidin and 0.05 µg/mL puromycin. Stable cell lines were first tested *in vitro* using 2 µM 4-hydroxytamoxifen (4-OHT; Sigma Aldrich). Images were obtained using Olympus IX70 microscope (Center Valley, PA).

**In vivo studies** – Mice (SCID/beige, female, 8 weeks old) were purchased from Taconic Biosciences, Inc. (CBSCBG-F, Hudson, NY). Karpas 299 cells ( $2.0 \times 10^6$ ) expressing either empty vector miR-30a or miR-30d were subcutaneously injected into the left flank. On the day of injection, 2 mg/mL 4-OHT (dissolved in ethanol and corn oil in 1:9 ratio) was administered for 21 days by *i.p.* injection. Tumor size was measured every 3 days using Vernier calipers, and tumor burden was calculated using the formula:  $3.14 \times \text{long axis} \times \text{short}$

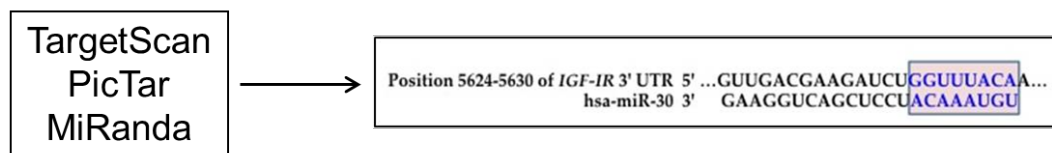
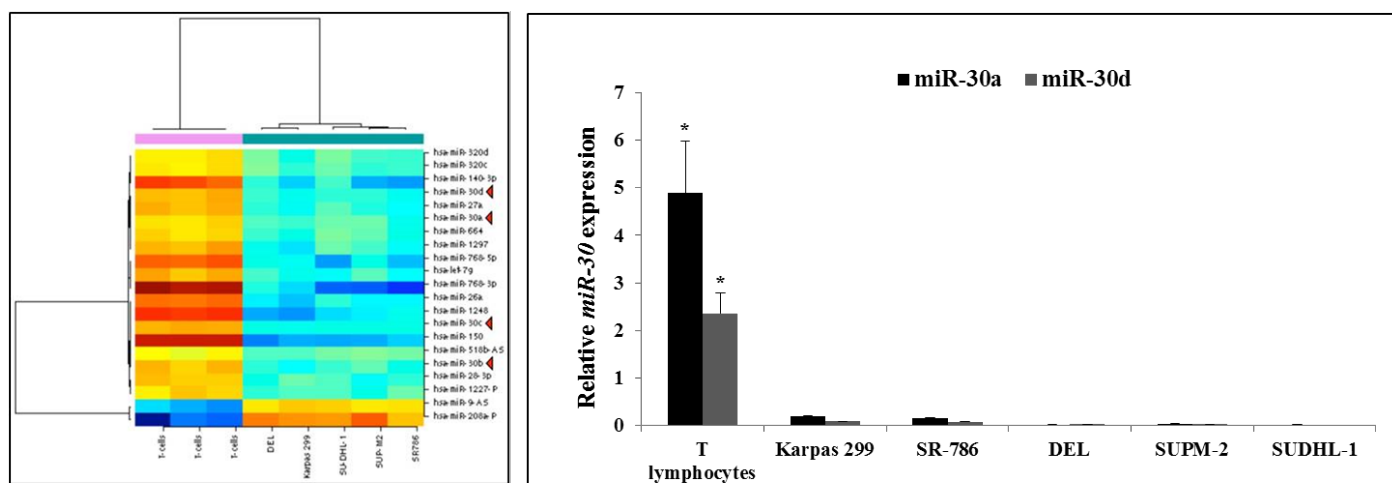
axis<sup>2</sup> × 0.6 cm<sup>3</sup>. Mice were euthanized when tumors reached 1.5 cm. To measure miRNA levels, some were sacrificed at day 21.

***Statistical analysis*** – Statistical analysis was performed using GraphPad Prism software. The student's *t*-test, Tukey's multiple comparisons test, Log Rank Mantel-Cox test, and 2-way ANOVA were used for statistical comparison, whenever appropriate. *P* < 0.05 was considered statistically significant.

### 3.3.2.2. Results

***MiR-30a and miR-30d are downregulated in NPM-ALK<sup>+</sup> ALCL cells:*** To examine whether deregulated miRs exist in NPM-ALK<sup>+</sup> ALCL cells, an miR array analysis was performed using 5 NPM-ALK<sup>+</sup> ALCL cell lines (Karpas 299, SR-786, SUP-M2, SU-DHL-1, DEL) compared to normal human T lymphocytes (Figure 1A). The array generated a list of potentially downregulated or upregulated miRs in NPM-ALK<sup>+</sup> ALCL cells. Because of our interest in IGF-IR, 3 web-based algorithms, TargetScan, PicTar, and miRANDA, were utilized to explore whether any of the highly ranked miRs have potential binding sites with the *IGF-IR* 3'-UTR. We identified that members of the miR-30 family of miRNAs could potentially bind the *IGF-IR* 3'-UTR (**Figure 16A**). Although several members of this family appeared to be deregulated based on the heat map, two of these miRs, miR-30a and miR-30d, appeared with the highest binding probability. The low expression levels of miR-30a and miR-30d, relative to human T lymphocytes, were confirmed by qPCR (**Figure 16A**). Examination of miR-30a and miR-30d expression levels in lymphoid tumors from patients revealed that these miRs were significantly decreased in these tissues compared to normal lymph nodes ( $P < 0.0001$ , **Figure 16B**).

A.



B.

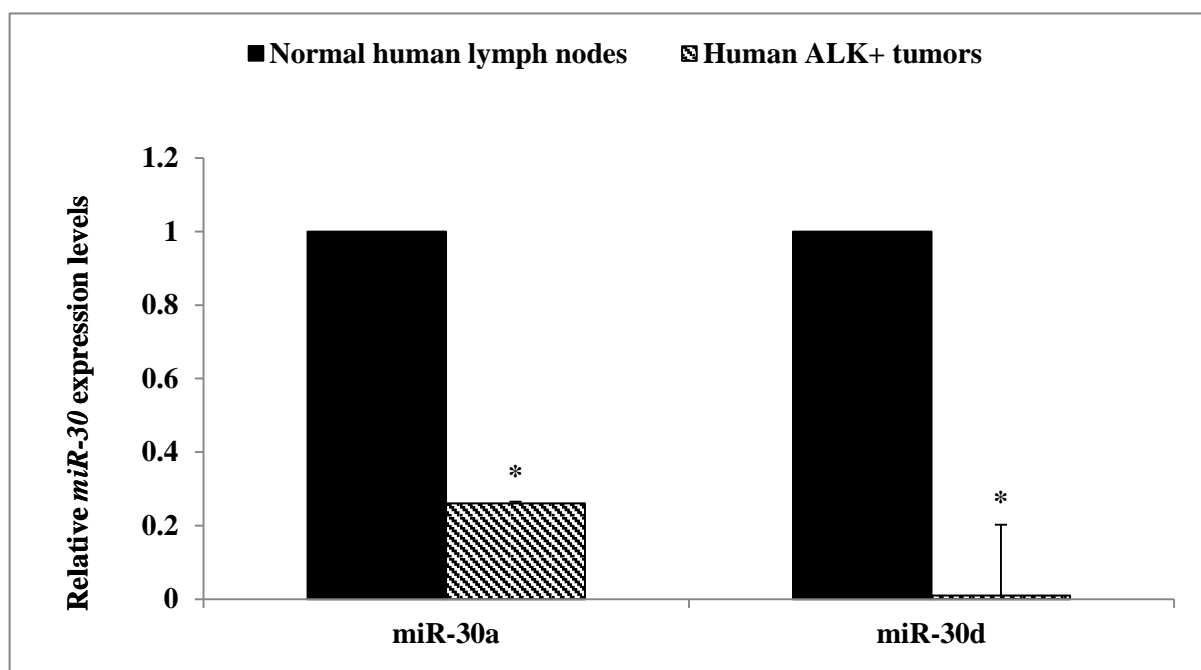


**FIGURE 16. Array analysis of differential expression of miR in NPM-ALK<sup>+</sup> ALCL cell lines vs. normal human T lymphocytes.** (A) MicroRNA array analysis identified numerous miR to be downregulated (green/blue) or upregulated (yellow/orange/red) in NPM-ALK<sup>+</sup> ALCL cell lines vs. normal human T lymphocytes. Because of our interest in whether any of these miRs is involved in the regulation of IGF-IR expression, we used the web based algorithms, TargetScan, MiRanda, and PicTar, to identify miRs with the potential to bind the 3'-UTR of *IGF-IR*. These algorithms predicted members of miR-30 family to bind with 3'-UTR-*IGF-IR* (> 0.9). We focused on miR-30a and miR-30d because they demonstrated the highest differential expression. The algorithms also proposed the potential binding sites of miR-30a and miR-30d within the *IGF-IR* 3'-UTR (bottom panel). According to the miR array, these miR are markedly downregulated in the lymphoma cell lines than the normal human T-cell (upper left panel). Decreased expression of these miR was further confirmed by qPCR (upper right panel) (T lymphocytes vs. NPM-ALK<sup>+</sup> ALCL cell lines: \* = p<0.00005). (B) qPCR also shows that miR-30a and miR-30d are significantly downregulated in FFPE tumor tissues from ALK<sup>+</sup> ALCL patients compared to normal lymph nodes (\* = p<0.05).

***MiR-30a and miR-30d bind IGF-IR 3'-UTR and decrease IGF-IR protein, but not IGF-IR mRNA levels:*** We explored whether miR-30a and miR-30d possess the ability to bind and regulate *IGF-IR* 3'-UTR by performing a luciferase assay using a wild type *IGF-IR* 3'-UTR luciferase construct along with control, miR-30a or miR-30d mimics transfected into R<sup>-</sup> cells, which lack the expression of IGF-IR. Simultaneously, a luciferase assay using mutated *IGF-IR* 3'-UTR luciferase construct lacking binding domains to miR-30a and miR-30d was performed after transfection of control or miR mimics. MiR-30a and miR-30d, but not the control mimic, decreased the luciferase activity of wild type *IGF-IR* 3'-UTR. Furthermore, changes were not observed in the luciferase activity of the mutated *IGF-IR* 3'-UTR. These findings suggest that miR-30a and miR-30d bind and negatively regulate *IGF-IR* 3'-UTR (**Figure 17**). Next, the effects of miR-30a and miR-30d on endogenously expressed IGF-IR were examined by transfecting Karpas 299 and DEL cells with either control, miR-30a or miR-30d mimic and then measuring IGF-IR protein and mRNA levels by Western blotting and qPCR, respectively (**Figure 18**). Although miR-30a and miR-30d significantly decreased IGF-IR protein, they failed to decrease *IGF-IR* mRNA, suggesting that these miRs induce negative regulation of IGF-IR expression posttranscriptionally (**Figure 18**). We further examined the phosphorylation levels of IGF-IR and its important downstream signaling targets. Transfection of miR-30a and miR-30d was associated with decreased pIGF-IR<sup>Tyr1131</sup>, and also decreased pIRS-1<sup>Ser639</sup> and pAKT<sup>Ser473</sup> levels, with no changes in total IRS-1 and AKT. It has been previously demonstrated that IRS-1 and AKT are downstream targets of IGF-IR signaling. MiR-30a and miR-30d also decreased pNPM-ALK<sup>Tyr664</sup> expression levels. This finding is consistent with our previous observations that IGF-IR functions to maintain the phosphorylation of NPM-ALK [128]. In addition, miR-30a and miR-30d also decreased total NPM-ALK protein expression. We have previously demonstrated that IGF-IR is able to

maintain NPM-ALK protein stability [127]. However, to rule out that these 2 miRs have direct inhibitory effects on NPM-ALK, we searched the web-based miR target prediction algorithms, and found that NPM-ALK does not represent a target of miR-30a or miR-30d. These findings provide strong evidence to support that the decrease in total NPM-ALK expression levels resulted from the decrease in IGF-IR and its effects on promoting the stability of NPM-ALK protein. Finally, miR-30a and miR-30d decreased the expression of important proteins involved in cell migration and adhesion and known to contribute to IGF-IR oncogenic effects, namely integrin  $\alpha 5/\beta 1$ .

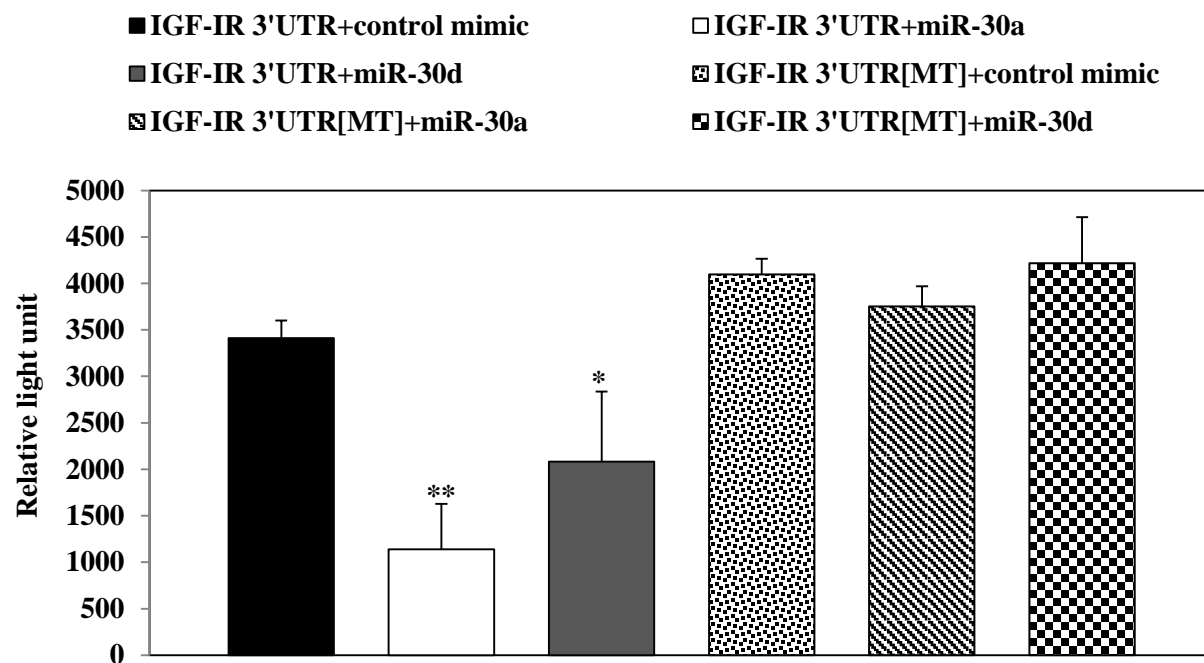




**FIGURE 17. MiR-30a and miR-30d decrease *IGF-IR-3'*-UTR activity.** A luciferase assay in R<sup>-</sup> cells transfected with wild type *IGF-IR* 3'-UTR luciferase reporter construct along with control mimic, miR-30a or miR-30d mimics revealed that miR-30a and miR-30d can bind and regulate *IGF-IR* 3'-UTR. In contrast, R<sup>-</sup> cells transfected with control mimic or mutated [MT] *IGF-IR* 3'-UTR failed to show similar decrease in *IGF-IR* 3'-UTR activity (\*: p<0.05; \*\*: p<0.001). The results are shown as means ± SD of 3 consistent experiments.

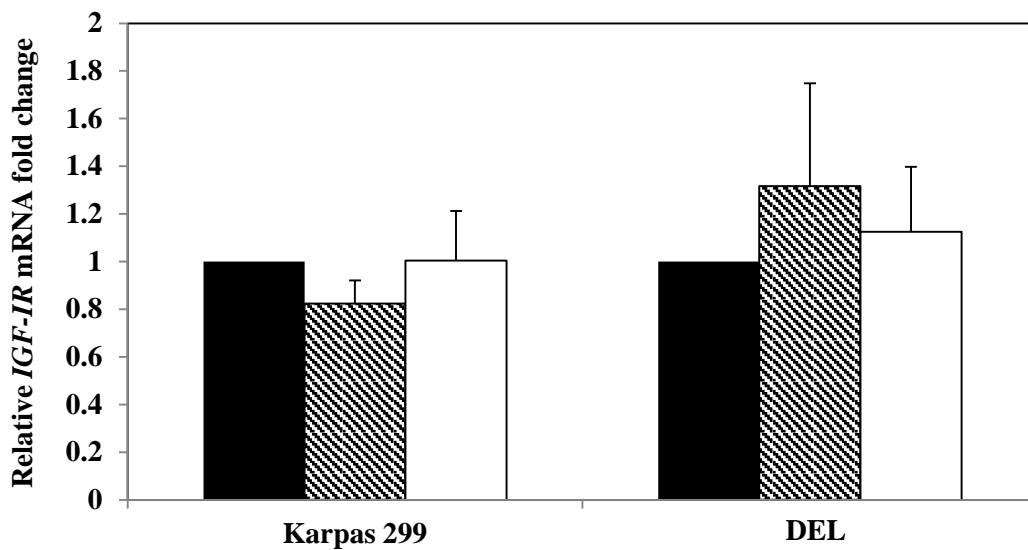
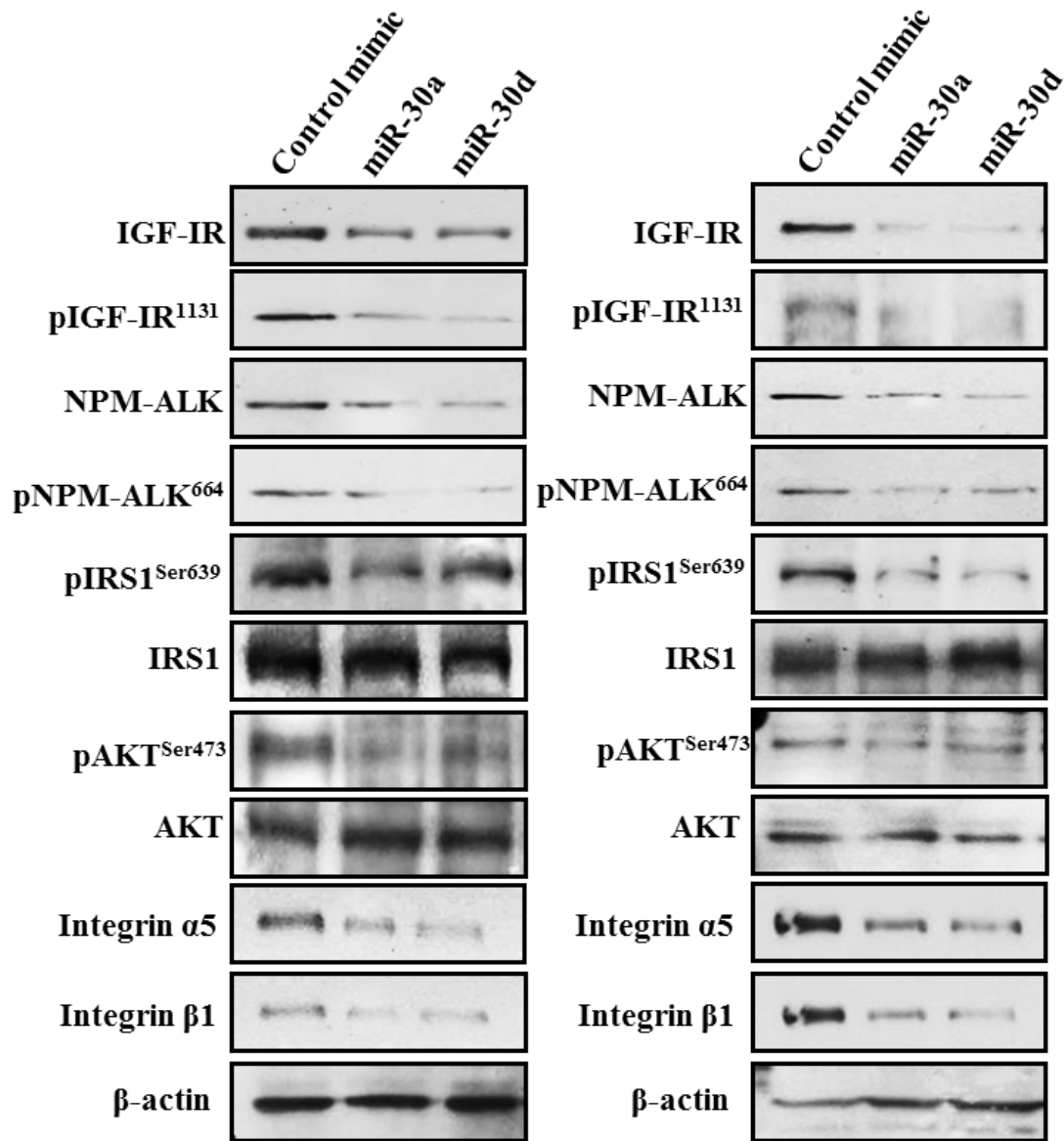
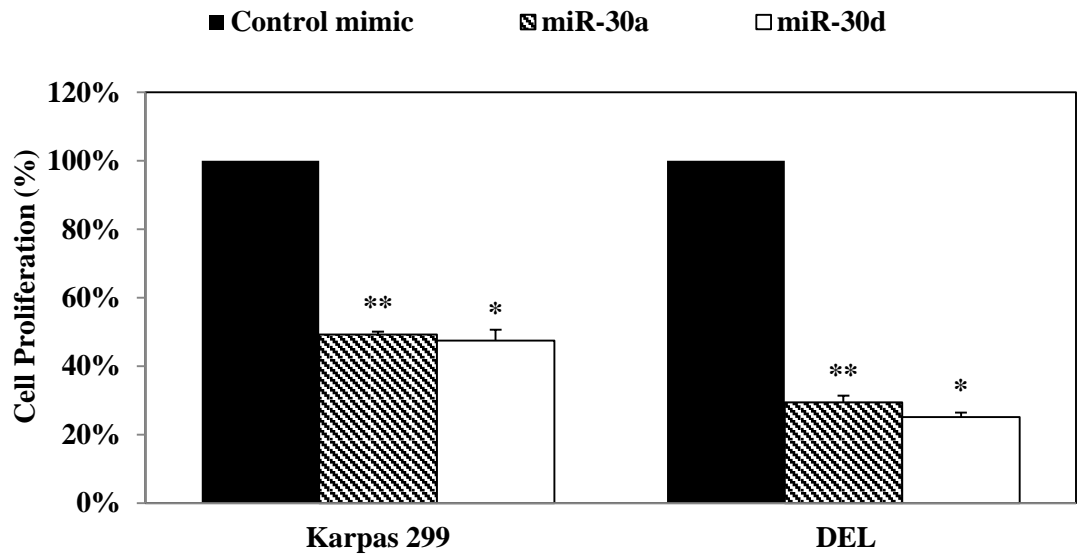


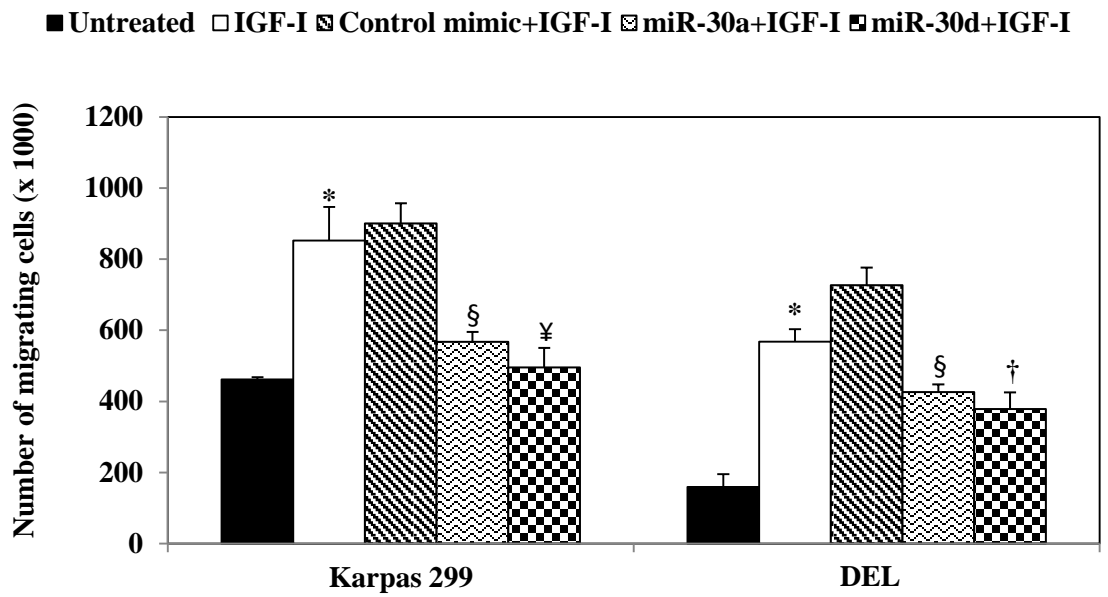
**FIGURE 18. MiR-30a and miR-30d decrease IGF-IR protein expression, but not *IGF-IR* mRNA expression.** Forced expression of control mimic, miR-30a or miR-30d mimics in Karpas 299 and DEL cell lines induced marked downregulation of IGF-IR protein (upper panel), but not *IGF-IR* mRNA (lower panel), indicating that these miRs regulate IGF-IR expression posttranscriptionally. The results are shown as means  $\pm$  SD of 3 consistent experiments. In addition, there were significant decreases in pIGF-IR<sup>Tyr1131</sup>, pNPM-ALK<sup>Tyr664</sup>, pIRS-1<sup>Ser639</sup>, and pAKT<sup>Ser473</sup> without any changes in total IRS-1 or total AKT. In contrast, the basal levels of NPM-ALK were significantly reduced, which is in agreement with our previous findings that IGF-IR sustains the stability of NPM-ALK protein. Furthermore, there was significant decrease in the tumor cell invasion-related proteins, integrins  $\alpha 5/\beta 1$ . To our knowledge, which was further supported by searching the web-based miR prediction search algorithms, integrins  $\alpha 5/\beta 1$  are not potential direct targets of miR-30a or miR-30d, and therefore their downregulation most likely resulted from IGF-IR downregulation.

*MiR-30a and miR-30d decrease cell proliferation, migration, and anchorage-independent colony formation potential of NPM-ALK<sup>+</sup> ALCL cells:* Thereafter, we proceeded to test the impact of miR-30a and miR-30d-mediated downregulation of IGF-IR on the neoplastic potential of NPM-ALK<sup>+</sup> ALCL. Transfection of Karpas 299 and DEL with either miR-30a or miR-30d significantly decreased lymphoma cell proliferation (**Figure 19A**), migration in response to IGF-I (**Figure 19B**), and anchorage-independent colony formation potential. Similar effects were not observed in control cells transfected with control mimic (**Figure 19C**).

A.



B.



C.

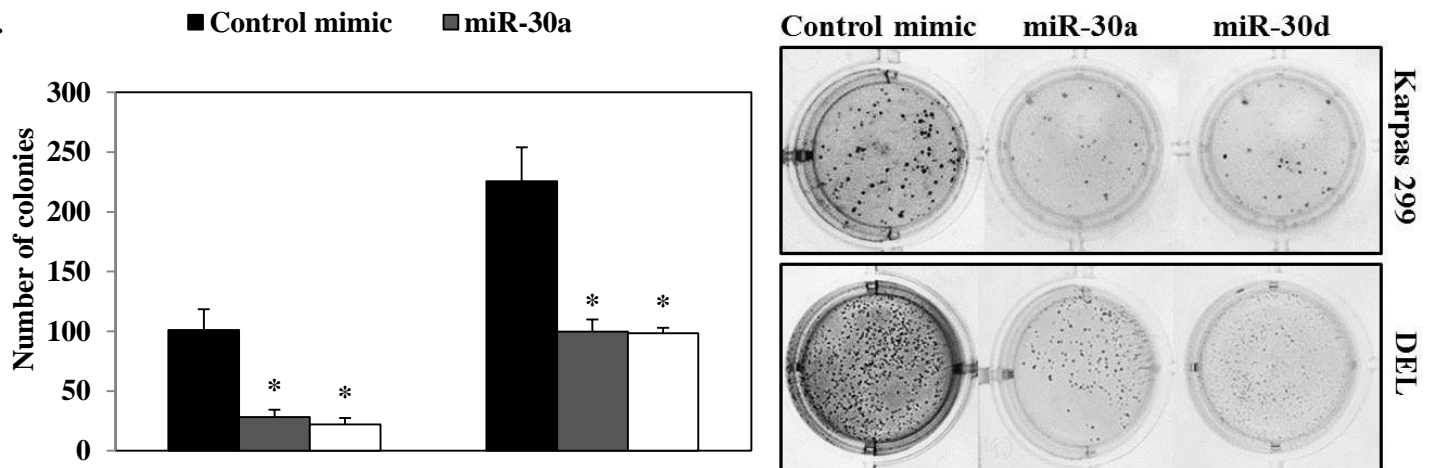


**FIGURE 4. MiR-30a and miR-30d decrease cell proliferation, migration, and colony formation potential in NPM-ALK<sup>+</sup> ALCL cells.** (A) Transfection of Karpas 299 and DEL cells with miR-30a or miR-30d, but not control mimic, resulted in significant decrease in the proliferation of these cells after 48 h. (B) In addition, miR-30a and miR-30d decreased significantly the migration of the lymphoma cells in response to IGF-I (500 ng/mL). (C) The 2 miRs abrogated Karpas 299 and DEL cell colony forming potential. The number of colonies is shown on the left and representative images are shown on the right. \*: p<0.05; \*\*: p<0.001; §: control mimic vs. miR-30a [p<0.05]; ¥: control mimic vs. miR-30d (p<0.05); †: control mimic vs. miR-30d (p<0.001). The results are shown as means ± SD of 3 consistent experiments.

*Methylation contributes to downregulation of miR-30a and miR-30d expression in NPM-ALK<sup>+</sup> ALCL:* At this point, we sought to define the mechanisms that could lead to downregulation of miR-30a and miR-30d expression in NPM-ALK<sup>+</sup> ALCL. To determine whether the decrease in miR-30a and miR-30d was due to effects elicited by NPM-ALK, Karpas 299 and DEL cells were transfected with scrambled siRNA or ALK siRNA for various time points, and miR-30a and miR-30d levels were measured by qPCR. Even after sufficient knockdown of NPM-ALK, there were no significant changes in miR expression, suggesting that NPM-ALK most likely does not induce the decrease in miR-30a and miR-30d (data not shown).

Several miRs have been previously shown to be decreased in cancer cells due to epigenetic events, such as methylation of their gene promoters [187]. To test whether methylation is suppressing expression of miR-30a and miR-30d in NPM-ALK<sup>+</sup> ALCL, Karpas 299 and SUP-M2 cells were treated with the demethylating agent 5'-azacytidine (5'-aza) for 48 h and levels of miR-30a and miR-30d were measured by qPCR (**Figure 20**). 5'-aza significantly increased miR-30a by 2, 2, and 3-fold in Karpas 299, DEL, and SUP-M2, respectively. In addition, 5'-aza increased miR-30d by 2.5, 2, and 4-fold in Karpas 299, DEL, and SUP-M2, respectively. These results suggest that methylation could represent one possible mechanism underlying decreased expression of miR-30a and miR-30d in NPM-ALK<sup>+</sup> ALCL.

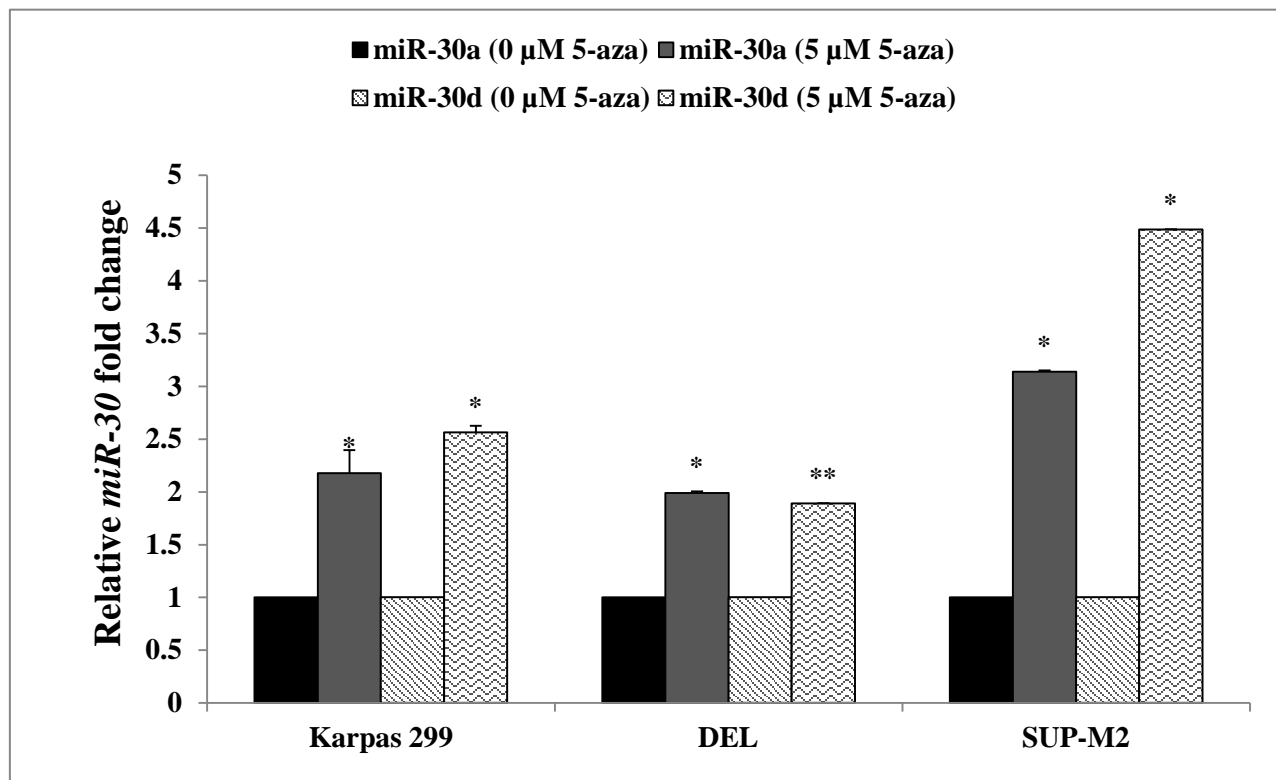




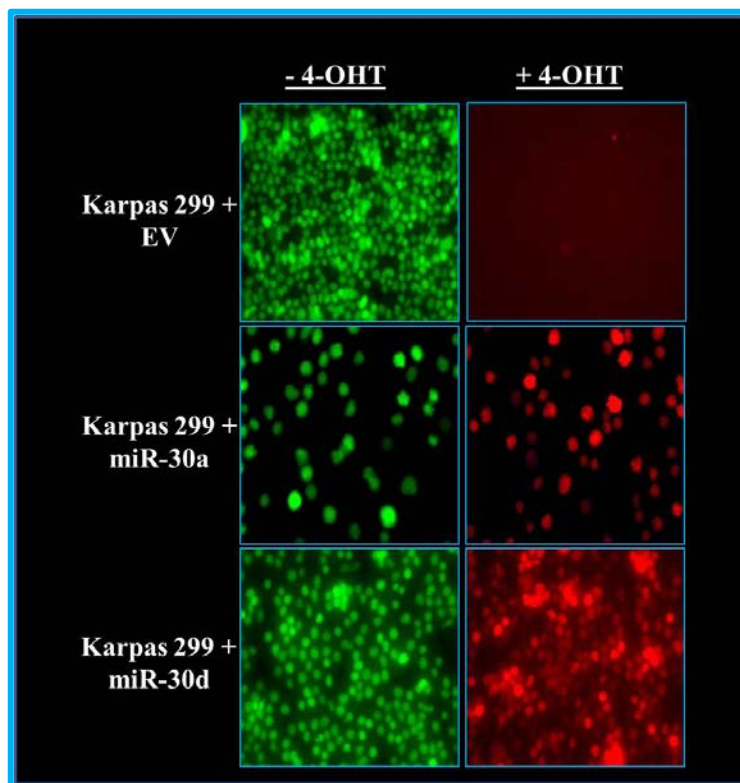
**FIGURE 20. 5'-aza increases miR-30a and miR-30d expression in NPM-ALK<sup>+</sup> ALCL cells.** Treatment of Karpas 299, DEL, and SUP-M2 with the demethylating agent 5'-azacytidine (5  $\mu$ M for 48 h) resulted in increased miR-30a (2 fold, 2 fold, and 3 fold for Karpas 299, DEL, and SUP-M2, respectively) and miR-30d expression (2.5 fold, 2 fold, and 4 fold for Karpas 299, DEL, and SUP-M2, respectively) (\* =  $p < 0.05$ , \*\* =  $p < 0.001$ ). The results are shown as means  $\pm$  SE of 3 consistent experiments.

***MiR-30a and miR-30d suppress NPM-ALK<sup>+</sup> ALCL tumor progression in mice:*** Tamoxifen-inducible stable cell line variants of Karpas 299 cells that express EV, miR-30a or miR-30d were developed to test the effect of miR-30a and miR-30d on NPM-ALK<sup>+</sup> ALCL *in vivo*. To create these cell lines, a vector containing miR-30a or miR-30d juxtaposed to a red fluorescent protein (RFP) coding sequence, was obtained. The vector also contained a green fluorescent protein (GFP), which is flanked by lox P sites. The miR expressing vectors were sequentially transfected with a second plasmid encoding Cre recombinase. With the treatment of 4-hydroxy tamoxifen (4-OHT), the Cre recombinase was activated, which resulted in excision of "floxed" GFP and the termination sequence allowing RFP and miR to be expressed. *Ex vivo* analysis revealed that miR-30a and miR-30d were stably expressed, as indicated by expression of RFP after the cells were treated with 4-OHT for 48 h, compared to untreated cells that still showed GFP expression (**Figure 21**). In addition, cells transfected with EV showed only GFP expression.

Stable cell lines expressing EV, miR-30a or miR-30d were subcutaneously injected into 3 different groups of SCID/beige mice. On the day of injection, 2 mg/mL 4-OHT was administered i.p. to induce the expression of the miRs, and thereafter was administered daily for 21 days to maintain the expression of miRs (**Figure 22**). Importantly, during the course of administration of 4-OHT, mice in which miRs were induced displayed much slower tumor establishment rate compared to control mice. By day 21, all of the mice in the control group had already been euthanized, whereas all of the mice from the miR-30a and miR-30d groups were alive. To measure miR levels after induction, some mice from the miR groups were sacrificed at day 21. The level of expression of miR-30a and miR-30d were also measured in tumors from control mice with lack of induction of miR. The remaining mice in were monitored past day 21 without 4-OHT administration. After cessation of miR induction at

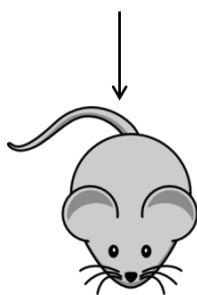
day 21, tumors present in mice with activated miR-30a and miR-30d slowly began to increase in size, although never reached the size of the control group. Furthermore, we noticed that miR-30a and miR-30d groups of mice had much smaller tumors that were more localized to the injection site relative to the control group (**Figure 22A**). Control mice, in contrast, displayed larger tumors that were sometimes disseminated and spread to the dorsal areas away from the injection site (**Figure 22B**). Measurement of miR-30a and miR-30d in mouse tumors revealed both miRs to be decreased in control mice, but demonstrated high expression in tumors from miR-induced mice. Furthermore, miR seemed to be continually expressed at low levels after stopping 4-OHT treatment, which may account for the fact that these tumors only gradually increased in size after 4-OHT cessation (**Figure 23**).

A.



B.

2 x 10<sup>6</sup> cells injected subcutaneously;  
administer 4-OHT (2mg/mL), once a day  
i.p.



Monitor tumor burden for 21+ days; measure tumor every 3 days

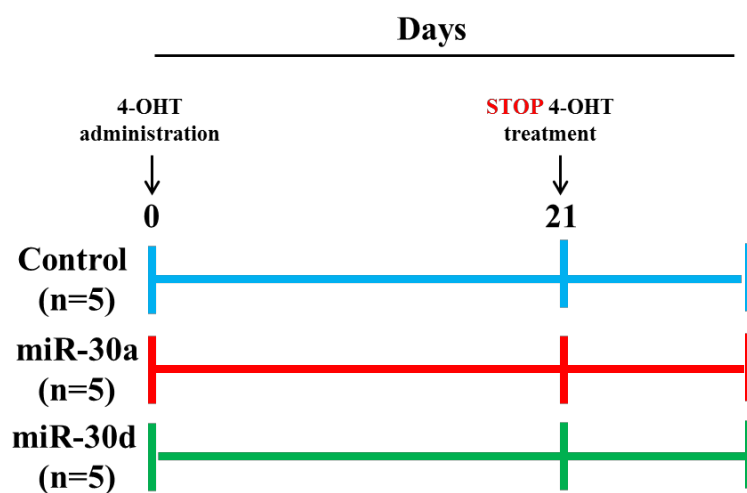
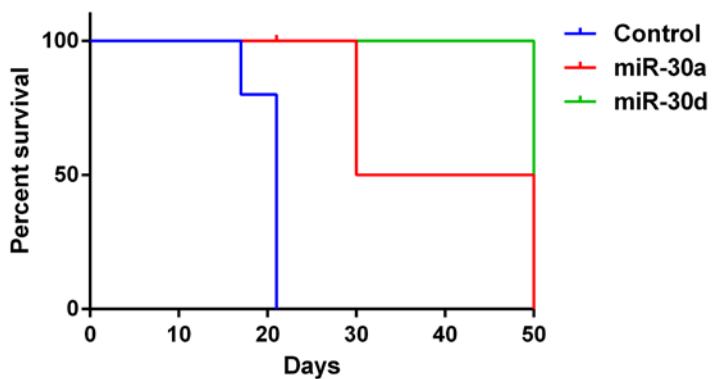
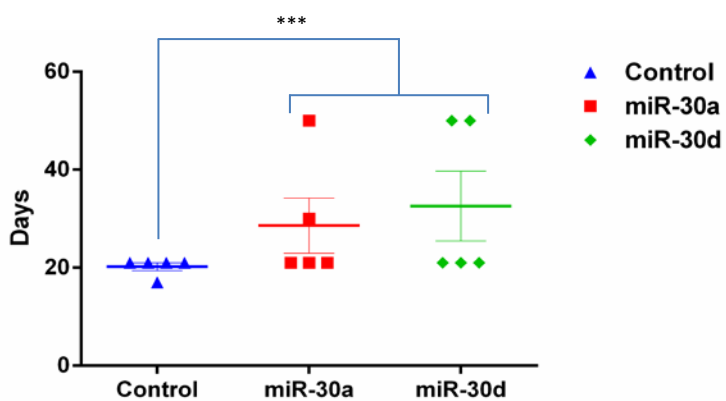
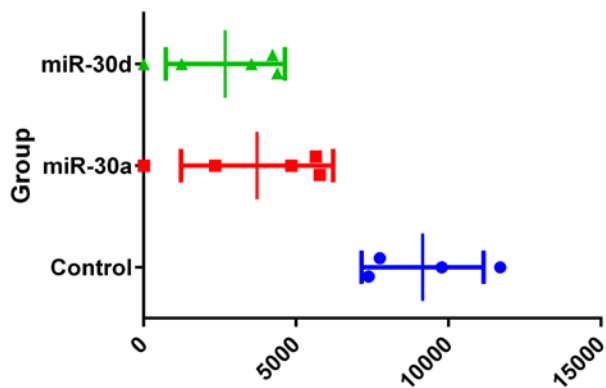
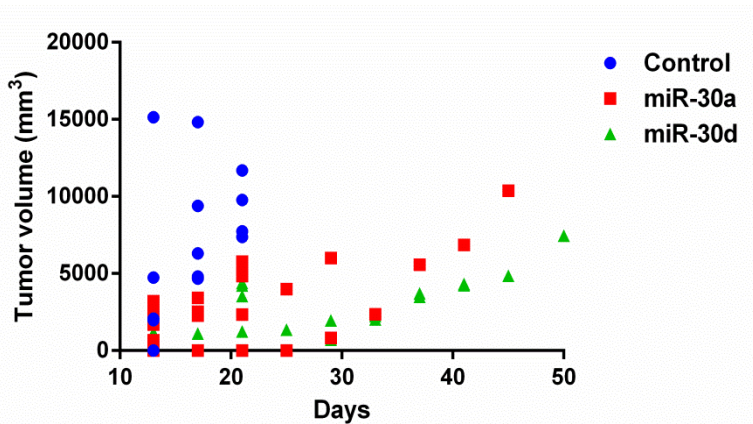


**FIGURE 21. Inducible miR-30a and miR-30d mouse model.** (A) Stable Karpas 299 cell lines were tested *ex vivo* before utilizing in mice. 4-OHT was added to Karpas 299 cells expressing EV, miR-30a (pEGFP/RFP-miR-30a/pCreER-IRES-Puro) or miR-30d (pEGFP/RFP-miR-30d/pCreER-IRES-Puro) for 48 h. Fluorescent microscopy revealed conversion of GFP to RFP in cells transfected with miR-30a or miR-30d, indicating expression of miRs, whereas cells expressing EV had no RFP signal, and thereby lack miR. (B) Mice experiments scheme illustrating that 8-week old female SCID/beige mice were injected s.c. with  $2 \times 10^6$  Karpas 299 cells expressing EV, miR-30a or miR-30d. In miR-30a and miR-30d groups, 4-OHT (2 mg/mL) was administered i.p. once daily and tumor burden was measured every 3 days up to 21 days. After stopping 4-OHT at 21 days, some mice were sacrificed to measure miRs levels in the tumors and the remainder observed until euthanized.

A.



B.

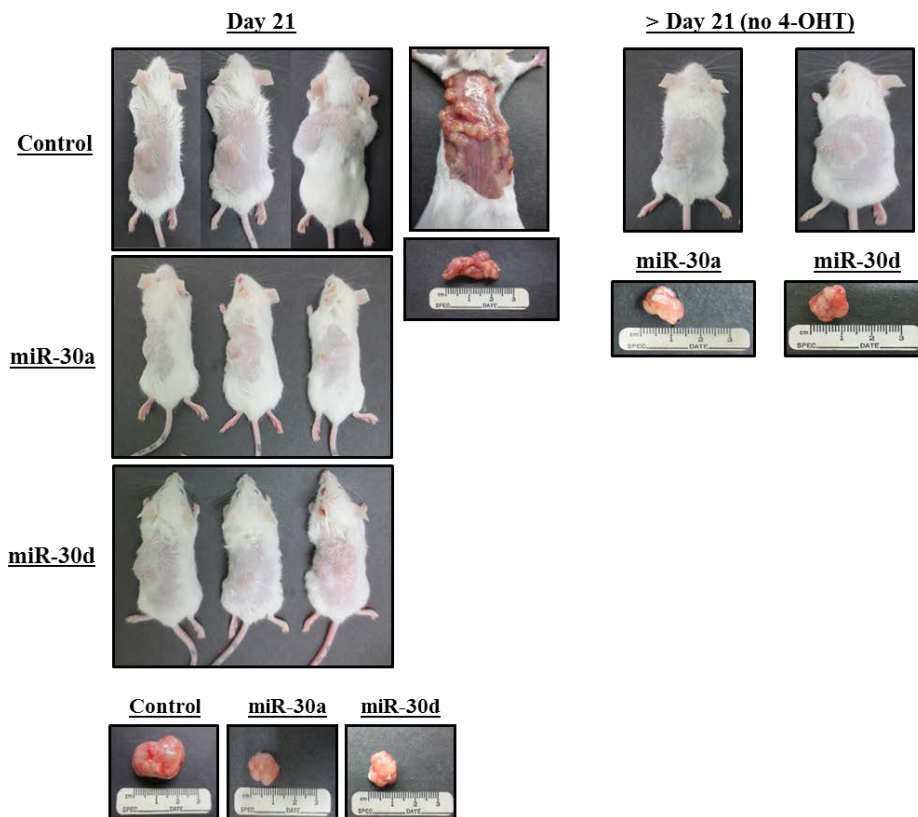


**FIGURE 22. MiR-30a and miR-30d suppress NPM-ALK<sup>+</sup> ALCL tumor growth *in vivo*.** (A) *Upper left panel*; during administration of 4-OHT, mice in which miR-30a or miR-30d was activated developed tumors substantially slower than the control mice. More importantly, all control mice had been euthanized due to excessive tumor burden at day 21 or before, whereas no mice from the miR-30a or miR-30d groups required to be euthanized during this period. By day 29, tumor burden in miR-30a or miR-30d groups began to gradually increase although for most of the tumors over 50 days their size was still considerably less than control group tumors (overall tumor volume significance over 50 days: control vs. miR-30;  $p=0.0004$ ) *Upper right panel*; day 21 tumor volume only ( $*= p < 0.05$ ); *Lower panel*; survival for miR-30a and miR-30d groups of mice was significantly longer relative to control groups ( $***= p=0.0006$ ). (B) Representative images at day 21 (with 4-OHT) or > day 21 (no 4-OHT). Control mice displayed larger tumors, including one mouse that displayed disseminated tumors (example shown; all tumors from this example are shown as tumor aggregate below image), whereas mice from miR-30a and miR-30d groups at 21 days displayed tumors that were smaller and localized to the site of injection. Although the mice in the miR-30 groups in which 4-OHT treatment was stopped displayed slightly larger tumors after 21 days, the tumor volume was still considerable less compared to controls.

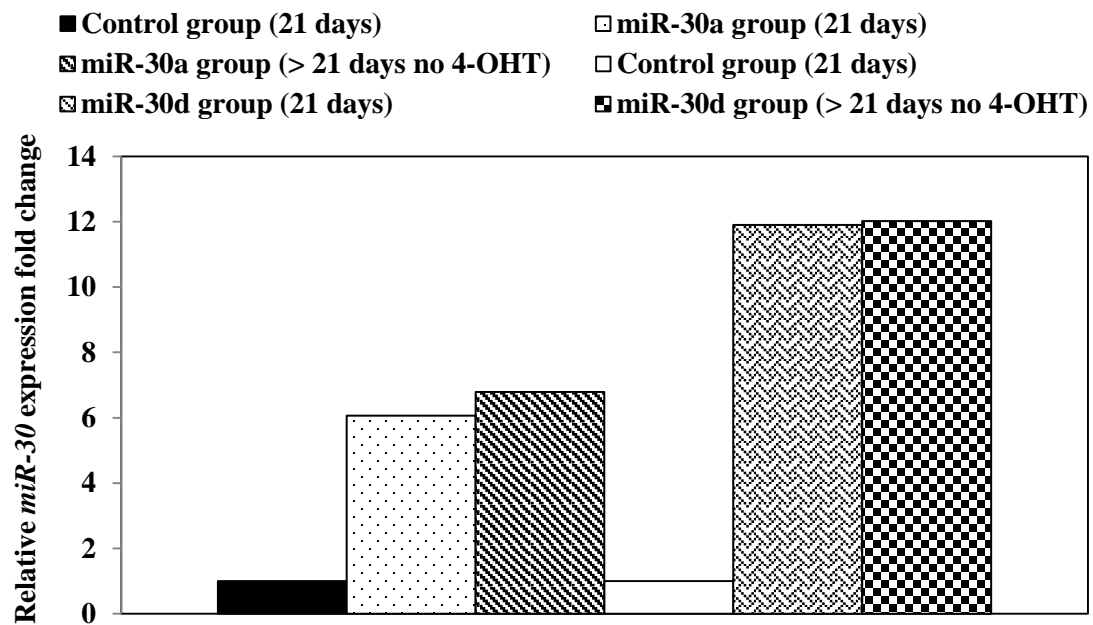




**FIGURE 23. Adequate induction of miR-30a and miR-30d expression by administration of 4-OHT in mice.** miR-30a and miR-30d expression levels increased in tumors from mice administrated 4-OHT for 21 days. High levels of miRs expression continued even after cessation of 4-OHT, perhaps indicating that induction of miRs led to persistent expression in the system.

### **3.3.3. Posttranscriptional Regulation of IGF-IR: mRNA Stability**

### 3.3.3.1 Materials and Methods

**Cell lines** – Five NPM-ALK<sup>+</sup> ALCL cell lines were used: Karpas 299, DEL, SUP-M2, SR-786, and SU-DHL-1 (DSMZ, Germany). Normal T lymphocytes were purchased from StemCell Technologies (Catalog # 70024, Vancouver, British Columbia). Lymphoma cell lines and normal T lymphocytes were maintained in RPMI 1640 medium (HyClone, South Logan, UT) supplemented with 10% FBS (Sigma, St. Louis, MO), glutamine (2 mM), penicillin (100 U/ml), and streptomycin (100 µg/ml) at 37°C in a humidified 5% CO<sub>2</sub> in air chamber.

**Actinomycin D treatment** – Briefly, actinomycin D (Sigma) was dissolved in DMSO (final concentration: 1 mg/mL). Human T lymphocytes or NPM-ALK<sup>+</sup> ALCL cell lines were treated with 1 µM actinomycin D and samples were collected at 0, 0.5, 1, 2, 4, and 8 h.

**RNA extraction, cDNA synthesis and absolute quantitative real time PCR (qPCR)** – Total RNA was isolated and purified using RNeasy Mini Kit (Qiagen, Valencia, CA). Briefly,  $2 \times 10^6$  cells were collected by centrifugation at 200× g for 5 min, washed twice in sterile PBS, and subjected to lysis and homogenization in RLT buffer using QiaShredder spin columns. Homogenized cells were resuspended in an equal volume of 70% ethanol and passed through provided spin columns. Two additional washing steps were performed with appropriate buffers: Buffer RW1 and Buffer RPE. Total RNA was collected upon elution with RNase-free water. Optical density readings were detected using Nanodrop (Thermo Scientific).

cDNA synthesis was performed through a two-step procedure using Superscript III RT protocol (Invitrogen, Carlsbad, CA). Approximately 0.3 µg total RNA was used for reverse transcription. First, total RNA, oligo (dT), and dNTP mix were added to a mixture that was

adjusted to a final volume of 10  $\mu\text{L}$  with Rnase-free water. RNA mixture and primer was denatured by incubating at 65°C for 5 min and then placed on ice. Second, a master reaction mix consisting of 10 $\times$  cDNA synthesis buffer, 0.1 DTT, RNaseOUT, SuperscriptIII RT,  $\text{MgCl}_2$ , and RNase-free water was prepared on ice and vortexed gently. Approximately 10  $\mu\text{L}$  of reaction mix was pipetted into each reaction tube on ice bringing the final volume to 20  $\mu\text{L}$ . The samples were then transferred to a thermal cycler preheated to the appropriate cDNA synthesis temperature and incubated for 60 min at 50°C, then terminated at 85°C for 5 min. 1  $\mu\text{L}$  of RNase H was added and samples were incubated at 37°C for 20 min to remove template RNA.

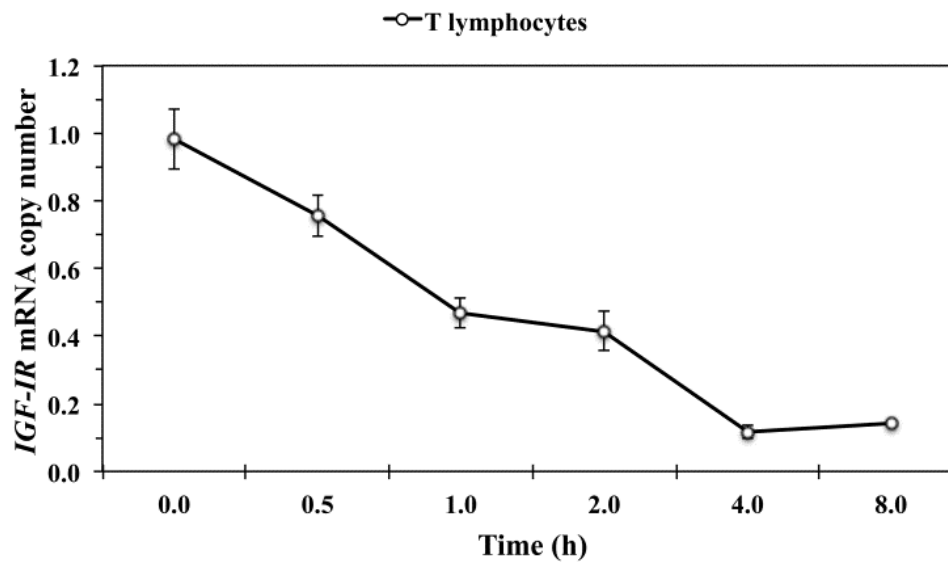
Absolute Quantitation real-time PCR was used to examine levels of *IGF-IR* mRNA in NPM-ALK<sup>+</sup> ALCL cell lines and normal T lymphocytes in a 25  $\mu\text{L}$  reaction using 1  $\mu\text{L}$  of the reverse transcribed cDNA, 20 $\times$  *IGF-IR* copy number primer/probe, and Taqman Genotyping Mastermix (Applied Biosystems). The primer/probe sets used were obtained from Applied Biosystems (sequences not provided). To create a standard curve, serial ten-fold dilutions (30, 300, 3000, 30,000, 300,000 copies) of an IGF-IR plasmid [128] were used.

### 3.3.3.2. Results

#### ***Rate of IGF-IR mRNA decay in ALK<sup>+</sup> ALCL cell lines and normal human T lymphocytes:***

Consistent with our previously published results [128], basal levels of *IGF-IR* were much higher in the NPM-ALK<sup>+</sup> ALCL cell lines than in the normal human T lymphocytes (**Figure 24A, 24B**). In T lymphocytes, *IGF-IR* mRNA decreased to 50% of its basal levels at 0.8 h (Fig. 1A). The decay of *IGF-IR* mRNA varied among the 5 different NPM-ALK<sup>+</sup> ALCL cell lines, yet it consistently occurred at a more prolonged rate than T lymphocytes (**Figure 24B**), decreasing to 50% of the basal *IGF-IR* mRNA at  $2.62 \pm 0.4$  h (mean  $\pm$  SE).

A



B

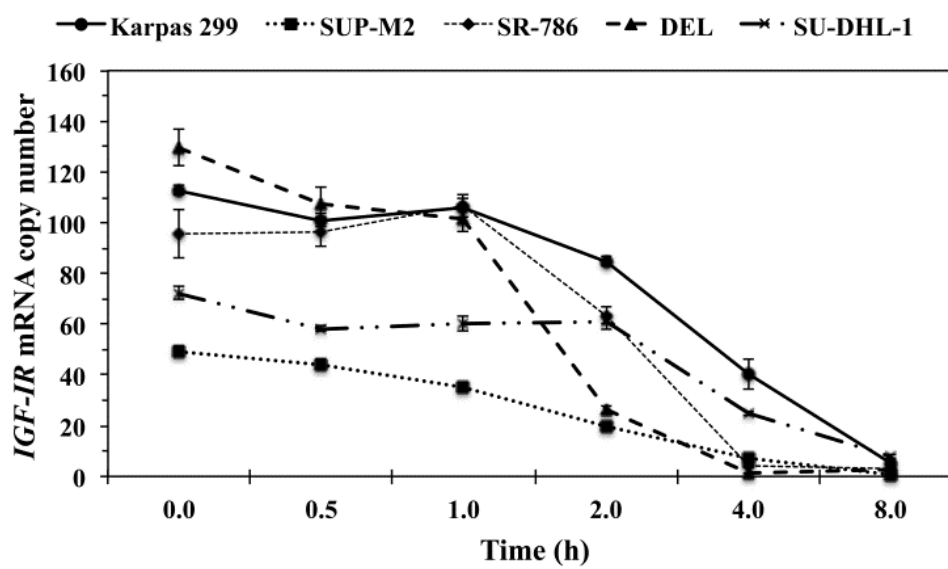


**FIGURE 24. *IGF-IR* mRNA expressed in NPM-ALK<sup>+</sup> ALCL cells exhibits prolonged decay time compared with *IGF-IR* mRNA from normal human T lymphocytes.** (A) The 50% level of *IGF-IR* mRNA was detected at 0.8 h in normal human T lymphocytes. (B) In contrast with T lymphocytes, the NPM-ALK<sup>+</sup> ALCL cell lines expressed remarkably higher basal levels of *IGF-IR* mRNA, with DEL and SUP-M2 cells demonstrating the highest and lowest levels, respectively. The 50% *IGF-IR* mRNA level was achieved after longer periods of time in the lymphoma cells than in normal T lymphocytes (SU-DHL-1: 3.7 h, Karpas 299: 3.4 h, SR-786: 2.6 h, SUP-M2: 1.9 h, DEL: 1.5 h). The mean of the *IGF-IR* mRNA decay time in the lymphoma cells was  $2.62 \pm 0.4$  h (SE). Results shown represent the means  $\pm$  SE of 3 experiments.

### 3.4. Discussion for Aim 2

In this aim, we identified deregulated posttranscriptional mechanisms that could contribute to the pathogenesis of NPM-ALK<sup>+</sup> ALCL. First, we identified miR-30a and miR-30d as potential regulators of IGF-IR expression at the posttranscriptional stage. Relative to normal T lymphocytes and reactive human lymphoid tissues, miR-30a and miR-30d were significantly decreased in the NPM-ALK<sup>+</sup> ALCL cell lines and tissues from lymphoma patients. Binding of miR-30a and miR-30d to respective binding sites located within the *IGF-IR* 3'-UTR decreased substantially the activity of the *IGF-IR* 3'-UTR. Furthermore, both miRs decreased IGF-IR protein levels but not *IGF-IR* mRNA levels, suggesting that these miRs do not cleave *IGF-IR* mRNA, but inhibit IGF-IR translation. Downregulation of IGF-IR by miR-30a and miR-30d resulted in decreased phosphorylation of several important IGF-IR interacting proteins and induced reduction in cell proliferation, migration, and colony formation. Treatment with the demethylating agent, 5'-aza-cytidine, was associated with increased miR-30a and miR-30d levels in NPM-ALK<sup>+</sup> ALCL cell lines, alluding to the possibility that these miRs are suppressed by epigenetic silencing. Importantly, the 2 miRs hindered NPM-ALK<sup>+</sup> ALCL tumor growth in immune-compromised mice. These results suggest that miR-30a and miR-30d can negatively regulate the progression of NPM-ALK<sup>+</sup> ALCL. At the posttranscriptional level, we also determined that *IGF-IR* mRNA turnover was considerably slower in the NPM-ALK<sup>+</sup> ALCL cells compared with normal T lymphocytes.

When we measured the expression levels of miR-30a and miR-30d, both miRNAs were significantly decreased in the NPM-ALK<sup>+</sup> ALCL cell lines and patient tumors compared to normal T lymphocytes and reactive lymph nodes. To the best of our knowledge, the gene from which miR-30a and miR-30d are transcribed has not been identified, and therefore, this proved to be a limitation for us to further investigate how the expression of these miRs is



negatively regulated. Nonetheless, there have been reports showing that certain oncogenes can directly inhibit the expression of miRs [188-192]. Thus, we sought to examine whether the key oncogene in NPM-ALK<sup>+</sup> ALCL, namely NPM-ALK, is involved in the suppression of miR-30a and miR-30d. Effective targeting NPM-ALK by siRNA did not result in increased expression of either miR-30a or miR-30d, suggesting that NPM-ALK is not contributing to downregulation of miR-30a and miR-30d expression (data not shown). However, there have been a variety of other mechanisms proposed for the deregulation of miRs in cancer such as epigenetic silencing [187]. A large proportion of tumor suppressor miRs are located within CpG islands, and therefore, are prone to DNA hypermethylation, as in the case of miR-127, miR-9-1, miR-34b/c cluster, and the DNMT1-derived miR-124a [193-196]. In our study, treating the NPM-ALK<sup>+</sup> ALCL cell lines with demethylating agent 5-aza-cytidine increased the expression of miR-30a and miR-30d, suggesting that the gene promoter from which miR-30a and miR-30d are transcribed is methylated.

Although there are few studies that have shown that some members of the miR-30 family possess oncogenic potential, the majority of these studies have described these miRs as tumor suppressors [197-201]. In line with these studies, our data show that miR-30a and miR-30d induced significant posttranscriptional decrease in IGF-IR protein expression,. To further support this notion, both miR-30a and miR-30d decreased significantly the activity of the *IGF-IR* 3'-UTR, which resulted in decreased cell proliferation, migration, and colony formation potential of NPM-ALK<sup>+</sup> ALCL cell lines, testifying to the tumor suppressor properties of these miRs.

Exogenous expression of miR-30a and miR-30d in the NPM-ALK<sup>+</sup> ALCL cells decreased the phosphorylation of NPM-ALK as well as its basal protein levels. We have

recently demonstrated that IGF-IR and NPM-ALK are physically associated via the Y646 and Y664 residues of NPM-ALK and Y950 residue of IGF-IR, which are located within their respective C-terminus. Through this association, a positive feedback loop appears to sustain their activation/phosphorylation [127, 128]. We also previously found that specific abrogation of IGF-IR by siRNA significantly decreased NPM-ALK protein levels, further attesting to the contribution of IGF-IR to sustaining NPM-ALK protein stability [127]. Using the 3 web-based miR prediction algorithms, we found that miR-30a and miR-30d do not have potential binding sites within NPM-ALK, implying that the decrease seen in NPM-ALK protein expression levels most likely resulted from IGF-IR downregulation.

Decreased IGF-IR level after transfection with miR-30a and miR-30d was associated with decreased phosphorylation of important IGF-IR downstream signaling partners, including pIRS-1 and pAKT, with no changes in total IRS-1 or AKT, which further demonstrates that miR-30a and miR-30d possess tumor suppressor properties in this lymphoma. Previous *in vitro* and *in vivo* studies showed that members of the miR-30 family are involved in the regulation of migration, invasion, and adhesion in a variety of cancer cells including those of the prostate, pancreas, and breast. These effects occur through modulating key proteins such as Ets-related gene (ERG), vimentin, integrin  $\beta 3$ , and other epithelial-to-mesenchymal transition molecules [199, 202, 203]. In the NPM-ALK<sup>+</sup> ALCL cells, another cellular protein involved in cell adhesion and migration, integrin  $\alpha 5/\beta 1$ , significantly decreased after miR-30-induced downregulation of IGF-IR. There have been previous reports indicating that IGF-IR or its primary ligand IGF-I can promote the stability and expression of  $\alpha 5/\beta 1$  to support the progression of different carcinomas, such as plasma cell myeloma, prostate cancer, and chondrosarcoma by enhancing cell motility, migration, adhesion of the malignant cells, and contributes to therapeutic resistance [204-208]. Because  $\alpha 5/\beta 1$  is not a

direct target of miR-30a or miR-30d, as indicated by the three online algorithms, downregulation of IGF-IR by miR-30a and miR-30d most likely caused the decrease in  $\alpha 5/\beta 1$  and thus contributed to the inhibition of the migratory potential of the NPM-ALK<sup>+</sup> ALCL cells.

MiR-30a and miR-30d were able to inhibit the NPM-ALK<sup>+</sup> ALCL tumor growth in SCID/beige mice. Even after withdrawing the administration of 4-OHT at 21 days, miR expression remained elevated in the mice, suggesting that although the tumor growth in some of these mice increased gradually, the overall average of the tumors in miR-30-induced group of mice never reached the overall average of tumor growth in control mice, perhaps due to the persistent effects of miR-30, which continuously slowed the progression of the tumors. In addition, some control mice displayed disseminated tumors, whereas all the miR-30a and miR-30d groups displayed smaller tumors that were confined to site of injection. Although these miRs can regulate different proteins involved in migration and invasion, it is possible that in our system, this effect was due to downregulation of integrin  $\alpha 5/\beta 1$  and thereby limiting the migration of these cells to other sites.

Because we found that the lack of expression of miR-30a and miR-30d is independent from NPM-ALK, we decided to study whether these miRs are also capable of regulating the expression of IGF-IR in other cancer types that are known to have high expression of IGF-IR such as breast cancer and colon cancer [209, 210]. Similar to the NPM-ALK<sup>+</sup> ALCL, miR-30a and miR-30d were significantly decreased in the MCF-7 and SW480 breast cancer and colon cancer cell lines, respectively, as well as primary tissue specimens from patients (**Figure S1**). Ectopic expression of miR-30a and miR-30d in MCF-7 and SW-480 cells induced remarkable downregulation of IGF-IR protein, but not *IGF-IR* mRNA (**Figure S2**). Downregulation of IGF-IR decreased pIGF-IR, pAKT, pIRS-1, integrin  $\alpha 5/\beta 1$ , and led to

significant reduction in cell proliferation, migration, and anchorage-independent colony formation potential (**Figures S2 and S3**). It has been previously shown that upregulation of integrin  $\alpha 5/\beta 1$  in MCF-7 cells contribute to multidrug resistance (MDR) [205]. Downregulation of integrin  $\alpha 5/\beta 1$  through reduction in IGF-IR protein by miR-30a and miR-30d may provide a mechanism to overcome MDR in these cells. Furthermore, both miR-30a and miR-30d significantly hindered progression of mammary tumors in female Balb/c nude mice (**Figures S5 and S6**). Recently, it has been shown that IRS-2 is a target for miR-30a in colon cancer [211]. In addition, miR-30a has been previously documented to reduce breast cancer by targeting vimentin, AVEN, metadherin, and Eya2 [212-215]. This further stresses the importance of these miRs for the survival of these cancers. In our study, we provide substantial evidence demonstrating IGF-IR as a novel target for miR-30a and miR-30d in these cancers.

Our data also show that the posttranscriptional decay of *IGF-IR* mRNA in NPM-ALK<sup>+</sup> ALCL occurs over a remarkably prolonged time compared with the decay of *IGF-IR* mRNA that is physiologically expressed in human T lymphocytes, suggesting an additional deregulated mechanism in which IGF-IR is upregulated posttranscriptionally. Very few studies have examined the rate of *IGF-IR* mRNA decay in other types of cancer, but these few studies support our findings [216-218]. For instance, when we treated the NPM-ALK<sup>+</sup> ALCL cells with actinomycin D, the average half-life for the lymphoma cells was around 3 h. This is similar to what was observed in other types of cancer, such as in the pancreatic cells MIA-PaCa-2 in which the half-life of *IGF-IR* mRNA was 4 h, compared to control cells in which 50% of *IGF-IR* mRNA was decayed in as little as 20 min after actinomycin D treatment [218]. Similar rates of decay were observed in breast cancer cells after treatment with antiestrogen ICI 182780 in a separate study [219]. Some mechanisms have been

proposed to explain the sustained stability of *IGF-IR* mRNA. For example, in one study, treatment of the osteogenic sarcoma-derived cell line Saos-2 with TNF $\alpha$ , decreased substantially *IGF-IR* mRNA stability relative to untreated cells [220]. It has been previously reported that NPM-ALK<sup>+</sup> ALCL cells lack the expression of TNF $\alpha$  due to DNA methylation of the TNF $\alpha$  promoter [221]. Furthermore, TNF $\alpha$  is highly expressed in normal activated T lymphocytes, where it is frequently involved in immune responses, especially in regards to inflammatory and immunomodulatory processes [222-225]. The lack of expression of this cytokine in the NPM-ALK<sup>+</sup> ALCL cells may be one possibility why *IGF-IR* mRNA is able to remain stable for longer periods of time compared to the normal T lymphocytes. In two other separate studies, *IGF-IR* mRNA stability was greatly influenced by the expression of HuR, an mRNA-binding protein involved in regulating the stability of a variety of mRNAs [216, 217]. Whether either of these mechanisms plays a role in NPM-ALK<sup>+</sup> ALCL is a direction of future study.

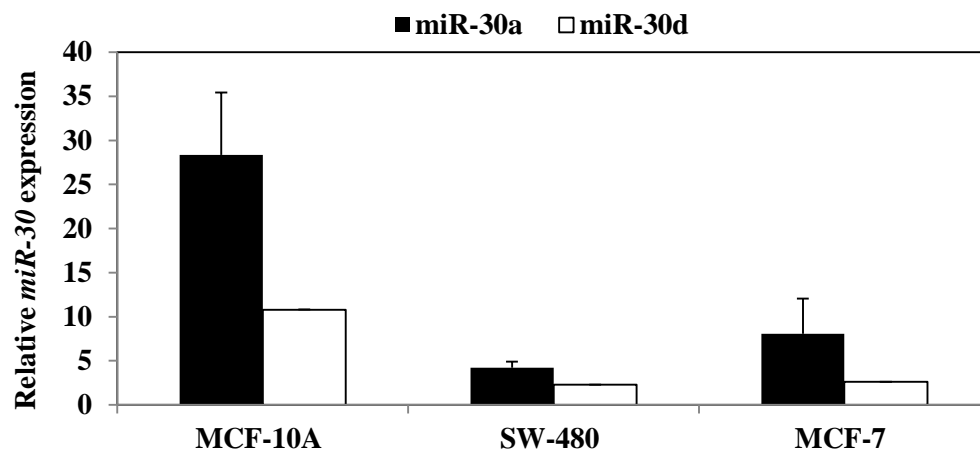
Overall, in this aim, we have determined the tumor suppressing properties of miR-30a and miR-30d in NPM-ALK<sup>+</sup> ALCL through targeting IGF-IR. Negative regulation of IGF-IR by miR-30a and miR-30d significantly reduces the oncogenic potential of these cells. In addition, the delay in *IGF-IR* mRNA decay further contributes to the upregulation of IGF-IR. Our results provide novel mechanisms in which IGF-IR is posttranscriptionally deregulated in this lymphoma, which may be beneficial to develop new therapeutic approaches to treat and ultimately eliminate the aggressive NPM-ALK<sup>+</sup> ALCL.

### 3.4.1. Supplemental

**Stable cell lines** – For MCF-7 Tet-inducible stable cell lines, miR-30a and miR-30d sequences were first subcloned into pmRi-mCherry vector (Clontech, catalog # 631119). Next, the pmRi-mCherry vectors expressing miR-30a or miR-30d were transfected into MCF-7 Tet-On Advanced cell line (catalog # 631153, Clontech) along with hygromycin B linear marker (200 ng; catalog# 631118, Clontech). Cells were cultured in DMEM media containing 100 µg/mL hygromycin B and 200 µg/mL G418 antibiotics for 2 weeks. Positive clones were expanded and maintained in DMEM media containing 50 µg/mL hygromycin B and 100 µg/mL G418.

**In vivo studies** – For MCF-7 Tet-inducible miR *in vivo* experiments, mice (Balb/c nude, catalog # BALBNU-F, 6-weeks old, female) were first primed with 2.5 µg/50 µL 17-estradiol (E2) diluted in peanut oil and injected s.c. for 1 week to assist MCF-7 cell proliferation. Then, mice were injected s.c. in the left mammary fat pad with  $2 \times 10^6$  cells expressing MCF-7 Tet-ON, pmRi-mCherry-miR-30a or pmRi-mCherry-miR-30d. Doxycycline (2 mg/mL) plus 5% sucrose and 2.5 µg of E2 was administered starting on the day of cell injection in the drinking water that was changed every 3 days in order to activate the miR. Once tumors developed, tumor burden was measured every 3 days for 100 days after cell injection. Tumor burden was calculated using the formula  $3.14 \times \text{long axis} \times \text{short axis}^2 \times 0.6$ . Doxycycline was administered during the entire 100 days, until mice were sacrificed.

A.



B.

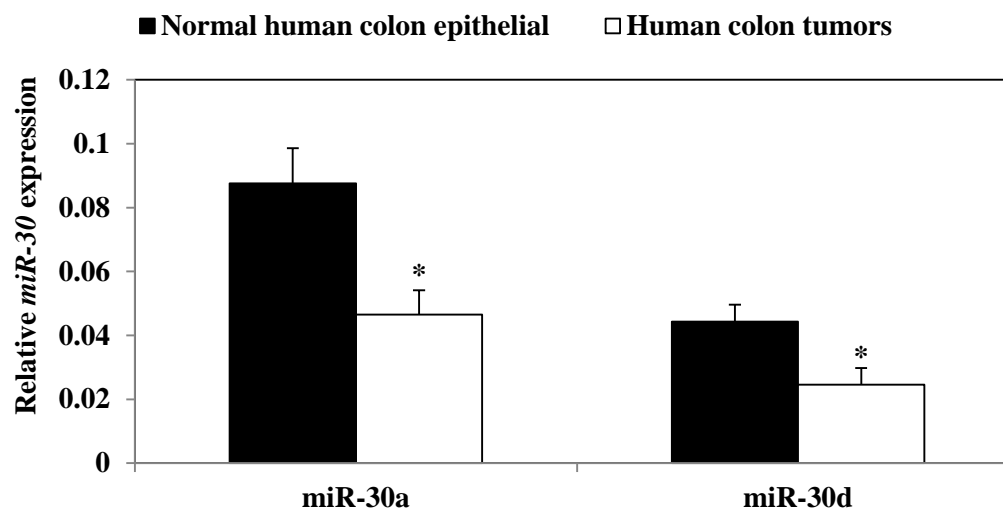
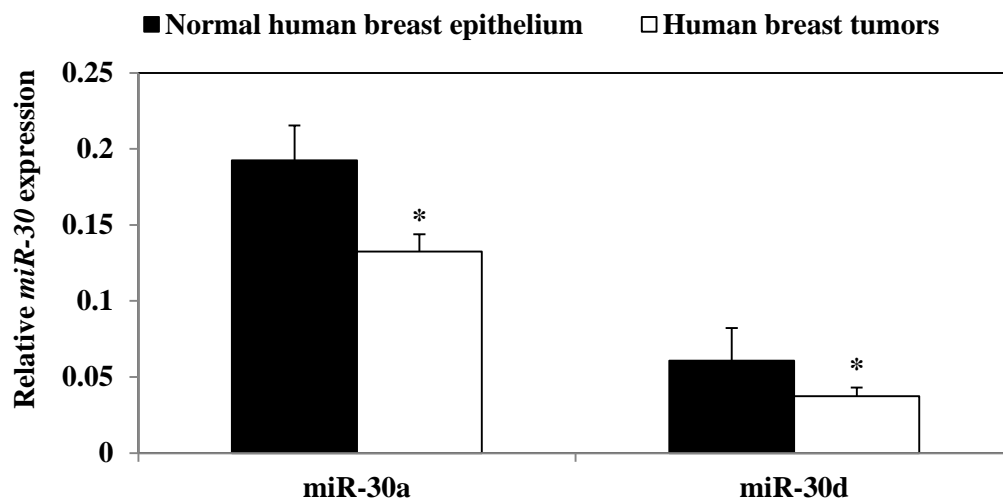


**FIGURE S1. MiR-30a and miR-30d are downregulated in MCF-7 and SW480 cells.** (A) qPCR analysis identified the expression of miR-30a and miR-30d to be remarkably downregulated in MCF-7 and SW480 cells compared with normal epithelial cells (MCF-10a). (B) A similar pattern of expression was identified in breast cancer patients and colon cancer patients compared to their respective normal counterparts (\* =  $p < 0.05$ ).



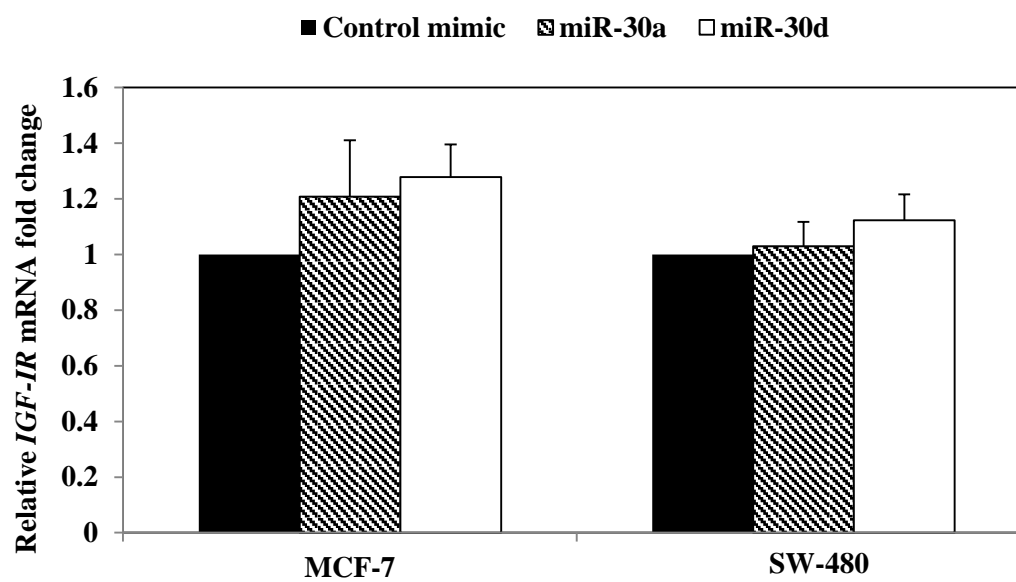
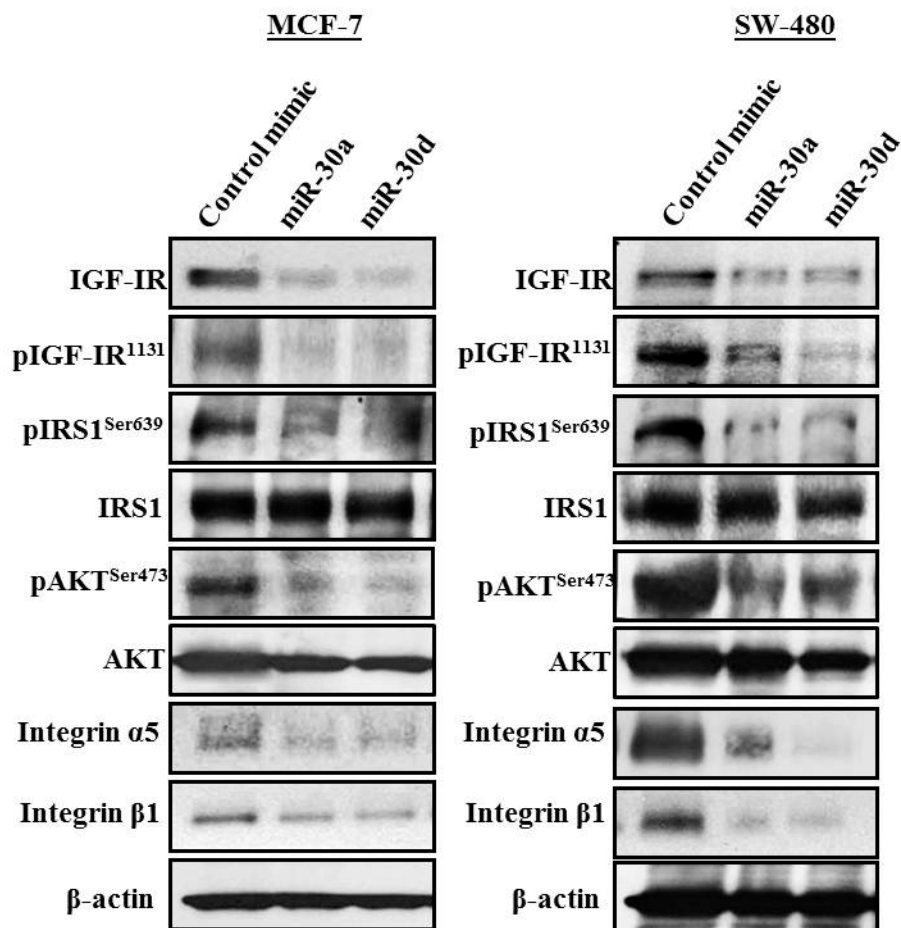
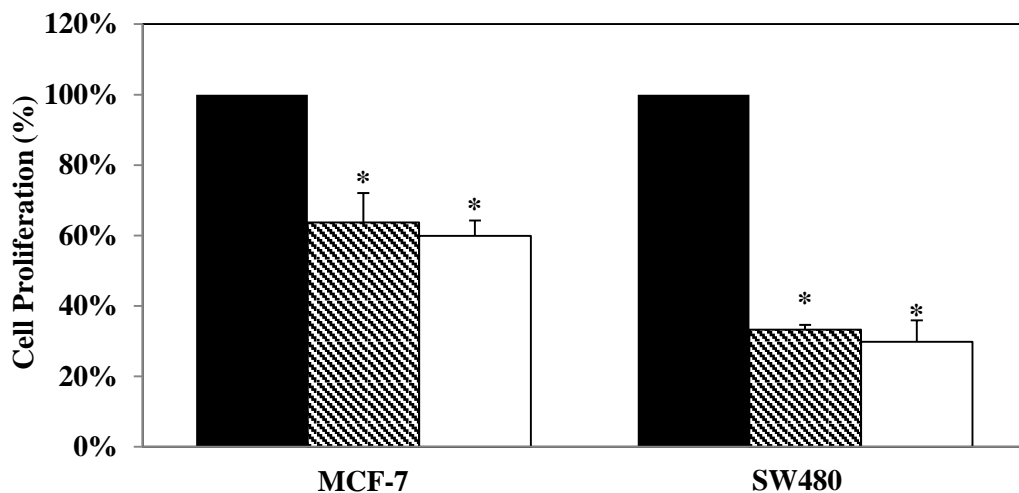


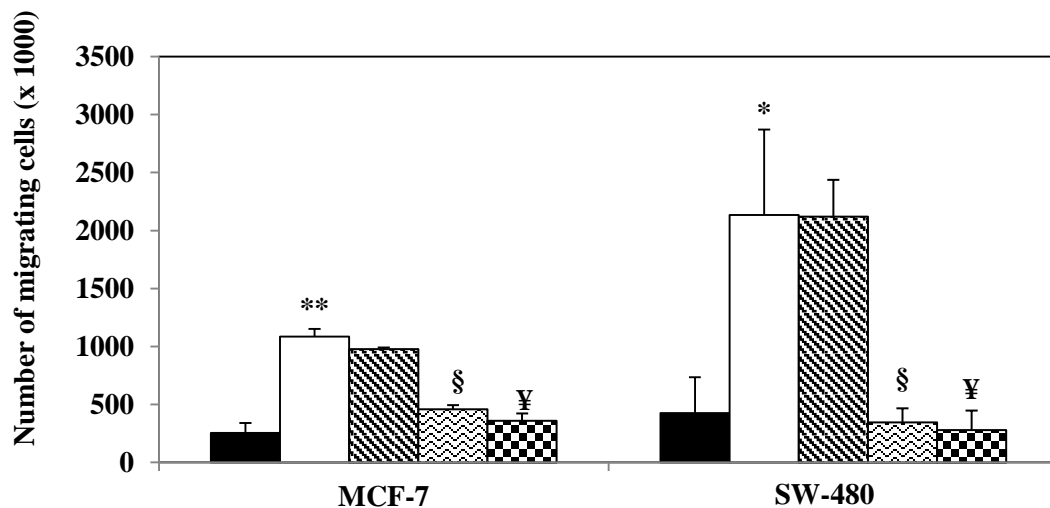
**FIGURE S2. MiR-30a and miR-30d decrease IGF-IR protein expression, but not *IGF-IR* mRNA expression in MCF-7 and SW480 cells.** Forced expression of control mimic, miR-30a mimic or miR-30d mimic in MCF-7 and SW480 cell lines induced marked downregulation of IGF-IR protein levels (upper panel), but not of *IGF-IR* mRNA levels (lower panel). The results are shown as means  $\pm$  SD of 3 consistent experiments. In addition, as shown in upper panel, there were significant decreases in downstream signaling proteins such as pIGF-IR<sup>1131</sup>, p-IRS-1<sup>Ser605</sup>, and pAKT<sup>Ser445</sup> without notable changes in total IRS-1 and AKT. Furthermore, miR-30a and miR-30d decreased the expression of integrin  $\alpha 5/\beta 1$ .

**A.** ■ Control mimic    ▨ miR-30a    □ miR-30d



**B.**

■ Untreated    □ IGF-I    ▨ Control mimic+IGF-I    ▩ miR-30a+IGF-I    ▪ miR-30d+IGF-I



**C.**

■ Control mimic    ■ miR-30a    □ miR-30d

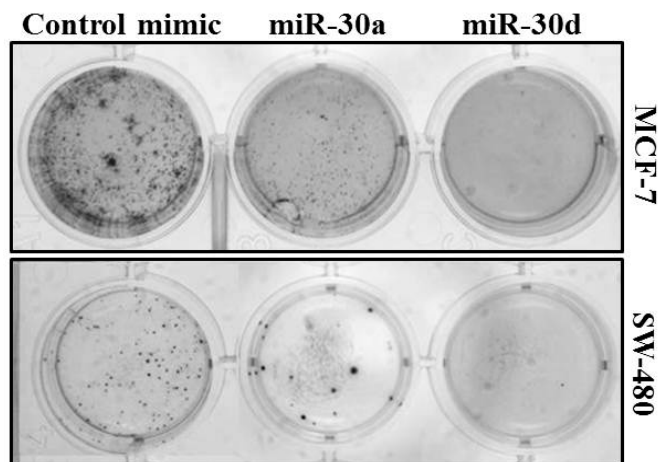
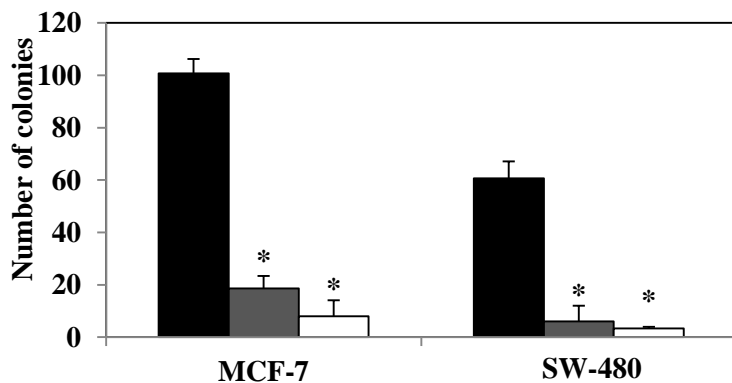


**FIGURE S3. MiR-30a and miR-30d decrease cell proliferation, migration, and colony formation potential in MCF-7 and SW480 cells.** (A) Transfection of MCF-7 and SW480 cells with miR-30a and miR-30d, but not control mimic, resulted in significant decrease in their proliferation after 48 h. (B) In addition, miR-30a and miR-30d decreased significantly the migration of the cells in response to IGF-I (500 ng/mL). (C) The two miRs decreased colony formation potential of MCF-7 and SW480 cells. Numbers of colonies are shown on the left and representative images are shown on the right. \*:  $p < 0.05$ ; \*\*:  $p < 0.001$ ; §: control mimic vs. miR-30a [ $p < 0.05$ ]; ¥: control mimic vs. miR-30d [ $p < 0.05$ ]. The results are shown as means  $\pm$  SD of 3 consistent experiments.

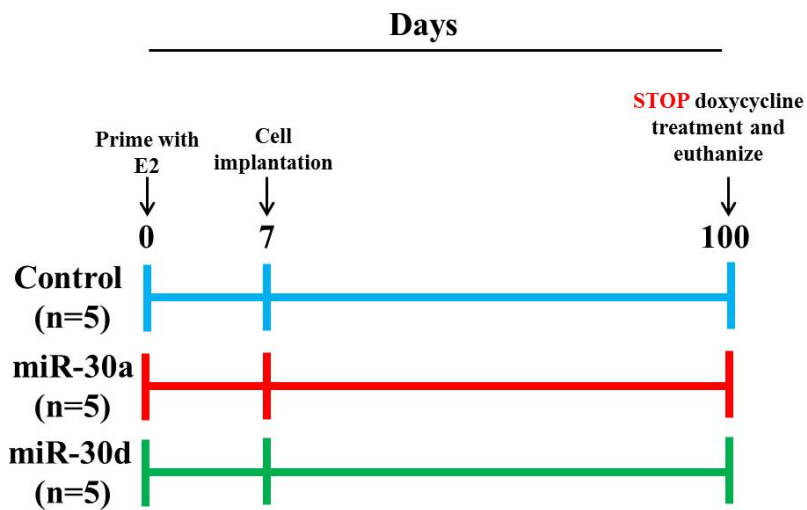
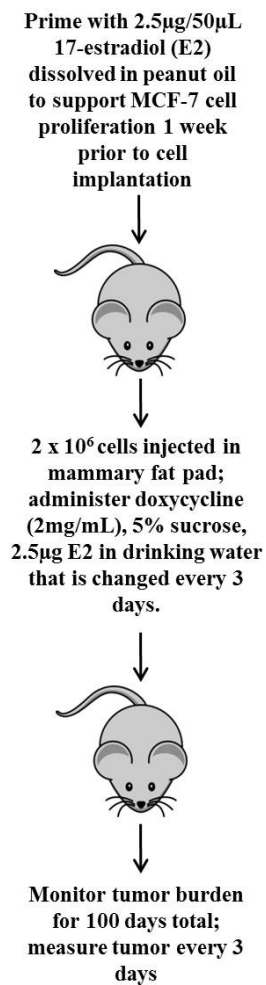
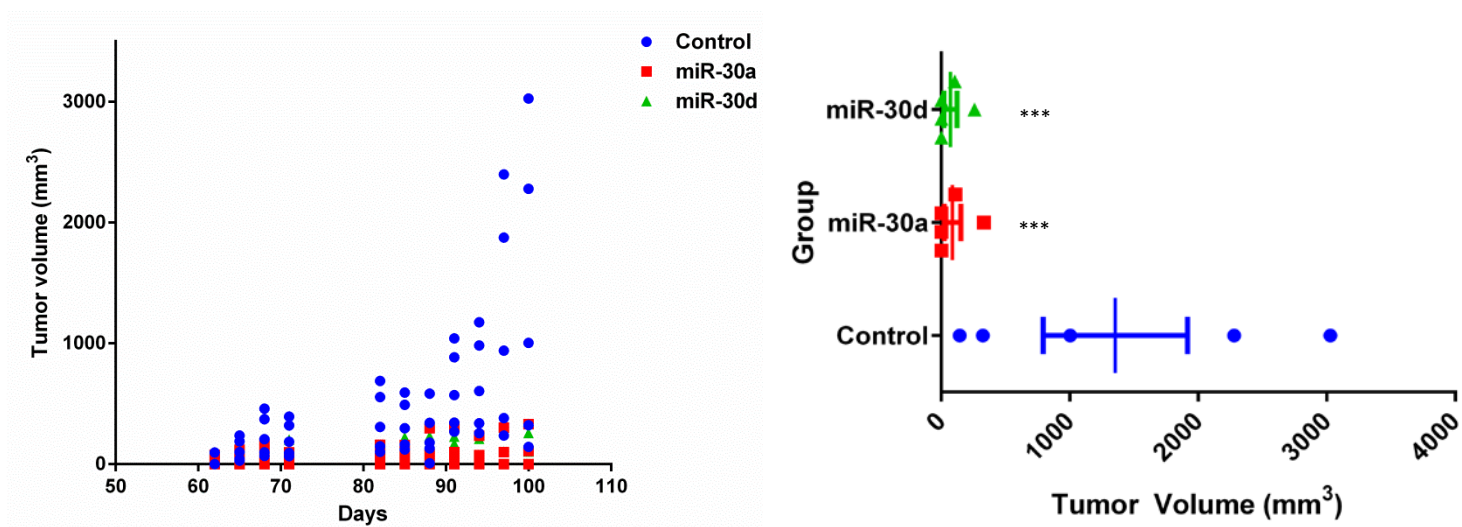


**FIGURE S4. Breast cancer mouse model with inducible expression of miR-30a or miR-30d.** Six-weeks old female Balb/c nude mice were first primed with s.c. injection of 2.5  $\mu\text{g}/50 \mu\text{L}$  17-estradiol (E2) diluted in peanut oil subcutaneously for 1 week before cell injection in order to assist MCF-7 cell proliferation. Then, mice were injected s.c. in the left mammary fat pad with  $2 \times 10^6$  cells expressing MCF-7 Tet-ON, pmRi-mCherry-miR-30a or pmRi-mCherry-miR-30d. Doxycycline (2 mg/mL) plus 5% sucrose and 2.5  $\mu\text{g}$  of E2 was administered on the day of cell implantation in the drinking water that was changed every 3 days for entire 100 days in order to activate the miR. Once tumors developed, tumor burden was measured every 3 days for 100 days total from time of cell implantation.

A.



Day 100 (+ doxycycline)

B.

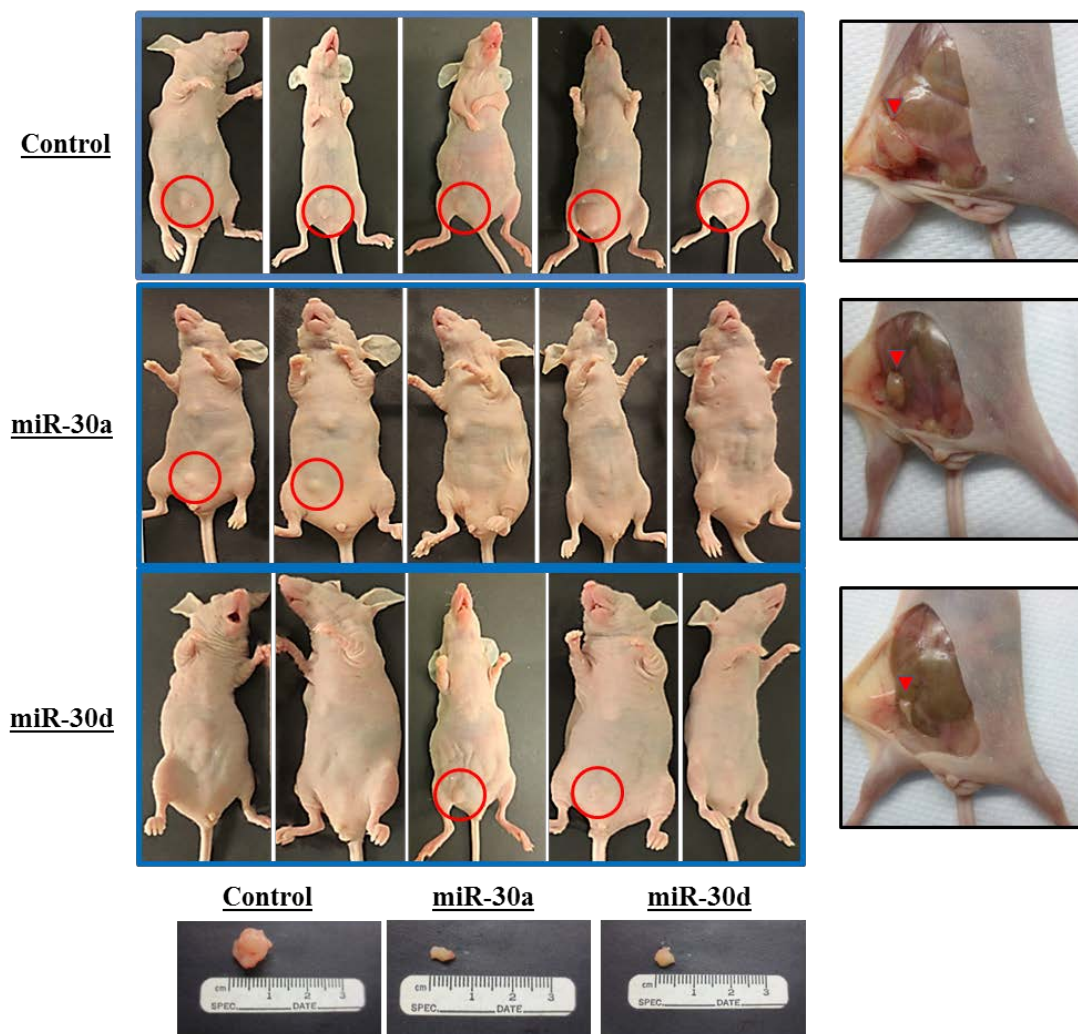


**FIGURE S5. Inducible expression of miR-30a and miR-30d suppresses breast cancer tumor growth *in vivo*.** (A) *Right panel*; tumors developed in all control mice at 62 days after MCF-7 cell s.c. implantation. In miR-30a and miR-30d groups, only 2/5 mice developed tumors. Tumors in control mice grew significantly faster, and the average tumor volume was greater than the miR-30a and miR-30d groups of mice, whose sizes were smaller and stabilized over the course of the study (100 days). *Left panel*; at day 100, control and miR-30 groups were euthanized to collect tumors [tumor burden significance at day 100 only, \*\*\*=  $p < 0.0001$ ; overall tumor burden significance: control vs. miR-30;  $p < 0.0001$ ]. (B) At day 100, control mice displayed tumors of variable sizes but were generally larger with greater average tumor volume than mice from miR-30a and miR-30d groups that displayed smaller average tumor sizes.



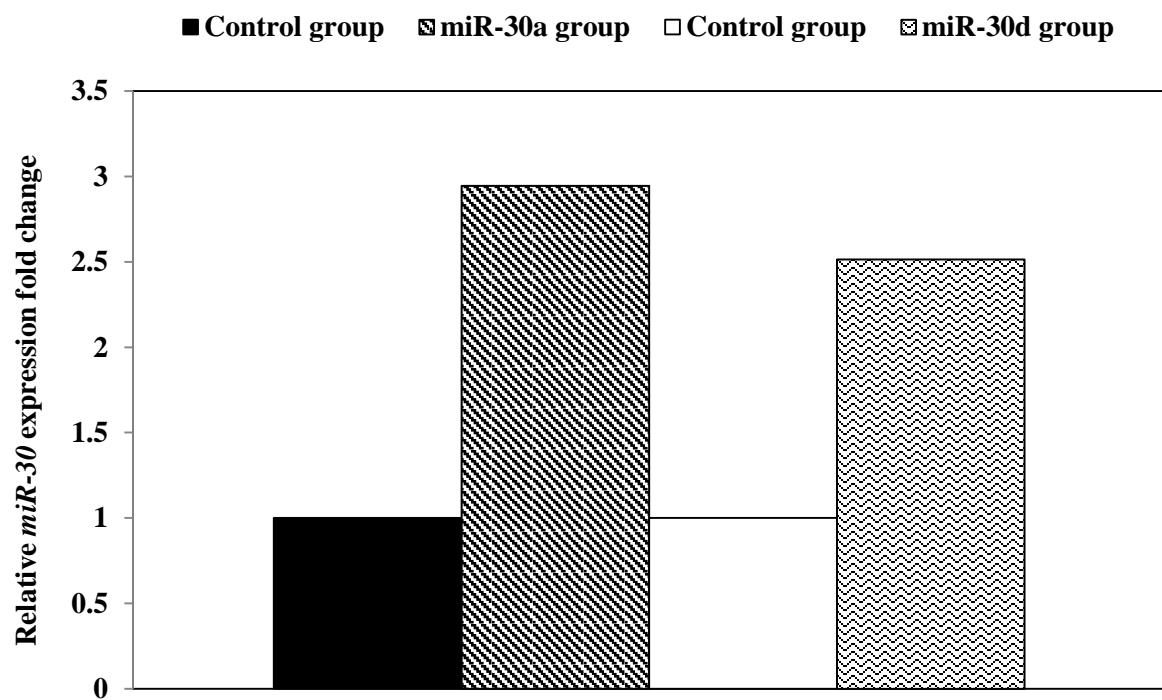


**FIGURE S6. Doxycyclin increased efficiently the levels of miR-30a and miR-30d *in vivo*.** MiR-30a and miR-30d expression levels increased in tumors that miRs were activated by doxycycline treatment at 100 days.

### **3.5. Posttranslational Regulation of NPM-ALK & IGF-IR**

### 3.5.1. Introduction

Posttranslational modifications contribute to critical signaling events that occur during neoplastic transformation. SUMOylation is a posttranslational modification that is characterized by the covalent and reversible binding of small ubiquitin-like modifiers (SUMO), including SUMO-1, SUMO-2/3, and SUMO-4, with their target proteins [226-228]. Although SUMOylation has some similarities with ubiquitination [229, 230], it has been shown that SUMO proteins compete with ubiquitin for substrate binding and thus SUMOylation appears to protect target proteins from proteasomal degradation [231, 232]. In addition to enhancing protein stability, SUMO proteins are involved in nuclear translocation of target proteins, which affects processes essential for cellular homeostasis [233, 234]. The SUMO family also includes the sentrin-specific proteases (SENPs): SENP1-3 and SENP5-7 [226, 235]. The roles of SENPs encompass removal of SUMO from target proteins; thus suppressing protein stabilization induced by SUMOylation. It has been recently demonstrated that SUMOylation plays a key role in the progression of cancer by stabilizing oncoproteins or targeting tumor suppressors to proteasomal degradation [236-240]. SUMOylation in NPM-ALK<sup>+</sup> ALCL has not been previously studied; therefore, one of our goals in this aim is to analyze SUMOylation in this aggressive lymphoma.

Posttranslational modifications also include ligand-mediated activation of target proteins. It has been previously shown that chimeric oncogenes, e.g., the Ewing sarcoma fusion proteins, transcriptionally induce the expression of IGF-I [68]. The increase in secreted IGF-I, as we have previously demonstrated in this lymphoma, leads to phosphorylation and activation of IGF-IR protein through dimerization. Whether NPM-ALK upregulates IGF-I expression and, as a result, promotes IGF-I-induced activation of IGF-IR is not known. In this aim, we also examined the potential role of NPM-ALK in regulating IGF-I expression.

### **3.5.2. Aberrant Posttranslational Mechanisms: SUMOylation**

### 3.5.2.1. Materials and Methods

**Web-based search** – To identify potential SUMOylation consensus binding sites within NPM-ALK and IGF-IR amino acid sequences, the online algorithm SUMOplot was used: <http://www.abgent.com/SUMOplot>.

**Cell lines** – Five characterized NPM-ALK<sup>+</sup> ALCL cell lines were used, including Karpas 299, DEL, SUP-M2, SR-786, and SU-DHL-1 (DSMZ, Germany). The 786-O (renal adenocarcinoma cell line; CRL-1932, ATCC) was used as a negative control for SUMO proteins. Jurkat cells (T lymphoblastic leukemia/lymphoma; ATCC) were used as host cells in protein degradation experiments and as a positive control. The normal human CD3<sup>+</sup> pan-T cells were purchased (Catalog number: 70024, StemCell Technologies, Vancouver, British Columbia, Canada). Cells were maintained in RPMI 1640 medium (HyClone, South Logan, UT) supplemented with 10% FBS (Sigma, St. Louis, MO), glutamine (2 mM), penicillin (100 U/mL), and streptomycin (100 µg/mL) at 37°C in a chamber containing humidified air with 5% CO<sub>2</sub>.

**Western blotting** – Western blotting was used to analyze the expression of various proteins. Cells were collected and subjected to lysis using lysis buffer as previously described [128]. Concentrations were measured using a Bio-Rad protein assay (Bio-Rad, Hercules, CA), and OD values were obtained using an ELISA plate reader (Bio-Tek Instruments, Winooski, VT). Proteins (50 µg) were subjected to electrophoresis with sodium dodecyl sulfate on 8% SDS-PAGE. Proteins were transferred to polyvinylidene fluoride (PVDF) membranes and probed with specific primary antibodies and then with appropriate horseradish peroxidase-conjugated secondary antibodies (Santa Cruz Biotechnology, Santa Cruz, CA, and GE Healthcare, Cardiff, UK). Proteins detection was performed using chemiluminescence (Amersham Life Sciences, Arlington Heights, IL).

**Antibodies** – Antibodies included SUMO-1 (4940), SUMO-2/3 (4971), Ubc9 (4786), SENP1 (11929), Ubiquitin (3933), Myc-tag (2276) (Cell Signaling Technology, Danvers, MA), ALK (M7195; DAKO, Carpinteria, CA), and  $\beta$ -actin (a5316; Sigma, St. Louis, MO).

**Immunoprecipitation** – Cells were lysed using lysis buffer containing 25 mM HEPES (pH 7.7), 400 mM NaCl, 1.5 mM MgCl<sub>2</sub>, 2 mM EDTA, 0.5% Triton X-100, 0.1 mM phenylmethylsulfonyl fluoride (PMSF), 2 mM dithiothreitol (DTT), Halt protease and phosphatase inhibitor cocktails 100 $\times$  (Thermo Scientific), and N-Ethylmaleimide (NEM; 10 mM) (Thermo Scientific) to inhibit deSUMOylation [241]. For immunoprecipitation, protein A/G agarose beads (Millipore, Billerica, MA) were blocked with 5% bovine serum albumin (BSA) overnight in order to reduce non-specific binding. In addition, lysates were pre-cleared using 2.5  $\mu$ g normal IgG with rocking for 1 h at 4°C, followed by centrifugation for 1 min at 13,000 rpm and removal of supernatant. Thereafter, 800  $\mu$ g of lysate was incubated with 2.5  $\mu$ g of primary antibody or mouse IgG control antibody along with the blocked protein A/G agarose beads overnight at 4°C. The next day, immunocomplexes were spun and supernatant was removed. The beads were washed 3 times with cold phosphate-buffered saline solution (PBS) for 15 min each at 13,000 rpm and once with lysis buffer, and then resuspended with 2 $\times$  sample buffer (Bio-Rad). The samples were then subjected to SDS-PAGE.

**Recombinant proteins** – The NPM-ALK recombinant protein was constructed using the TnT T7/SP6 Coupled Rabbit Reticulocyte Lysate System (Promega, Fitchburg, WI). The template for the TnT reaction was a plasmid previously described [128]. The following reaction components were assembled in a 1.5 mL microcentrifuge tube: TNT Rabbit Reticulocyte Lysate (25  $\mu$ L), TNT Reaction Buffer (2  $\mu$ L), TNT T7 RNA Polymerase (1  $\mu$ L), Amino Acid

Mixture Minus Leucine 1 mM (0.5  $\mu$ L), Amino Acid Mixture Minus Methionine 1 mM (0.5  $\mu$ L), RNasin Ribonuclease Inhibitor, 40 u/ $\mu$ l (1  $\mu$ L), NPM-ALK plasmid template (2  $\mu$ L), Transcend Biotin-Lysyl-tRNA (1  $\mu$ L), and nuclease-free water to a final volume of 50  $\mu$ L. Thereafter, the reactions were incubated at 30°C for 90 min. Aliquots of these reactions (5  $\mu$ L) were analyzed by Western blotting to confirm the translation of NPM-ALK.

**SUMOylation assay** – The *in vitro* SUMOylation assay was performed by using the SUMO-1 and SUMO-2/3 SUMOlink Kits (Active Motif, Carlsbad, CA). Briefly, the following reaction components were assembled in a 1.5 mL microcentrifuge tube: protein buffer (1  $\mu$ L), 5 $\times$  SUMOylation buffer (1  $\mu$ L), NPM-ALK recombinant protein (4  $\mu$ L), E1 activating enzyme (1  $\mu$ L), E2 conjugating enzyme (1  $\mu$ L), SUMO-1, -2 or -3 protein (1  $\mu$ L), and nuclease-free water to a final volume of 20  $\mu$ L. For baseline mutated reactions, the SUMO proteins were substituted with their corresponding mutated proteins, provided in the kit. The reactions were mixed gently and incubated at 30°C for 3 h. Thereafter, the reactions were stopped by adding an equal volume of 2 $\times$  SDS-PAGE loading buffer and analyzed by Western blotting.

**Site-directed mutagenesis** – NPM-ALK<sup>K24R</sup> and NPM-ALK<sup>K32R</sup> constructs were created by using the QuickChange II XL Site-Directed Mutagenesis kit (Agilent Technologies, Santa Clara, CA) and the following set of primers according to the manufacturer's instructions:

**Table 11.** Primers used to create NPM-ALK<sup>K24R</sup> and NPM-ALK<sup>K32R</sup> constructs by site-directed mutagenesis.

NPM-ALK <sup>K24R</sup> Forward	5'-TTTTCGGTTGTGAACTACGGGCCGACAAAGATTATC-3'
NPM-ALK <sup>K24R</sup> Reverse	5'-GATAATCTTTGTGCGCCCGTAGTTCACAACCGAAAAG-3'
NPM-ALK <sup>K32R</sup> Forward	5'-GCCGACAAAGATTATCACTITCGCGTGGATAATGATGAAAATGAG -3'
NPM-ALK <sup>K32R</sup> Reverse	5'-CTCATTTTCATCATTATCCACGCGAAAGTGATAATCTTTGTCGGC-3'

The polymerase chain reaction (PCR) products (5  $\mu$ L) were transformed using MaxEfficiency DH5alpha competent cells (Invitrogen), and the transformation reactions



were plated on ampicillin-resistant plates. Colonies containing the correct insert were confirmed by direct sequencing and amplified in ampicillin-containing LB broth overnight at 37°C with shaking at 225 rpm. The following day, the colonies were processed with the QiaPrep Spin Miniprep Kit (Qiagen, Germantown, MD) to isolate plasmids. For *in vitro* SUMOylation assays, the mutated plasmids were used as templates for the TnT reactions to create mutated recombinant proteins.

**Transfection** – Transfection of NPM-ALK<sup>+</sup> ALCL cells with the SENP1 expression plasmid (Origene, Rockville, MD) was performed by electroporation using the Amaxa 4D nucleofection system in 100 µL cuvettes (Solution SF, Program CA-150; Lonza, Houston, TX); Transfection of Jurkat cells using the wild-type NPM-ALK, NPM-ALK<sup>K24R</sup> or NPM-ALK<sup>K32R</sup> plasmid was performed using the Nucleofector System (Solution V, Program X-001; Lonza, Houston, TX); thereafter, cells were incubated for 48 h.

**Protein degradation assay** – Cells were transfected, using the conditions described in the previous section, with either wild type or mutated NPM-ALK constructs for 48 h. The cells were then treated with cyclohexamide (CHX, Sigma-Aldrich; 100 µg/mL) for another 24 or 48 h, then harvested and subjected to lysis and Western blotting.

**Immunofluorescence** – Cytospins were prepared from EV or myc-tagged SENP1 transfected cells, followed by fixation with 4% paraformaldehyde (PFA) at the following timepoints: 0 min, 15 min, 30 min, 1 h, 3h, 6 h, 12 h, 24 h, and 48 h. After fixation, cells were subjected to permeabilization with 0.2% Triton-X in PBS for 30 min at room temperature. Subsequently, cells were blocked with 0.3% Triton-X/2% BSA in PBS solution for 1 h at room temperature. Thereafter, Myc-tag primary antibody was added at 1:2000 dilution in order to detect exogenous SENP1 and slides were incubated at 4°C overnight. The following day, slides were washed 3 times in PBS and Alexa 647 fluorochrome-conjugated secondary antibody

was added at 1:200 dilution for 1.5 h at room temperature. Thereafter, slides were washed 3 times in PBS and counterstained with DAPI. Prolong Gold Antifade Mountant (catalog # P36934; Invitrogen) was added, slides were coverslipped, and sealed with nail polish to prevent dehydration. Images were captured using Deltavision Image Restoration microscope (Olympus IX71; GE Healthcare; total magnification is  $\times 400$ ).

***Cell fractionation*** – Cell fractionation was performed using the Nuclear/Cytosol Fractionation kit (BioVision, Milipitas, CA). For expression of cytoplasmic and nuclear proteins at baseline levels as well as after transfection with EV or SENP1 expression plasmids, cells were collected by centrifuging at  $600 \times g$  for 5 min at  $4^{\circ}\text{C}$ . CEB-A buffer (0.2 mL) containing DTT and protease inhibitors (provided in the kit) was added and samples were spun at  $500 \times g$  for 3 min at  $4^{\circ}\text{C}$ . The supernatant was removed and the pellet was resuspended in 0.2 mL of the CEB-A mix and subjected to vigorous vortexing at the highest setting for 15 sec to fully resuspend the pellet. Thereafter, the samples were incubated on ice for 10 min. Ice-cold CEB-B buffer (11  $\mu\text{L}$ ) was added to the tube, which was subjected to vortexing and placed on ice for 1 min, and then spun at maximum speed for 5 min. Immediately, the supernatant (containing the cytoplasmic extract) was transferred into a clean, pre-chilled tube. The remaining pellet was washed 5 times in ice-cold PBS by centrifugation at maximum speed for 1 min. Then, the pellet was resuspended in 30  $\mu\text{L}$  of ice-cold NEB buffer and subjected to vortexing for 15 sec and returned to ice for 10 min. This step was repeated 4 times. Finally, the samples were subjected to centrifugation at maximum speed for 15 min, and the supernatant (containing nuclear extract) was transferred into a clean, pre-chilled tube.

***Colony formation assay*** – Methylcellulose (3 mL; Methocult H4230) was added to 15 mL tubes. Transfected cells were resuspended to eliminate clumping and then added in a 1:10

(v/v) ratio to the methylcellulose. Tubes were tightly capped, and the mixtures were gently inverted several times. Then, 1.0 mL of the mix was dispensed into 24-well plates in triplicate. Plates were placed in a humidified incubator at 37°C in 5% CO<sub>2</sub> for 7 days and then *p*-iodonitrotetrazolium violet was added for 24 hours for staining. Colonies were visualized using the AlphaImager system (ProteinSimple, San Jose, CA).

**Cell viability assay** – Cell viability was evaluated by the CellTiter 96 AQueous One Solution Cell Proliferation Assay (MTS) kit (Promega). Cells were seeded in 96-well plates at a concentration of 10,000 cells/well in 100 µL of RPMI medium supplemented with 10% FBS. MTS reagent (20 µL) was added and then incubated at 37°C in a humidified chamber containing 5% CO<sub>2</sub> in air for approximately 4 hours. OD measurements were obtained by using an ELISA plate reader.

**BrdU assay** – Cell proliferation was measured by using the 5-bromo-2'-deoxyuridine (BrdU) assay kit (ExAlpha, Shirley, MA). Briefly,  $2 \times 10^5$  cells/mL were plated into a 96-well plate. The BrdU label (1:500 dilution) was added, and the plate was incubated at 37°C for 24 h. Cells were fixed for 30 min at room temperature. The anti-BrdU antibody was added for 1 h after washing, followed by peroxidase goat anti-mouse IgG conjugate (1:2000 dilution) for 30 min. Thereafter, the 3,3',5,5'-tetramethylbenzidine peroxidase substrate was added to the cells and the plate incubated for 30 min at room temperature in the dark. The acid Stop Solution was then added and the plate was read at 450 nm by using an ELISA plate reader.

**Protein extraction from FFPE tissues** – Proteins were recovered from these sections by using the Qiagen Qproteome FFPE Tissue Kit (Catalog # 37623). Briefly, 2 µM tissue sections were subjected to the following sequence of deparaffinization conditions: (1) xylene (2 × 5 min); (2) 100% ethanol (3 × 5 min); (3) 95% ethanol (3 × 5 min); and (4) 80% ethanol (3 × 5 min). Areas of interest were excised from the slide with a needle and transferred to a

1.5 mL collection tube. The supplied Extraction Buffer EXB Plus without  $\beta$ -mercaptoethanol was provided with the kit. For each extraction procedure, 6  $\mu$ L of  $\beta$ -mercaptoethanol was first added to 94  $\mu$ L of Extraction Buffer EXB Plus to obtain a working solution. Extraction Buffer EXB Plus supplemented with  $\beta$ -mercaptoethanol (100  $\mu$ L) was added into the tube containing the excised tissue and mixed by vortexing. Each tube was sealed with a Collection Tube Sealing Clip (supplied) and incubated on ice for 5 min, then mixed again by vortexing. The samples were incubated on a heating block at 100°C for 20 min, and then incubated in an oven with rotators at 80°C for 2 h with agitation at 750 rpm. Thereafter, the tubes were held at 4°C for 1 min and the Collection Tube Sealing Clips were removed. The samples were subjected to centrifugation for 15 min at 14,000  $\times g$  at 4°C. The supernatant containing the extracted proteins was transferred to a new 1.5 mL tube. For quantification of protein yield, the Bio-Rad assay was used.

### 3.5.2.2. Results

*SUMOylation pathway is upregulated in NPM-ALK<sup>+</sup> ALCL cells:* SUMOylation of IGF-IR has been previously characterized in other types of cancers. In addition, we found SUMOylation of IGF-IR in NPM-ALK<sup>+</sup> ALCL cells (**Supplemental Figures**), which supports previously published literature [238, 242-244]. Nonetheless, we decided to focus on whether SUMOylation also contributes to NPM-ALK protein stability, which has not been previously studied. To determine whether there are SUMO consensus motifs located within the NPM-ALK amino acid sequence, we searched the online algorithm SUMOPlot and identified several potential SUMO consensus motifs (**Figure 25**). Screening of the 5 NPM-ALK<sup>+</sup> ALCL cell lines relative to normal human T lymphocytes revealed Ubc9 and SUMO-1 to be moderately overexpressed in 3/5 cell lines, whereas SUMO-2/3 demonstrated significant overexpression in all cell lines. In contrast, SENP1 protein was substantially decreased in all cell lines, suggesting that the SUMOylation pathway is deregulated in NPM-ALK<sup>+</sup> ALCL cells (**Figure 26A**). A similar pattern was observed in patient samples extracted from FFPE lymphoma tumor sections (**Figure 26B**).

## SUMO consensus motifs in NPM-ALK

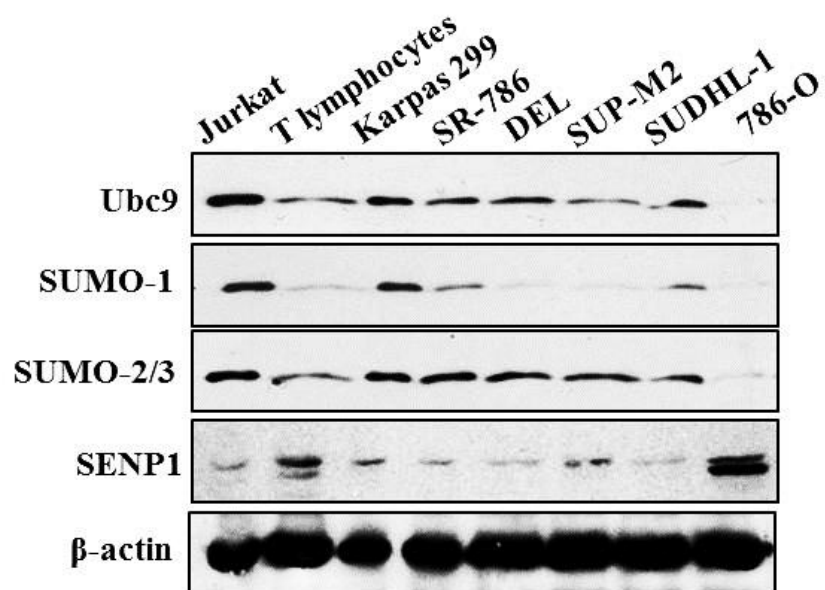
1	MEDSMDMDMS	PLRPQNYLFG	CEL <b>KAD</b> KDYH	<b>FKVD</b> NDENEH	QLSLRTVSLG
51	AG <b>AKDE</b> LHIV	EAEAMNYEGS	PIKVTLATLK	MSVQPTVSLG	GFEITPPVVL
101	RLKCGSGPVH	ISGQHLVVYR	RKHQELQAMA	MELQSPEYKL	SKLRTSTIMT
151	DYNPNYCFAG	KTSSISDLKE	VPRKNITLIR	GLGHGAFGEV	YEQVSGMPN
201	DPSPLQVAVK	TLPEVCSEQD	ELDFLMEALI	ISKFNHQNIV	RCIGVSLQSL
251	PRFILLELMA	GGD <b>LKS</b> FLRE	TRPRPSQPSS	LAMDLLHVA	RDIACGCQYL
301	EENHFIHRDI	AARNCLLTCP	GPGRV <b>AKIG</b> D	FGMARDIYRA	SY <b>YRKG</b> GCAM
351	LPVKWMPPEA	FMEGIFTSKT	DTWSFGVLLW	EIFSLGYMPY	PSKSNQEVLE
401	FVTSGGRMDP	PKNCPGPVYR	IMTQCWQHQP	EDRPNFAIL	ERIEYCTQDP
451	DVINTALPIE	YGPLVEEEE <b>K</b>	<b>VPVRPKD</b> PEG	VPLLV <b>SQQA</b>	<b>KRE</b> EERSPA
501	PPPLPTSSG	<b>KAAKKP</b> TAAE	VSVRVP <b>R</b> GPA	VEGGHV <b>N</b> MAF	SQSNPPSELH
551	KVHGSRNKPT	SLWNPTYGSW	FTEKPT <b>K</b> KNN	<b>PLAKKE</b> PHDR	GNLGLEGSCT
601	VPPNVATGRL	PGASLLLEPS	SLTANMKEVP	LFRLRH <b>F</b> PCG	NVNYGYQQQG
651	LPLEAATAPG	AGHYEDTILK	SKNSMNQPGP		

No.	Pos.	Group	Score	No.	Pos.	Group	Score
1	K24	LFGCE <u>LKAD</u> <u>KDYHF</u>	0.91	8	K327	GPGRV <u>AKIG</u> DFGMA	0.62
2	K32	DKDYH <u>FKVD</u> NDENE	0.85	9	K265	MAGGD <u>LKSF</u> LRETR	0.56
3	K54	SLGAG <u>AKDE</u> LHIVE	0.79	10	K476	KVPVR <u>PKDP</u> EGVP	0.50
4	K491	LVSQQ <u>AKRE</u> EERSP	0.79	11	K470	LVEEE <u>EKVP</u> VRPKD	0.39
5	K584	KNNPI <u>AKKE</u> PHDRG	0.79	12	K585	NNPIA <u>KKEP</u> HDRGN	0.37
6	K103	PVVLRL <u>LKCG</u> SGPVH	0.73	13	K345	RASYR <u>RKGG</u> CAMLP	0.27
7	K514	SSGKA <u>AKKP</u> TAAEV	0.69				

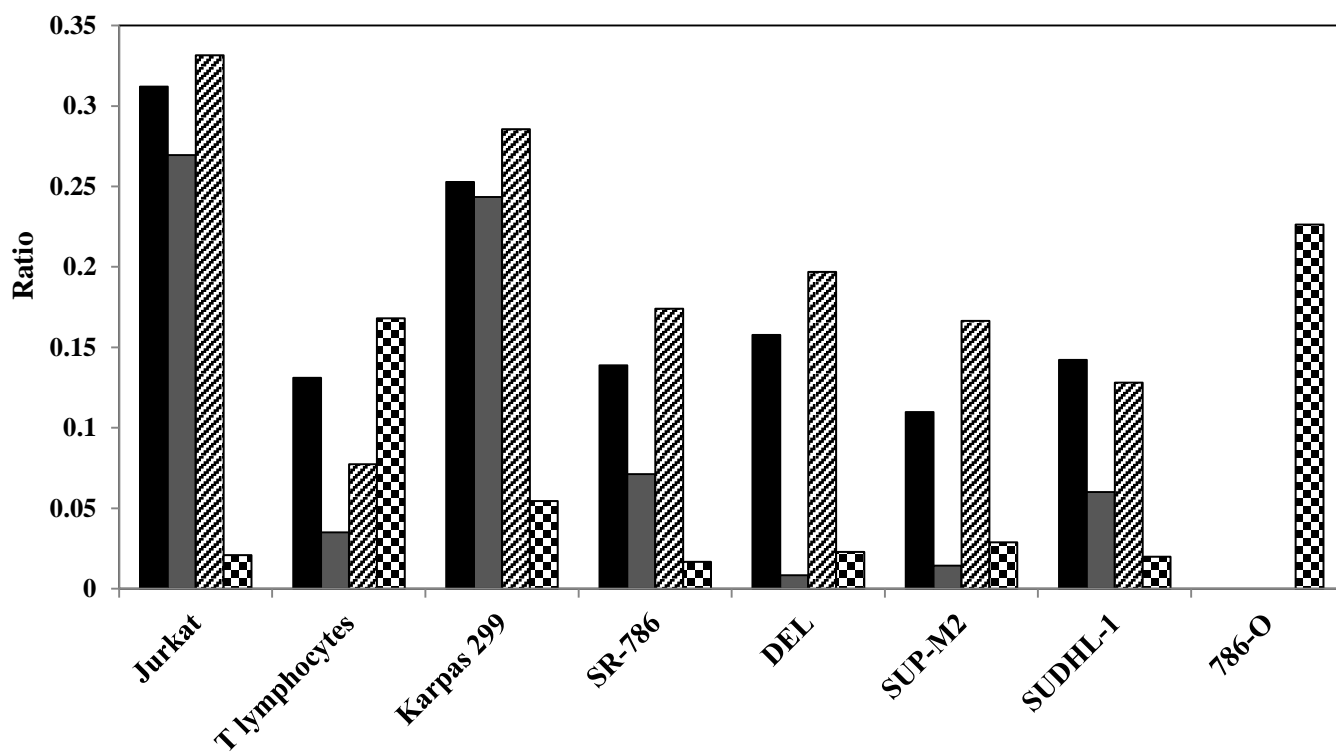
- Motifs with high probability
- Motifs with low probability
- Overlapping Motifs

**FIGURE 25. SUMO consensus motifs within NPM-ALK amino acid sequence.** The online software SUMOplot revealed several SUMO consensus motifs within the NPM-ALK amino acid sequence, two of which appeared with the highest probability of conjugation with the SUMO proteins ( $>0.80$ ). Red: motifs with high probability; Green: motifs with low probability; Blue: overlapping motifs.

A.

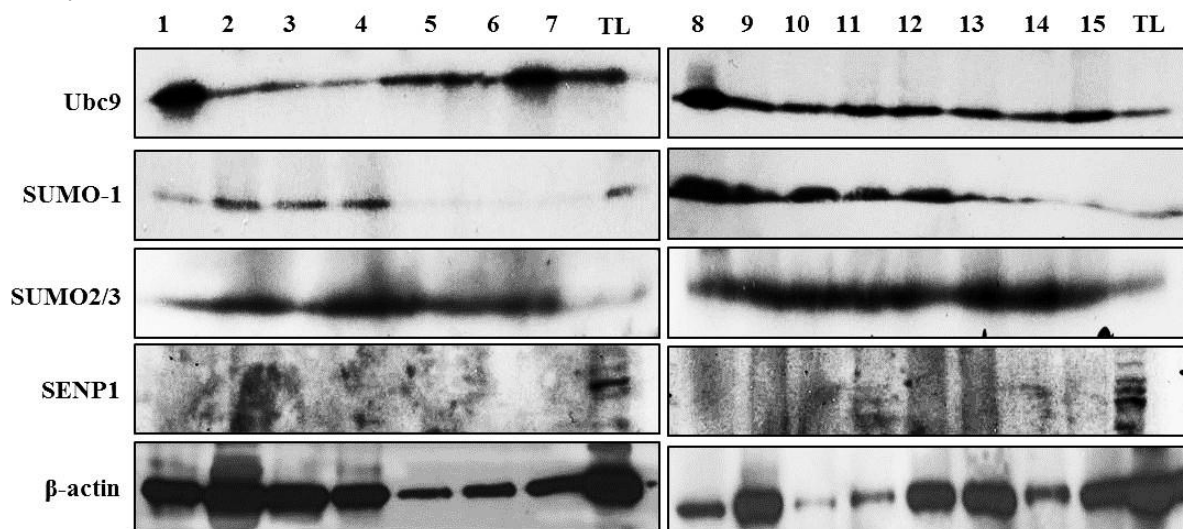


■ Ubc9:  $\beta$ -actin    ■ SUMO-1:  $\beta$ -actin    ▨ SUMO-2/3:  $\beta$ -actin    ▩ SENP1:  $\beta$ -actin

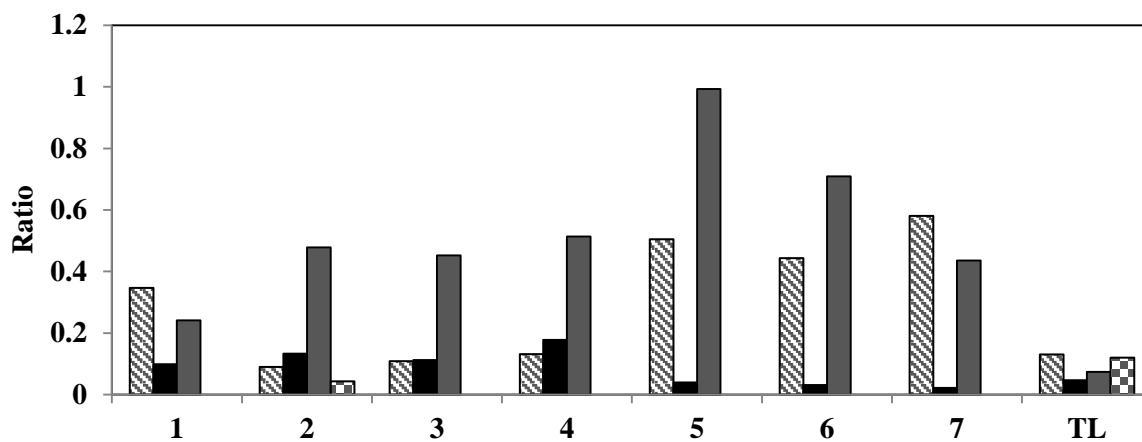




B.



▨ Ubc9:  $\beta$ -actin   ■ SUMO-1:  $\beta$ -actin   ■ SUMO-2/3:  $\beta$ -actin   ▨ SENP-1:  $\beta$ -actin



▨ Ubc9:  $\beta$ -actin   ■ SUMO-1:  $\beta$ -actin   ■ SUMO-2/3:  $\beta$ -actin   ▨ SENP-1:  $\beta$ -actin

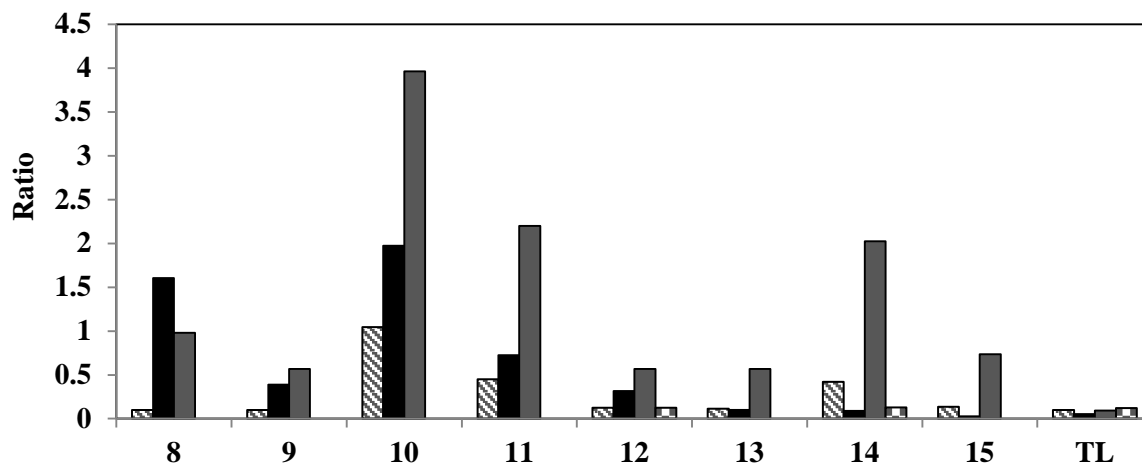


**FIGURE 26. SUMO is upregulated in NPM-ALK<sup>+</sup> ALCL.** (A) *Upper panel*; screening of the NPM-ALK<sup>+</sup> ALCL cells lines Karpas 299, SR-786, DEL, SUP-M2, and SU-DHL-1 by Western blotting revealed overexpression of Ubc9 and SUMO-1 in the majority of the cell lines (4/5 and 3/5 cell lines, respectively) relative to normal T lymphocytes (TL). SUMO-2/3 was upregulated in the lymphoma cell lines, relative to TL. In contrast, SENP1 protease was decreased in the lymphoma cell lines compared to TL.  $\beta$ -actin was used as a loading control. Jurkat and 786-O cells were used as positive and negative controls, respectively. *Lower panel*; densitometry of SUMO proteins relative to  $\beta$ -actin is shown. (B) *Upper panel*; Western blot performed on protein extracted from FFPE tissue sections of patient specimens (1-15) revealed a similar pattern of expression: Ubc9 and SUMO-1 was overexpressed in 7/15 and 9/15 patients, whereas SUMO-2/3 was overexpressed in all patients. In contrast, SENP1 was decreased in 13/15 patients.  $\beta$ -actin was used as loading control. *Lower panel*; densitometry of SUMO proteins relative to  $\beta$ -actin is shown. Variability in  $\beta$ -actin levels was due to the poor quality of some of the FFPE tumor sections.

***SUMO proteins physically associate with NPM-ALK:*** To test whether the SUMO proteins can physically associate with NPM-ALK, NPM-ALK protein was immunoprecipitated in the Karpas 299 and SR786 cell lines and the expression of SUMO-1, SUMO-2/3, and Ubc9 was analyzed by Western blotting. We found that all 3 of the SUMO proteins can interact with NPM-ALK (**Figure 27A**). Furthermore, an *in vitro* SUMOylation assay showed that all SUMO modifiers are capable of SUMOylating NPM-ALK *in vitro*, as indicated by the presence of the higher molecular weight band above the baseline NPM-ALK protein levels. In contrast, mutated SUMO-1 and SUMO-2/3 proteins failed to SUMOylate NPM-ALK (**Figure 27B**).

SUMOplot showed several potential SUMO consensus motifs for NPM-ALK: K24 and K32 were identified as having the highest probability of conjugation with SUMO proteins. To determine whether these potential sites are indeed capable of binding the SUMO modifiers, a second *in vitro* SUMOylation assay was performed using either the wild-type NPM-ALK protein or NPM-ALK protein mutated at either K24 or K32 (**Figure 28A**). SUMOylation was abolished with NPM-ALK<sup>K24R</sup> for both SUMO-1 and SUMO-3 and with NPM-ALK<sup>K32R</sup> for SUMO-3 only (**Figure 28B**). This suggests that SUMO-1 and SUMO-3 are most likely the primary SUMO modifiers for NPM-ALK at K24 and K32. In contrast, mutations at K24 and K32 failed to prevent SUMO-2 from conjugating to NPM-ALK; SUMO-2 most likely conjugates to lysine residues found within other consensus motifs in NPM-ALK.

Next, we sought to determine the effects of K24 and K32 mutations on NPM-ALK protein stability. Jurkat cells, which lack NPM-ALK but contain high levels of SUMO modifiers and Ubc9 proteins, were transfected with wild-type NPM-ALK, NPM-ALK<sup>K24R</sup>, NPM-ALK<sup>K32R</sup> or the NPM-ALK<sup>K24R/K32R</sup> construct, and then treated with the protein

synthesis inhibitor CHX for 24 or 48 h. While degradation of NPM-ALK protein was minimal at 24 h, CHX inhibited protein synthesis significantly in cells expressing NPM-ALK<sup>K24R</sup>, NPM-ALK<sup>K32R</sup>, and most with the NPM-ALK<sup>K24R/K32R</sup> combination at 48 h. NPM-ALK mutated at K24 induced an increase in degradation by 42% compared to wild type NPM-ALK. Similarly, NPM-ALK mutated at K32 led to an increase of its degradation level by 56% vs. wild type NPM-ALK. Notably, NPM-ALK dual mutation at K24 and K32 was associated with more pronounced increase in degradation; 67% in comparison with wild type NPM-ALK. In contrast, CHX did not inhibit wild-type NPM-ALK at either time point (**Figure 29**). These findings suggest that SUMOylation contributes to the stability of NPM-ALK in NPM-ALK<sup>+</sup> ALCL cells.

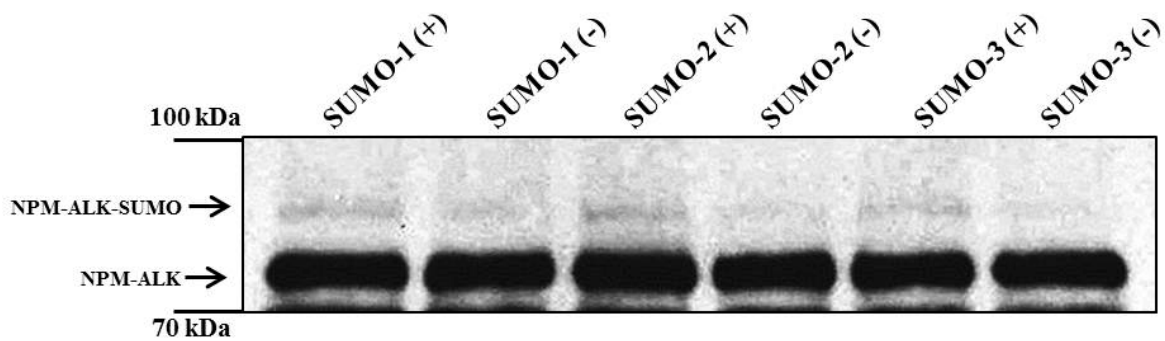
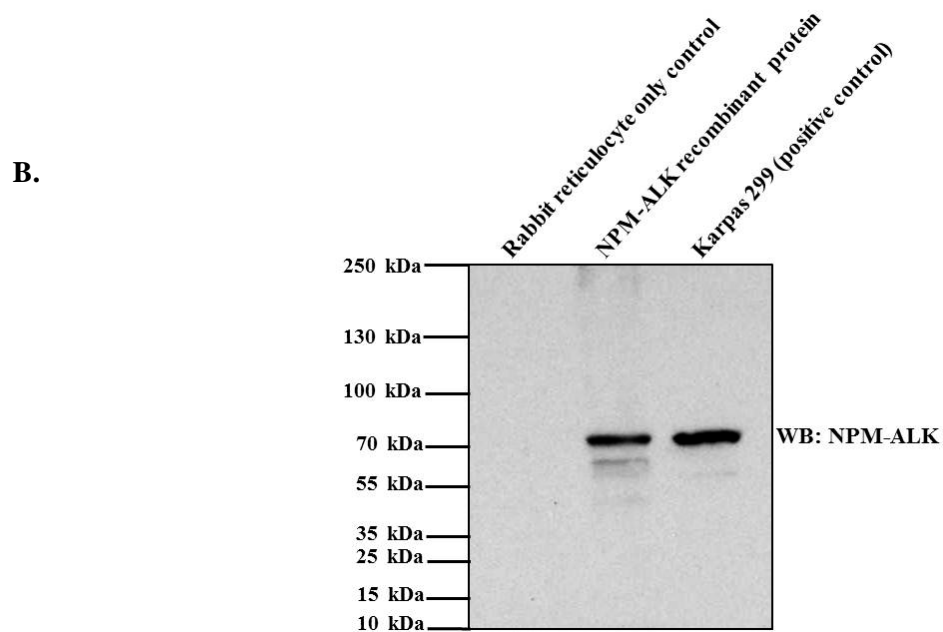
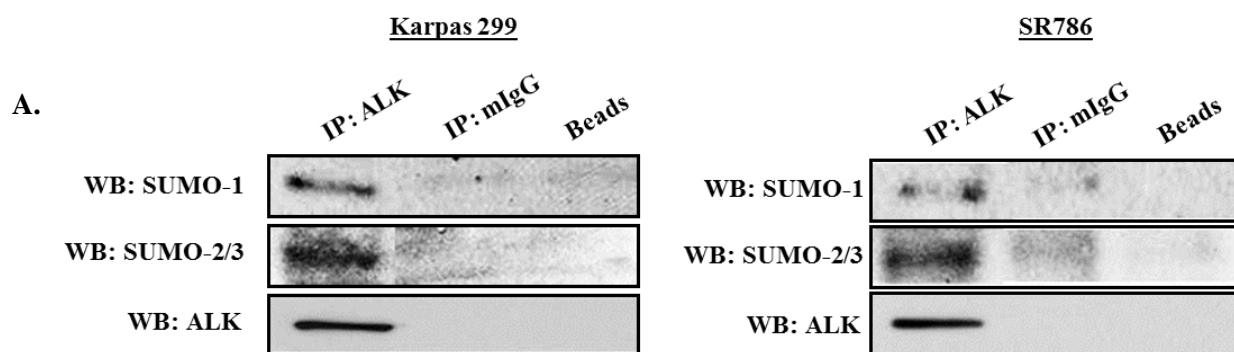


**FIGURE 27. NPM-ALK is SUMOylated.** (A) NPM-ALK was immunoprecipitated in Karpas 299 and SR-786 cells, and the expression of SUMO proteins was detected by Western blotting. These studies showed that SUMO-1 and SUMO-2/3 can interact with NPM-ALK, as indicated by bands present in lane 1 (NPM-ALK immunoprecipitation) but not in lanes 2 and 3, where normal mouse IgG was immunoprecipitated or beads alone were used in the IP reaction, respectively. (B) *Upper panel*; NPM-ALK recombinant protein was created using the TnT coupled rabbit reticulocyte kit. Western blotting was performed to test the expression of the NPM-ALK recombinant protein (entire membrane shown): no expression of NPM-ALK in rabbit reticulocyte lysate only (lane 1), positive band corresponding to NPM-ALK in the NPM-ALK recombinant protein at 80 kDa (lane 2), and in the positive control Karpas 299 cell line (lane 3). *Lower panel*; recombinant NPM-ALK protein was subjected to *in vitro* SUMOylation assay. Presence of a band with a molecular weight that is ~20 kDa higher than baseline NPM-ALK molecular weight was detected in lanes incubated with wild type SUMO-1 (lane 1), SUMO-2 (lane 3), or SUMO-3 (lane 5); incubation with mutated SUMO forms (lanes 2, 4, and 6) did not show higher molecular weight band.

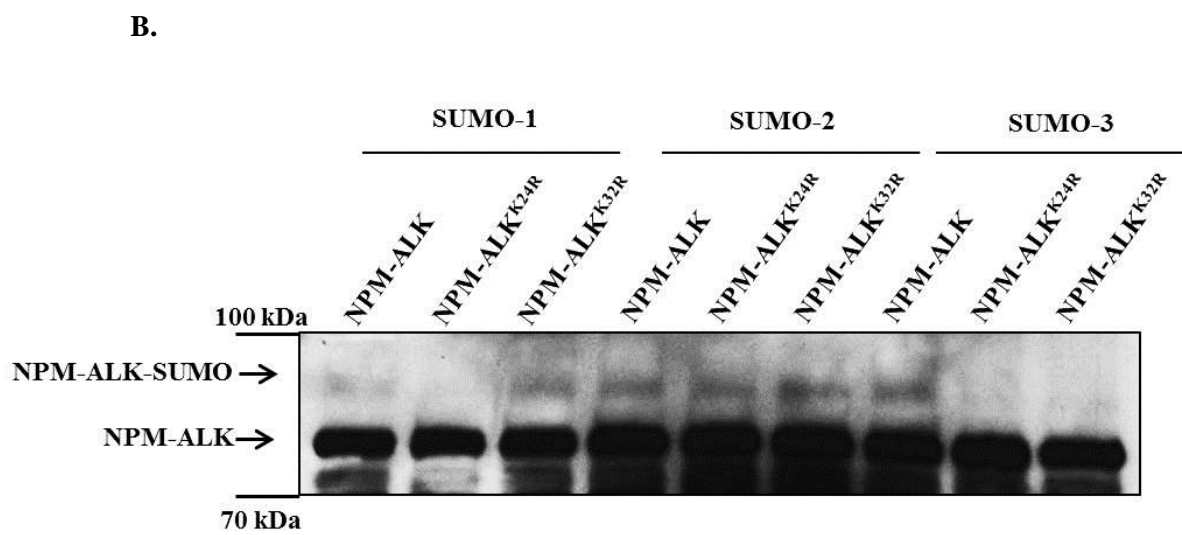
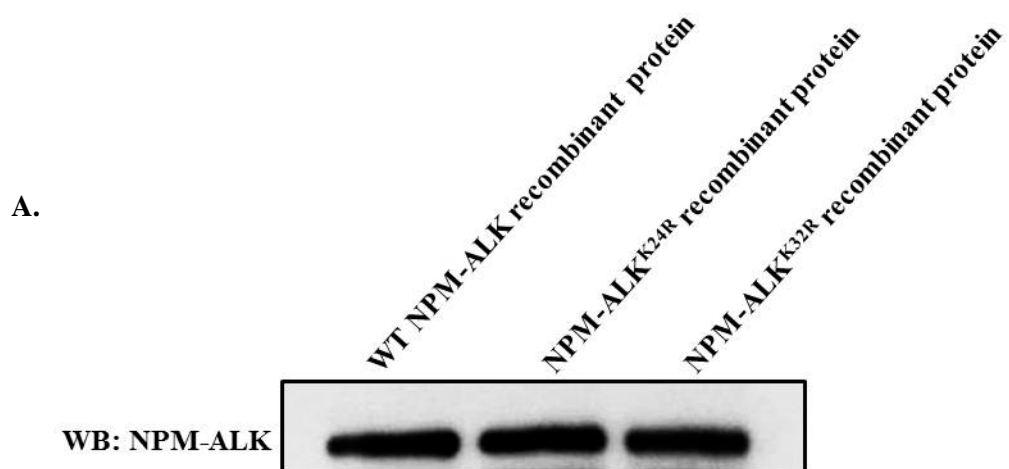


**FIGURE 28. NPM-ALK is SUMOylated at Lys<sup>24</sup> and Lys<sup>32</sup>.** (A) Mutated NPM-ALK recombinant proteins (NPM-ALK<sup>K24R</sup> and NPM-ALK<sup>K32R</sup>) were created using the TnT coupled rabbit reticulocyte kit. Western blotting was performed to test NPM-ALK protein expression of recombinant proteins: wild-type (WT) NPM-ALK recombinant protein (lane 1), NPM-ALK<sup>K24R</sup> recombinant protein (lane 2), and NPM-ALK<sup>K32R</sup> recombinant protein (lane 3). (B) Wild type and mutated recombinant NPM-ALK proteins were subjected to an *in vitro* SUMOylation assay. SUMOylation was abolished with the K24R mutation for SUMO-1 and SUMO-3 and with the K32R mutation for SUMO-3. These two mutations failed to deSUMOylate SUMO-2.





**FIGURE 29. SUMOylation promotes the stability of NPM-ALK protein.** *Upper panel;* Jurkat cells were transfected with wild type NPM-ALK, NPM-ALK<sup>K24R</sup>, NPM-ALK<sup>K32R</sup> or NPM-ALK<sup>K24R/K32R</sup> for 48 h and then treated with the protein synthesis inhibitor cyclohexamide (CHX) for an additional 0, 24, or 48 h. NPM-ALK<sup>K24R</sup> and NPM-ALK<sup>K32R</sup> substantially decreased NPM-ALK protein expression at 48 h (42% and 50% protein reduction, respectively), which was further enhanced with NPM-ALK<sup>K24R/K32R</sup> (67% protein reduction). In contrast, wild type NPM-ALK protein expression did not decrease even after 48 h. *Lower panel;* densitometry of NPM-ALK compared to  $\beta$ -actin.  $\beta$ -actin loading was unequal due to limited amount of protein available in some samples for Western blot after prolonged transfection.

*Abolishment of SUMOylation prevents nuclear NPM-ALK accumulation in NPM-ALK<sup>+</sup> ALCL cells:* It is well established that NPM-ALK gains the ability to translocate to the nucleus through the process of heterodimerization between wild type NPM and NPM-ALK [50]. Whether other unidentified factors contribute to this phenomenon remain unclear. SUMOylation has been shown to play important roles in the translocation of target proteins into the nucleus [233]. We set to study whether SUMOylation contributes to the translocation of NPM-ALK and its accumulation in the nucleus. To elucidate whether there is abundance of NPM-ALK inside the nucleus in NPM-ALK<sup>+</sup> ALCL cells, we fractionated Karpas 299 and SR-786 (2 cell lines showing low expression levels of endogenous SENP1, but higher expression of SUMO modifiers). As previously described [47], there was significantly higher expression of NPM-ALK in the nuclear extracts than in the cytoplasmic extracts, as well as higher expression of SUMO proteins in the nucleus (**Figure 30**). The strong presence of NPM-ALK inside the nucleus may be due to the enhanced SUMOylation process in NPM-ALK<sup>+</sup> ALCL cells. To further investigate this interesting observation, Karpas 299 and SR-786 cells were transfected with SENP1, one of the proteases responsible for removing the SUMO modifier from the target and thereby destabilizing the target, and cell fractionation was performed again. Consistent with previous studies [245, 246], we found that SENP1 is able to rapidly shuttle between the nucleus and cytoplasm in NPM-ALK<sup>+</sup> ALCL cells (**Figure 31; upper panel**). Importantly, SENP1 decreased the expression of SUMO proteins in the nucleus. This decrease was associated with reduction of nuclear NPM-ALK levels in both cell lines. This event further led to a decrease in the cytoplasmic expression of NPM-ALK, suggesting that SUMOylation contributes to the accumulation of NPM-ALK in the nucleus in NPM-ALK<sup>+</sup> ALCL cells, which appears to hinder its export from the nucleus to the cytoplasm (**Figure 31; lower panel**).

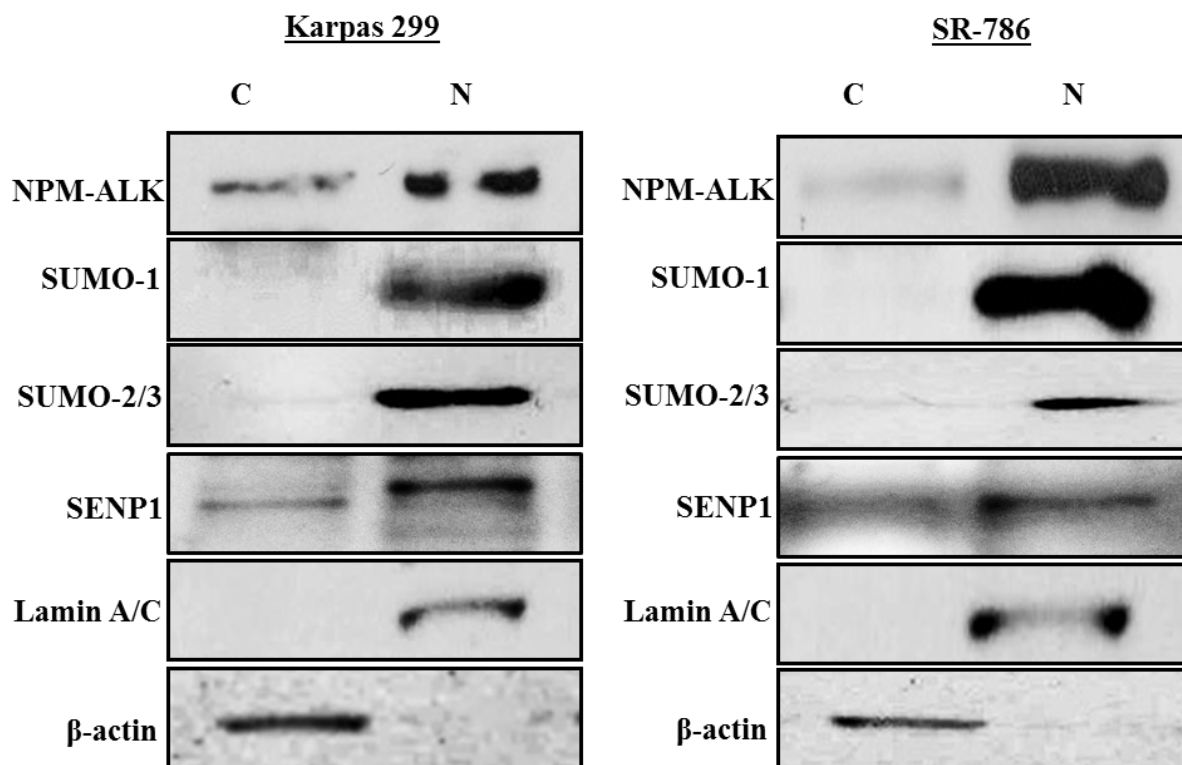


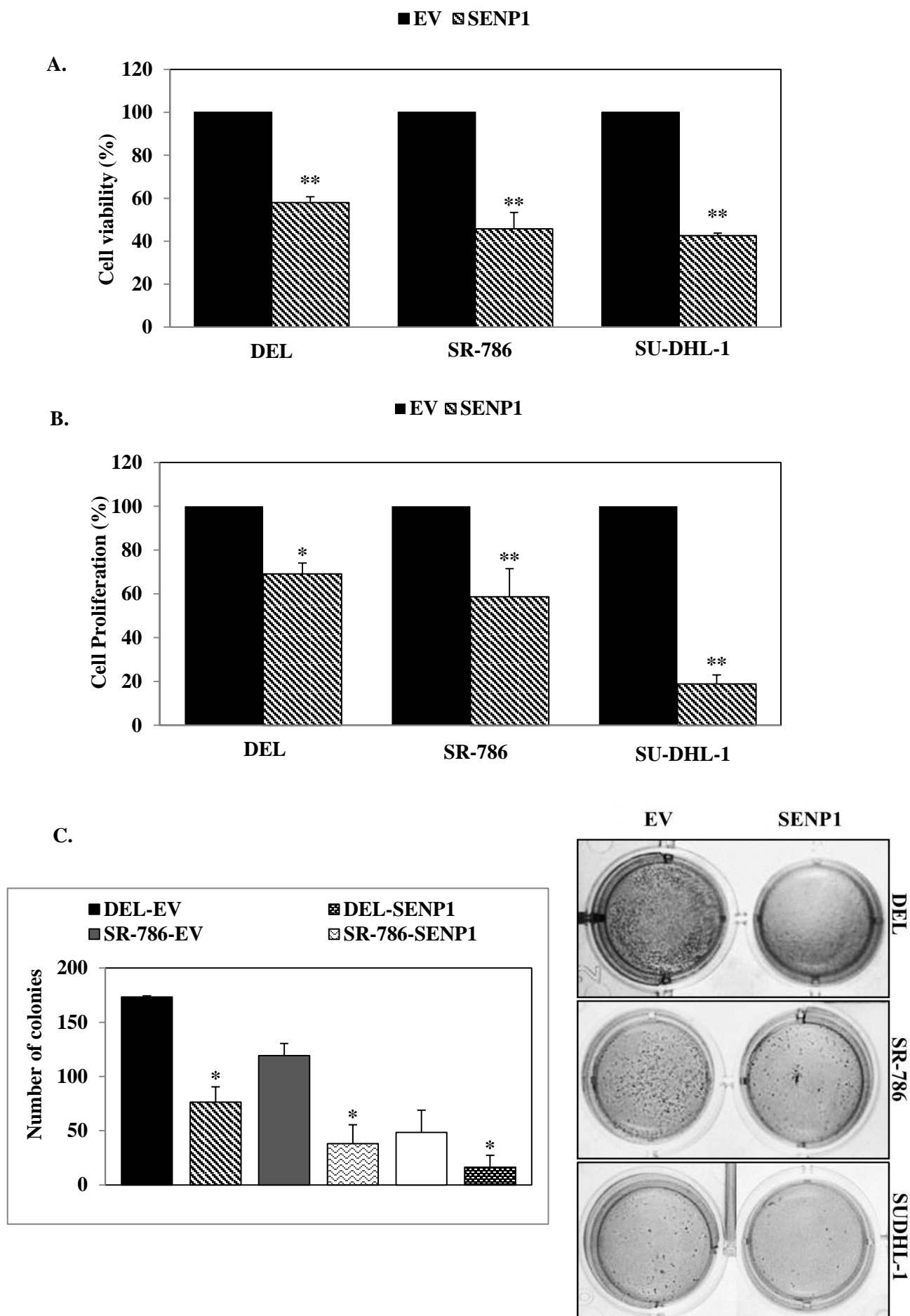
**FIGURE 30. NPM-ALK is predominantly expressed in the nucleus.** Cell fractionation experiments in Karpas 299 and SR-786 revealed higher expression of NPM-ALK protein in the nucleus, relative to cytoplasm. In addition, SUMO proteins were mainly nuclear. Lamin A/C and  $\beta$ -actin were used as nuclear and cytoplasmic loading controls, respectively.



**FIGURE 31. SENP1 decreases NPM-ALK expression.** *Upper panel;* Karpas 299 and SR-786 cells were transfected with EV or SENP1 expression plasmid. Then, immunofluorescence staining for the detection of SENP1 was performed at various time points. Up to 1 h, SENP1 was predominantly localized in the cytoplasm, and then it became predominantly nuclear at 3 to 6 h. At 24 h most of SENP1 appeared to be shuttling back to the cytoplasm, whereas at 48 h strong levels of expression of SENP1 were detected in the nucleus and cytoplasm. *Lower panel;* cellular fractionation shows that transfection of SENP1 in Karpas 299 and SR-786 cells resulted in decreased expression of SUMO-1 and SUMO-2/3 proteins at 48 h after transfection. The decrease in SUMO was associated with decreased NPM-ALK protein expression in the nucleus and cytoplasm at 48 h after transfection. The decrease in NPM-ALK levels appears to be more pronounced in the nucleus. Lamin A/C and  $\beta$ -actin were used as nuclear and cytoplasmic loading controls, respectively.

*Downregulation of the SUMOylation pathway decreases cell proliferation, viability, and colony formation potential in NPM-ALK<sup>+</sup> ALCL cells, and enhances the ubiquitination of NPM-ALK:* To test the biological impact of overexpressing SENP1, we transfected DEL, SR-786, and SU-DHL-1 (3 cell lines showing low expression levels of endogenous SENP1), with either empty vector or SENP1 full-length expression plasmid for 48 h. SENP1 significantly decreased cell viability, cell proliferation, and colony formation potential of lymphoma cells (**Figure 32A, 32B, 32C**). In addition, SENP1 increased the covalent modification of ubiquitin on NPM-ALK, suggesting that deSUMOylation by SENP1 switches target proteins to the ubiquitination pathway (**Figure 32D**).





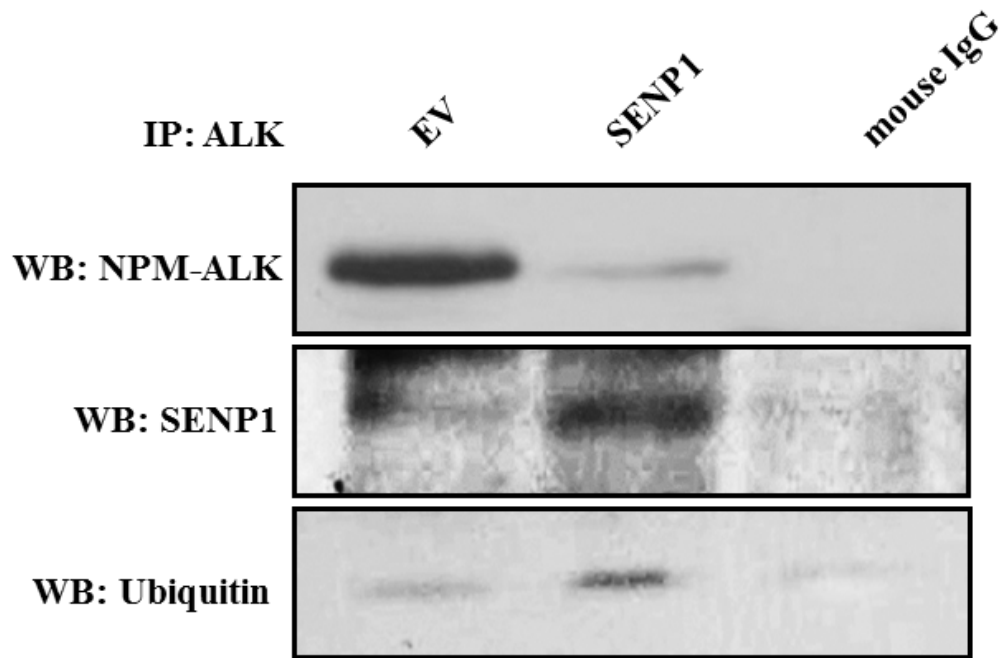


**FIGURE 32. SENP1 decreases cell viability, proliferation, and colony formation potential in NPM-ALK<sup>+</sup> ALCL cells.** (A) Transfection of DEL, SR-786, and SU-DHL-1 cells with EV or the SENP1 protease expression plasmid in resulted in a significant decrease in their viability after 48 h. (B) In addition, SENP1 decreased significantly the proliferation of these cells, and (C) decreased their colony formation potential. Numbers of colonies are shown on the left and representative images are shown on the right (\*: p<0.05; \*\*: p<0.001). (D) SENP1 decreased NPM-ALK expression, which was simultaneously associated with increased binding between ubiquitin and NPM-ALK, suggesting that deSUMOylation directs NPM-ALK to the ubiquitination pathway.

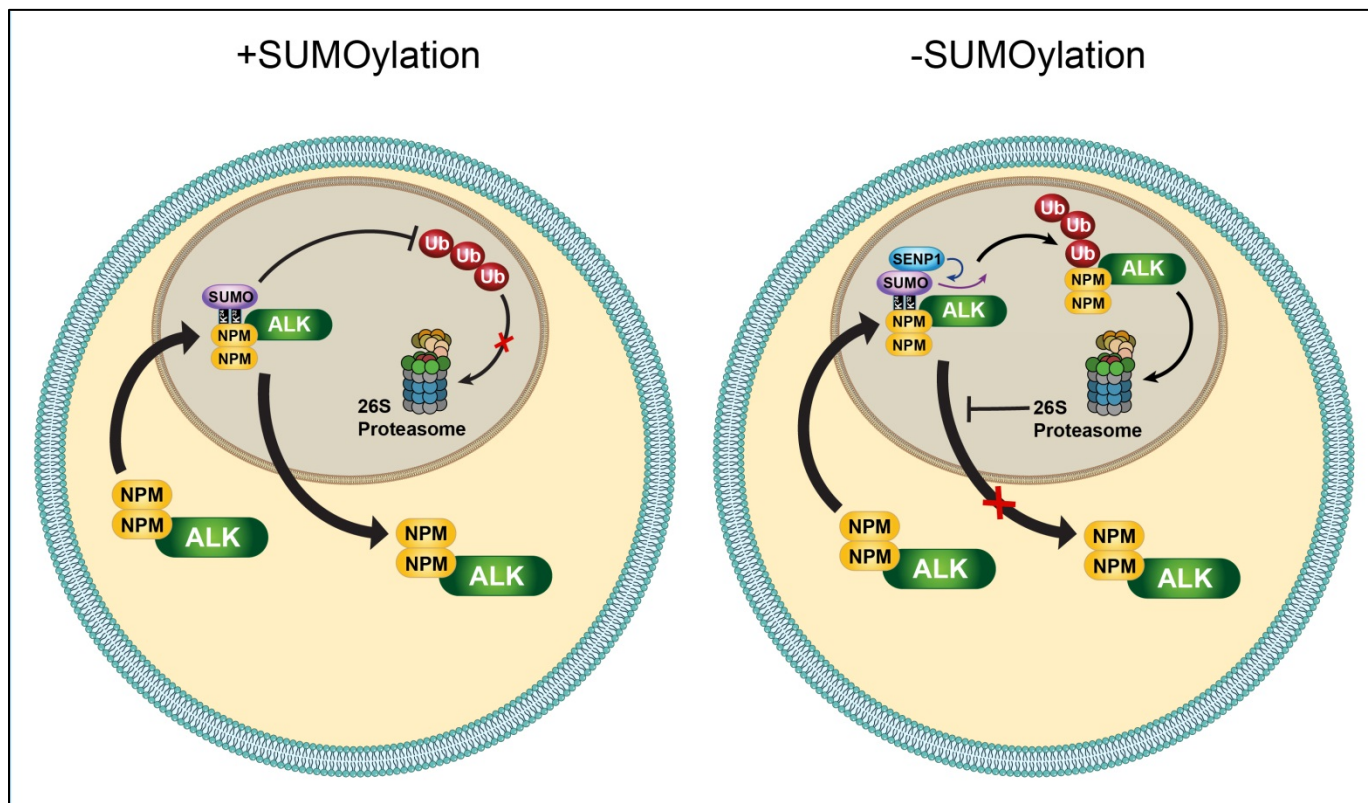


**FIGURE 33. Schematic model illustrating the SUMOylation of NPM-ALK.** We have identified that SUMOylation plays an important role in stabilizing NPM-ALK protein. NPM-ALK is able to form heterodimers with wild type NPM, which facilitates shuttling of NPM-ALK between the cytoplasm and nucleus. *Left panel;* SUMOylation of NPM-ALK at Lys<sup>24/32</sup> results in its stabilization in the nucleus, which leads to efficient shuttling of NPM-ALK into the cytoplasm. *Right panel;* in the presence of deSUMOylating protease SENP1, the SUMO modifier is removed from the NPM-ALK heterodimer in the nucleus which allows the binding of ubiquitin, which mediates its degradation via 26s proteasome, as has been previously demonstrated [247]. Degradation of the NPM-ALK heterodimer in the nucleus decreases its nuclear accumulation and subsequently reduces its translocation and expression in the cytoplasmic compartment.

### **3.5.3. Aberrant Posttranslational Mechanisms: IGF-I**

### 3.5.3.1. Materials and Methods

**Cell lines** – Three NPM-ALK<sup>+</sup> ALCL cell lines were used in this study: DEL, SUP-M2, and SR-786. The cell lines were maintained in RPMI 1640 medium (HyClone, South Logan, Utah) supplemented with 10% FBS (Sigma, St. Louis, MO), glutamine (2 mM), penicillin (100 U/ml), and streptomycin (100 µg/ml) at 37°C in a humidified 5% CO<sub>2</sub> in air chamber.

**Transfection** – Transfection of the cells with scrambled or NPM-ALK siRNA (Dharmacon) was performed by electroporation using Amaxa 4D nucleofection system in 100 µL cuvettes (Lonza; Solution SF, Program CA-150) and, thereafter, cells were incubated for 48 h.

**Western blotting** – Western blotting was used to analyze the expression of IGF-I and NPM-ALK proteins. Cells were collected and lysed using lysis buffer containing 25 mM HEPES (pH 7.7), 400 mM NaCl, 1.5 mM MgCl<sub>2</sub>, 2 mM EDTA, 0.5% Triton X-100, 0.1 mM PMSF, 2 mM DTT, phosphatase inhibitor (20 mM B-GP, 1 mM Na<sub>3</sub>VO<sub>4</sub>, Roche), and protease inhibitor cocktails (10 µg/ml leupeptine, 2 µg/ml pepstatin, 50 µg/ml antipain, 1x benzamidine, 2 µg/ml chymostatin; Roche). Concentrations were measured using Bio-Rad protein assay and OD values were obtained using an ELISA plate reader (Bio-Tek Instruments, Winooski, VT). Proteins (50 µg) were electrophoresed on 8% SDS-PAGE. The proteins were transferred to PVDF membranes and probed with specific primary antibodies and then with appropriate horseradish peroxidase-conjugated secondary antibodies (Santa Cruz; and GE Healthcare, Cardiff, UK). Proteins were detected using chemiluminescence-based kit (Amersham Life Sciences, Arlington Heights, IL).

**Antibodies** – Antibodies used were ALK (M719501-2; Dako, Carpinteria, CA); IGF-I (05-172; Millipore, Billerica, MA); and β-actin (A-5316; Sigma).

*ELISA* – To measure the levels of IGF-I secreted in cell culture supernatant, a standard ELISA-based approach was used. Briefly, cells were transfected with scrambled or ALK siRNA for 48 h. Thereafter, cells were switched to serum free media for 24 h. The medium was then collected and concentrated using Amicon Ultra-15 centrifugal tubes (UFC900308; Millipore). ELISA assay was performed using the IGF-I cytokine kit (R&D Systems).



### 3.5.3.2. Results

*NPM-ALK does not affect the levels of expression of IGF-IR or IGF-I:* Previous studies in our lab demonstrated that the levels of IGF-IR as well as endogenous IGF-I and secreted IGF-I were increased in NPM-ALK<sup>+</sup> ALCL [128] (**Figure 34**). To explore whether NPM-ALK plays a role in the increased levels of expression of IGF-IR and IGF-I, we transfected SR-786, DEL, and SU-DHL-1 cells with ALK siRNA for extended periods of time. Although siRNA effectively decreased NPM-ALK levels, the levels of IGF-IR protein (**Figure 35A**) and mRNA (**Figure 35B**) remained unchanged. In addition, decreased levels of NPM-ALK by siRNA were not associated with decreased levels of endogenous pro-IGF-I or IGF-I proteins (**Figure 35A**) or levels of secreted IGF-I (**Figure 35C**).

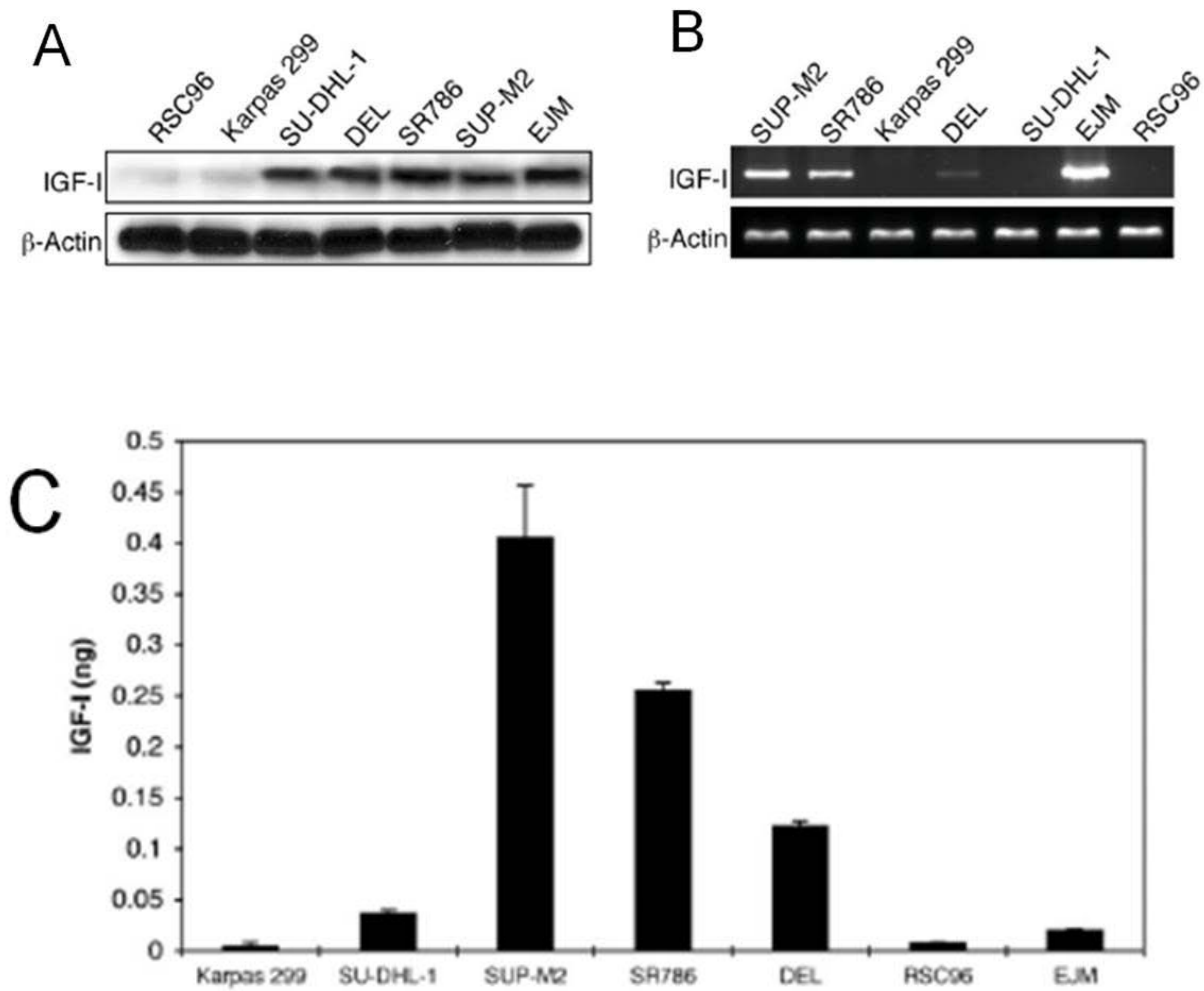


**FIGURE 34. Expression of IGF-I in NPM-ALK<sup>+</sup> ALCL cell lines.** (A) Western blotting shows overexpression of endogenous IGF-I in 4/5 NPM-ALK<sup>+</sup> ALCL cell lines. EJM (plasma cell myeloma) and RSC96 (Schwann cells) cell lines were used as positive and negative controls, respectively. (B) RT-PCR shows the presence of IGF-I mRNA in SUP-M2, SR-786, DEL (low level), and EJM, and its absence in Karpas 299, SU-DHL-1, and RSC96. (C) SUP-M2, SR-786, and DEL cell lines demonstrate the presence of secreted IGF-I in cell culture supernatants. The EJM cell line was included because it expresses IGF-I protein and mRNA. IGF-I is almost undetectable in cell culture supernatants from Karpas 299 and RSC96 cells. The experiment was repeated 3 times, and the results shown are the mean  $\pm$  SD.  $P < 0.01$  for SUP-M2, SR-786, and DEL compared with other cell lines. **Adapted by direct permission from BLOOD (Shi P, Lai R, Lin Q, Iqbal AS, Young LC, Kwak LW, Ford RJ, Amin HM. IGF-IR tyrosine kinase interacts with NPM-ALK oncogene to induce survival of T-cell ALK<sup>+</sup> anaplastic large-cell lymphoma cells. Blood. 2009 Jul 9;114(2):360-70.), copyright 2009.**

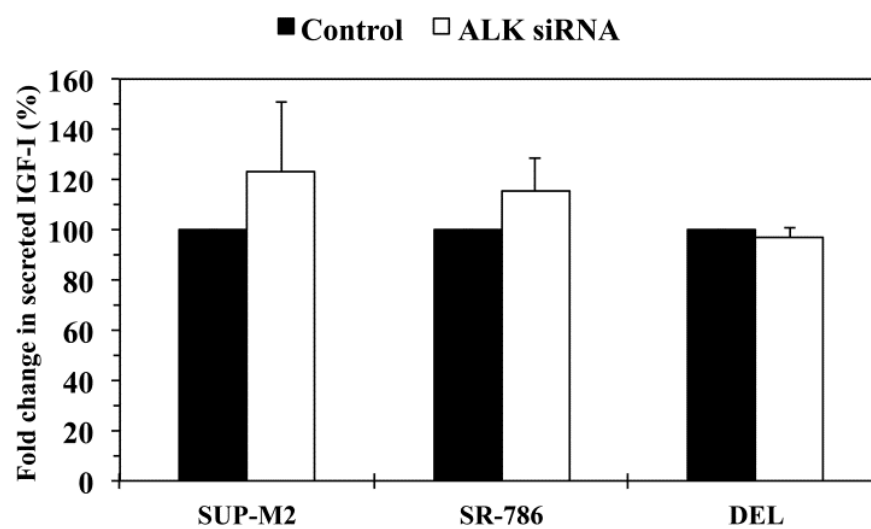
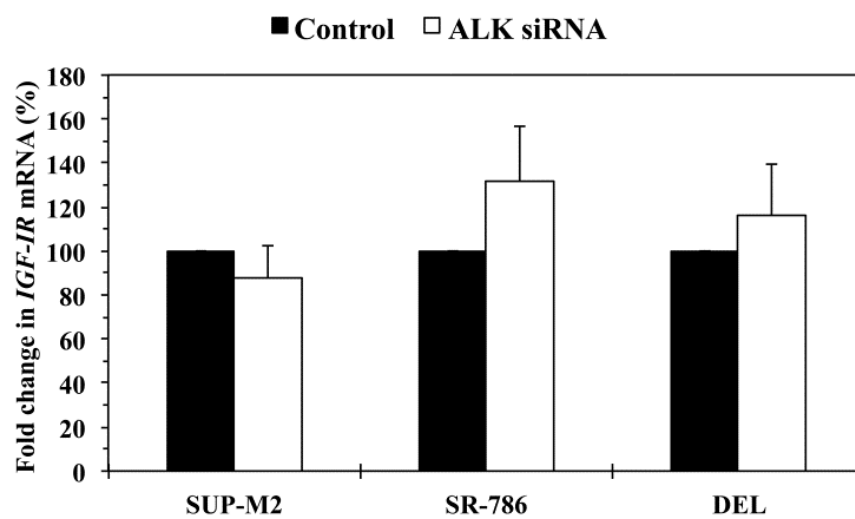
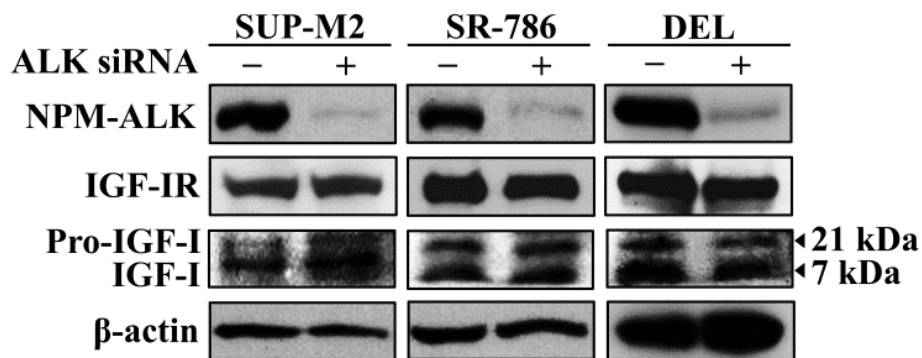


**FIGURE 35. NPM-ALK does not affect the levels of expression of IGF-IR and IGF-I.** (A) Western blotting shows that at 48 h, downregulation of NPM-ALK by ALK siRNA was not associated with decreased expression of IGF-IR, pro-IGF-I or IGF-I proteins in SUP-M2, SR-786, and DEL cell lines. Analysis of IGF-IR levels after transfection of the cells with ALK siRNA was performed at extended time points (12, 24, 48, 72, and 96 h), and also in other cell lines including Karpas 299 and SU-DHL-1, with similar results (data not shown).  $\beta$ -Actin shows equal protein loading. (B) Downregulation of NPM-ALK in the 3 cell lines did not decrease the levels of *IGF-IR* mRNA. The example shown is at 48 h after transfection of the cells with ALK siRNA. The results are shown as means  $\pm$  SE of 4 consistent experiments. In addition, analysis of *IGF-IR* mRNA was performed at other time points and cell lines as described in Fig. 6A. Changes in *IGF-IR* mRNA levels were not detected at any time point (data not shown). (C) An ELISA assay showing that specific downregulation of NPM-ALK did not decrease the levels of secreted IGF-I in the 3 NPM-ALK<sup>+</sup> ALCL cell lines SUP-M2, SR-786, and DEL. The results represent means  $\pm$  SE of 3 experiments.

### 3.6. Discussion for Aim 3

In this aim we show that posttranslational defects exist and contribute to the pathogenesis of NPM-ALK<sup>+</sup> ALCL. Firstly, we found that there was an overall upregulation of SUMO proteins expression in 5 NPM-ALK<sup>+</sup> ALCL cell lines as well as in ALK<sup>+</sup> ALCL patients' specimens compared to normal human T lymphocytes. Specifically, the expression of SUMO-2/3 was increased in the lymphoma cell lines and patients' tumor samples. In addition, the expression of SUMO-1 was increased in majority of cell lines and patients' tumors. In contrast, expression of the SUMOylation inhibitor SENP1 was decreased in the cell lines and patients' tumors than the T lymphocytes. We also showed that NPM-ALK is SUMOylated via covalent modification by SUMO proteins, which protects it from degradation. In support of this idea, inhibition of SUMOylation through restoration of the deSUMOylating SENP1 protease decreased SUMO protein expression, and induced a substantial decrease in NPM-ALK protein expression in the cytoplasm and nucleus. Our data provide strong evidence that SUMOylation contributes to the stability of NPM-ALK protein in NPM-ALK<sup>+</sup> ALCL. Downregulation of SUMOylation by SENP1 resulted in decreased viability, proliferation, and colony formation potential of the lymphoma cells, suggesting that disruption of the SUMOylation pathway induces tumor-suppressing effects in this type of cancer. Secondly, we found that NPM-ALK does not regulate the expression of IGF-I and IGF-IR proteins. IGF-I is the main ligand for IGF-IR and causes posttranslational modifications of IGF-IR thorough phosphorylation and subsequent activation.

SUMOylation is a dynamic process that induces major impact on target proteins including changing their stability, localization, and activity. Whereas SUMOylation is important for physiological processes, it is deregulated in cancer cells [248]. In line with this possibility, our data showed that the SUMO proteins were aberrantly overexpressed and

SENPI1 protease was decreased in NPM-ALK<sup>+</sup> ALCL compared to normal T lymphocytes. It has been established that an important outcome of SUMOylation is the maintenance of protein stability by protecting targets from proteosomal degradation [237, 249-254]. We were able to identify K24 and K32 within the NPM domain as targets for SUMOylation in NPM-ALK oncogenic protein. Indeed, all SUMO modifiers were capable of modifying NPM-ALK at these lysine residues. Mutations induced at K24 and K32 in the SUMO consensus motifs of NPM-ALK prevented SUMO-1 and SUMO-3 from modifying NPM-ALK as well as resulted in significant degradation of NPM-ALK protein, testifying to the stabilizing effect of SUMOylation on NPM-ALK. Moreover, both SUMO-1 and SUMO-3 were required to induce substantial degradation, in contrast to the level of degradation achieved individually by these modifiers. This observation suggests that this dual mutation that prevents both SUMO modifiers from modifying NPM-ALK is required for NPM-ALK to undergo degradation. Also, the finding that NPM-ALK double mutant was not degraded entirely because NPM-ALK double mutant maintained its ability to bind with SUMO-2. Therefore, we cannot completely exclude that other SUMO binding motifs may encompass potential binding sites for other SUMO modifiers, such as SUMO-2, which also conveys protection of NPM-ALK from degradation.

We elected to study SENPI1 because of its ability to deSUMOylate all 3 SUMO modifiers, unlike other SENPs that have preferential deSUMOylation activities [255-257]. SENPs have 2 primary functions: 1) the conversion of SUMO precursors to mature SUMO via removal of a portion of the C-terminus; and 2) the removal of SUMO from target proteins. These SENP-controlled processes contribute to the dynamic nature of SUMOylation. In fact, using immunofluorescence staining we found that SENPI1 moves from the nucleus to cytoplasm in only 15 min. This is in line with previous studies which showed the very short time required

by SENP1 to shuttle between the nucleus and cytoplasm, and how this mechanism allows SENP1 to elicit different functions in multiple compartments within the cell [245, 246, 258-260]. It has been shown that amino acid residues located at positions 171-177, within the N-terminal region of SENP1, are essential for SENP1 nuclear targeting. This was directly demonstrated through substitution experiments in which the basic residues within this short motif hindered significantly SENP1 nuclear accumulation and restricted its expression in the cytoplasm. Although this motif does not fit the classical consensus NLS sequence, these results provided evidence that this region can be classified as a nonconsensus NLS and more importantly, is required for SENP1 nuclear import as well as modulating SENP1 activity [260]. Reestablishment of SENP1 in NPM-ALK<sup>+</sup> ALCL cells resulted in increased deSUMOylation activity, which was associated with decreased expression of the SUMO proteins and NPM-ALK protein levels. As a result, downregulation of the SUMOylation pathway by SENP1 decreased cell viability, proliferation, and colony formation.

NPM is inherently capable of moving between the nucleus and cytoplasm [50]. The nuclear localization signal (NLS) of NPM is present within its C-terminus [17]. Nonetheless, the NPM segment that associates with ALK to form the NPM-ALK chimera is derived from the more proximal N-terminus that lacks the NLS, explaining why NPM-ALK lacks the ability to move to the nucleus [50]. However, nuclear translocation of NPM-ALK still occurs primarily because of the formation of heterodimers between wild type NPM and NPM-ALK. Our experiments showed that the expression of NPM-ALK in the nucleus, as well as cytoplasm, was significantly reduced after SENP1 transfection. This may be explained by: 1) SENP1 activity increased in the nucleus upon transfection with SENP1 plasmid, allowing for deSUMOylation to simultaneously increase in the nucleus leading to NPM-ALK destabilization; and 2) SENP1-mediated degradation of NPM-ALK heterodimers in the



nucleus makes them less available for nuclear export into the cytoplasm. Our results suggest a model in which SUMOylation provides stabilization of NPM-ALK protein, which appears to further sustain NPM-ALK expression and accumulation in the nucleus and cytoplasm.

SUMOylation can lead to alteration of protein surfaces, which greatly affects interactions of the target protein with other molecules that can also indirectly influence the target's stability. For instance, it has been shown that SUMOylation can promote protein-protein interactions [261-265]; however, in many cases, SUMOylation leads to protein-protein interaction interference [266-268]. For instance, SUMOylated E2-25K prevents interaction with the ubiquitin E1 activating enzyme [268]. Similarly, there have been studies indicating that disruption of SUMOylation reveals ubiquitin-acceptor lysine residues located elsewhere in the protein, whose subsequent ubiquitination will promote protein degradation [250, 251, 269]. In NPM-ALK<sup>+</sup> ALCL cells, deSUMOylation of NPM-ALK by SENP1 led to an increase in the association of ubiquitin and NPM-ALK, suggesting that SUMOylation may be able to prevent NPM-ALK from entering the proteosomal degradation pathway. NPM-ALK has been previously shown to be ubiquitinated through hsp70-mediated proteosomal degradation, although a specific lysine residue for ubiquitination has not been identified [247]. Our data suggest that transfection of SENP1 resulted in the removal of the SUMO modifiers, which unmasked lysine residues in NPM-ALK and made them available for modification by ubiquitin for proteosomal degradation. To this end, there is no direct evidence that ubiquitin binds to and modifies K24 and K32 that we identified as sites of modification by SUMO proteins, however, we cannot completely rule out that at least one of these residues possess ability to be modified by ubiquitin. Indeed, entering the amino acid sequence in a web-based ubiquitination prediction search algorithm (UbPred; [www.ubpred.org](http://www.ubpred.org)) revealed that NPM-ALK contains potential ubiquitination site at K32

(intermediate statistical confidence of  $p=0.71$ ). Importantly, we have provided evidence that ubiquitin and NPM-ALK are physically associated after SENP1 transfection, and it is likely that deSUMOylation triggers the ubiquitination pathway.

It has been previously shown that IGF-IR undergoes ligand-dependent SUMOylation, which appears to be a prerequisite for its nuclear translocation [238, 270]. It has also been shown that this nuclear translocation requires the phosphorylation of IGF-IR [271]. In our lymphoma cells, IGF-I stimulation induced nuclear expression of pIGF-IR (**Figure S7**). We also determined that IGF-IR is capable of interacting with SUMO proteins in NPM-ALK<sup>+</sup> ALCL cells (**Figure S8**), and that transfection of SENP1 leads to decreased expression of IGF-IR in the cytoplasm as well as decreased pIGF-IR nuclear expression (**Figure S9**). We have recently demonstrated that the physical association between NPM-ALK and IGF-IR proteins enhances the stability of NPM-ALK [127]. In support of this idea, specific targeting of IGF-IR by siRNA significantly decreased NPM-ALK protein levels, attesting to the contribution of IGF-IR to maintaining NPM-ALK protein stability [127]. In contrast, NPM-ALK has no effect on IGF-IR protein stability (**Figure 35 in section 3.5.3.2.**). Therefore, it can be postulated that deSUMOylation of IGF-IR by SENP1 perhaps causes interference of its association with NPM-ALK, which would lead to NPM-ALK protein instability. However, further studies need to be performed to establish such a claim. Jointly, these alternative mechanisms also provide novel evidence in which SUMOylation contributes to NPM-ALK protein stability.

It was previously demonstrated that chimeric oncogenes such as the Ewing sarcoma oncogenic fusion proteins induce the expression of IGF-I, the primary ligand of IGF-IR, which enhances the phosphorylation/activation of IGF-IR through dimerization [68]. In this aim, we tested whether NPM-ALK induces effects similar to Ewing sarcoma fusion proteins

on IGF-I levels. Specific abrogation of NPM-ALK by siRNA failed to reduce pro-IGF-I or IGF-I protein levels, which suggests that NPM-ALK lacks ability to upregulate IGF-I expression, and therefore does not possess a posttranslational effect on IGF-IR, at least from this aspect.

In this aim, we identified for the first time that SUMOylation contributes to maintaining NPM-ALK protein stability, and hinders its proteosomal degradation. In contrast, SENP1-mediated disruption of SUMOylation causes degradation of NPM-ALK, which thereby reduces the oncogenic potential of this oncogenic protein. At the other hand, we found that NPM-ALK does not regulate IGF-I-mediated posttranslational modulation of IGF-IR.

## 3.6.1. Supplemental

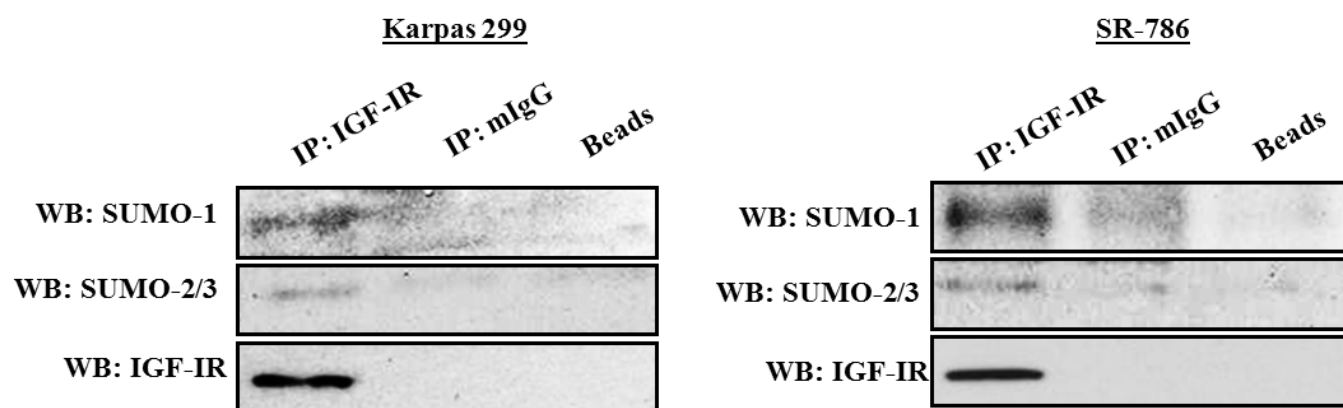
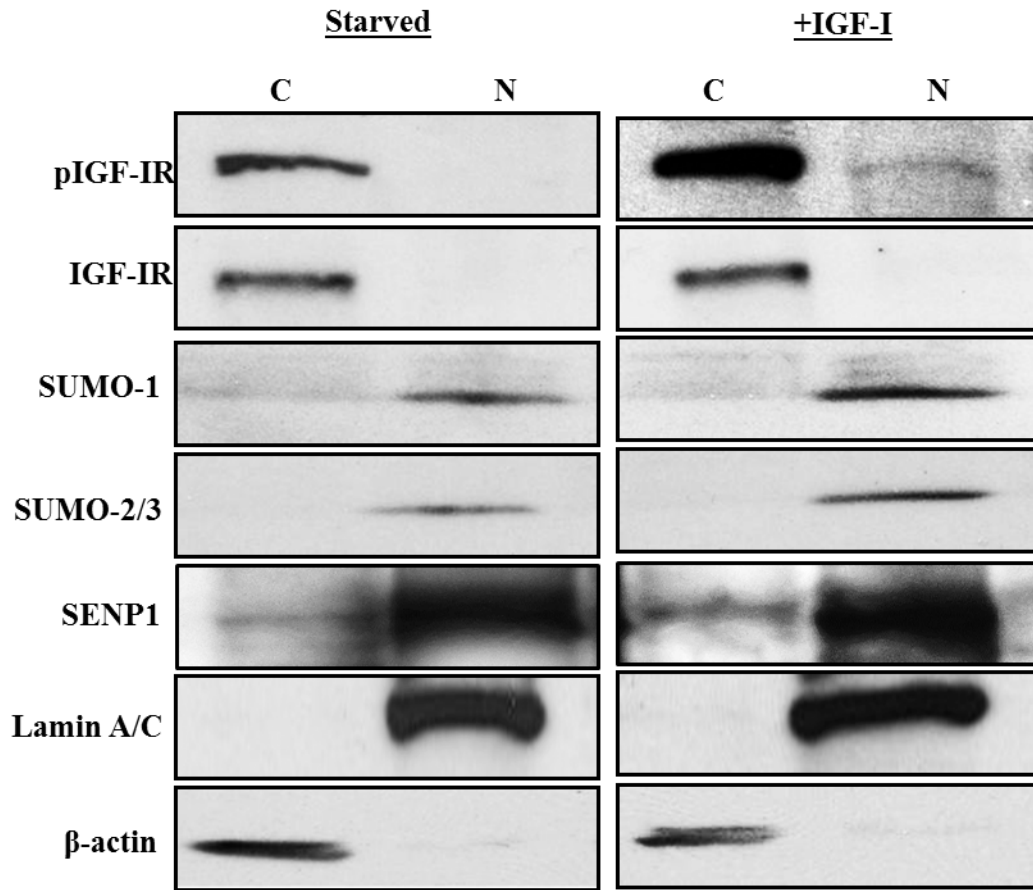


**FIGURE S7. IGF-IR is SUMOylated.** IGF-IR was immunoprecipitated in Karpas 299 and SR-786 cells, and expression of SUMO proteins was evaluated by Western blotting. These studies revealed SUMO-1 and SUMO-2/3 are associated with IGF-IR, as indicated by bands present in lane 1 (IGF-IR immunoprecipitation) and not in lanes 2 and 3, where mouse IgG was immunoprecipitated or beads alone, respectively.



**SR-786**

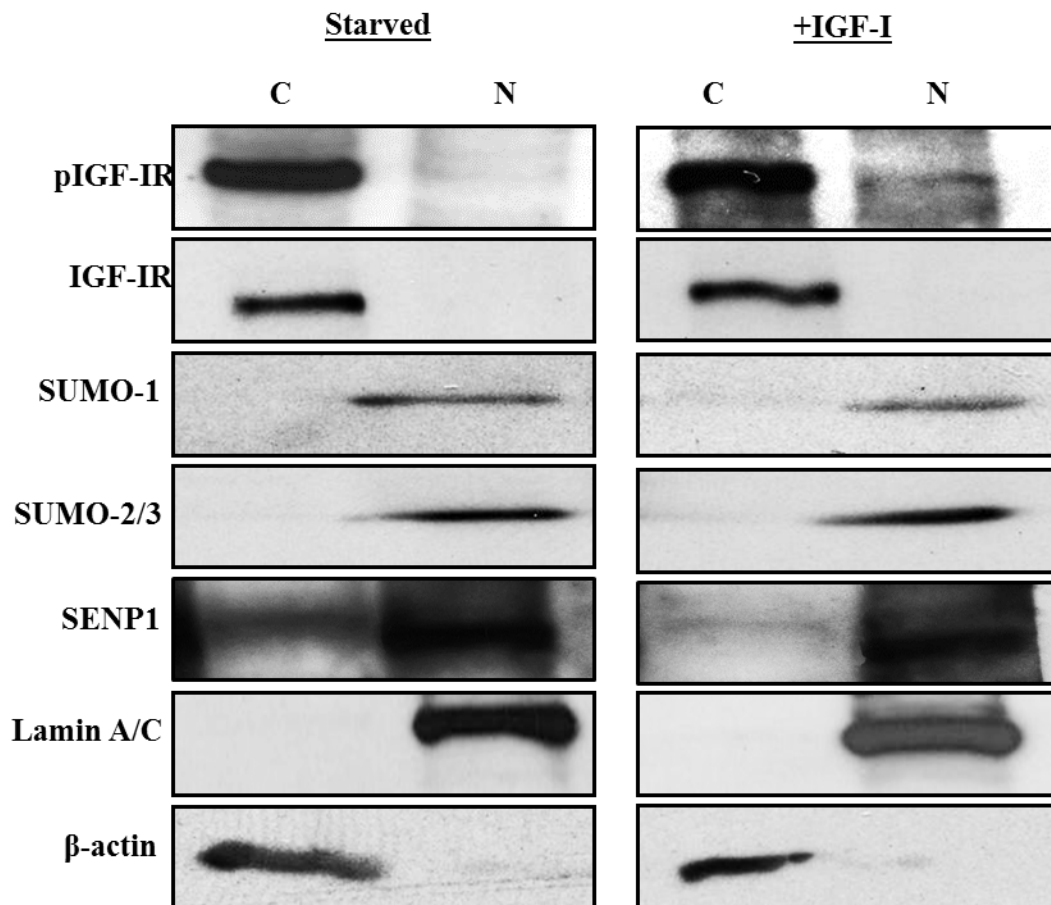


**FIGURE S8. IGF-IR and pIGF-IR are expressed in the cytoplasm, whereas pIGF-IR is expressed in the cytoplasm and nucleus after IGF-I stimulation.** Cell fractionation experiments in Karpas 299 and SR-786 cells reveals expression of IGF-IR protein in the cytoplasm, with no expression in the nucleus with or without IGF-I stimulation. In contrast, pIGF-IR is predominantly located in the cytoplasm under non-stimulated conditions. After IGF-I stimulation, however, pIGF-IR is expressed in the cytoplasm and nucleus. In addition, SUMO proteins predominantly showed nuclear expression. Lamin A/C and  $\beta$ -actin were used as nuclear and cytoplasmic loading controls, respectively.

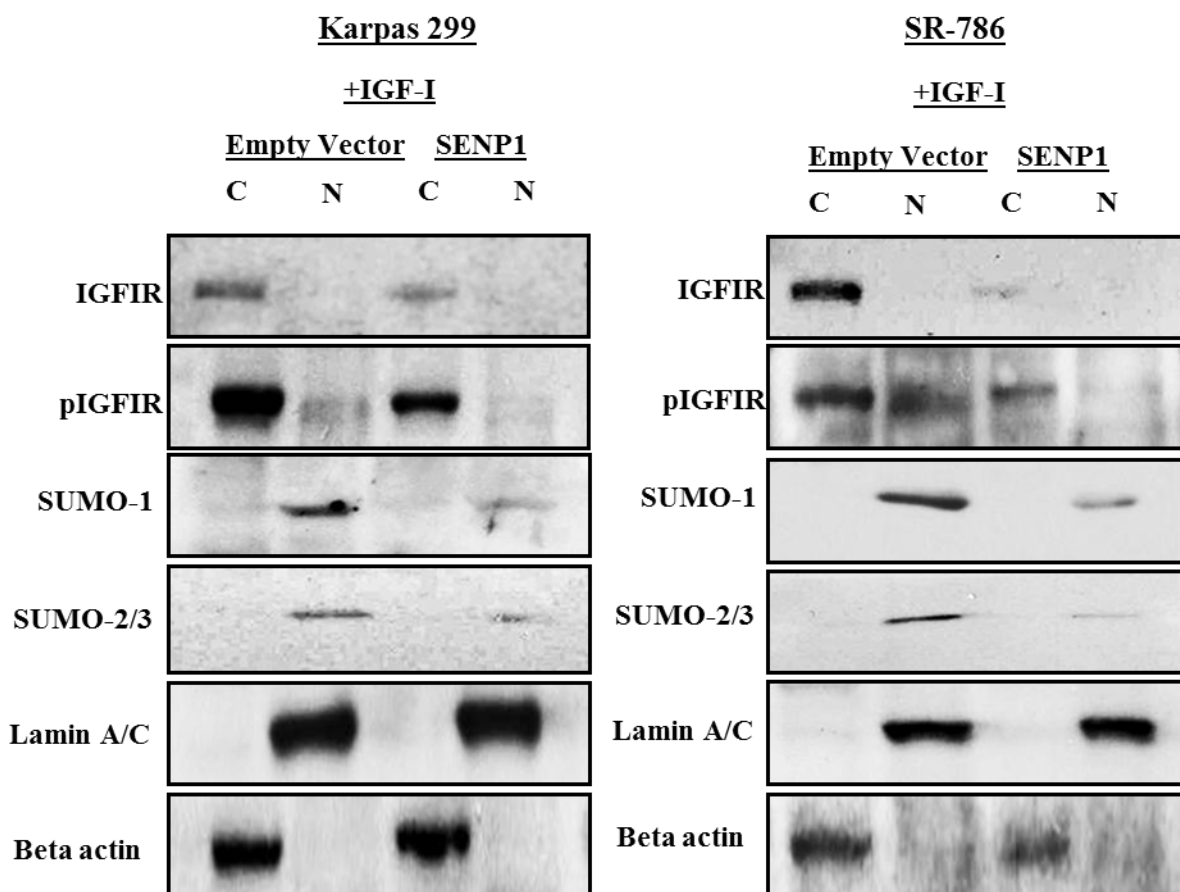




**FIGURE S9. SENP1 decreases IGF-IR nuclear and cytoplasmic expression.** Transfection of empty vector or SENP1 expression plasmid in Karpas 299 and SR-786 cells decreased the expression of SUMO proteins after 48 h. Subsequently, IGF-IR and pIGF-IR expression decreased in the cytoplasm. In addition, pIGF-IR expression decreased significantly in the nucleus as well. Lamin A/C and  $\beta$ -actin were used as nuclear and cytoplasmic loading controls, respectively.

## **Conclusions**

In this work, we identified novel deregulated mechanisms that determine the pathogenic expression of IGF-IR and NPM-ALK, two potent oncogenic proteins that play important roles in the survival of NPM-ALK<sup>+</sup> ALCL; an aggressive type of cancer that predominantly affects children and young adults.

At the transcriptional level, we found that two transcription factors, namely Ik-1 and MZF1, are markedly decreased in NPM-ALK<sup>+</sup> ALCL cell lines and patients lymphoma tissues. Importantly, we provided evidence that Ik-1 and MZF1 negatively regulate the *IGF-IR* gene promoter, which leads to a significant decrease in the expression of IGF-IR mRNA and protein. We also used FISH analysis and found no evidence to support amplification of the *IGF-IR* gene in this lymphoma. It is important to note that although we performed FISH analysis in 5 established NPM-ALK<sup>+</sup> ALCL cell lines and obtained consistent findings, it cannot be ruled out that if a large cohort of patient samples were analyzed, rare cases with *IGF-IR* gene amplification might have been discovered.

At the posttranscriptional level, we found that the time required for the decay of *IGF-IR* mRNA is significantly longer in the NPM-ALK<sup>+</sup> ALCL cell lines than normal human T lymphocytes, which supports the idea that more *IGF-IR* mRNA transcripts are available for translation into IGF-IR protein, resulting in the overexpression of IGF-IR in this lymphoma. Also at the posttranscriptional levels, we showed that miR-30a and miR-30d are substantially decreased in NPM-ALK<sup>+</sup> ALCL cell lines and human lymphoma tissues. Importantly, we demonstrated that miR-30a and miR-30d are capable of binding and inhibiting the *IGF-IR*-3'UTR to decrease IGF-IR protein expression.

At the posttranslational level, we identified for the first time that SUMOylation, a posttranslational modification mechanism, is deregulated in NPM-ALK<sup>+</sup> ALCL. In this

regard, SUMOylation appears to sustain the stability of NPM-ALK protein and facilitates its nuclear and cytoplasmic accumulation. Although it has been demonstrated in other types of cancer, herein our data support that SUMOylation sustains IGF-IR protein stability also in NPM-ALK<sup>+</sup> ALCL. On the other hand, there was no evidence to support that NPM-ALK is involved in the regulation of IGF-I expression, and hence doesn't impact IGF-I-mediated phosphorylation/activation of IGF-IR.

Intriguingly, our data support that increased expression of IGF-IR protein and decreased expression of miR-30a and miR-30d appear not to be directly resulting from the expression of NPM-ALK. Although NPM-ALK has significant oncogenic potential and its expression is considered the mainstay feature in NPM-ALK<sup>+</sup> ALCL, most likely NPM-ALK is not the only factor that governs the clinicopathological and the immunophenotypic features of NPM-ALK<sup>+</sup> ALCL as known in human patients. Evidence suggests the oncogenic effects of NPM-ALK stem from its ability to collaborate with other survival-promoting proteins within the lymphoma cells. Although the lymphomagenic potential of NPM-ALK has been demonstrated in chimeric as well as transgenic (Tg) mice models, mice typically developed significant B-cell lymphoma and plasma cell tumors with a smaller proportion developing T-cell neoplasms. [272]. For instance, it has been shown that in an NPM-ALK Tg mouse model under the control of a murine *CD4* promoter, mice developed lymphoma tumors of B-cell origin [56]. In addition, the lymphoma tumors found in some these mice were exclusively plasmablastic [56]. In another model, NPM-ALK transgenic mice under the control of the *Vav*-promoter also gave rise almost exclusively to tumors of a B-cell origin [273]. This is particularly interesting because the *Vav*-promoter is directly involved in the development and expression of all the types of hematopoietic lineages. Furthermore, in a transgenic mouse model in which NPM-ALK was under the control of the *lck* promoter, the developed tumors

were of immature T lymphoblastic type [274]. While the *lck* promoter model is more suitable for studying T-cell lineage tumors (*lck* promoter is active in T cells), the authors concluded that this animal model does not reflect the classic human NPM-ALK<sup>+</sup> ALCL development. Lastly, in a chimeric animal model, irradiated mice transplanted with bone marrow cells infected with a retroviral construct, pSR $\alpha$ MSVtkneo–*NPM-ALK* that contains the human *NPM-ALK* cDNA, developed lymphomas that were composed of immunoblast-like B-cells [53]. Collectively, these observations indicate that NPM-ALK may be inclined to transform B-cell lineages in mice, in contrast to tumors of T-cell origin such as those of human NPM-ALK<sup>+</sup> ALCL [275]. More importantly, these data are inline with our results that failed to show that NPM-ALK, despite being a very important survival molecule in NPM-ALK<sup>+</sup> T-cell lymphoma, does not necessarily regulate all factors contributing to the survival of these cells, e.g., the increase in IGF-IR or the decrease in miR-30a/miR-30d expressions.

The evidence provided by the animal studies supporting how NPM-ALK is very important for development of lymphoma tumors yet, these tumors are not necessarily similar to NPM-ALK<sup>+</sup> ALCL in humans further strengthens the argument that the multilevel deregulation identified in our experiments carry important potential in the pathogenesis of this aggressive disease. However, there are limitations to *in vitro* studies including that this experimental system lacks essential components that affect the cells under physiological conditions such as the microenvironment that includes surrounding stromal tissue and blood vessels. These elements are not found in a purely *in vitro* system, and can influence the outcome of the result. *In vivo* experiments, although more closely related to human conditions, also have their limitations. While animal models do contain the microenvironment, they do not represent human conditions exactly. Differences in species, even subtly, can produce different outcomes. Therefore, perhaps the ideal way to examine if

truly a specific oncogenic mechanism is deregulated is by directly analyzing this mechanism in a large cohort of patients with correlation to clinicopathological features and response to therapy and survival data. In our study, we analyzed the expression of Ik-1, MZF1, miR-30, and SUMO proteins in relatively small patient populations. Although such analysis supports that these aberrancies indeed exist in patients, more extensive analysis in a larger cohort of patients is expected to help to provide concrete conclusions.

It has been shown that NPM-ALK interacts with several molecules known to regulate cellular survival. In preliminary studies conducted in our lab, we found that NPM-ALK interacts with IGF-IR to maintain the latter's phosphorylation status. Reciprocally, our data suggested that IGF-IR not only maintains NPM-ALK phosphorylation, but also sustains its stability. In the current study, we have further demonstrated using several experimental approaches in which modifications of transcriptional, posttranscriptional, and posttranslational pathways resulted in abrogation of IGF-IR signaling system was associated with a remarkable decrease in NPM-ALK protein expression attesting that IGF-IR sustains the stability of NPM-ALK. At least from these data, IGF-IR could represent a unique oncogenic entity in this lymphoma.

The aberrant expression/function of key molecules at each regulatory stage, beginning at the "gene level" and ending at the "protein level", allows IGF-IR to escape tight regulatory systems in this lymphoma; in contrast to normal human T lymphocytes, in which these systems keep IGF-IR expression at low physiologic levels. This observation further emphasizes the contributions of every single system. It also suggests that the failure of one mechanism to maintain overexpression of IGF-IR might result in alternative pathways that rescue IGF-IR expression and maintain it at very high levels for it to continue to elicit oncogenic effects. Targeting IGF-IR not only provides opportunities to decrease the

oncogenic effects mediated by IGF-IR alone, but could also affect significantly the oncogenic potential of NPM-ALK due to IGF-IR's regulatory effects on the stability of the fusion protein. Exploring how these individual mechanisms are themselves deregulated could be an important direction for future studies (**Figure 36**).

Our model supports the multifaceted nature of NPM-ALK<sup>+</sup> lymphoma, and that disturbances in more than one regulatory mechanism exist, which reflects the complex survival network in these lymphoma cells in particular as well as in cancer cells in general. Even though this lymphoma is driven by a major oncogene such as *NPM-ALK*, our data strongly suggest that the regulation of the expression of IGF-I/IGF-IR molecules is largely independent from NPM-ALK. Despite the fact that this lymphoma, similar to few other types of cancer, is driven by a major oncogene, numerous epithelial, mesenchymal, neural, and hematological cancers are instead driven by several oncogenic molecules that work in harmony to promote cell survival. Notably, upregulation of IGF-IR is a common feature among the majority of these tumors. Thus, the findings in our lymphoma model could be applied to other types of cancer. In support of this idea, our data show that miR-30a and miR-30d can negatively regulate IGF-IR posttranscriptionally; not only in NPM-ALK<sup>+</sup> ALCL but also in breast and colon cancers as well. Our study also demonstrates that upregulation of *IGF-IR* gene expression results from aberrancies in transcriptional regulatory mechanisms, namely Iκ-1 and MZF1 transcription factors, resembling what was found before with other transcription factors that regulate IGF-IR in epithelial and mesenchymal tumors. In a similar fashion, our data support that aberrant SUMOylation of IGF-IR occurs in NPM-ALK<sup>+</sup> ALCL, and these findings are in line with previously established findings in other types of cancer where SUMOylation of IGF-IR plays important roles in their pathogenesis. Furthermore, our current study supports that SUMOylation plays an additional important role

via maintaining the stability of NPM-ALK. These observations highlight that although different types of cancer exhibit remarkably heterogeneous clinical and pathological features, certain molecular characteristics are still common among them.

Overall, we provide novel evidence that multilevel deregulation of survival mechanisms contributes to the pathogenesis of NPM-ALK<sup>+</sup> ALCL. We hope that our findings will further current knowledge of the pathobiology of NPM-ALK<sup>+</sup> ALCL and provide a framework for the tailoring of novel therapeutic strategies to eradicate this lymphoma.



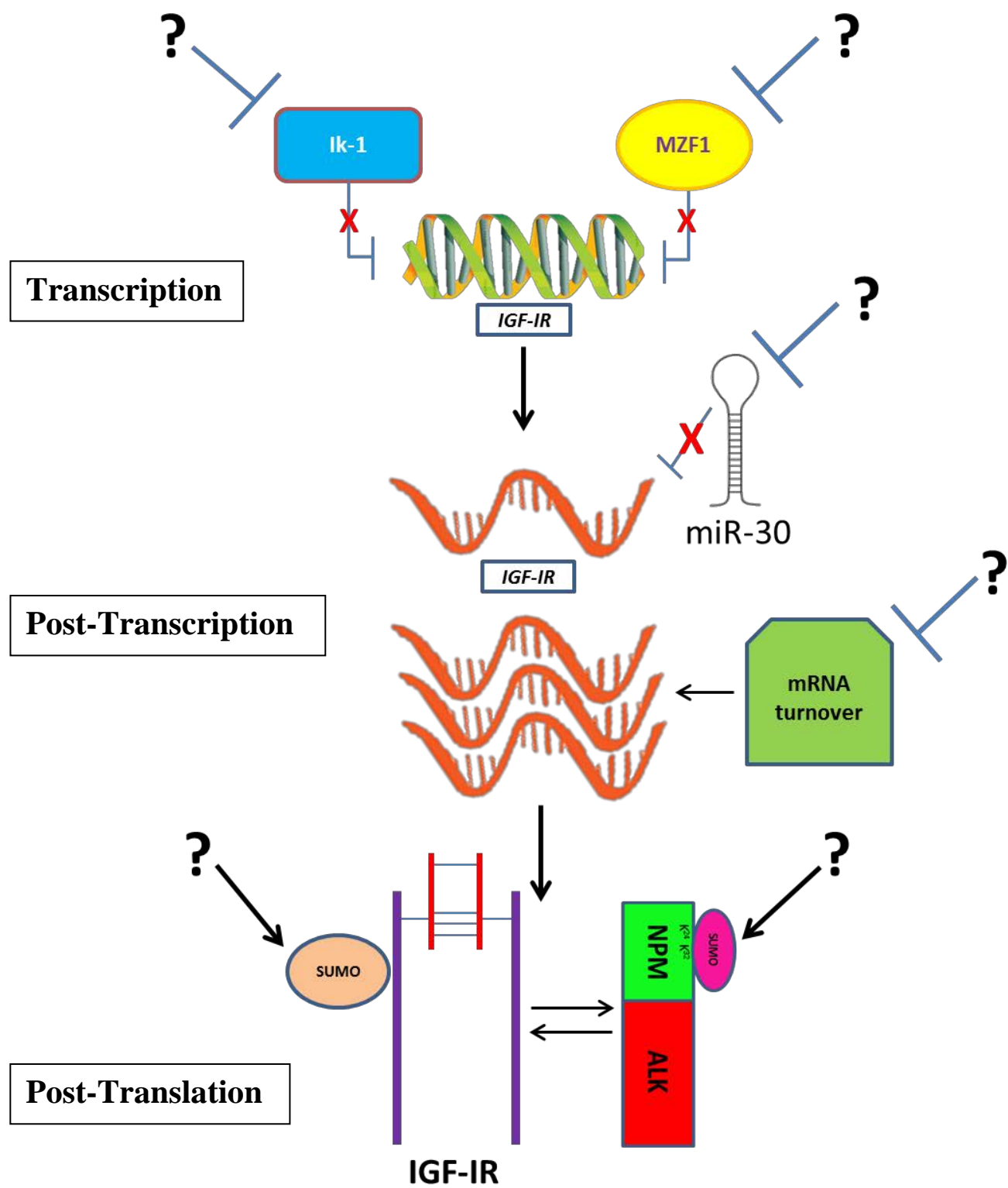


**FIGURE 36. Mechanisms contributing to deregulated survival mechanisms in NPM-ALK<sup>+</sup> ALCL.** Ik-1 and MZF1 expression levels are significantly decreased, preventing them from transcriptionally inhibiting *IGF-IR* gene expression and allowing *IGF-IR* mRNA to be transcribed. MiR-30a and miR-30d are markedly decreased in NPM-ALK<sup>+</sup> ALCL. Lack of suppression of the IGF-IR-3'UTR by these miRs allows IGF-IR protein to stabilize. Furthermore, slower decay of *IGF-IR* mRNA increases its bioavailability for protein translation. Fully translated IGF-IR is further stabilized by the posttranslational modification SUMOylation. SUMOylated IGF-IR can indirectly stabilize NPM-ALK, which is itself capable of being SUMOylated. How these mechanisms are regulated (indicated by “?”) is a direction of future study.

## Future Directions

Apart from the future studies mentioned in the individual discussion sections, identifying whether each of our identified mechanisms have regulatory effects on each other as well as determining how these aberrant mechanisms are deregulated would be worth pursuing, as illustrated in **Figure 36**. Some of the important mechanisms that require further analysis include:

1. Determining whether NPM-ALK contributes to the decreased expression levels of Ik-1 and MZF1 in these lymphoma cells. *Preliminary experiment:* Transfect NPM-ALK<sup>+</sup> ALCL cells with scrambled siRNA or ALK siRNA, and check Ik-1 and MZF1 expression levels by qPCR and Western blotting.
2. Identifying the host genes of miR-30a and miR-30d may lead to better understanding of how these microRNAs are deregulated, not only in NPM-ALK<sup>+</sup> ALCL but also in any other type of cancer. It is possible that Ik-1 and MZF1 help support the transcription of miR-30 by regulating its host gene. *Preliminary experiment:* Identify miR-30 genes. In addition, overexpression of Ik-1 and MZF1 in NPM-ALK<sup>+</sup> ALCL cells by transfection, and measure miR-30 expression levels by qPCR.
3. It has been previously shown that miR-30 directly targets the SUMO conjugating enzyme Ubc9, and that restoration of a previously decreased miR-30 expression level inhibits Ubc9 expression. Exploring whether the aberrantly decreased expression of miR-30 in NPM-ALK<sup>+</sup> ALCL cells contributes to upregulation of SUMOylation would also support IGF-IR and NPM-ALK protein stability. *Preliminary experiment:* Overexpress miR-30a and miR-30d in NPM-ALK<sup>+</sup> ALCL cells, and measure Ubc9 and SUMO expression by qPCR and Western blotting.

## Bibliography:

1. Gascoyne RD, Aoun P, Wu D, Chhanabhai M, Skinnider BF, Greiner TC, Morris SW, Connors JM, Vose JM, Viswanatha DS, Coldman A and Weisenburger DD. Prognostic significance of anaplastic lymphoma kinase (ALK) protein expression in adults with anaplastic large cell lymphoma. *Blood*. 1999; 93(11):3913-3921.
2. Stein H, Mason DY, Gerdes J, O'Connor N, Wainscoat J, Pallesen G, Gatter K, Falini B, Delsol G, Lemke H and et al. The expression of the Hodgkin's disease associated antigen Ki-1 in reactive and neoplastic lymphoid tissue: evidence that Reed-Sternberg cells and histiocytic malignancies are derived from activated lymphoid cells. *Blood*. 1985; 66(4):848-858.
3. Stein H, Foss HD, Durkop H, Marafioti T, Delsol G, Pulford K, Pileri S and Falini B. CD30(+) anaplastic large cell lymphoma: a review of its histopathologic, genetic, and clinical features. *Blood*. 2000; 96(12):3681-3695.
4. Kadin ME, Sako D, Berliner N, Franklin W, Woda B, Borowitz M, Ireland K, Schweid A, Herzog P, Lange B and et al. Childhood Ki-1 lymphoma presenting with skin lesions and peripheral lymphadenopathy. *Blood*. 1986; 68(5):1042-1049.
5. Falini B, Pileri S, Zinzani PL, Carbone A, Zagonel V, Wolf-Peeters C, Verhoef G, Menestrina F, Todeschini G, Paulli M, Lazzarino M, Giardini R, Aiello A, Foss HD, Araujo I, Fizzotti M, et al. ALK+ lymphoma: clinico-pathological findings and outcome. *Blood*. 1999; 93(8):2697-2706.
6. Savage KJ, Harris NL, Vose JM, Ullrich F, Jaffe ES, Connors JM, Rimsza L, Pileri SA, Chhanabhai M, Gascoyne RD, Armitage JO, Weisenburger DD and International Peripheral TCLP. ALK- anaplastic large-cell lymphoma is clinically and immunophenotypically different from both ALK+ ALCL and peripheral T-cell lymphoma, not otherwise specified: report from the International Peripheral T-Cell Lymphoma Project. *Blood*. 2008; 111(12):5496-5504.
7. Pulford K, Morris SW and Turturro F. Anaplastic lymphoma kinase proteins in growth control and cancer. *Journal of cellular physiology*. 2004; 199(3):330-358.
8. Shiota M, Nakamura S, Ichinohasama R, Abe M, Akagi T, Takeshita M, Mori N, Fujimoto J, Miyauchi J, Mikata A, Nanba K, Takami T, Yamabe H, Takano Y, Izumo T, Nagatani T, et al. Anaplastic large cell lymphomas expressing the novel chimeric protein p80NPM/ALK: a distinct clinicopathologic entity. *Blood*. 1995; 86(5):1954-1960.
9. Ferreri AJ, Govi S, Pileri SA and Savage KJ. Anaplastic large cell lymphoma, ALK-positive. *Critical reviews in oncology/hematology*. 2012; 83(2):293-302.
10. Ferreri AJ, Govi S, Pileri SA and Savage KJ. Anaplastic large cell lymphoma, ALK-negative. *Critical reviews in oncology/hematology*. 2013; 85(2):206-215.
11. Butrynski JE, D'Adamo DR, Hornick JL, Dal Cin P, Antonescu CR, Jhanwar SC, Ladanyi M, Capelletti M, Rodig SJ, Ramaiya N, Kwak EL, Clark JW, Wilner KD, Christensen JG, Janne PA, Maki RG, et al. Crizotinib in ALK-rearranged inflammatory myofibroblastic tumor. *The New England journal of medicine*. 2010; 363(18):1727-1733.
12. Carpenter EL and Mosse YP. Targeting ALK in neuroblastoma--preclinical and clinical advancements. *Nature reviews Clinical oncology*. 2012; 9(7):391-399.
13. Kwak EL, Bang YJ, Camidge DR, Shaw AT, Solomon B, Maki RG, Ou SH, Dezube BJ, Janne PA, Costa DB, Varella-Garcia M, Kim WH, Lynch TJ, Fidias P, Stubbs H, Engelman JA, et al. Anaplastic lymphoma kinase inhibition in non-small-cell lung cancer. *The New England journal of medicine*. 2010; 363(18):1693-1703.
14. Mori M, Ueno Y, Konagai S, Fushiki H, Shimada I, Kondoh Y, Saito R, Mori K, Shindou N, Soga T, Sakagami H, Furutani T, Doihara H, Kudoh M and Kuromitsu S. The selective anaplastic lymphoma receptor tyrosine kinase inhibitor ASP3026 induces tumor regression and prolongs survival in non-small cell lung cancer model mice. *Molecular cancer therapeutics*. 2014; 13(2):329-340.

15. Ceccon M, Mologni L, Bisson W, Scapozza L and Gambacorti-Passerini C. Crizotinib-resistant NPM-ALK mutants confer differential sensitivity to unrelated Alk inhibitors. *Molecular cancer research : MCR*. 2013; 11(2):122-132.
16. Gambacorti Passerini C, Farina F, Stasia A, Redaelli S, Ceccon M, Mologni L, Messa C, Guerra L, Giudici G, Sala E, Mussolin L, Deeren D, King MH, Steurer M, Ordemann R, Cohen AM, et al. Crizotinib in advanced, chemoresistant anaplastic lymphoma kinase-positive lymphoma patients. *Journal of the National Cancer Institute*. 2014; 106(2):djt378.
17. Hingorani K, Szebeni A and Olson MO. Mapping the functional domains of nucleolar protein B23. *The Journal of biological chemistry*. 2000; 275(32):24451-24457.
18. Szebeni A and Olson MO. Nucleolar protein B23 has molecular chaperone activities. *Protein science : a publication of the Protein Society*. 1999; 8(4):905-912.
19. Okuwaki M, Matsumoto K, Tsujimoto M and Nagata K. Function of nucleophosmin/B23, a nucleolar acidic protein, as a histone chaperone. *FEBS letters*. 2001; 506(3):272-276.
20. Nishimura Y, Ohkubo T, Furuichi Y and Umekawa H. Tryptophans 286 and 288 in the C-terminal region of protein B23.1 are important for its nucleolar localization. *Bioscience, biotechnology, and biochemistry*. 2002; 66(10):2239-2242.
21. Wang W, Budhu A, Forgues M and Wang XW. Temporal and spatial control of nucleophosmin by the Ran-Crm1 complex in centrosome duplication. *Nature cell biology*. 2005; 7(8):823-830.
22. Iwahara T, Fujimoto J, Wen D, Cupples R, Bucay N, Arakawa T, Mori S, Ratzkin B and Yamamoto T. Molecular characterization of ALK, a receptor tyrosine kinase expressed specifically in the nervous system. *Oncogene*. 1997; 14(4):439-449.
23. Morris SW, Naeve C, Mathew P, James PL, Kirstein MN, Cui X and Witte DP. ALK, the chromosome 2 gene locus altered by the t(2;5) in non-Hodgkin's lymphoma, encodes a novel neural receptor tyrosine kinase that is highly related to leukocyte tyrosine kinase (LTK). *Oncogene*. 1997; 14(18):2175-2188.
24. Vernersson E, Khoo NK, Henriksson ML, Roos G, Palmer RH and Hallberg B. Characterization of the expression of the ALK receptor tyrosine kinase in mice. *Gene expression patterns : GEP*. 2006; 6(5):448-461.
25. Souttou B, Carvalho NB, Raulais D and Vigny M. Activation of anaplastic lymphoma kinase receptor tyrosine kinase induces neuronal differentiation through the mitogen-activated protein kinase pathway. *The Journal of biological chemistry*. 2001; 276(12):9526-9531.
26. Motegi A, Fujimoto J, Kotani M, Sakuraba H and Yamamoto T. ALK receptor tyrosine kinase promotes cell growth and neurite outgrowth. *Journal of cell science*. 2004; 117(Pt 15):3319-3329.
27. Degoutin J, Vigny M and Gouzi JY. ALK activation induces Shc and FRS2 recruitment: Signaling and phenotypic outcomes in PC12 cells differentiation. *FEBS letters*. 2007; 581(4):727-734.
28. Donella-Deana A, Marin O, Cesaro L, Gunby RH, Ferrarese A, Coluccia AM, Tartari CJ, Mologni L, Scapozza L, Gambacorti-Passerini C and Pinna LA. Unique substrate specificity of anaplastic lymphoma kinase (ALK): development of phosphoacceptor peptides for the assay of ALK activity. *Biochemistry*. 2005; 44(23):8533-8542.
29. Tartari CJ, Gunby RH, Coluccia AM, Sottocornola R, Cimbri B, Scapozza L, Donella-Deana A, Pinna LA and Gambacorti-Passerini C. Characterization of some molecular mechanisms governing autoactivation of the catalytic domain of the anaplastic lymphoma kinase. *The Journal of biological chemistry*. 2008; 283(7):3743-3750.
30. Beckmann G and Bork P. An adhesive domain detected in functionally diverse receptors. *Trends in biochemical sciences*. 1993; 18(2):40-41.
31. Loren CE, Englund C, Grabbe C, Hallberg B, Hunter T and Palmer RH. A crucial role for the Anaplastic lymphoma kinase receptor tyrosine kinase in gut development in *Drosophila melanogaster*. *EMBO reports*. 2003; 4(8):781-786.

32. Stoica GE, Kuo A, Aigner A, Sunitha I, Souttou B, Malerczyk C, Caughey DJ, Wen D, Karavanov A, Riegel AT and Wellstein A. Identification of anaplastic lymphoma kinase as a receptor for the growth factor pleiotrophin. *The Journal of biological chemistry*. 2001; 276(20):16772-16779.
33. Shiota M and Mori S. Anaplastic large cell lymphomas expressing the novel chimeric protein p80NPM/ALK: a distinct clinicopathologic entity. *Leukemia*. 1997; 11 Suppl 3:538-540.
34. Morris SW, Kirstein MN, Valentine MB, Dittmer KG, Shapiro DN, Saltman DL and Look AT. Fusion of a kinase gene, ALK, to a nucleolar protein gene, NPM, in non-Hodgkin's lymphoma. *Science*. 1994; 263(5151):1281-1284.
35. Griffin CA, Hawkins AL, Dvorak C, Henkle C, Ellingham T and Perlman EJ. Recurrent involvement of 2p23 in inflammatory myofibroblastic tumors. *Cancer research*. 1999; 59(12):2776-2780.
36. Soda M, Choi YL, Enomoto M, Takada S, Yamashita Y, Ishikawa S, Fujiwara S, Watanabe H, Kurashina K, Hatanaka H, Bando M, Ohno S, Ishikawa Y, Aburatani H, Niki T, Sohara Y, et al. Identification of the transforming EML4-ALK fusion gene in non-small-cell lung cancer. *Nature*. 2007; 448(7153):561-566.
37. Arber DA, Sun LH and Weiss LM. Detection of the t(2;5)(p23;q35) chromosomal translocation in large B-cell lymphomas other than anaplastic large cell lymphoma. *Human pathology*. 1996; 27(6):590-594.
38. Du XL, Hu H, Lin DC, Xia SH, Shen XM, Zhang Y, Luo ML, Feng YB, Cai Y, Xu X, Han YL, Zhan QM and Wang MR. Proteomic profiling of proteins dysregulated in Chinese esophageal squamous cell carcinoma. *Journal of molecular medicine*. 2007; 85(8):863-875.
39. Dirks WG, Fahrnich S, Lis Y, Becker E, MacLeod RA and Drexler HG. Expression and functional analysis of the anaplastic lymphoma kinase (ALK) gene in tumor cell lines. *International journal of cancer Journal international du cancer*. 2002; 100(1):49-56.
40. Caren H, Abel F, Kogner P and Martinsson T. High incidence of DNA mutations and gene amplifications of the ALK gene in advanced sporadic neuroblastoma tumours. *The Biochemical journal*. 2008; 416(2):153-159.
41. Chen Y, Takita J, Choi YL, Kato M, Ohira M, Sanada M, Wang L, Soda M, Kikuchi A, Igarashi T, Nakagawara A, Hayashi Y, Mano H and Ogawa S. Oncogenic mutations of ALK kinase in neuroblastoma. *Nature*. 2008; 455(7215):971-974.
42. George RE, Sanda T, Hanna M, Frohling S, Luther W, 2nd, Zhang J, Ahn Y, Zhou W, London WB, McGrady P, Xue L, Zozulya S, Gregor VE, Webb TR, Gray NS, Gilliland DG, et al. Activating mutations in ALK provide a therapeutic target in neuroblastoma. *Nature*. 2008; 455(7215):975-978.
43. Janoueix-Lerosey I, Lequin D, Brugieres L, Ribeiro A, de Pontual L, Combaret V, Raynal V, Puisieux A, Schleiermacher G, Pierron G, Valteau-Couanet D, Frebourg T, Michon J, Lyonnet S, Amiel J and Delattre O. Somatic and germline activating mutations of the ALK kinase receptor in neuroblastoma. *Nature*. 2008; 455(7215):967-970.
44. Mosse YP, Laudenslager M, Longo L, Cole KA, Wood A, Attiyeh EF, Laquaglia MJ, Sennett R, Lynch JE, Perri P, Laureys G, Speleman F, Kim C, Hou C, Hakonarson H, Torkamani A, et al. Identification of ALK as a major familial neuroblastoma predisposition gene. *Nature*. 2008; 455(7215):930-935.
45. Li XQ, Hisaoka M, Shi DR, Zhu XZ and Hashimoto H. Expression of anaplastic lymphoma kinase in soft tissue tumors: an immunohistochemical and molecular study of 249 cases. *Human pathology*. 2004; 35(6):711-721.
46. Corao DA, Biegel JA, Coffin CM, Barr FG, Wainwright LM, Ernst LM, Choi JK, Zhang PJ and Pawel BR. ALK expression in rhabdomyosarcomas: correlation with histologic subtype and fusion status. *Pediatric and developmental pathology : the official journal of the Society for Pediatric Pathology and the Paediatric Pathology Society*. 2009; 12(4):275-283.
47. Pulford K, Lamant L, Morris SW, Butler LH, Wood KM, Stroud D, Delsol G and Mason DY. Detection of anaplastic lymphoma kinase (ALK) and nucleolar protein nucleophosmin (NPM)-ALK proteins in normal and neoplastic cells with the monoclonal antibody ALK1. *Blood*. 1997; 89(4):1394-1404.

48. Perez-Pinera P, Chang Y, Astudillo A, Mortimer J and Deuel TF. Anaplastic lymphoma kinase is expressed in different subtypes of human breast cancer. *Biochemical and biophysical research communications*. 2007; 358(2):399-403.
49. Delsol G, Lamant L, Mariame B, Pulford K, Dastugue N, Brousset P, Rigal-Huguet F, al Saati T, Cerretti DP, Morris SW and Mason DY. A new subtype of large B-cell lymphoma expressing the ALK kinase and lacking the 2; 5 translocation. *Blood*. 1997; 89(5):1483-1490.
50. Bischof D, Pulford K, Mason DY and Morris SW. Role of the nucleophosmin (NPM) portion of the non-Hodgkin's lymphoma-associated NPM-anaplastic lymphoma kinase fusion protein in oncogenesis. *Molecular and cellular biology*. 1997; 17(4):2312-2325.
51. Mason DY, Pulford KA, Bischof D, Kuefer MU, Butler LH, Lamant L, Delsol G and Morris SW. Nucleolar localization of the nucleophosmin-anaplastic lymphoma kinase is not required for malignant transformation. *Cancer research*. 1998; 58(5):1057-1062.
52. Fujimoto J, Shiota M, Iwahara T, Seki N, Satoh H, Mori S and Yamamoto T. Characterization of the transforming activity of p80, a hyperphosphorylated protein in a Ki-1 lymphoma cell line with chromosomal translocation t(2;5). *Proceedings of the National Academy of Sciences of the United States of America*. 1996; 93(9):4181-4186.
53. Kuefer MU, Look AT, Pulford K, Behm FG, Pattengale PK, Mason DY and Morris SW. Retrovirus-mediated gene transfer of NPM-ALK causes lymphoid malignancy in mice. *Blood*. 1997; 90(8):2901-2910.
54. Bai RY, Dieter P, Peschel C, Morris SW and Duyster J. Nucleophosmin-anaplastic lymphoma kinase of large-cell anaplastic lymphoma is a constitutively active tyrosine kinase that utilizes phospholipase C-gamma to mediate its mitogenicity. *Molecular and cellular biology*. 1998; 18(12):6951-6961.
55. Lange K, Uckert W, Blankenstein T, Nadrowitz R, Bittner C, Renauld JC, van Snick J, Feller AC and Merz H. Overexpression of NPM-ALK induces different types of malignant lymphomas in IL-9 transgenic mice. *Oncogene*. 2003; 22(4):517-527.
56. Chiarle R, Gong JZ, Guasparri I, Pesci A, Cai J, Liu J, Simmons WJ, Dhall G, Howes J, Piva R and Inghirami G. NPM-ALK transgenic mice spontaneously develop T-cell lymphomas and plasma cell tumors. *Blood*. 2003; 101(5):1919-1927.
57. Chiarle R, Simmons WJ, Cai H, Dhall G, Zamo A, Raz R, Karras JG, Levy DE and Inghirami G. Stat3 is required for ALK-mediated lymphomagenesis and provides a possible therapeutic target. *Nature medicine*. 2005; 11(6):623-629.
58. Zamo A, Chiarle R, Piva R, Howes J, Fan Y, Chilosi M, Levy DE and Inghirami G. Anaplastic lymphoma kinase (ALK) activates Stat3 and protects hematopoietic cells from cell death. *Oncogene*. 2002; 21(7):1038-1047.
59. Han Y, Amin HM, Franko B, Frantz C, Shi X and Lai R. Loss of SHP1 enhances JAK3/STAT3 signaling and decreases proteasome degradation of JAK3 and NPM-ALK in ALK+ anaplastic large-cell lymphoma. *Blood*. 2006; 108(8):2796-2803.
60. Amin HM, McDonnell TJ, Ma Y, Lin Q, Fujio Y, Kunisada K, Leventaki V, Das P, Rassidakis GZ, Cutler C, Medeiros LJ and Lai R. Selective inhibition of STAT3 induces apoptosis and G(1) cell cycle arrest in ALK-positive anaplastic large cell lymphoma. *Oncogene*. 2004; 23(32):5426-5434.
61. Zhu H, Vishwamitra D, Curry CV, Manshoury R, Diao L, Khan A and Amin HM. NPM-ALK up-regulates iNOS expression through a STAT3/microRNA-26a-dependent mechanism. *The Journal of pathology*. 2013; 230(1):82-94.
62. Amin HM, Medeiros LJ, Ma Y, Feretzaki M, Das P, Leventaki V, Rassidakis GZ, O'Connor SL, McDonnell TJ and Lai R. Inhibition of JAK3 induces apoptosis and decreases anaplastic lymphoma kinase activity in anaplastic large cell lymphoma. *Oncogene*. 2003; 22(35):5399-5407.
63. Coluccia AM, Perego S, Cleris L, Gunby RH, Passoni L, Marchesi E, Formelli F and Gambacorti-Passerini C. Bcl-XL down-regulation suppresses the tumorigenic potential of NPM/ALK in vitro and in vivo. *Blood*. 2004; 103(7):2787-2794.
64. Piva R, Pellegrino E, Mattioli M, Agnelli L, Lombardi L, Boccalatte F, Costa G, Ruggeri BA, Cheng M, Chiarle R, Palestro G, Neri A and Inghirami G. Functional validation of the anaplastic

- lymphoma kinase signature identifies CEBPB and BCL2A1 as critical target genes. *The Journal of clinical investigation*. 2006; 116(12):3171-3182.
65. Lai R, Rassidakis GZ, Medeiros LJ, Ramdas L, Goy AH, Cutler C, Fujio Y, Kunisada K, Amin HM and Gilles F. Signal transducer and activator of transcription-3 activation contributes to high tissue inhibitor of metalloproteinase-1 expression in anaplastic lymphoma kinase-positive anaplastic large cell lymphoma. *The American journal of pathology*. 2004; 164(6):2251-2258.
  66. Nieborowska-Skorska M, Slupianek A, Xue L, Zhang Q, Raghunath PN, Hoser G, Wasik MA, Morris SW and Skorski T. Role of signal transducer and activator of transcription 5 in nucleophosmin/ anaplastic lymphoma kinase-mediated malignant transformation of lymphoid cells. *Cancer research*. 2001; 61(17):6517-6523.
  67. Ruchatz H, Coluccia AM, Stano P, Marchesi E and Gambacorti-Passerini C. Constitutive activation of Jak2 contributes to proliferation and resistance to apoptosis in NPM/ALK-transformed cells. *Experimental hematology*. 2003; 31(4):309-315.
  68. Zhang Q, Wang HY, Liu X and Wasik MA. STAT5A is epigenetically silenced by the tyrosine kinase NPM1-ALK and acts as a tumor suppressor by reciprocally inhibiting NPM1-ALK expression. *Nature medicine*. 2007; 13(11):1341-1348.
  69. Voena C, Conte C, Ambrogio C, Boeri Erba E, Boccalatte F, Mohammed S, Jensen ON, Palestro G, Inghirami G and Chiarle R. The tyrosine phosphatase Shp2 interacts with NPM-ALK and regulates anaplastic lymphoma cell growth and migration. *Cancer research*. 2007; 67(9):4278-4286.
  70. Leventaki V, Drakos E, Medeiros LJ, Lim MS, Elenitoba-Johnson KS, Claret FX and Rassidakis GZ. NPM-ALK oncogenic kinase promotes cell-cycle progression through activation of JNK/cJun signaling in anaplastic large-cell lymphoma. *Blood*. 2007; 110(5):1621-1630.
  71. Rassidakis GZ, Feretzaki M, Atwell C, Grammatikakis I, Lin Q, Lai R, Claret FX, Medeiros LJ and Amin HM. Inhibition of Akt increases p27Kip1 levels and induces cell cycle arrest in anaplastic large cell lymphoma. *Blood*. 2005; 105(2):827-829.
  72. Bai RY, Ouyang T, Miething C, Morris SW, Peschel C and Duyster J. Nucleophosmin-anaplastic lymphoma kinase associated with anaplastic large-cell lymphoma activates the phosphatidylinositol 3-kinase/Akt antiapoptotic signaling pathway. *Blood*. 2000; 96(13):4319-4327.
  73. Gu TL, Tothova Z, Scheijen B, Griffin JD, Gilliland DG and Sternberg DW. NPM-ALK fusion kinase of anaplastic large-cell lymphoma regulates survival and proliferative signaling through modulation of FOXO3a. *Blood*. 2004; 103(12):4622-4629.
  74. Marzec M, Kasprzycka M, Liu X, El-Salem M, Halasa K, Raghunath PN, Bucki R, Wlodarski P and Wasik MA. Oncogenic tyrosine kinase NPM/ALK induces activation of the rapamycin-sensitive mTOR signaling pathway. *Oncogene*. 2007; 26(38):5606-5614.
  75. Lelbach A, Muzes G and Feher J. The insulin-like growth factor system: IGFs, IGF-binding proteins and IGFBP-proteases. *Acta Physiol Hung*. 2005; 92(2):97-107.
  76. He J, Rosen CJ, Adams DJ and Kream BE. Postnatal growth and bone mass in mice with IGF-I haploinsufficiency. *Bone*. 2006; 38(6):826-835.
  77. Rosen CJ and Pollak M. Circulating IGF-I: New Perspectives for a New Century. *Trends Endocrinol Metab*. 1999; 10(4):136-141.
  78. Rubin J, Fan X, Rahnert J, Sen B, Hsieh CL, Murphy TC, Nanes MS, Horton LG, Beamer WG and Rosen CJ. IGF-I secretion by prostate carcinoma cells does not alter tumor-bone cell interactions in vitro or in vivo. *Prostate*. 2006; 66(8):789-800.
  79. Yakar S, Wu Y, Setser J and Rosen CJ. The role of circulating IGF-I: lessons from human and animal models. *Endocrine*. 2002; 19(3):239-248.
  80. Yao W, Zhong J, Rosen CJ, Hock JM and Lee WH. IGF-I and postnatal growth of weaver mutant mice. *Endocrine*. 2005; 26(2):117-125.
  81. Bing-You RG, Denis MC and Rosen CJ. Low bone mineral density in adults with previous hypothalamic-pituitary tumors: correlations with serum growth hormone responses to GH-releasing hormone, insulin-like growth factor I, and IGF binding protein 3. *Calcif Tissue Int*. 1993; 52(3):183-187.



82. Wang J, Zhou J, Cheng CM, Kopchick JJ and Bondy CA. Evidence supporting dual, IGF-I-independent and IGF-I-dependent, roles for GH in promoting longitudinal bone growth. *J Endocrinol.* 2004; 180(2):247-255.
83. Jenkins PJ and Bustin SA. Evidence for a link between IGF-I and cancer. *Eur J Endocrinol.* 2004; 151 Suppl 1:S17-22.
84. Borugian MJ, Spinelli JJ, Sun Z, Kolonel LN, Oakley-Girvan I, Pollak MD, Whittemore AS, Wu AH and Gallagher RP. Prostate cancer risk in relation to insulin-like growth factor (IGF)-I and IGF-binding protein-3: a prospective multiethnic study. *Cancer Epidemiol Biomarkers Prev.* 2008; 17(1):252-254.
85. Chen T, Lukanova A, Grankvist K, Zeleniuch-Jacquotte A, Wulff M, Johansson R, Schock H, Lenner P, Hallmans G, Wadell G, Toniolo P and Lundin E. IGF-I during primiparous pregnancy and maternal risk of breast cancer. *Breast Cancer Res Treat.* 2009.
86. LeRoith D and Roberts CT, Jr. The insulin-like growth factor system and cancer. *Cancer Lett.* 2003; 195(2):127-137.
87. Wu Y, Yakar S, Zhao L, Hennighausen L and LeRoith D. Circulating insulin-like growth factor-I levels regulate colon cancer growth and metastasis. *Cancer research.* 2002; 62(4):1030-1035.
88. Peters G, Gongoll S, Langner C, Mengel M, Piso P, Klempnauer J, Ruschoff J, Kreipe H and von Wasielewski R. IGF-1R, IGF-1 and IGF-2 expression as potential prognostic and predictive markers in colorectal-cancer. *Virchows Arch.* 2003; 443(2):139-145.
89. Pollak M, Beamer W and Zhang JC. Insulin-like growth factors and prostate cancer. *Cancer metastasis reviews.* 1998; 17(4):383-390.
90. Mairet-Coello G, Tury A and DiCicco-Bloom E. Insulin-like growth factor-1 promotes G(1)/S cell cycle progression through bidirectional regulation of cyclins and cyclin-dependent kinase inhibitors via the phosphatidylinositol 3-kinase/Akt pathway in developing rat cerebral cortex. *J Neurosci.* 2009; 29(3):775-788.
91. Werner H, Hernandez-Sanchez C, Karnieli E and Leroith D. The regulation of IGF-I receptor gene expression. *Int J Biochem Cell Biol.* 1995; 27(10):987-994.
92. Adams TE, Epa VC, Garrett TP and Ward CW. Structure and function of the type 1 insulin-like growth factor receptor. *Cellular and molecular life sciences : CMLS.* 2000; 57(7):1050-1093.
93. Chitnis MM, Yuen JS, Protheroe AS, Pollak M and Macaulay VM. The type 1 insulin-like growth factor receptor pathway. *Clinical cancer research : an official journal of the American Association for Cancer Research.* 2008; 14(20):6364-6370.
94. Bertrand FE, Steelman LS, Chappell WH, Abrams SL, Shelton JG, White ER, Ludwig DL and McCubrey JA. Synergy between an IGF-1R antibody and Raf/MEK/ERK and PI3K/Akt/mTOR pathway inhibitors in suppressing IGF-1R-mediated growth in hematopoietic cells. *Leukemia.* 2006; 20(7):1254-1260.
95. Himpe E and Kooijman R. Insulin-like growth factor-I receptor signal transduction and the Janus Kinase/Signal Transducer and Activator of Transcription (JAK-STAT) pathway. *BioFactors.* 2009; 35(1):76-81.
96. Foulstone E, Prince S, Zaccheo O, Burns JL, Harper J, Jacobs C, Church D and Hassan AB. Insulin-like growth factor ligands, receptors, and binding proteins in cancer. *J Pathol.* 2005; 205(2):145-153.
97. Inagaki K, Tiulpakov A, Rubtsov P, Sverdlova P, Peterkova V, Yakar S, Terekhov S and LeRoith D. A familial insulin-like growth factor-I receptor mutant leads to short stature: clinical and biochemical characterization. *J Clin Endocrinol Metab.* 2007; 92(4):1542-1548.
98. Sadagurski M, Yakar S, Weingarten G, Holzenberger M, Rhodes CJ, Breitkreutz D, Leroith D and Wertheimer E. Insulin-like growth factor 1 receptor signaling regulates skin development and inhibits skin keratinocyte differentiation. *Mol Cell Biol.* 2006; 26(7):2675-2687.
99. Scavo LM, Karas M, Murray M and Leroith D. Insulin-like growth factor-I stimulates both cell growth and lipogenesis during differentiation of human mesenchymal stem cells into adipocytes. *J Clin Endocrinol Metab.* 2004; 89(7):3543-3553.

100. Liu JP, Baker J, Perkins AS, Robertson EJ and Efstratiadis A. Mice carrying null mutations of the genes encoding insulin-like growth factor I (Igf-1) and type 1 IGF receptor (Igf1r). *Cell*. 1993; 75(1):59-72.
101. Rosen CJ, Ackert-Bicknell CL, Adamo ML, Shultz KL, Rubin J, Donahue LR, Horton LG, Delahunty KM, Beamer WG, Sipos J, Clemmons D, Nelson T, Bouxsein ML and Horowitz M. Congenic mice with low serum IGF-I have increased body fat, reduced bone mineral density, and an altered osteoblast differentiation program. *Bone*. 2004; 35(5):1046-1058.
102. Rosen CJ, Dimai HP, Vereault D, Donahue LR, Beamer WG, Farley J, Linkhart S, Linkhart T, Mohan S and Baylink DJ. Circulating and skeletal insulin-like growth factor-I (IGF-I) concentrations in two inbred strains of mice with different bone mineral densities. *Bone*. 1997; 21(3):217-223.
103. Wu Y, Sun H, Yakar S and LeRoith D. Elevated levels of insulin-like growth factor (IGF)-I in serum rescue the severe growth retardation of IGF-I null mice. *Endocrinology*. 2009; 150(9):4395-4403.
104. Gualberto A and Pollak M. Clinical Development of Inhibitors of the Insulin-like Growth Factor Receptor in Oncology. *Curr Drug Targets*. 2009.
105. Gualco E, Wang JY, Del Valle L, Urbanska K, Peruzzi F, Khalili K, Amini S and Reiss K. IGF-IR in neuroprotection and brain tumors. *Front Biosci*. 2009; 14:352-375.
106. LeRoith D, Baserga R, Helman L and Roberts CT, Jr. Insulin-like growth factors and cancer. *Annals of internal medicine*. 1995; 122(1):54-59.
107. Macaulay VM. Insulin-like growth factors and cancer. *Br J Cancer*. 1992; 65(3):311-320.
108. Mitsiades CS and Mitsiades N. Treatment of hematologic malignancies and solid tumors by inhibiting IGF receptor signaling. *Expert Rev Anticancer Ther*. 2005; 5(3):487-499.
109. Moore T, Carbajal S, Beltran L, Perkins SN, Yakar S, Leroith D, Hursting SD and Digiovanni J. Reduced susceptibility to two-stage skin carcinogenesis in mice with low circulating insulin-like growth factor I levels. *Cancer Res*. 2008; 68(10):3680-3688.
110. Pandini G, Vigneri R, Costantino A, Frasca F, Ippolito A, Fujita-Yamaguchi Y, Siddle K, Goldfine ID and Belfiore A. Insulin and insulin-like growth factor-I (IGF-I) receptor overexpression in breast cancers leads to insulin/IGF-I hybrid receptor overexpression: evidence for a second mechanism of IGF-I signaling. *Clin Cancer Res*. 1999; 5(7):1935-1944.
111. Pollak M. Insulin and insulin-like growth factor signalling in neoplasia. *Nat Rev Cancer*. 2008; 8(12):915-928.
112. Pollak M. Targeting insulin and insulin-like growth factor signalling in oncology. *Curr Opin Pharmacol*. 2008; 8(4):384-392.
113. Samani AA, Yakar S, LeRoith D and Brodt P. The role of the IGF system in cancer growth and metastasis: overview and recent insights. *Endocr Rev*. 2007; 28(1):20-47.
114. Wolpin BM, Meyerhardt JA, Chan AT, Ng K, Chan JA, Wu K, Pollak MN, Giovannucci EL and Fuchs CS. Insulin, the insulin-like growth factor axis, and mortality in patients with nonmetastatic colorectal cancer. *J Clin Oncol*. 2009; 27(2):176-185.
115. Yu H and Rohan T. Role of the insulin-like growth factor family in cancer development and progression. *J Natl Cancer Inst*. 2000; 92(18):1472-1489.
116. Jones RA, Campbell CI, Petrik JJ and Moorehead RA. Characterization of a novel primary mammary tumor cell line reveals that cyclin D1 is regulated by the type I insulin-like growth factor receptor. *Mol Cancer Res*. 2008; 6(5):819-828.
117. Rubini M, Hongo A, D'Ambrosio C and Baserga R. The IGF-I receptor in mitogenesis and transformation of mouse embryo cells: role of receptor number. *Exp Cell Res*. 1997; 230(2):284-292.
118. Zhang D, Samani AA and Brodt P. The role of the IGF-I receptor in the regulation of matrix metalloproteinases, tumor invasion and metastasis. *Horm Metab Res*. 2003; 35(11-12):802-808.
119. Flossmann-Kast BB, Jehle PM, Hoefflich A, Adler G and Lutz MP. Src stimulates insulin-like growth factor I (IGF-I)-dependent cell proliferation by increasing IGF-I receptor number in human pancreatic carcinoma cells. *Cancer Res*. 1998; 58(16):3551-3554.

120. Dupont J, Karas M and LeRoith D. The potentiation of estrogen on insulin-like growth factor I action in MCF-7 human breast cancer cells includes cell cycle components. *J Biol Chem.* 2000; 275(46):35893-35901.
121. Lann D and LeRoith D. The role of endocrine insulin-like growth factor-I and insulin in breast cancer. *J Mammary Gland Biol Neoplasia.* 2008; 13(4):371-379.
122. Sciacca L, Costantino A, Pandini G, Mineo R, Frasca F, Scalia P, Sbraccia P, Goldfine ID, Vigneri R and Belfiore A. Insulin receptor activation by IGF-II in breast cancers: evidence for a new autocrine/paracrine mechanism. *Oncogene.* 1999; 18(15):2471-2479.
123. Shukla V, Coumoul X, Cao L, Wang RH, Xiao C, Xu X, Ando S, Yakar S, Leroith D and Deng C. Absence of the full-length breast cancer-associated gene-1 leads to increased expression of insulin-like growth factor signaling axis members. *Cancer Res.* 2006; 66(14):7151-7157.
124. Monti S, Proietti-Pannunzi L, Sciarra A, Lolli F, Falasca P, Poggi M, Celi FS and Toscano V. The IGF axis in prostate cancer. *Curr Pharm Des.* 2007; 13(7):719-727.
125. Mitsiades CS, Mitsiades NS, McMullan CJ, Poulaki V, Shringarpure R, Akiyama M, Hideshima T, Chauhan D, Joseph M, Libermann TA, Garcia-Echeverria C, Pearson MA, Hofmann F, Anderson KC and Kung AL. Inhibition of the insulin-like growth factor receptor-1 tyrosine kinase activity as a therapeutic strategy for multiple myeloma, other hematologic malignancies, and solid tumors. *Cancer cell.* 2004; 5(3):221-230.
126. Chng WJ, Gualberto A and Fonseca R. IGF-1R is overexpressed in poor-prognostic subtypes of multiple myeloma. *Leukemia.* 2006; 20(1):174-176.
127. Shi B, Vishwamitra D, Granda JG, Whitton T, Shi P and Amin HM. Molecular and functional characterizations of the association and interactions between nucleophosmin-anaplastic lymphoma kinase and type I insulin-like growth factor receptor. *Neoplasia.* 2013; 15(6):669-683.
128. Shi P, Lai R, Lin Q, Iqbal AS, Young LC, Kwak LW, Ford RJ and Amin HM. IGF-1R tyrosine kinase interacts with NPM-ALK oncogene to induce survival of T-cell ALK+ anaplastic large-cell lymphoma cells. *Blood.* 2009; 114(2):360-370.
129. Vishwamitra D, Shi P, Wilson D, Manshouri R, Vega F, Schlette EJ and Amin HM. Expression and effects of inhibition of type I insulin-like growth factor receptor tyrosine kinase in mantle cell lymphoma. *Haematologica.* 2011; 96(6):871-880.
130. Shi P, Chandra J, Sun X, Gergely M, Cortes JE, Garcia-Manero G, Arlinghaus RB, Lai R and Amin HM. Inhibition of IGF-1R tyrosine kinase induces apoptosis and cell cycle arrest in imatinib-resistant chronic myeloid leukaemia cells. *Journal of cellular and molecular medicine.* 2010; 14(6B):1777-1792.
131. Amin HM and Lai R. Pathobiology of ALK+ anaplastic large-cell lymphoma. *Blood.* 2007; 110(7):2259-2267.
132. Vishwamitra D, Li Y, Wilson D, Manshouri R, Curry CV, Shi B, Tang XM, Sheehan AM, Wistuba, II, Shi P and Amin HM. MicroRNA 96 is a post-transcriptional suppressor of anaplastic lymphoma kinase expression. *The American journal of pathology.* 2012; 180(5):1772-1780.
133. Ribeiro TC, Jorge AA, Almeida MQ, Mariani BM, Nishi MY, Mendonca BB, Fragoso MC and Latronico AC. Amplification of the insulin-like growth factor 1 receptor gene is a rare event in adrenocortical adenocarcinomas: searching for potential mechanisms of overexpression. *BioMed research international.* 2014; 2014:936031.
134. Tran TN, Selinger CI, Yu B, Ng CC, Kohonen-Corish MR, McCaughan B, Kennedy C, O'Toole SA and Cooper WA. Alterations of insulin-like growth factor-1 receptor gene copy number and protein expression are common in non-small cell lung cancer. *Journal of clinical pathology.* 2014; 67(11):985-991.
135. Badzio A, Wynes MW, Dziadziuszko R, Merrick DT, Pardo M, Rzyman W, Kowalczyk A, Singh S, Ranger-Moore J, Manriquez G, Gaire F, Jassem J and Hirsch FR. Increased insulin-like growth factor 1 receptor protein expression and gene copy number in small cell lung cancer. *Journal of thoracic oncology : official publication of the International Association for the Study of Lung Cancer.* 2010; 5(12):1905-1911.
136. Dziadziuszko R, Merrick DT, Witta SE, Mendoza AD, Szostakiewicz B, Szymanowska A, Rzyman W, Dziadziuszko K, Jassem J, Bunn PA, Jr., Varella-Garcia M and Hirsch FR. Insulin-like

- growth factor receptor 1 (IGF1R) gene copy number is associated with survival in operable non-small-cell lung cancer: a comparison between IGF1R fluorescent in situ hybridization, protein expression, and mRNA expression. *Journal of clinical oncology : official journal of the American Society of Clinical Oncology*. 2010; 28(13):2174-2180.
137. Janeway KA, Zhu MJ, Barretina J, Perez-Atayde A, Demetri GD and Fletcher JA. Strong expression of IGF1R in pediatric gastrointestinal stromal tumors without IGF1R genomic amplification. *International journal of cancer Journal international du cancer*. 2010; 127(11):2718-2722.
138. Tarn C, Rink L, Merkel E, Flieder D, Pathak H, Koumbi D, Testa JR, Eisenberg B, von Mehren M and Godwin AK. Insulin-like growth factor 1 receptor is a potential therapeutic target for gastrointestinal stromal tumors. *Proceedings of the National Academy of Sciences of the United States of America*. 2008; 105(24):8387-8392.
139. Almeida A, Muleris M, Dutrillaux B and Malfoy B. The insulin-like growth factor I receptor gene is the target for the 15q26 amplicon in breast cancer. *Genes, chromosomes & cancer*. 1994; 11(1):63-65.
140. Takahashi K, Nishiyama C, Hasegawa M, Akizawa Y and Ra C. Regulation of the human high affinity IgE receptor beta-chain gene expression via an intronic element. *Journal of immunology*. 2003; 171(5):2478-2484.
141. Sun L, Goodman PA, Wood CM, Crotty ML, Sensel M, Sather H, Navara C, Nachman J, Steinherz PG, Gaynon PS, Seibel N, Vassilev A, Juran BD, Reaman GH and Uckun FM. Expression of aberrantly spliced oncogenic ikaros isoforms in childhood acute lymphoblastic leukemia. *Journal of clinical oncology : official journal of the American Society of Clinical Oncology*. 1999; 17(12):3753-3766.
142. Georgopoulos K, Bigby M, Wang JH, Molnar A, Wu P, Winandy S and Sharpe A. The Ikaros gene is required for the development of all lymphoid lineages. *Cell*. 1994; 79(1):143-156.
143. Winandy S, Wu L, Wang JH and Georgopoulos K. Pre-T cell receptor (TCR) and TCR-controlled checkpoints in T cell differentiation are set by Ikaros. *The Journal of experimental medicine*. 1999; 190(8):1039-1048.
144. Morris JF, Rauscher FJ, 3rd, Davis B, Klemsz M, Xu D, Tenen D and Hromas R. The myeloid zinc finger gene, MZF-1, regulates the CD34 promoter in vitro. *Blood*. 1995; 86(10):3640-3647.
145. Perrotti D, Melotti P, Skorski T, Casella I, Peschle C and Calabretta B. Overexpression of the zinc finger protein MZF1 inhibits hematopoietic development from embryonic stem cells: correlation with negative regulation of CD34 and c-myc promoter activity. *Molecular and cellular biology*. 1995; 15(11):6075-6087.
146. Kathrein KL, Lorenz R, Innes AM, Griffiths E and Winandy S. Ikaros induces quiescence and T-cell differentiation in a leukemia cell line. *Molecular and cellular biology*. 2005; 25(5):1645-1654.
147. Geimer Le Lay AS, Oravec A, Mastio J, Jung C, Marchal P, Ebel C, Dembele D, Jost B, Le Gras S, Thibault C, Borggreffe T, Kastner P and Chan S. The tumor suppressor Ikaros shapes the repertoire of notch target genes in T cells. *Science signaling*. 2014; 7(317):ra28.
148. Theocharides AP, Dobson SM, Laurenti E, Notta F, Voisin V, Cheng PY, Yuan JS, Guidos CJ, Minden MD, Mullighan CG, Torlakovic E and Dick JE. Dominant-negative Ikaros cooperates with BCR-ABL1 to induce human acute myeloid leukemia in xenografts. *Leukemia*. 2015; 29(1):177-187.
149. Hromas R, Morris J, Cornetta K, Berebitsky D, Davidson A, Sha M, Sledge G and Rauscher F, 3rd. Aberrant expression of the myeloid zinc finger gene, MZF-1, is oncogenic. *Cancer research*. 1995; 55(16):3610-3614.
150. Robertson KA, Hill DP, Kelley MR, Tritt R, Crum B, Van Epps S, Srour E, Rice S and Hromas R. The myeloid zinc finger gene (MZF-1) delays retinoic acid-induced apoptosis and differentiation in myeloid leukemia cells. *Leukemia*. 1998; 12(5):690-698.
151. Rafn B, Nielsen CF, Andersen SH, Szyniarowski P, Corcelle-Termeau E, Valo E, Fehrenbacher N, Olsen CJ, Daugaard M, Egebjerg C, Bottzauw T, Kohonen P, Nylandsted J,

- Hautaniemi S, Moreira J, Jaattela M, et al. ErbB2-driven breast cancer cell invasion depends on a complex signaling network activating myeloid zinc finger-1-dependent cathepsin B expression. *Molecular cell*. 2012; 45(6):764-776.
152. Gaboli M, Kotsi PA, Gurrieri C, Cattoretti G, Ronchetti S, Cordon-Cardo C, Broxmeyer HE, Hromas R and Pandolfi PP. Mzf1 controls cell proliferation and tumorigenesis. *Genes & development*. 2001; 15(13):1625-1630.
153. Yan QW, Reed E, Zhong XS, Thornton K, Guo Y and Yu JJ. MZF1 possesses a repressively regulatory function in ERCC1 expression. *Biochemical pharmacology*. 2006; 71(6):761-771.
154. Tsai SJ, Hwang JM, Hsieh SC, Ying TH and Hsieh YH. Overexpression of myeloid zinc finger 1 suppresses matrix metalloproteinase-2 expression and reduces invasiveness of SiHa human cervical cancer cells. *Biochemical and biophysical research communications*. 2012; 425(2):462-467.
155. Werner H, Woloschak M, Adamo M, Shen-Orr Z, Roberts CT, Jr. and LeRoith D. Developmental regulation of the rat insulin-like growth factor I receptor gene. *Proceedings of the National Academy of Sciences of the United States of America*. 1989; 86(19):7451-7455.
156. Werner H, Stannard B, Bach MA, LeRoith D and Roberts CT, Jr. Cloning and characterization of the proximal promoter region of the rat insulin-like growth factor I (IGF-I) receptor gene. *Biochemical and biophysical research communications*. 1990; 169(3):1021-1027.
157. Cooke DW, Bankert LA, Roberts CT, Jr., LeRoith D and Casella SJ. Analysis of the human type I insulin-like growth factor receptor promoter region. *Biochemical and biophysical research communications*. 1991; 177(3):1113-1120.
158. Mamula PW and Goldfine ID. Cloning and characterization of the human insulin-like growth factor-I receptor gene 5'-flanking region. *DNA and cell biology*. 1992; 11(1):43-50.
159. Werner H, Bach MA, Stannard B, Roberts CT, Jr. and LeRoith D. Structural and functional analysis of the insulin-like growth factor I receptor gene promoter. *Mol Endocrinol*. 1992; 6(10):1545-1558.
160. Smale ST and Baltimore D. The "initiator" as a transcription control element. *Cell*. 1989; 57(1):103-113.
161. Werner H and Roberts CT, Jr. The IGFI receptor gene: a molecular target for disrupted transcription factors. *Genes, chromosomes & cancer*. 2003; 36(2):113-120.
162. Beitner-Johnson D, Werner H, Roberts CT, Jr. and LeRoith D. Regulation of insulin-like growth factor I receptor gene expression by Sp1: physical and functional interactions of Sp1 at GC boxes and at a CT element. *Mol Endocrinol*. 1995; 9(9):1147-1156.
163. Werner H, Rauscher FJ, 3rd, Sukhatme VP, Drummond IA, Roberts CT, Jr. and LeRoith D. Transcriptional repression of the insulin-like growth factor I receptor (IGF-I-R) gene by the tumor suppressor WT1 involves binding to sequences both upstream and downstream of the IGF-I-R gene transcription start site. *The Journal of biological chemistry*. 1994; 269(17):12577-12582.
164. Werner H, Roberts CT, Jr., Rauscher FJ, 3rd and LeRoith D. Regulation of insulin-like growth factor I receptor gene expression by the Wilms' tumor suppressor WT1. *Journal of molecular neuroscience : MN*. 1996; 7(2):111-123.
165. Damon SE, Plymate SR, Carroll JM, Sprenger CC, Dechsukhum C, Ware JL and Roberts CT, Jr. Transcriptional regulation of insulin-like growth factor-I receptor gene expression in prostate cancer cells. *Endocrinology*. 2001; 142(1):21-27.
166. Chen MY, Clark AJ, Chan DC, Ware JL, Holt SE, Chidambaram A, Fillmore HL and Broaddus WC. Wilms' tumor 1 silencing decreases the viability and chemoresistance of glioblastoma cells in vitro: a potential role for IGF-1R de-repression. *Journal of neuro-oncology*. 2011; 103(1):87-102.
167. Shalita-Chesner M, Glaser T and Werner H. Signal transducer and activator of transcription-1 (STAT1), but not STAT5b, regulates IGF-I receptor gene expression in an osteosarcoma cell line. *Journal of pediatric endocrinology & metabolism : JPEM*. 2004; 17(2):211-218.
168. Schayek H, Bentov I, Rotem I, Pasmanik-Chor M, Ginsberg D, Plymate SR and Werner H. Transcription factor E2F1 is a potent transactivator of the insulin-like growth factor-I receptor (IGF-IR) gene. *Growth hormone & IGF research : official journal of the Growth Hormone Research Society and the International IGF Research Society*. 2010; 20(1):68-72.

169. Ma Y, Cheng Q, Ren Z, Xu L, Zhao Y, Sun J, Hu S and Xiao W. Induction of IGF-1R expression by EGR-1 facilitates the growth of prostate cancer cells. *Cancer letters*. 2012; 317(2):150-156.
170. Maor SB, Abramovitch S, Erdos MR, Brody LC and Werner H. BRCA1 suppresses insulin-like growth factor-I receptor promoter activity: potential interaction between BRCA1 and Sp1. *Molecular genetics and metabolism*. 2000; 69(2):130-136.
171. Abramovitch S, Glaser T, Ouchi T and Werner H. BRCA1-Sp1 interactions in transcriptional regulation of the IGF-IR gene. *FEBS letters*. 2003; 541(1-3):149-154.
172. Maor S, Mayer D, Yarden RI, Lee AV, Sarfstein R, Werner H and Papa MZ. Estrogen receptor regulates insulin-like growth factor-I receptor gene expression in breast tumor cells: involvement of transcription factor Sp1. *The Journal of endocrinology*. 2006; 191(3):605-612.
173. Reizner N, Maor S, Sarfstein R, Abramovitch S, Welshons WV, Curran EM, Lee AV and Werner H. The WT1 Wilms' tumor suppressor gene product interacts with estrogen receptor-alpha and regulates IGF-I receptor gene transcription in breast cancer cells. *Journal of molecular endocrinology*. 2005; 35(1):135-144.
174. Glait C, Tencer L, Ravid D, Sarfstein R, Liscovitch M and Werner H. Caveolin-1 up-regulates IGF-I receptor gene transcription in breast cancer cells via Sp1- and p53-dependent pathways. *Experimental cell research*. 2006; 312(19):3899-3908.
175. Rubinstein M, Idelman G, Plymate SR, Narla G, Friedman SL and Werner H. Transcriptional activation of the insulin-like growth factor I receptor gene by the Kruppel-like factor 6 (KLF6) tumor suppressor protein: potential interactions between KLF6 and p53. *Endocrinology*. 2004; 145(8):3769-3777.
176. Werner H, Karnieli E, Rauscher FJ and LeRoith D. Wild-type and mutant p53 differentially regulate transcription of the insulin-like growth factor I receptor gene. *Proceedings of the National Academy of Sciences of the United States of America*. 1996; 93(16):8318-8323.
177. Prisco M, Hongo A, Rizzo MG, Sacchi A and Baserga R. The insulin-like growth factor I receptor as a physiologically relevant target of p53 in apoptosis caused by interleukin-3 withdrawal. *Molecular and cellular biology*. 1997; 17(3):1084-1092.
178. Girnita L, Girnita A, Brodin B, Xie Y, Nilsson G, Dricu A, Lundeberg J, Wejde J, Bartolazzi A, Wiman KG and Larsson O. Increased expression of insulin-like growth factor I receptor in malignant cells expressing aberrant p53: functional impact. *Cancer research*. 2000; 60(18):5278-5283.
179. Molnar A and Georgopoulos K. The Ikaros gene encodes a family of functionally diverse zinc finger DNA-binding proteins. *Molecular and cellular biology*. 1994; 14(12):8292-8303.
180. Garzon R, Calin GA and Croce CM. MicroRNAs in Cancer. *Annual review of medicine*. 2009; 60:167-179.
181. Esquela-Kerscher A and Slack FJ. Oncomirs - microRNAs with a role in cancer. *Nature reviews Cancer*. 2006; 6(4):259-269.
182. Merkel O, Hamacher F, Laimer D, Sift E, Trajanoski Z, Scheideler M, Egger G, Hassler MR, Thallinger C, Schmatz A, Turner SD, Greil R and Kenner L. Identification of differential and functionally active miRNAs in both anaplastic lymphoma kinase (ALK)+ and ALK- anaplastic large-cell lymphoma. *Proceedings of the National Academy of Sciences of the United States of America*. 2010; 107(37):16228-16233.
183. Dejean E, Renalier MH, Foisseau M, Agirre X, Joseph N, de Paiva GR, Al Saati T, Soulier J, Desjobert C, Lamant L, Prosper F, Felsher DW, Cavaille J, Prats H, Delsol G, Giuriato S, et al. Hypoxia-microRNA-16 downregulation induces VEGF expression in anaplastic lymphoma kinase (ALK)-positive anaplastic large-cell lymphomas. *Leukemia*. 2011; 25(12):1882-1890.
184. Matsuyama H, Suzuki HI, Nishimori H, Noguchi M, Yao T, Komatsu N, Mano H, Sugimoto K and Miyazono K. miR-135b mediates NPM-ALK-driven oncogenicity and renders IL-17-producing immunophenotype to anaplastic large cell lymphoma. *Blood*. 2011; 118(26):6881-6892.
185. Desjobert C, Renalier MH, Bergalet J, Dejean E, Joseph N, Kruczynski A, Soulier J, Espinos E, Meggetto F, Cavaille J, Delsol G and Lamant L. MiR-29a down-regulation in ALK-positive anaplastic large cell lymphomas contributes to apoptosis blockade through MCL-1 overexpression. *Blood*. 2011; 117(24):6627-6637.

186. Liu CG, Calin GA, Volinia S and Croce CM. MicroRNA expression profiling using microarrays. *Nature protocols*. 2008; 3(4):563-578.
187. Weber B, Stresmann C, Brueckner B and Lyko F. Methylation of human microRNA genes in normal and neoplastic cells. *Cell cycle*. 2007; 6(9):1001-1005.
188. Fazi F, Racanicchi S, Zardo G, Starnes LM, Mancini M, Travaglini L, Diverio D, Ammatuna E, Cimino G, Lo-Coco F, Grignani F and Nervi C. Epigenetic silencing of the myelopoiesis regulator microRNA-223 by the AML1/ETO oncoprotein. *Cancer cell*. 2007; 12(5):457-466.
189. Kent OA, Chivukula RR, Mullendore M, Wentzel EA, Feldmann G, Lee KH, Liu S, Leach SD, Maitra A and Mendell JT. Repression of the miR-143/145 cluster by oncogenic Ras initiates a tumor-promoting feed-forward pathway. *Genes & development*. 2010; 24(24):2754-2759.
190. Li Y, Choi PS, Casey SC, Dill DL and Felsher DW. MYC through miR-17-92 Suppresses Specific Target Genes to Maintain Survival, Autonomous Proliferation, and a Neoplastic State. *Cancer cell*. 2014; 26(2):262-272.
191. He L, Thomson JM, Hemann MT, Hernando-Monge E, Mu D, Goodson S, Powers S, Cordon-Cardo C, Lowe SW, Hannon GJ and Hammond SM. A microRNA polycistron as a potential human oncogene. *Nature*. 2005; 435(7043):828-833.
192. Bui TV and Mendell JT. Myc: Maestro of MicroRNAs. *Genes & cancer*. 2010; 1(6):568-575.
193. Saito Y, Liang G, Egger G, Friedman JM, Chuang JC, Coetzee GA and Jones PA. Specific activation of microRNA-127 with downregulation of the proto-oncogene BCL6 by chromatin-modifying drugs in human cancer cells. *Cancer cell*. 2006; 9(6):435-443.
194. Lehmann U, Hasemeier B, Christgen M, Muller M, Romermann D, Langer F and Kreipe H. Epigenetic inactivation of microRNA gene hsa-mir-9-1 in human breast cancer. *The Journal of pathology*. 2008; 214(1):17-24.
195. Toyota M, Suzuki H, Sasaki Y, Maruyama R, Imai K, Shinomura Y and Tokino T. Epigenetic silencing of microRNA-34b/c and B-cell translocation gene 4 is associated with CpG island methylation in colorectal cancer. *Cancer research*. 2008; 68(11):4123-4132.
196. Lujambio A, Ropero S, Ballestar E, Fraga MF, Cerrato C, Setien F, Casado S, Suarez-Gauthier A, Sanchez-Cespedes M, Git A, Spiteri I, Das PP, Caldas C, Miska E and Esteller M. Genetic unmasking of an epigenetically silenced microRNA in human cancer cells. *Cancer research*. 2007; 67(4):1424-1429.
197. Zhong Z, Xia Y, Wang P, Liu B and Chen Y. Low expression of microRNA-30c promotes invasion by inducing epithelial mesenchymal transition in non-small cell lung cancer. *Molecular medicine reports*. 2014.
198. Zhao JJ, Lin J, Zhu D, Wang X, Brooks D, Chen M, Chu ZB, Takada K, Ciccarelli B, Admin S, Tao J, Tai YT, Treon S, Pinkus G, Kuo WP, Hideshima T, et al. miR-30-5p functions as a tumor suppressor and novel therapeutic tool by targeting the oncogenic Wnt/beta-catenin/BCL9 pathway. *Cancer research*. 2014; 74(6):1801-1813.
199. Kao CJ, Martiniez A, Shi XB, Yang J, Evans CP, Dobi A, deVere White RW and Kung HJ. miR-30 as a tumor suppressor connects EGF/Src signal to ERG and EMT. *Oncogene*. 2014; 33(19):2495-2503.
200. Quintavalle C, Donnarumma E, Iaboni M, Roscigno G, Garofalo M, Romano G, Fiore D, De Marinis P, Croce CM and Condorelli G. Effect of miR-21 and miR-30b/c on TRAIL-induced apoptosis in glioma cells. *Oncogene*. 2013; 32(34):4001-4008.
201. Li J, Donath S, Li Y, Qin D, Prabhakar BS and Li P. miR-30 regulates mitochondrial fission through targeting p53 and the dynamin-related protein-1 pathway. *PLoS genetics*. 2010; 6(1):e1000795.
202. Ozcan S. MiR-30 family and EMT in human fetal pancreatic islets. *Islets*. 2009; 1(3):283-285.
203. Yu F, Deng H, Yao H, Liu Q, Su F and Song E. Mir-30 reduction maintains self-renewal and inhibits apoptosis in breast tumor-initiating cells. *Oncogene*. 2010; 29(29):4194-4204.
204. Morozevich GE, Kozlova NI, Cheglakov IB, Ushakova NA, Preobrazhenskaya ME and Berman AE. Implication of alpha5beta1 integrin in invasion of drug-resistant MCF-7/ADR breast carcinoma cells: a role for MMP-2 collagenase. *Biochemistry Biokhimiia*. 2008; 73(7):791-796.

205. Morozevich GE, Kozlova NI, Preobrazhenskaya ME, Ushakova NA, Eltsov IA, Shtil AA and Berman AE. The role of beta1 integrin subfamily in anchorage-dependent apoptosis of breast carcinoma cells differing in multidrug resistance. *Biochemistry Biokhimiia*. 2006; 71(5):489-495.
206. Tai YT, Podar K, Catley L, Tseng YH, Akiyama M, Shringarpure R, Burger R, Hideshima T, Chauhan D, Mitsiades N, Richardson P, Munshi NC, Kahn CR, Mitsiades C and Anderson KC. Insulin-like growth factor-1 induces adhesion and migration in human multiple myeloma cells via activation of beta1-integrin and phosphatidylinositol 3'-kinase/AKT signaling. *Cancer research*. 2003; 63(18):5850-5858.
207. Sayeed A, Fedele C, Trerotola M, Ganguly KK and Languino LR. IGF-IR promotes prostate cancer growth by stabilizing alpha5beta1 integrin protein levels. *PLoS one*. 2013; 8(10):e76513.
208. Wu CM, Li TM, Hsu SF, Su YC, Kao ST, Fong YC and Tang CH. IGF-I enhances alpha5beta1 integrin expression and cell motility in human chondrosarcoma cells. *Journal of cellular physiology*. 2011; 226(12):3270-3277.
209. Surmacz E. Function of the IGF-I receptor in breast cancer. *Journal of mammary gland biology and neoplasia*. 2000; 5(1):95-105.
210. Durai R, Yang W, Gupta S, Seifalian AM and Winslet MC. The role of the insulin-like growth factor system in colorectal cancer: review of current knowledge. *International journal of colorectal disease*. 2005; 20(3):203-220.
211. Zhang Q, Tang Q, Qin D, Yu L, Huang R, Lv G, Zou Z, Jiang XC, Zou C, Liu W, Luo J, Zhao Z, Muhammad S, Wang G, Chen YG and Wang X. Role of MicroRNA 30a Targeting Insulin Receptor Substrate 2 in Colorectal Tumorigenesis. *Molecular and cellular biology*. 2015; 35(6):988-1000.
212. Fu J, Xu X, Kang L, Zhou L, Wang S, Lu J, Cheng L, Fan Z, Yuan B, Tian P, Zheng X, Yu C, Ye Q and Lv Z. miR-30a suppresses breast cancer cell proliferation and migration by targeting Eya2. *Biochemical and biophysical research communications*. 2014; 445(2):314-319.
213. Zhang N, Wang X, Huo Q, Sun M, Cai C, Liu Z, Hu G and Yang Q. MicroRNA-30a suppresses breast tumor growth and metastasis by targeting metadherin. *Oncogene*. 2014; 33(24):3119-3128.
214. Ouzounova M, Vuong T, Ancy PB, Ferrand M, Durand G, Le-Calvez Kelm F, Croce C, Matar C, Herceg Z and Hernandez-Vargas H. MicroRNA miR-30 family regulates non-attachment growth of breast cancer cells. *BMC genomics*. 2013; 14:139.
215. Cheng CW, Wang HW, Chang CW, Chu HW, Chen CY, Yu JC, Chao JI, Liu HF, Ding SL and Shen CY. MicroRNA-30a inhibits cell migration and invasion by downregulating vimentin expression and is a potential prognostic marker in breast cancer. *Breast cancer research and treatment*. 2012; 134(3):1081-1093.
216. Chu PC, Kulp SK and Chen CS. Insulin-like growth factor-I receptor is suppressed through transcriptional repression and mRNA destabilization by a novel energy restriction-mimetic agent. *Carcinogenesis*. 2013; 34(12):2694-2705.
217. Meng Z, King PH, Nabors LB, Jackson NL, Chen CY, Emanuel PD and Blume SW. The ELAV RNA-stability factor HuR binds the 5'-untranslated region of the human IGF-IR transcript and differentially represses cap-dependent and IRES-mediated translation. *Nucleic acids research*. 2005; 33(9):2962-2979.
218. Nair PN, De Armond DT, Adamo ML, Strodel WE and Freeman JW. Aberrant expression and activation of insulin-like growth factor-1 receptor (IGF-1R) are mediated by an induction of IGF-1R promoter activity and stabilization of IGF-1R mRNA and contributes to growth factor independence and increased survival of the pancreatic cancer cell line MIA PaCa-2. *Oncogene*. 2001; 20(57):8203-8214.
219. Huynh H, Nickerson T, Pollak M and Yang X. Regulation of insulin-like growth factor I receptor expression by the pure antiestrogen ICI 182780. *Clinical cancer research : an official journal of the American Association for Cancer Research*. 1996; 2(12):2037-2042.
220. Shalita-Chesner M, Katz J, Shemer J and Werner H. Regulation of insulin-like growth factor-I receptor gene expression by tumor necrosis factor-alpha and interferon-gamma. *Molecular and cellular endocrinology*. 2001; 176(1-2):1-12.



221. Zhang Q, Wang HY, Bhutani G, Liu X, Paessler M, Tobias JW, Baldwin D, Swaminathan K, Milone MC and Wasik MA. Lack of TNF $\alpha$  expression protects anaplastic lymphoma kinase-positive T-cell lymphoma (ALK+ TCL) cells from apoptosis. *Proceedings of the National Academy of Sciences of the United States of America*. 2009; 106(37):15843-15848.
222. Goldfeld AE, McCaffrey PG, Strominger JL and Rao A. Identification of a novel cyclosporin-sensitive element in the human tumor necrosis factor alpha gene promoter. *The Journal of experimental medicine*. 1993; 178(4):1365-1379.
223. Muller S, Rihs S, Schneider JM, Paredes BE, Seibold I, Brunner T and Mueller C. Soluble TNF-alpha but not transmembrane TNF-alpha sensitizes T cells for enhanced activation-induced cell death. *European journal of immunology*. 2009; 39(11):3171-3180.
224. Tsai EY, Jain J, Pesavento PA, Rao A and Goldfeld AE. Tumor necrosis factor alpha gene regulation in activated T cells involves ATF-2/Jun and NFATp. *Molecular and cellular biology*. 1996; 16(2):459-467.
225. van Horssen R, Ten Hagen TL and Eggermont AM. TNF-alpha in cancer treatment: molecular insights, antitumor effects, and clinical utility. *The oncologist*. 2006; 11(4):397-408.
226. Johnson ES. Protein modification by SUMO. *Annual review of biochemistry*. 2004; 73:355-382.
227. Kim KI, Baek SH, Jeon YJ, Nishimori S, Suzuki T, Uchida S, Shimbara N, Saitoh H, Tanaka K and Chung CH. A new SUMO-1-specific protease, SUSP1, that is highly expressed in reproductive organs. *The Journal of biological chemistry*. 2000; 275(19):14102-14106.
228. Tatham MH, Jaffray E, Vaughan OA, Desterro JM, Botting CH, Naismith JH and Hay RT. Polymeric chains of SUMO-2 and SUMO-3 are conjugated to protein substrates by SAE1/SAE2 and Ubc9. *The Journal of biological chemistry*. 2001; 276(38):35368-35374.
229. Bayer P, Arndt A, Metzger S, Mahajan R, Melchior F, Jaenicke R and Becker J. Structure determination of the small ubiquitin-related modifier SUMO-1. *J Mol Biol*. 1998; 280(2):275-286.
230. Kim KI, Baek SH and Chung CH. Versatile protein tag, SUMO: its enzymology and biological function. *J Cell Physiol*. 2002; 191(3):257-268.
231. Melchior F. SUMO--nonclassical ubiquitin. *Annu Rev Cell Dev Biol*. 2000; 16:591-626.
232. Muller S, Hoege C, Pyrowolakis G and Jentsch S. SUMO, ubiquitin's mysterious cousin. *Nat Rev Mol Cell Biol*. 2001; 2(3):202-210.
233. Seeler JS and Dejean A. Nuclear and unclear functions of SUMO. *Nat Rev Mol Cell Biol*. 2003; 4(9):690-699.
234. Andreou AM and Tavernarakis N. SUMOylation and cell signalling. *Biotechnol J*. 2009; 4(12):1740-1752.
235. Melchior F, Schergaut M and Pichler A. SUMO: ligases, isopeptidases and nuclear pores. *Trends in biochemical sciences*. 2003; 28(11):612-618.
236. Desterro JM, Rodriguez MS and Hay RT. SUMO-1 modification of IkappaBalpha inhibits NF-kappaB activation. *Molecular cell*. 1998; 2(2):233-239.
237. Bae SH, Jeong JW, Park JA, Kim SH, Bae MK, Choi SJ and Kim KW. Sumoylation increases HIF-1alpha stability and its transcriptional activity. *Biochemical and biophysical research communications*. 2004; 324(1):394-400.
238. Sehat B, Tofigh A, Lin Y, Trocme E, Liljedahl U, Lagergren J and Larsson O. SUMOylation mediates the nuclear translocation and signaling of the IGF-1 receptor. *Science signaling*. 2010; 3(108):ra10.
239. Chen SF, Gong C, Luo M, Yao HR, Zeng YJ and Su FX. Ubc9 expression predicts chemoresistance in breast cancer. *Chin J Cancer*. 2011; 30(9):638-644.
240. Kim JH, Lee JM, Nam HJ, Choi HJ, Yang JW, Lee JS, Kim MH, Kim SI, Chung CH, Kim KI and Baek SH. SUMOylation of pontin chromatin-remodeling complex reveals a signal integration code in prostate cancer cells. *Proceedings of the National Academy of Sciences of the United States of America*. 2007; 104(52):20793-20798.
241. Sarge KD and Park-Sarge OK. Detection of proteins sumoylated in vivo and in vitro. *Methods Mol Biol*. 2009; 590:265-277.

242. Deng H, Lin Y, Badin M, Vasilcanu D, Stromberg T, Jernberg-Wiklund H, Sehat B and Larsson O. Over-accumulation of nuclear IGF-1 receptor in tumor cells requires elevated expression of the receptor and the SUMO-conjugating enzyme Ubc9. *Biochemical and biophysical research communications*. 2011; 404(2):667-671.
243. Zhang J, Huang FF, Wu DS, Li WJ, Zhan HE, Peng MY, Fang P, Cao PF, Zhang MM, Zeng H and Chen FP. SUMOylation of insulin-like growth factor 1 receptor, promotes proliferation in acute myeloid leukemia. *Cancer letters*. 2015; 357(1):297-306.
244. Packham S, Warsito D, Lin Y, Sadi S, Karlsson R, Sehat B and Larsson O. Nuclear translocation of IGF-1R via p150 and an importin-beta/RanBP2-dependent pathway in cancer cells. *Oncogene*. 2014.
245. Kim YH, Sung KS, Lee SJ, Kim YO, Choi CY and Kim Y. Desumoylation of homeodomain-interacting protein kinase 2 (HIPK2) through the cytoplasmic-nuclear shuttling of the SUMO-specific protease SENP1. *FEBS letters*. 2005; 579(27):6272-6278.
246. Li X, Luo Y, Yu L, Lin Y, Luo D, Zhang H, He Y, Kim YO, Kim Y, Tang S and Min W. SENP1 mediates TNF-induced desumoylation and cytoplasmic translocation of HIPK1 to enhance ASK1-dependent apoptosis. *Cell death and differentiation*. 2008; 15(4):739-750.
247. Bonvini P, Dalla Rosa H, Vignes N and Rosolen A. Ubiquitination and proteasomal degradation of nucleophosmin-anaplastic lymphoma kinase induced by 17-allylamino-demethoxygeldanamycin: role of the co-chaperone carboxyl heat shock protein 70-interacting protein. *Cancer research*. 2004; 64(9):3256-3264.
248. Sarge KD and Park-Sarge OK. Sumoylation and human disease pathogenesis. *Trends in biochemical sciences*. 2009; 34(4):200-205.
249. Zhou W, Hannoun Z, Jaffray E, Medine CN, Black JR, Greenhough S, Zhu L, Ross JA, Forbes S, Wilmut I, Iredale JP, Hay RT and Hay DC. SUMOylation of HNF4alpha regulates protein stability and hepatocyte function. *Journal of cell science*. 2012; 125(Pt 15):3630-3635.
250. Klenk C, Humrich J, Qwitterer U and Lohse MJ. SUMO-1 controls the protein stability and the biological function of phosphatidylinositol-3-OH kinase. *The Journal of biological chemistry*. 2006; 281(13):8357-8364.
251. de Cristofaro T, Mascia A, Pappalardo A, D'Andrea B, Nitsch L and Zannini M. Pax8 protein stability is controlled by sumoylation. *Journal of molecular endocrinology*. 2009; 42(1):35-46.
252. Giri R, Yeh HH, Wu CH and Liu HS. SUMO-1 overexpression increases RbAp46 protein stability and suppresses cell growth. *Anticancer research*. 2008; 28(6A):3749-3756.
253. Belaguli NS, Zhang M, Brunnicardi FC and Berger DH. Forkhead box protein A2 (FOXA2) protein stability and activity are regulated by sumoylation. *PloS one*. 2012; 7(10):e48019.
254. Manente AG, Pinton G, Tavian D, Lopez-Rodas G, Brunelli E and Moro L. Coordinated sumoylation and ubiquitination modulate EGF induced EGR1 expression and stability. *PloS one*. 2011; 6(10):e25676.
255. Gong L, Millas S, Maul GG and Yeh ET. Differential regulation of sumoylated proteins by a novel sumoin-specific protease. *The Journal of biological chemistry*. 2000; 275(5):3355-3359.
256. Mikolajczyk J, Drag M, Bekes M, Cao JT, Ronai Z and Salvesen GS. Small ubiquitin-related modifier (SUMO)-specific proteases: profiling the specificities and activities of human SENPs. *The Journal of biological chemistry*. 2007; 282(36):26217-26224.
257. Xu Z and Au SW. Mapping residues of SUMO precursors essential in differential maturation by SUMO-specific protease, SENP1. *The Biochemical journal*. 2005; 386(Pt 2):325-330.
258. Ihara M, Koyama H, Uchimura Y, Saitoh H and Kikuchi A. Noncovalent binding of small ubiquitin-related modifier (SUMO) protease to SUMO is necessary for enzymatic activities and cell growth. *The Journal of biological chemistry*. 2007; 282(22):16465-16475.
259. Mukhopadhyay D and Dasso M. Modification in reverse: the SUMO proteases. *Trends in biochemical sciences*. 2007; 32(6):286-295.
260. Bailey D and O'Hare P. Characterization of the localization and proteolytic activity of the SUMO-specific protease, SENP1. *The Journal of biological chemistry*. 2004; 279(1):692-703.
261. Matunis MJ, Coutavas E and Blobel G. A novel ubiquitin-like modification modulates the partitioning of the Ran-GTPase-activating protein RanGAP1 between the cytosol and the nuclear pore complex. *The Journal of cell biology*. 1996; 135(6 Pt 1):1457-1470.

262. Mahajan R, Delphin C, Guan T, Gerace L and Melchior F. A small ubiquitin-related polypeptide involved in targeting RanGAP1 to nuclear pore complex protein RanBP2. *Cell*. 1997; 88(1):97-107.
263. Girdwood D, Bumpass D, Vaughan OA, Thain A, Anderson LA, Snowden AW, Garcia-Wilson E, Perkins ND and Hay RT. P300 transcriptional repression is mediated by SUMO modification. *Molecular cell*. 2003; 11(4):1043-1054.
264. Papouli E, Chen S, Davies AA, Huttner D, Krejci L, Sung P and Ulrich HD. Crosstalk between SUMO and ubiquitin on PCNA is mediated by recruitment of the helicase Srs2p. *Molecular cell*. 2005; 19(1):123-133.
265. Pfander B, Moldovan GL, Sacher M, Hoege C and Jentsch S. SUMO-modified PCNA recruits Srs2 to prevent recombination during S phase. *Nature*. 2005; 436(7049):428-433.
266. Zheng G and Yang YC. ZNF76, a novel transcriptional repressor targeting TATA-binding protein, is modulated by sumoylation. *The Journal of biological chemistry*. 2004; 279(41):42410-42421.
267. Lin X, Sun B, Liang M, Liang YY, Gast A, Hildebrand J, Brunnicardi FC, Melchior F and Feng XH. Opposed regulation of corepressor CtBP by SUMOylation and PDZ binding. *Molecular cell*. 2003; 11(5):1389-1396.
268. Pichler A, Knipscheer P, Oberhofer E, van Dijk WJ, Korner R, Olsen JV, Jentsch S, Melchior F and Sixma TK. SUMO modification of the ubiquitin-conjugating enzyme E2-25K. *Nature structural & molecular biology*. 2005; 12(3):264-269.
269. Mooney SM, Grande JP, Salisbury JL and Janknecht R. Sumoylation of p68 and p72 RNA helicases affects protein stability and transactivation potential. *Biochemistry*. 2010; 49(1):1-10.
270. Sarfstein R, Pasmanik-Chor M, Yeheskel A, Edry L, Shomron N, Warman N, Wertheimer E, Maor S, Shochat L and Werner H. Insulin-like growth factor-I receptor (IGF-IR) translocates to nucleus and autoregulates IGF-IR gene expression in breast cancer cells. *The Journal of biological chemistry*. 2012; 287(4):2766-2776.
271. Aleksic T, Chitnis MM, Perestenko OV, Gao S, Thomas PH, Turner GD, Protheroe AS, Howarth M and Macaulay VM. Type 1 insulin-like growth factor receptor translocates to the nucleus of human tumor cells. *Cancer research*. 2010; 70(16):6412-6419.
272. Turner SD and Alexander DR. What have we learnt from mouse models of NPM-ALK-induced lymphomagenesis? *Leukemia*. 2005; 19(7):1128-1134.
273. Turner SD, Tooze R, MacLennan K and Alexander DR. Vav-promoter regulated oncogenic fusion protein NPM-ALK in transgenic mice causes B-cell lymphomas with hyperactive Jun kinase. *Oncogene*. 2003; 22(49):7750-7761.
274. Jager R, Hahne J, Jacob A, Egert A, Schenkel J, Wernert N, Schorle H and Wellmann A. Mice transgenic for NPM-ALK develop non-Hodgkin lymphomas. *Anticancer research*. 2005; 25(5):3191-3196.
275. Ogilvy S, Metcalf D, Gibson L, Bath ML, Harris AW and Adams JM. Promoter elements of vav drive transgene expression in vivo throughout the hematopoietic compartment. *Blood*. 1999; 94(6):1855-1863.

**Vitae:**

Deeksha Vishwamitra was raised in Cincinnati, OH, the daughter of Nimi Rao and Teju Vishwamitra. After completing her work at Indian Hill High School, Cincinnati, OH, in 2003, she entered The Ohio State University in Columbus, OH. She received the degree of Bachelor of Science with a major in Molecular Genetics from OSU In June 2007. She began her Master's work in May 2008 at the University of Texas Graduate School of Biomedical Sciences at Houston. She earned her MS degree in January 2010 in Cancer Biology and Molecular Biology. She matriculated into the PhD program immediately at the University of Texas Graduate School of Biomedical Sciences at Houston in January 2010. She completed her PhD degree in April 2015 in Cancer Biology.